HELIUM ISOTOPE GEOCHEMISTRY OF OCEANIC VOLCANIC ROCKS: IMPLICATIONS FOR MANTLE HETEROGENEITY AND DEGASSING

by

MARK DAVID KURZ

B.S., University of Wisconsin, Madison
(1976)

SUBMITTED IN PARTIAL FULFILLMENT OF THE
REQUIREMENTS FOR THE DEGREE OF
DOCTOR OF PHILOSOPHY

at the

MASSACHUSETTS INSTITUTE OF TECHNOLOGY

and the

WOODS HOLE OCEANOGRAPHIC INSTITUTION

June, 1982

Signature of Author .....
Joint Program in Oceanography, Massachusetts Institute of Technology-Woods Hole Oceanographic Institution, March, 1982.

Certified by .....
Thesis Supervisor

Accepted by .....
Chairman, Joint Committee for Chemical Oceanography, Massachusetts Institute of Technology - Woods Hole Oceanographic Institution

Lindgren
MASSACHUSETTS INSTITUTE OF TECHNOLOGY
JUL 1 1982
LIBRARIES

MIT Libraries
Document Services

Room 14-0551
77 Massachusetts Avenue
Cambridge, MA 02139
Ph: 617.253.5668 Fax: 617.253.1690
Email: docs@mit.edu
http://libraries.mit.edu/docs

DISCLAIMER OF QUALITY

Due to the condition of the original material, there are unavoidable flaws in this reproduction. We have made every effort possible to provide you with the best copy available. If you are dissatisfied with this product and find it unusable, please contact Document Services as soon as possible.

Thank you.

Pages are missing from the original document.

Page 160

TABLE OF CONTENTS

	Page
LIST OF FIGURES	6
LIST OF TABLES	8
BIOGRAPHICAL SKETCH	10
ACKNOWLEDGEMENTS	11
ABSTRACT	12
CHAPTER 1: Introduction	14
A. Helium Isotope Geochemistry and the Atmospheric Helium Inventory	14
B. Helium in Mantle Derived Rocks	18
C. Objectives	20
CHAPTER 2: Experimental Methods	25
A. Introduction	25
B. Sample Preparation	25
C. Extraction Methods	26
1. The Crusher	27
2. The Furnace	29
3. The First Processing Line	34
4. The Second Processing Line	36
D. Blanks	40
E. Mass Spectrometry	41
1. Procedure	43
2. Standardization	46
3. Precision and Reproducibility	50

CHAPTER 3: The Distribution of Helium in Oceanic Basalt Glasses..... 53

A. Introduction..... 53

B. Experimental..... 56

1. Methods..... 56

2. Samples..... 60

C. Results..... 63

1. Glass-Vesicle Partitioning..... 65

2. Glass-Phenocryst Partitioning..... 72

3. Determination of Diffusion Rates by Stepwise Heating... 75

4. $^{3}He/^{4}He$ Ratios..... 80

D. Discussion..... 82

E. Summary..... 85

CHAPTER 4: Helium Isotopic Variations in Mid-Ocean Ridge Basalts.... 87

A. Introduction..... 87

B. Results and Discussion: Global Variations..... 93

1. Overall Isotopic Variations..... 93

2. Helium in Normal MORB..... 97

C. Results and Discussion: Central North Atlantic Samples..... 102

1. Helium Isotopic Variations..... 102

2. Concentration variations and Glass-Vesicle Partitioning 109

3. Isotope Systematics..... 115

C. Results and Discussion: South Atlantic Near the Bouvet.....

Triple Junction..... 121

D. Isotopic Variations and Mantle Heterogeneity..... 128

E. Conclusions..... 131

CHAPTER 5: Helium Isotopic Systematics of Oceanic Islands..... 135

A. Introduction..... 135

B. Samples..... 142

C. Results..... 145

1. Islands of the Atlantic and Indian Oceans..... 145

2. Iceland..... 145

3. Loihi Seamount and the Island of Hawaii..... 148

4. Evaluation of Methods..... 152

D. Discussion..... 152

1. Crystal-Melt Partitioning..... 152

2. Overall Helium Isotopic Variability..... 153

3. Iceland..... 159

4. Loihi Seamount and the Island of Hawaii..... 166

a. Background..... 166

b. Loihi Seamount: Glass-Vesicle Partitioning..... 170

c. Loihi Seamount: Isotopic Variations..... 175

d. Helium Isotopic Variations: Hawaiian Volcanoes... 183

e. A Model for Volcanism on the Hawaiian Islands..... 186

5. Implications for Mantle Heterogeneity..... 190

1. The Mantle Plume Model..... 190

2. The Layered Mantle..... 193

E. Conclusions..... 196

CHAPTER 6: Implications for Mantle Heterogeneity and Degassing..... 199

A. Introduction..... 199

B. Mantle Models: Constraints form the Helium Isotopes..... 204

1. Identification of the Undepleted End-Member..... 204

2. Identification of the Recycled End-Member..... 209

3. Proposed Mantle Model..... 220

4. Geochemical Consistency of the Model..... 228

C. Implications for Mantle Degassing..... 231

1. Catastrophic of Continuous degassing..... 231

2. Origin of the ^{3}He Flux..... 235

3. Implications for Degassing History..... 239

D. Conclusions..... 245

APPENDIX I: Stepwise Heating Data..... 248

APPENDIX II: Sample Descriptions and Petrography..... 253

REFERENCES..... 265

LIST OF FIGURES

Page

CHAPTER 2

2.1 Sketch of Rock Crusher..... 28

2.2 Simplified Sketch of the Furnace Hot Zone..... 32

2.3 Cross Section of Furnace Sample Delivery System..... 33

2.4 Diagram of the First Gas Processing Line..... 36

2.5 Diagram of the Second Gas Processing Line..... 39

2.6 Sketch of W.H.O.I. Branch Tube Mass Spectrometer MS-2..... 44

2.7 Magnet Scan of Atmospheric Helium..... 45

2.8 Typical Calibration Curve for Air Standards..... 49

CHAPTER 3

3.1 Plot of Glass-Melt Partitioning for MORB Glasses..... 68

3.2 Plot of lnD vs 1/T for Helium Diffusion in Basaltic Glass..... 76

3.3 Plot of 3He vs. 4He for MORB Several MORB Glasses..... 81

CHAPTER 4

4.1 Map of Mid-Ocean Ridges With Sample Locations Indicated..... 92

4.2 Histogram of All Helium Isotope Ratio Measurements for MORB... 98

4.3 Histogram of Helium Isotope Ratios for Normal MORB Samples.... 100

4.4 Histogram of Helium Concentrations in Normal MORB Samples..... 101

4.5 Dredge Locations for Central North Atlantic Samples..... 103

4.6 Helium and Strontium Isotopic Variation Along the Mid-Atlantic Ridge from 25° to 65° N Latitude..... 105

4.7 Plot of $^{3}He/^{4}He$ versus $^{87}Sr/^{86}Sr$ for the Central North..... Atlantic Samples..... 108

4.8 Vesicularity and Helium Concentration Variations Along the.... Mid-Atlantic Ridge..... 110
4.9 Plots of Helium versus Cl Content and Vesicularity..... 112
4.10 Plot of Total Helium Versus $^{3}He/^{4}He$ for the Central North..... North Atlantic Samples..... 114
4.11 Plot of K Content Versus $^{3}He/^{4}He$ Ratio for the Central..... North Atlantic Samples..... 122
4.12 Map of South Atlantic Near the Bouvet Triple Junction..... 124
4.13 $^{3}He/^{4}He$ versus $^{87}Sr/^{86}Sr$ for the South Atlantic Samples..... 126

CHAPTER 5

5.1 Map Showing the Locations of the Oceanic Islands Studied..... 141
5.2 $^{3}He/^{4}He$ versus $^{87}Sr/^{86}Sr$ for Oceanic Islands..... 156
5.3 $^{3}He/^{4}He$ versus K_2O for Oceanic Islands..... 158
5.4 Map of Iceland with Sample Localities..... 161
5.5 Map of Hawaii with Sample Localities..... 168
5.6 Glass-Vesicle Partitioning Plot for Loihi Seamount Glasses.... 173
5.7 Histogram Plot of Isotopic Difference Between Helium Contained In Vesicles and Glass..... 177
5.8 $^{3}He/^{4}He$ versus $^{87}Sr/^{86}Sr$ for Loihi Seamount Glasses..... 181
5.9 $^{3}He/^{4}He$ Versus Volcano Age for the Hawaiian Volcanoes..... 184
5.10 $^{3}He/^{4}He$ Versus Volcano Volume for the Hawaiian Volcanoes..... 189

CHAPTER 6

6.1 Closed System Helium Isotopic Evolution for Chondritic Earth.. 208
6.2 Simplified Plot of $^{3}He/^{4}He$ versus $^{87}Sr/^{86}Sr$ for Terrestrial and Meteoritic Materials..... 208
6.3 Two Component Mixing Diagram 211

6.4 Idealized Structure of Oceanic Lithosphere and Subduction Zone 216

6.5 Helium Isotopic Evolution Curves for Oceanic Crust..... 218

6.6 Sketch of the Proposed Mantle Model..... 227

6.7 $^{3}He/^{4}He$ Versus $^{207}Pb/^{204}Pb$ for Oceanic Islands..... 229

LIST OF TABLES

CHAPTER 2

2.1 Components of the Helium Blank for Melting Rocks..... 42

2.2 Typical Contributions to the Uncertainty of Helium Isotope Ratio Measurements..... 51

2.3 Reproducibility of the Replicate Standard Rock..... 53

CHAPTER 3

3.1 Major Element Chemistry of Glasses..... 57

3.2 Helium Results: Basaltic Glasses..... 65

3.3 Glass-vesicle Partitioning Results..... 66

3.4 Plagioclase-glass Partitioning Results..... 74

CHAPTER 4

4.1 Helium Results for North Atlantic Samples..... 94

4.2 Helium Results for South Atlantic Samples..... 95

4.3 Helium Results for Samples from Atlantic, Pacific, and Indian Oceans..... 96

CHAPTER 5

5.1 Helium Results: Atlantic and Indian Ocean..... 146

5.2 Helium Results: Iceland..... 147

5.3 Helium Results: Loihi Glasses..... 149

5.4 Helium Results: Loihi Xenoliths..... 150

5.5 Helium Results: Hawaiian Volcanoes..... 151

5.6 Vesicularity and Partitioning for Loihi Glasses..... 171

ACKNOWLEDGEMENTS

I sincerely thank my thesis advisor Bill Jenkins, for his interest, patience, and good humor during the course of this work. His sensible approach to problems, both scientific and human, has been an inspiration. I also thank my thesis committee, Bill Bryan, Henry Dick, Stan Hart, and Geoff Thompson for timely advice and encouragement. Interesting discussions with Anton le Roex, Fred Frey, Dave Clague, John Edmond, Dan McKenzie, Dan Repeta, and my fellow students have been particularly stimulating. All the members of the helium isotope lab helped provide a pleasant, if not always sane, working environment; Dempsey Lott provided "positive vibrations" when experimental problems seemed insurmountable.

I also thank all the people who unselfishly donated samples that were studied in this thesis: Claude Allegre, John Bender, Dave Claque, Dan Fornari, Andrew Graham, Susan Humphris, Robert Hutchison, Anton le Roex, Sven Maaloe, Bill Melson, Jim Moore, Keith O'Nions, Mike Rhodes, Peter Rona, J.G. Schilling, Hubert Staudigel, B. Upton, and W. Voerwoerd.

Finally, I thank my family - Robb, Pam, Max, and Kay - and especially my wife, Slim, for always being there.

HELIUM ISOTOPE GEOCHEMISTRY OF OCEANIC VOLCANIC ROCKS: IMPLICATIONS FOR MANTLE HETEROGENEITY AND DEGASSING

by

MARK DAVID KURZ

Submitted to the Massachusetts Institute of Technology - Woods Hole Oceanography Institution Joint Program in Oceanography on March 31, 1982 in partial fulfillment of the requirements for the degree of Doctor of Philosophy.

ABSTRACT

The concentrations and isotopic compositions of helium have been measured in a number of mantle derived oceanic basalts. The goal of this research is to use the helium isotopic systematics to constrain the nature and origin of mantle heterogeneity in the oceanic mantle.

Studies of helium partitioning in mid-ocean ridge basalt (MORB) glass, performed by crushing and melting in vacuo, show that a significant fraction of the helium resides within vesicles. Measured concentrations are therefore a function of original helium content, magmatic history, vesicle size and quantity, and grain size analyzed. The helium solubility inferred from the results is 3.7×10^{-4} cc STP/g-atm), which is significantly higher (by a factor of 5) than the enstatite value (Kirsten, 1968) most often used in the literature. Concentrations obtained from basaltic phenocrysts and glasses suggest that helium behaves as an incompatible element with respect to olivine, clinopyroxene, and plagioclase.

Diffusion rates for helium in basaltic glass (in the temperature range 125-400°C), determined using the method of stepwise heating, yielded an activation energy of 19.9 ± 1 Kcal/mole and $\ln D_0 = -2.7 \pm .6$ (cgs units). Extrapolation of these results to ocean floor temperatures (0°C) gives a diffusivity of $1.0 \pm .6 \times 10^{-17}$ cm^2/sec, indicating that diffusion is an insignificant mechanism for helium loss from fresh basaltic glasses.

The diffusion and partitioning studies suggest that these processes will not alter the helium isotopic ratios in basaltic melts. Therefore, the isotopic composition of the oceanic mantle can be inferred by extracting the helium from basaltic glasses and phenocrysts.

A survey of the helium isotopic ratios in MORB glasses from all over the mid-ocean ridge system shows that there is considerable variation; the $^3He/^4He$ ratios range from 6.5 to 14.2 x atmospheric. The results from a number of oceanic island basalts show even more variability, with the $^3He/^4He$ ratios ranging from 5.0 x atmospheric (for alkali islands such as Gough and Tristan da Cunha) to 31.9 x atmospheric (for Loihi Seamount). The regional variability, and the correlations with $^{87}Sr/^{86}Sr$ can best be explained by the presence of three distinct reservoirs in the mantle which mix with one another. The three mantle

source regions are believed to be 1) the depleted source for normal MORB (with $^3He/^4He$ ~8.4 x atmospheric), presumed to be in the upper mantle; 2) an undepleted mantle reservoir with $^3He/^4He$ > 8.4 x atmospheric; and 3) a recycled oceanic crust reservoir with $^3He/^4He$ < 8.4 x atmospheric. A model for mantle structure that is consistent with the observations is proposed and discussed in light of the geophysical data.

^3He concentrations for the different mantle reservoirs are inferred from the measurements, and suggest that the present-day ^3He flux, and the ^3He in MORB glasses, is ultimately derived from the lower mantle. Consideration of the ^3He flux, available $^3He/^{36}Ar$ measurements, and the atmospheric ^{36}Ar inventory, shows that present-day degassing rates are insufficient to generate the atmospheric argon. It is suggested that an episode of more rapid mantle outgassing occurred in the past.

Thesis Supervisor: William J. Jenkins
Title: Associate Scientist

CHAPTER 1

INTRODUCTION

The origin of the atmosphere is a fundamental problem in earth science. Although it is generally agreed that the atmosphere formed by degassing of the earth's interior, the time dependence and physical nature of the degassing processes are controversial. The approach taken in this thesis is to use observable present-day degassing to constrain this problem. As the most voluminous volcanic rock on earth, oceanic basalts represent a major mechanism for degassing. In addition to carrying gases to the surface, the basalts carry information regarding the nature of their mantle source regions. Recent studies have shown that the mantle is heterogeneous, but models to explain the origin of the heterogeneities are diverse.

Helium is ideally suited to studying both mantle heterogeneity and degassing, since it has a primordial isotope, ^3He, and a radiogenic isotope ^4He, which is produced by decay of uranium and thorium. Thus the $^3He/^4He$ ratio is a measure of the relative proportion of primordial and radiogenic helium. In addition, helium escapes from the atmosphere, resulting in low atmospheric abundances, so that helium is the only noble gas for which a mantle flux can be measured. The goal of this thesis is to use the unique properties of helium to trace past and present mantle degassing processes.

A. Helium Isotope Geochemistry and Atmospheric Inventory

Although ^4He was isolated by Ramsay in 1895 (from the radioactive mineral cleveite; Ramsay, 1895), ^3He was not discovered until much

later, due to its low atmospheric abundance. In 1939, Alvarez and Cornog (1939a,b) used a cyclotron to discover ^3He in air and in well gas. They observed a difference of ~12 in the $^3He/^4He$ ratios of the two sources of helium, but could not accurately determine the absolute ratios. The presence of ^3He in the atmosphere and the isotopic variations were initially attributed to cosmic ray production (e.g. Hill, 1941). Using a gas-source mass spectrometer, Aldrich and Nier (1946) more accurately determined the atmospheric $^3He/^4He$ to be $1.2 \pm .3 \times 10^{-6}$, and confirmed that gas well helium typically has ratios lower by a factor of 10. The presently accepted value for atmospheric $^3He/^4He$ is 1.38×10^{-6} (Mamyrin et al., 1970; Clarke et al., 1976). In a subsequent study, Aldrich and Nier (1948) performed analyses on a number of mineral specimens, including beryl, uraninite, and spodumene. The Li-rich mineral spodumene had the highest $^3He/^4He$ ratio ($\sim 10^{-5}$), while the other minerals had ratios closer to well gas ($\sim 10^{-7}$). Morrison and Pine (1955) showed that the $^3He/^4He$ in the minerals could be explained by the production ratios of the two isotopes. ^3He is produced by the reaction:

$$^6Li(n,\alpha)^3H \xrightarrow[\beta]{} {}^3He$$

where the neutrons are provided by (α,n) reactions. Radiogenic ^4He is produced by decay of U and Th:

$$^{238}U \rightarrow {}^{206}Pb + 8\,{}^4He$$

$$^{235}U \rightarrow {}^{207}Pb + 7\,{}^4He$$

$$^{232}Th \rightarrow {}^{207}Pb + 6\,{}^4He$$

For a rock of granitic composition, Morrison and Pine (1955) calculated a $^3He/^4He$ production ratio of $\sim 10^{-7}$, in reasonable agreement with the well gas measurements. While recognizing that helium escaped from the atmosphere, they suggested that the atmosphere had a $^3He/^4He$ ratio higher than the production ratio due to cosmic ray production.

Consideration of the mechanisms by which helium escapes from the exosphere led to attempts at constructing mass-balance inventories for the atmosphere. Since the residence times of ^3He and ^4He are on the order of 10^6 years, it should be possible to balance the production and loss mechanisms, if the atmosphere is viewed as a steady state system. Each of the isotopes presents a different problem. For ^4He, the thermal loss rate is much lower than the crustal input rate, which led to the suggestion of nonthermal loss mechanisms (Nicolet, 1957; Kockarts and Nicolet, 1962; MacDonald, 1963). A number of mechanisms have been suggested, including loss of helium ions near the magnetic poles (Axford, 1968), and episodic loss during geomagnetic reversals (Sheldon and Kern, 1972). The escape of photoionized helium has now been experimentally verified (Raitt et al., 1978) and seems the most feasible loss mechanism.

The ^3He budget has been considered in the most detail by Johnson and Axford (1969). Using measured exospheric temperatures during one solar cycle (from 1947 to 1968), they calculated a mean ^3He thermal escape flux of 6 atoms cm^{-2} sec^{-1}, which is significantly greater than the estimated nonthermal escape flux of 1 atom cm^{-2} sec^{-1} for that isotope. Since the crustal and cosmogenic ^3He production rates (Morrison and Pine, 1955; Craig and Lal, 1961) are too low to balance

this total escape flux, Johnson and Axford (1969) showed that an additional ^3He source must be found; they favored auroral precipitation of solar wind ^3He at the earth's poles.

However, a previously unknown terrestrial ^3He source was indicated by the discovery of high $^3He/^4He$ ratios (relative to atmospheric) in Pacific deep water (Clarke et al., 1969) and in hot springs (Mamyrin et al., 1969). Clarke et al. (1969) suggested that the oceanic excess of ^3He was due to a primordial component leaking out of the ocean floor, and that this could balance the ^3He budget. Alternative interpretations included: in situ decay of cosmogenic tritium (Fairhall, 1969); spallation generated ^3He (Takagi, 1969); and helium leaking out of sedimentary cosmic dust on the sea floor (Krylov et al., 1973). Subsequent oceanographic studies have shown that excess ^3He is a general feature that is best explained by injection at mid-ocean ridges (Craig and Clarke, 1970; Craig et al., 1975; Jenkins et al., 1976; Lupton et al., 1980). Further proof has come from excess ^3He observed in oceanic basalt glasses (Krylov et al., 1974; Lupton and Craig, 1975) and in ocean floor hot springs (Lupton et al., 1976; Lupton et al., 1977; Jenkins et al., 1978)

Craig and Clarke (1970) used upwelling rates and the excess ^3He in the deep water to calculate an oceanic flux of 6 atoms cm^{-2} sec^{-1}. Using the ^3He/heat ratio from sea-floor hot springs and the oceanic heat flow deficit (Williams and von Herzen, 1974), Jenkins et al. (1978) showed that this flux is readily achieved by hydrothermal activity. Therefore, the oceanic ^3He flux approximately balances the exospheric escape rate. However, it should be noted that these rates

are probably uncertain to about a factor of two, and that the apparent balance does not preclude new refinements in the inventory.

B. Helium in Mantle Derived Rocks

Given the compelling evidence that the oceanic ^3He is derived from mantle sources, the oceanic basalts provide us with samples that can yield information about the mantle. Prior to the discovery of excess ^3He in oceanic basalts (Krylov et al., 1974; Lupton and Craig, 1975), a number of studies indicated that these rocks contained non-atmospheric gases. The first evidence came from attempts to use K-Ar dating on young basalts, which indicated the presence of excess ^{40}Ar (Dalrymple and Moore, 1968; Funkhouser et al., 1968). Fisher (1971, 1973) suggested that the glassy rims of oceanic basalts were "quenched" rapidly enough (on the ocean floor) to trap the magmatic gases derived from the mantle. In this now widely accepted scenario, the holocrystalline interiors of basalts cool more slowly, lose most of the magmatic gas, and interact more extensively with seawater (see also Dymond and Hogan, 1978). Dymond and Hogan (1973) measured the noble gases in several glasses, and interpreted the abundance patterns as being similar to "solar" gases found in meteorites (Pepin and Signer, 1967). This view was challenged by Fisher (1975), who showed that the relative abundance patterns could also be "planetary," and by Ozima and Alexander (1976), who suggested that magmatic fractionation processes may alter the abundance patterns. A potentially important mechanism for altering the noble gas abundances, which has largely been ignored, is the formation of vesicles in oceanic basalt glasses. As discussed by Moore et al. (1977), these vesicles are present in most glasses

(even those that are erupted at great depth on the ocean floor) and contain primarily CO_2. The removal of a gas phase will clearly alter the abundance pattern, since the noble gas abundances remaining in the glass (after removal) will be determined by their relative solubility, as well as the initial "mantle" concentrations.

The helium concentrations in these basaltic glasses are of importance to the helium budget described above. For example, Lupton and Craig (1975) observed helium concentrations of roughly 10^{-6}ccSTP/gram. Using a mean crustal production rate of 2 km^2/yr, they noted that if this were representative of the oceanic crust, degassing of a layer 50 km thick would be required to produce the observed oceanic ^3He flux. Since the oceanic crust reaches a maximum thickness of only 7 km, this concentration must be somewhat low, or an additional source of helium must be found. Fisher (1975) reported helium concentrations a factor of ten higher in glasses from a different part of the ocean ridge. However, it is not clear whether this difference is due to regional variability, or an analytical artifact. Lupton and Craig (1975) and Craig and Lupton (1976) crushed their samples before analysis; if a large part of the helium resides within the vesicles, their values may be low due to gas loss prior to analysis.

There is also considerable regional variation in the $^3He/^4He$ ratio. Krylov et al. (1974) measured a $^3He/^4He$ ratio of 8 x atmospheric (R_{atm}) in a MORB glass from the Indian Ocean. Lupton and Craig (1975) and Craig and Lupton (1976) reported $^3He/^4He$ ratios of 8.9 to 10.9 x R_{atm} in seven MORB glass samples from the

Atlantic and Pacific Oceans. Although this total variation is roughly 25 percent (and the quoted uncertainties are ~5 percent), Lupton and Craig (1976, 1981) have suggested that MORB glasses have uniform $^3He/^4He$ ratios. $^3He/^4He$ ratios higher than these MORB values have been observed in thermal spring and basalt samples from Iceland (Polak et al., 1976; Poreda et al., 1980), Hawaii (Craig and Lupton, 1976; Jenkins et al., 1978; Kaneoka and Takaoka, 1978, 1980), and Yellowstone National Park (Craig et al., 1978). Excess ^3He has also been reported for diamonds (Takaoka and Kaneoka, 1978), kaersutite from Kakanui, New Zealand (Saito et al., 1978), and Josephenite (Bochsler et al., 1976; Downing et al., 1977). However, several studies have shown that terrestrial samples can be contaminated in the laboratory by residual gases from previously analyzed meteorite samples (see Craig et al, 1979; Bernatowicz et al., 1979; Smith and Reynolds, 1981). It therefore seems likely that high values reported for Josephenite and Kakanui kaersutite reflect meteoritic contamination. Nevertheless, the available data show that there is considerable local and global variation in the $^3He/^4He$ ratios of volcanic gases. Recent reviews of the field have been given Tolstikhin (1978) and Craig and Lupton (1981).

C. Objectives

Relating helium isotopic variations to models of the mantle is of fundamental importance. In particular, Sr, Nd, and Pb isotopic studies of oceanic volcanic rocks have shown that the mantle has been heterogeneous for long periods of time (e.g., Allegre et al., 1979; Wasserburg and DePaulo, 1979; O'Nions et al., 1980; Sun, 1980; Hart and

Brooks, 1981). The models to explain these variations are clearly important to deciphering the terrestrial degassing history (and vice versa), since any mantle fractionation process that can alter the Rb/Sr, Sm/Nd, and U/Pb ratios will also affect the gases. One model to explain these variations is a layered mantle, with the upper mantle having been fractionated (or depleted) to produce the continents (Jacobsen and Wasserburg, 1979; O'Nions et al., 1979). The lower mantle would then be relatively undepleted, and would supply the source of oceanic islands or mantle plume volcanics (Morgan, 1971; Schilling, 1973; Sun and Hanson, 1975; Wasserburg and DePaulo, 1979). The striking anti-correlation between $^{87}Sr/^{86}Sr$ and $^{143}Nd/^{144}Nd$ is consistent with this two layer model, and allows the prediction of undepleted, or "bulk earth" isotopic composition (DePaulo and Wasserburg, 1976; Richard et al., 1976, O'Nions et al., 1977).

However, Anderson (1982a) has shown that the Nd-Sr correlation could also be produced by mixing of ancient depleted and enriched reservoirs. In this case, the samples that have isotopic compositions similar to bulk earth may not be derived from an unfractionated mantle source. An alternate model, that would be consistent with this, would explain the isotopic variation by recycling of oceanic crust into the mantle (Armstrong, 1968; Hofmann and White, 1980, 1982). Thus, the isotopic variations of Sr, Nd, and Pb show that mantle is heterogeneous, but the origins of the heterogeneities are not uniquely determined by the data.

Several important questions are brought to mind by relating the helium data to these mantle models. First, if the upper mantle is

truly depleted, having been through a fractionation process that produced the continents, then why do MORB glasses have $^3He/^4He$ ratios higher than atmospheric helium. Second, the hot spring helium, from Hawaii and Iceland, has even higher $^3He/^4He$ ratios than MORB, which is, at first glance, consistent with the mantle plume hypothesis. However, both Hawaii and Iceland have Sr and Nd isotopic compositions that are close to those of MORB, implying long-term depletion (O'Nions et al., 1977). Finally, if recycling of oceanic crust is an important process (Hofmann and White, 1980), then one might expect $^3He/^4He$ ratios lower than atmospheric.

Helium differs from the other isotopes in one very important respect: its volatility. Like the other isotopes, the rate of change of the isotopic ratio is controlled by the stable daughter/radioactive parent ratio, which is in this case $^3He/(Th + U)$. Due to the volatility of helium, any degassing event will lower this ratio in the residual mantle, and result, with time, in a decrease in $^3He/^4He$ ratio. Therefore, helium isotopes should provide an important means of distinguishing undepleted mantle reservoirs from those that are recyled (Hofmann and White, 1982) or ancient enriched reservoirs.

The objectives of this research are to 1) establish the possible causes of helium concentration and isotopic variations in oceanic basalts; 2) use the isotopic systematics to constrain the nature and origin of mantle heterogeneity; and 3) relate mantle evolution to degassing history.

Chapter 3 addresses the first of these objectives, and discusses the effects that diffusion, melt-vesicle partitioning, and melt-crystal

partitioning have on helium concentrations and isotopic ratios. It is found that vesiculation can strongly affect the observed concentration, but has little effect on the isotopic ratio. Thus the helium concentrations reported in the literature are at best lower limits to the original magmatic concentration. Diffusion experiments on basaltic glass show that at ocean floor temperatures, diffusion is an insignificant process in altering helium concentrations or isotopic ratios. Glass-plagioclase partitioning for one sample suggests that helium behaves as an incompatible element, which is supported by further analyses reported in chapter 5. To summarize, shallow and post-eruptive processes do not affect the $^{3}He/^{4}He$ ratios, which can therefore be interpreted as reflecting mantle source regions.

In chapters 4 and 5, helium isotopic analyses are reported for a wide variety of ocean floor and ocean island rocks. The helium and strontium isotopic systematics of these samples can best be explained by mixing between three distinct mantle sources, which are referred to here as depleted, undepleted, and recycled. The depleted source is characterized by $^{3}He/^{4}He$ of ~8.4 x atmospheric and $^{87}Sr/^{86}Sr$ of ~.7023-.7028. The undepleted source has higher $^{3}He/^{4}He$ and $^{87}Sr/^{86}Sr$ ratios, while the recycled source has lower $^{3}He/^{4}He$ and higher $^{87}Sr/^{86}Sr$. While the end-members for these two distinct mantle reservoirs cannot be identified, the recycled source is best explained by subducted oceanic crust that is remixed with the mantle. Undepleted mantle is presumed to be that reservoir which has remained least degassed over the age of the earth.

A model to explain the existence of these three mantle reservoirs

is proposed in chapter 6. The model consists of a mantle with two layers, the upper depleted layer (above 700 km) underlain by undepleted layer. The recycled oceanic crust is restricted to the upper mantle by the 700 km barrier, and either accumulates at this level, or mixes back into the upper layer. This accounts for the diverse isotopic chemistry of oceanic islands, in addition to the relative abundance of basalts bearing the isotopic signature of each mantle type.

Using mantle ^{3}He concentrations inferred from the measurements, it is concluded that the present-day oceanic ^{3}He is ultimately derived from the lower mantle. Consideration of the present-day ^{3}He degassing rate, available $^{3}He/^{36}Ar$ measurements, and the atmospheric ^{36}Ar inventory, shows that a catastrophic degassing event or episode may have occurred in the past. This conclusion is consistent with the proposed mantle model because the lower mantle contains most of the ^{3}He and is kept from degassing by the insulating effect of the upper mantle.

In summary, the helium isotopes are shown to be an extremely useful tracer of mantle processes. Parts of chapters 3, 4, and 5 have been published in Kurz and Jenkins (1981), Kurz, Jenkins, Schilling, and Hart (1982a) and Kurz, Jenkins, and Hart (1982a), respectively.

CHAPTER 2

EXPERIMENTAL METHODS

A. Introduction

The experimental methods described in this chapter changed slightly during the course of the thesis work. The first helium analyses (chapters 3 and 4) were performed using the extraction line discussed in section 3 and the first WHOI branch tube mass spectrometer (referred to as MS-1). When the construction of the second branch tube mass spectrometer (referred to as MS-2) was completed, the extraction line was rebuilt as described in section 4, and connected directly to the mass spectrometer.

B. Sample Preparation

The glass fragments or phenocrysts were hand-picked under a binocular microscope to avoid contaminants, and sonically cleaned in acetone or methanol. In some cases, the samples were sonically cleaned in distilled water to facilitate picking. All of the ocean island basalts and xenoliths were coarsely crushed in a steel anvil mill and sieved (using stainless steel ASTM sieves). If the phenocryst sizes were greater than 1 mm, the 10-18 mesh (1-2 mm) size fraction was then hand-picked. If the phenocryst grain sizes were smaller than 1 mm, the 18-35 mesh fraction (.5-1 mm) was run through the Franz isodynamic separator, and then hand-picked. In general, the largest grain size was used, as long as no contaminants were introduced. If the crystal grains of a given size fraction were not clear and free of cracks or grain boundaries, a smaller size was used.

The basaltic glasses from the ocean floor were chosen on the basis of freshness, and hand-picking was only necessary to eliminate oxide coatings, spherulitic grains, and phenocrysts. Due to the ubiquitous presence of vesicles in these glasses (see chapter 3), chunks larger than 2 mm were chosen for analysis.

A portion of each sample was selected for petrographic thin section to allow examination in transmitted light. Doubly polished thin sections of the ocean island basalts and xenoliths were prepared using standard techniques. The glass-vesicle partitioning study described in chapter 3 required thin sections of the same size glass chips that were analyzed for helium. The thin sections of these glass chips were prepared by mounting the grains (in epoxy) on a slide, grinding to flatness, and polishing, followed by remounting on another slide and repeating the grinding and polishing steps.

Major element analyses of some of the samples were performed using the MIT MAC 15K e.v. electron microprobe. The instrument was calibrated using appropriate standards (for basaltic glasses: Kakanui hornblende, apatite, orthoclase, Mn-ilmenite, and basaltic glass VG-2), and corrected for instrumental drift by periodically analyzing a replicate standard (VG-2). At least two grains of each sample were probed, including a total of at least seven different spot checks.

C. Extraction Methods

All of the extractions reported in this thesis were performed using metal, high-vacuum apparati; the only glass section of the extraction line consisted of a high-vacuum glass stopcock, and parts of the toepler pump (described below). At the outset, the emphasis was on

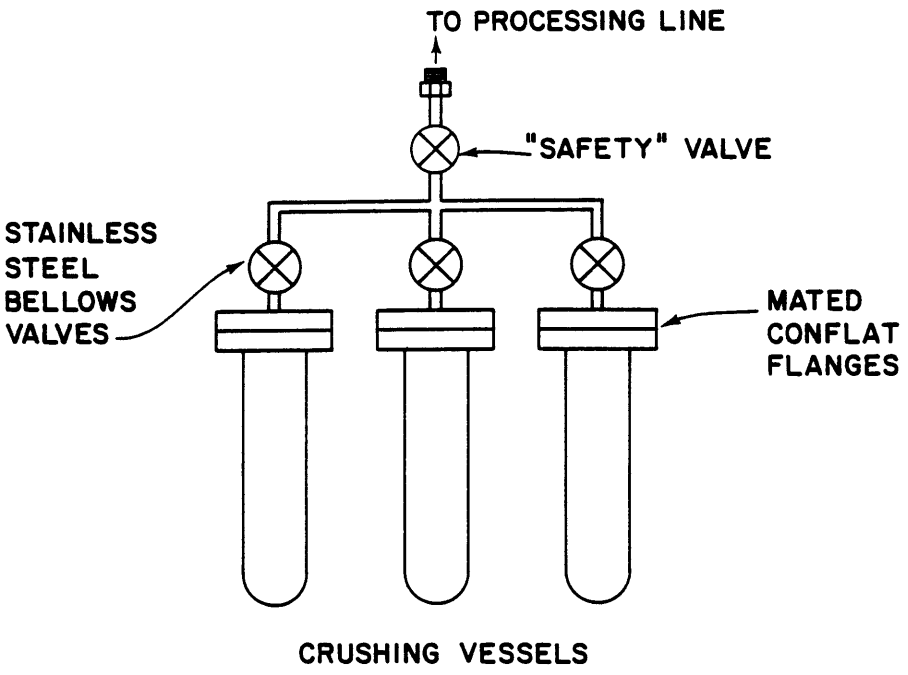
maintaining low helium blanks while extracting (and saving) the other noble gases at the same time. Since the first processing line was not connected directly to the mass spectrometer, the helium samples were saved in 1720 (Corning aluminum-silicate) or Pb glass breakseal tubes. The chemical composition of these glass types greatly reduces the rate of helium diffusion, making them suitable for storage of helium samples (see chapter 3).

Since part of the goal of this thesis was to further the understanding of noble gas distribution in igneous rocks, two extraction methods were used. Gases residing within vesicles and fluid inclusions were extracted using a stainless steel crushing vessel (the crusher). The gases dissolved within the rocks' silicate structure were extracted using a resistively heated, ultra-high vacuum furnace.

1. The crusher

The crusher was designed to allow crushing of rocks in vacuo; the essential details are shown in figure 2.1. The interior end walls of the cylindrical vessel were rounded, so that when a stainless steel ball bearing was placed inside with a rock sample and agitated, the rock chips were completely crushed. The "plug insert" confines the rock powder to the vessel, but allows transfer of gases through two stainless steel screens. The vessel was connected to the vacuum processing line via two mated conflat flanges, two valves, and a Nupro "VCR" nickel gasket coupling. The system was readily detachable from the line using the VCR coupling. The first crusher differed from the one shown in figure 2.1 only in that a single vessel (rather than three) was used, and also that the insert was threaded.

ROCK CRUSHING MANIFOLD



CROSS SECTION OF CRUSHING VESSEL

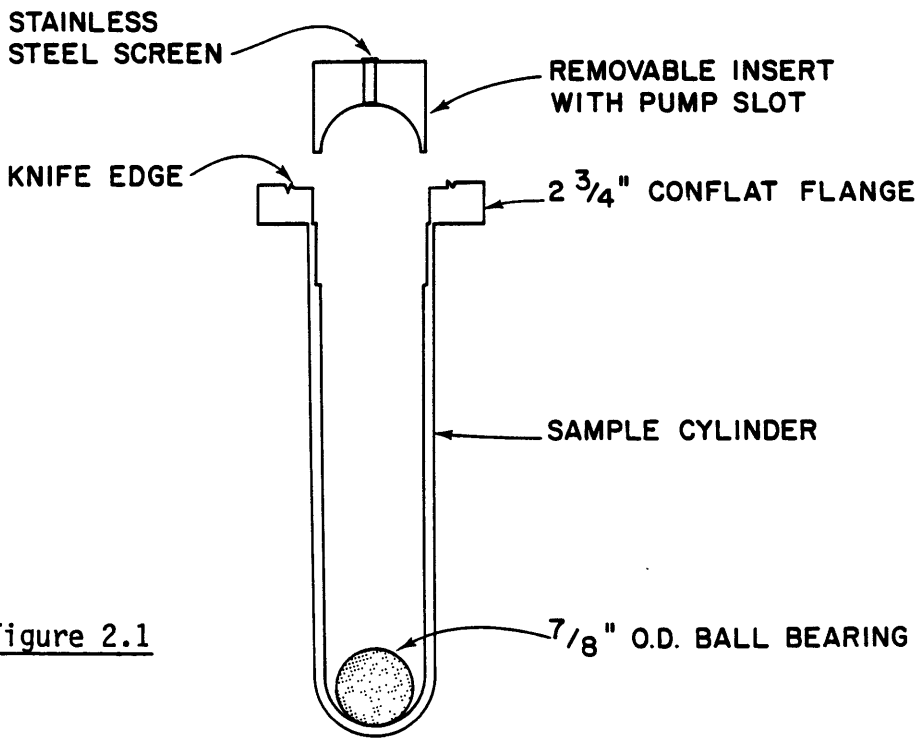


Figure 2.1

The first step of the procedure involved placing the rock sample in the vessel with a stainless steel ball bearing, mating the conflat flanges with a copper gasket, and coupling the VCR fitting to the processing line. When suitable vacuum was indicated by the ionization gauge, both valves were closed, the crusher was detached from the line and shaken, using a shaker table, for a period of 30 minutes. After reattachment and pump-out, the released gases were processed in the manner described below (section 3).

Initially, the vessels were cleaned between samples with 50 percent HF, which dissolved the silicates; this process was found to be cumbersome and unnecessary; stainless steel brushes attached to the end of a hand drill were more effective. After removing the previous sample, cleaning was completed with stainless stell brushes, washing with soap and water, and rinsing with distilled water, acetone, and methanol. A clean, new ball bearing was used for each sample. Numerous procedural blanks confirmed that cleaning was effective, that there was no "memory" of previous samples, and that the blank was reproducible.

The "efficiency" of the technique was tested by sieving several of the samples after crushing, to establish the grain size. For the MORB glasses discussed in chapter 3, 99 percent of the powder was smaller than 120μ and 70 percent smaller than 63μ. An additional test was performed by re-crushing several of the MORB glasses; in each case an insignificant amount of helium was released.

2. The furnace

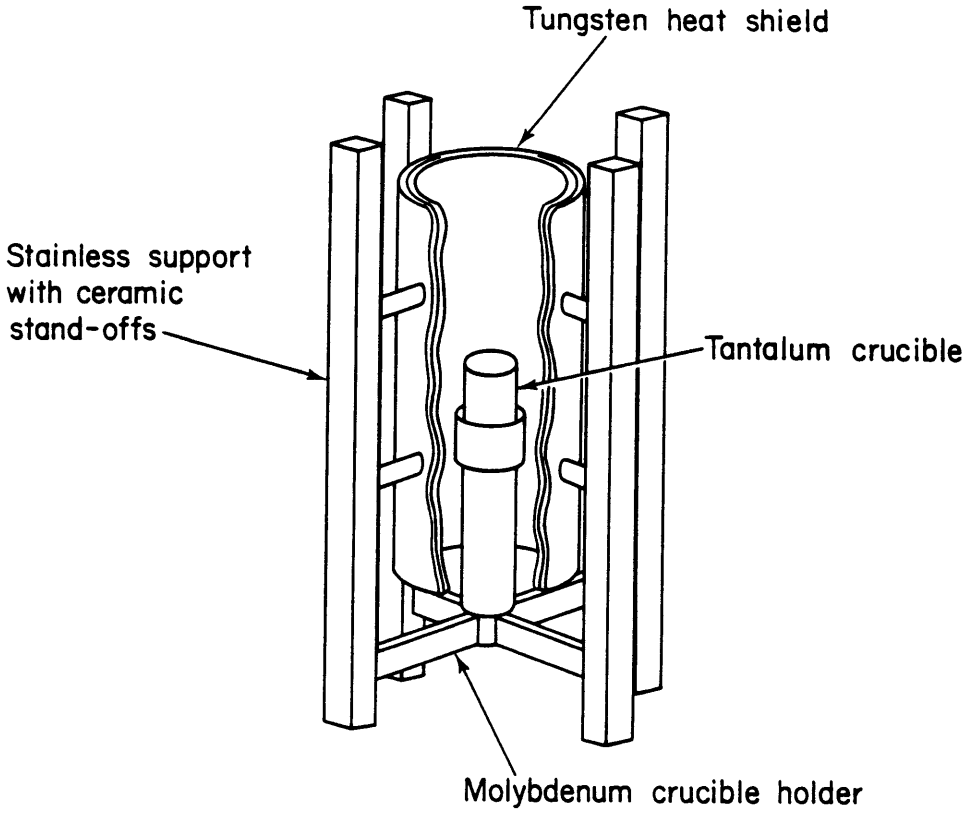
The essential details of the high-temperature furnace used are

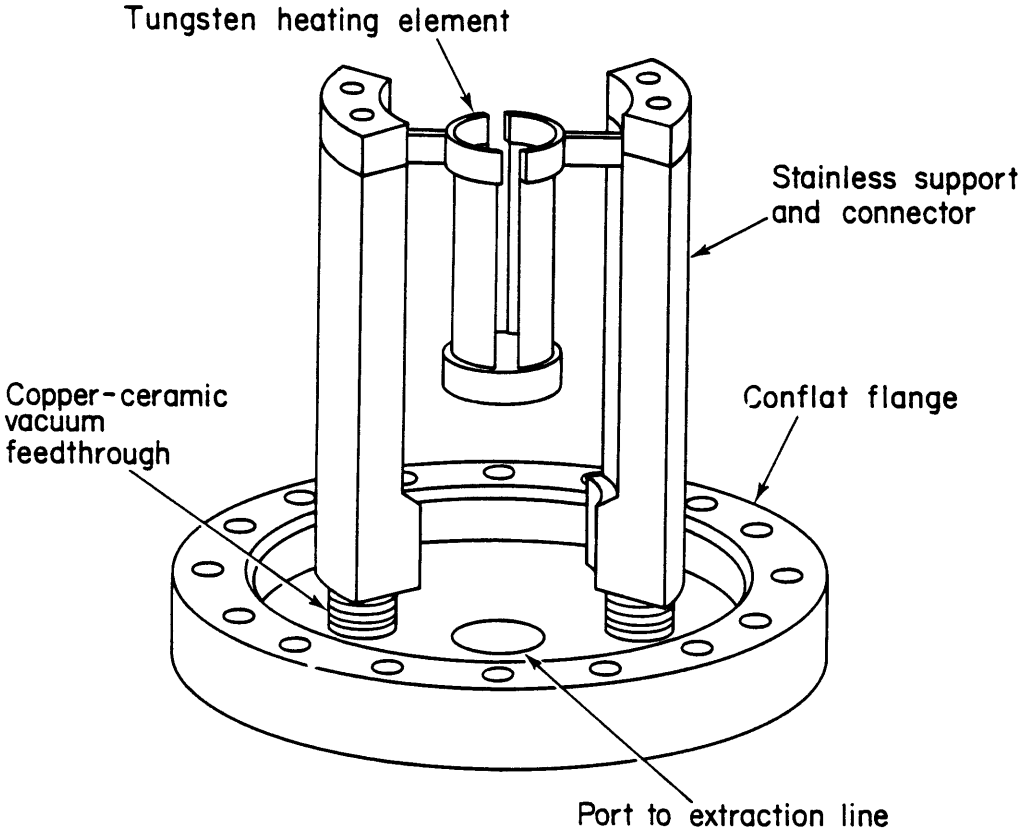
shown in figures 2.2 and 2.3. The tantalum crucible (Schwarzkopf Inc.) was resistively heated by current passing through the tungsten mesh heating element (GTE Sylvania). The current is delivered to the heating element via stainless-ceramic-copper feedthroughs (Ceramaseal) and the stainless posts shown in figure 2.2 (bottom). The layered tungsten heat shield insures that radiative losses from the hot zone are not serious. The necessary current was supplied by a 25:1 (10KVA) step-down transformer connected to the feedthrough (shown in figure 2.2) by copper bars and supplied by a 0-208V motor driven variac.

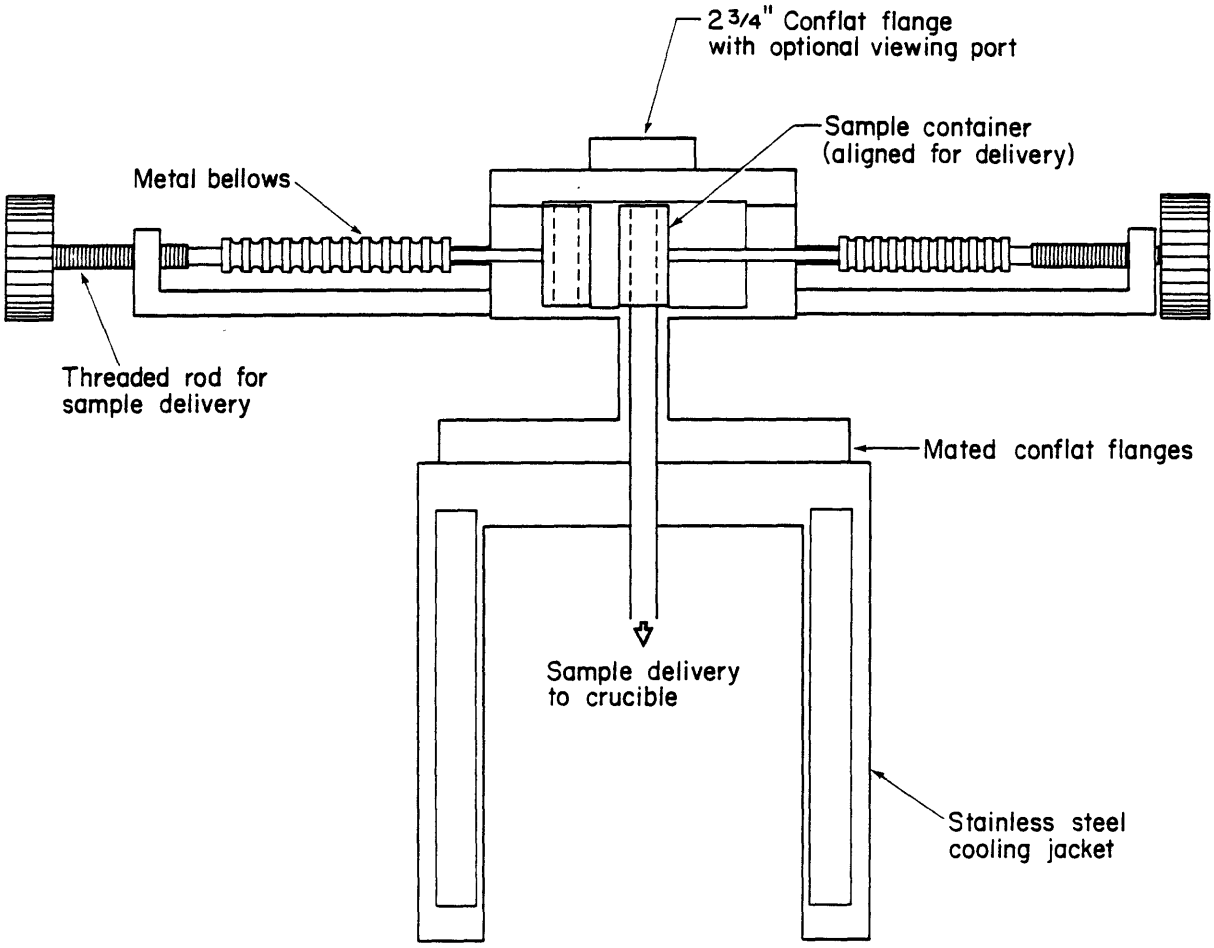
The sample loading mechanism and cooling jacket shown in figure 2.3 fit over the heater assembly shown in figure 2.2, and were connected with conflat knife-edge flanges. The bellows movement mechanism allows sample delivery without breaking vacuum for up to six samples (two sample holders are shown in figure 2.3). Rock chips are placed directly into the sample holders, and are dropped into the crucible when the sample holder aligns with the axis of the sample container. Aluminum foil boats were used to keep the powder samples in place.

Temperature calibration was accomplished by focusing an optical pyrometer on the crucible through the pyrex window. The temperature-power relationship was established with the window in place and the window was replaced by a stainless flange for sample analysis. The temperature was measured by the current and voltage across the tungsten heating element. In general, measuring the current flow was sufficient to infer a temperature, since the current-voltage-temperature relationship was stable. In only one case during the course of this study did the current-voltage-temperature

Figure 2.2: Simplified sketch of the furnace "hot zone." The crucible support and heat shield (top) attach to the conflat flange shown at the bottom. When assembled, the crucible is centered within the tungsten heating element, but the crucible and heat shield are electrically isolated from the heating element.


Tungsten heat shield
Stainless support with ceramic stand-offs
Tantalum crucible
Molybdenum crucible holder


Tungsten heating element
Stainless support and connector
Copper-ceramic vacuum feedthrough
Conflat flange
Port to extraction line



SIMPLIFIED CROSS SECTION OF FURNACE
SAMPLE DELIVERY SYSTEM

Figure 2.3: Cross section of furnace sample delivery system.

relationship change during analysis (due to a heating element-heat shield short). Recalibration was only necessary when the furnace was dismantled. Typically, 400 amps at 3.5V was necessary to raise the crucible to 1400°C. Frequent recalibration showed that in the range of 800-1500°C, the temperatures estimated in this manner were accurate to ±20°C.

3. The first processing line

Most of the mid-ocean ridge basalt samples discussed in chapters 3 and 4 were processed using the extraction line shown in figure 2.4. The gases released by crushing or melting were passed through a dry ice acetone U-tube trap (-70°C) to remove H_2O, and a charcoal trap cooled with liquid nitrogen to trap CO_2 and the heavy noble gases. Hydrogen was removed using a Ti sponge operated at room temperature. The He and Ne were collected in 1720 or Pb glass breakseal tubes using the toepler pump. After the He-Ne fraction was removed, the gases trapped on the charcoal trap were transferred to the charcoal-pyrex breakseal tube by heating the former and cooling the latter to -195°C. The heavy noble gases were then saved in the pyrex breakseal tube. After completing this step, new breakseal tubes were glass-blown onto the line, the whole system was briefly heated to ~200°C and the Ti sponge was heated to ~800°C for a minimum of 2 hours.

The timing of the various steps differed slightly for the crushing and melting extractions, which led to different helium blanks. In the case of the melting extractions, the furnace was raised to 1400°C and exposed to the Ti and charcoal traps for a period of 1-1/2 hours. During this time, the toepler section was open to the diffusion pump,

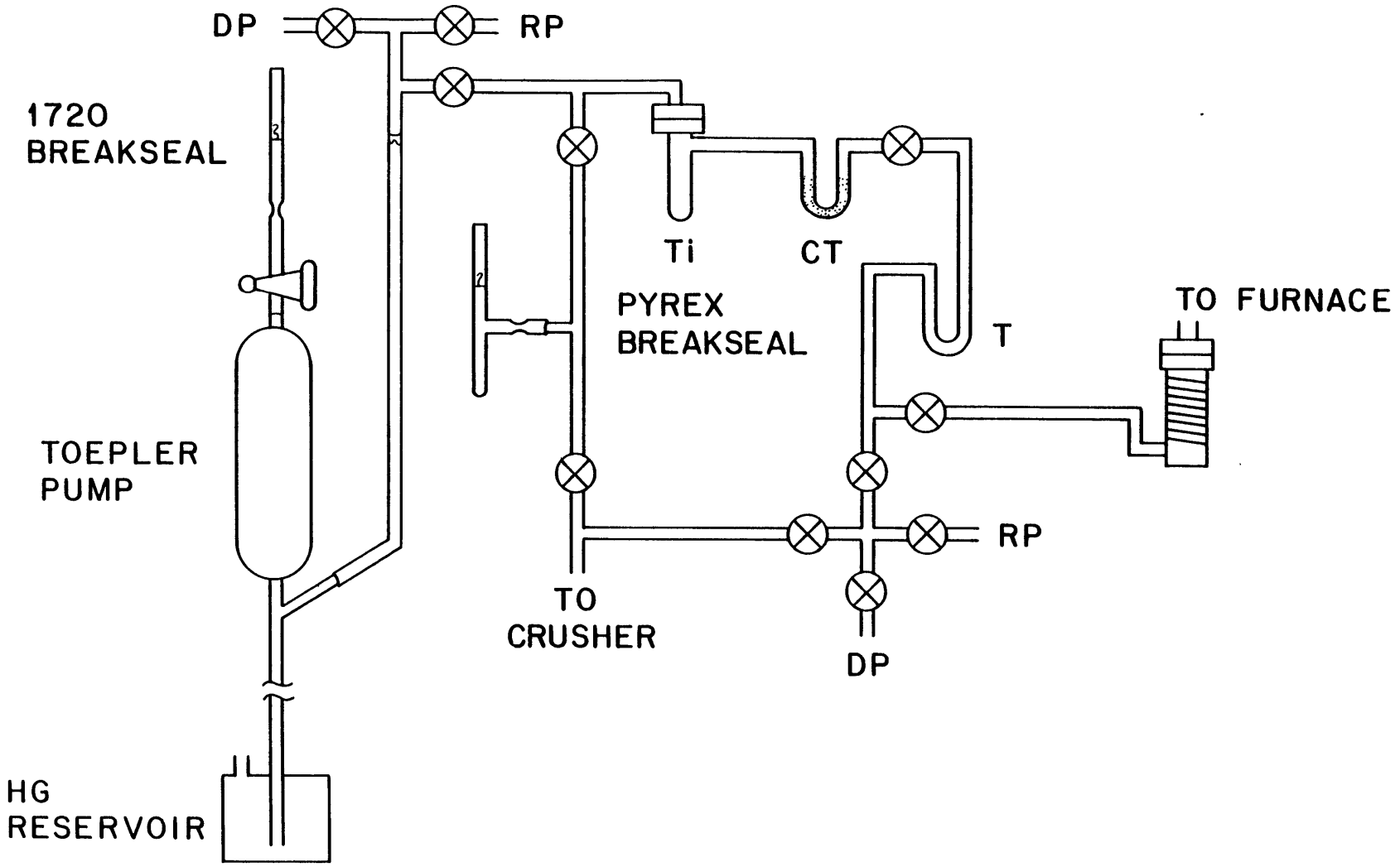


Figure 2.4: The first processing line. All stainless steel, except for the breakseals, the stopcock, and the connecting line to the toepler pump.
Key: Ti - titanium sponge trap; CT - charcoal trap; DP - diffusion pump; RP - rough pump.

the stopcock was worked to pump away any gas dissolved in the stopcock grease, and the mercury was raised and lowered several times to remove any possible contaminant trapped in the mercury. After the 1-1/2 hour period, the valve to the diffusion pump was closed, and the He-Ne split of the sample was toepler-pumped into the breakseal (total pumping time was 30 minutes). The long heating cycle was chosen to insure complete extraction of the heavy noble gases; the large concentrations of helium present in most MORB glasses allow the slightly higher blanks without sacrificing precision. When low concentration samples that required low blanks were encountered, this long procedure was abandoned.

In the crushing procedure, "the crusher" was attached to the line, pumped out, removed and agitated to crush the rock sample, and then re-attached to the processing line. During the steps that required coupling and decoupling from the line, nitrogen gas was introduced to minimize atmospheric contamination. After the final re-attachment, and after suitable vacuum was attained (determined by ionization gauge), the gas inside the crusher was exposed to the charcoal and Ti traps for 10 minutes via the same path as the gases released by melting (see figure 2.4). This was followed by toepler pumping the He-Ne fraction, and transfer of the heavy noble gases in exactly the fashion described above.

4. The second extraction line

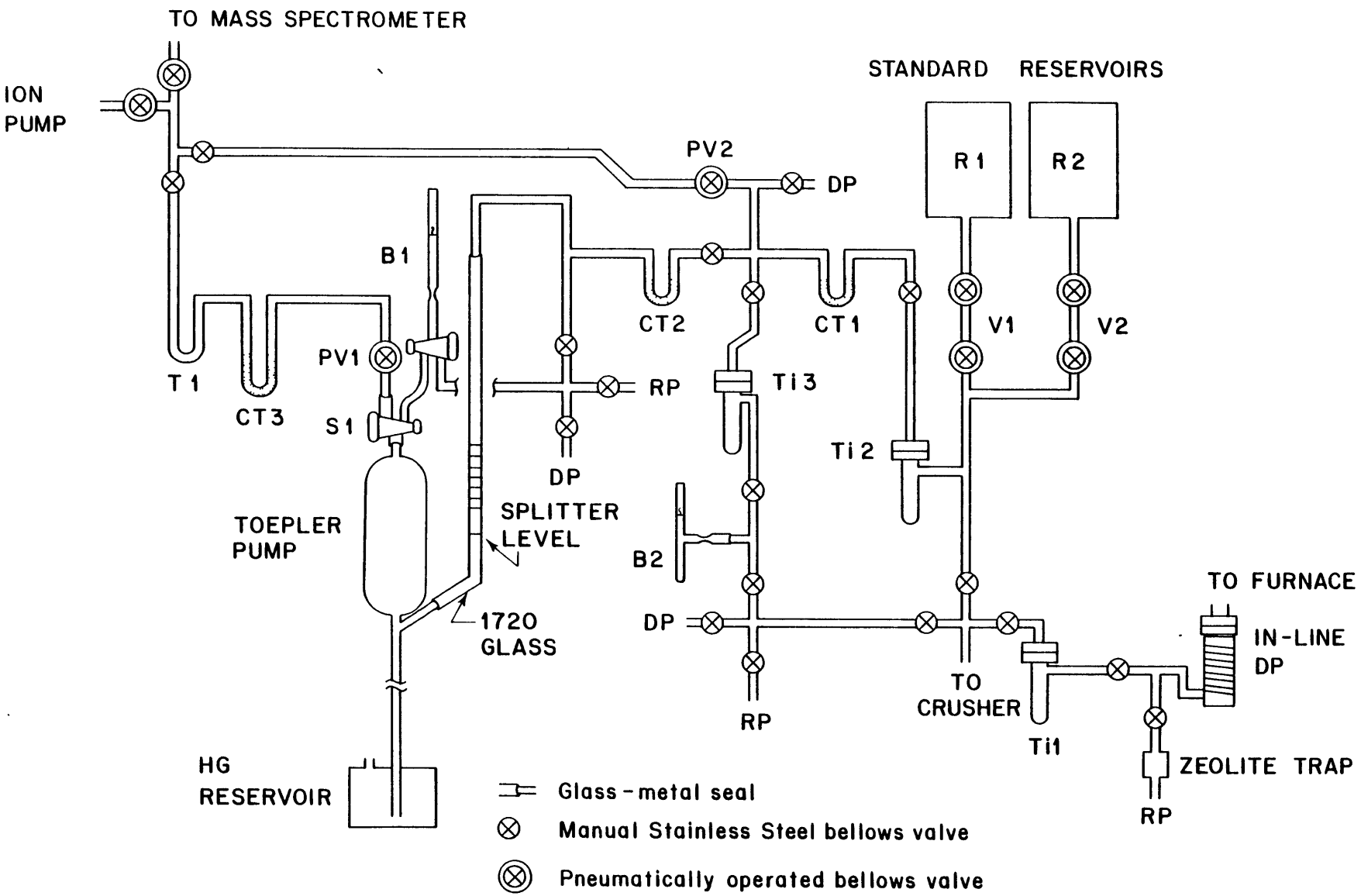
When the new multiple collection mass spectrometer (MS-2) was nearing completion, the first extraction line was modified to serve as an inlet line to the mass spectrometer. This modified second processing-inlet line is shown in figure 2.5. Several improvements

were implemented: a) The helium samples could be directly inlet into the mass spectrometer, resulting in lower blanks. b) The two three-way stopcocks gave the option of saving a sample in a breakseal tube, or of letting part of a sample into the mass spectrometer and saving the remainder in the breakseal tube.
c) Glass-blowing through the rough pump valve (RP near S1 in figure 2.5) did not expose the rest of the extraction line to atmosphere. The charcoal trap (CT2) protected the heavy noble gas section of the line from backstreaming and from mercury. d) There were two completely separate inlet paths to the mass spectrometer, one for He or Ne, and one for the heavy noble gases.

The helium extraction procedure was much the same as described in section 3, with the exception that the samples were expanded directly into the mass spectrometer via the pneumatic valve (PV1). As is discussed in the next section, the blanks are significantly lower than the earlier procedure. The additional Ti sponges (Ti1 and Ti3 in figure 2.5) give greater capacity for removing H_2, requiring less frequent recycling of the traps.

Since the helium concentrations in igneous rocks vary by four orders of magnitude (from 10^{-9} to 10^{-5} cc/g), it was often necessary to split samples before inlet, due to the pressure dependence of the measured $^3He/^4He$ ratio. In general, this was only necessary for the basaltic glass samples. Splitting was accomplished by adjusting the mercury level on the toepler pump. First, 1 percent of the sample was expanded into the mass spectrometer by lowering the mercury to the lowest "splitter level" (see figure 2.5), and closing

Figure 2.5: The second processing line. The standard reservoir system is somewhat simplified: separate ports to the pumps and to a breakseal port are not shown.
Key: B1 - 1720 glass breakseal for He-Ne fraction
B2 - pyrex breakseal for heavy noble gases
CT - charcoal trap
DP - diffusion pump (Varian HS-2)
RP - rough pump
Ti - titanium sponge trap
T1 - U tube trap to remove Hg
PV - pneumatic valve.


TO MASS SPECTROMETER
ION PUMP
STANDARD RESERVOIRS
R1
R2
PV2
DP
B1
CT2
CT1
V1
V2
T1
CT3
PV1
RP
Ti3
S1
DP
Ti2
TOEPLER PUMP
SPLITTER LEVEL
B2
TO FURNACE
IN-LINE DP
1720 GLASS
DP
TO CRUSHER
RP
Ti1
ZEOLITE TRAP
HG RESERVOIR
RP
Glass-metal seal
Manual Stainless Steel bellows valve
Pneumatically operated bellows valve

the stopcock. Only the fraction of the gas above the stopcock was inlet. The ^4He peak height of this fraction of the sample was then used to calculate the total sample size (to within 10 percent), and to determine if a reduction in size was necessary. The mercury level was then adjusted to the appropriate splitter level. The volume reduction was determined by the ratio of the volume between stopcock S1 and valve PV1, and the volume between stopcock S1 and the mercury level. The mercury levels indicated by marks on the glass tube were calibrated using air standard peak intensities. They were reproducible to better than ~1 percent above the neck of the mercury reservoir (volume reductions up to a factor of 3), and ~5 percent below the neck. This difference is due to the varying diameter of the reservoir, and the resulting uncertainty in volume that an uncertainty in the mercury level implies. After inlet, the remaining gas could be saved in breakseal B1 by raising the mercury through stopcock S2.

D. Helium Blanks

As discussed in the previous sections, the extraction procedures changed during the course of this study, resulting in changes in the helium blanks. The first procedure (described in section C.4), which involved saving the helium in breakseal tubes and splitting to allow later neon analysis, had distinctly higher blanks. For a 120-minute furnace heating cycle, the blank was typically $1.0 \pm .2 \times 10^{-8}$ cc ^4He with atmospheric $^3He/^4He$ ratio. The different contributions to the blank are listed in table 2.1. The total blank of $\sim 1 \times 10^{-8}$ was generally less than 1 percent of the sample size for mid-ocean ridge basalt glasses, and is applicable to most of the samples

discussed in chapters 3 and 4. The crusher blank was $5 \pm 2 \times 10^{-9}$, and consisted primarily of the processing line, toepler pump components in table 2.1. The crushing vessel contributed less than 1×10^{-9} cc ^4He to the blank.

When low concentration samples were encountered and the extraction line was attached directly to MS-2, several steps were taken to lower the blank:

i. The helium samples were inlet directly into the mass spectrometer.

ii. The original, in-line diffusion pump was replaced by an all-metal diffusion pump with a conflat flange seal (copper gasket between two knife edges).

iii. The overall heating time for the furnace extractions was reduced to 45 minutes (20 minutes to reach 1400°C, 25 minutes at temperature).

iv. The pyrex "splitter" section of the toepler pump was replaced with 1720 glass.

These changes significantly lowered the blank. For crushing or melting, the blank was $1\text{-}2 \times 10^{-9}$ cc ^4He, most of which was contributed by the toepler section of the line. The extraction efficiency of these procedures was tested by performing procedural blanks immediately after a sample.

E. Mass Spectrometry

The 90° sector, 25.4 cm radius-of-curvature mass spectrometers (MS-1 and MS-2) used for this study are similar in design to the one described by Jenkins (1974) and Clarke et al. (1976). The branch tube

Table 2.1: Components of the helium blank for melting rocks using the first extraction procedure

	cc STP ^4He
Furnace (120 minutes)	5×10^{-9}
Processing line	$1\text{-}2 \times 10^{-9}$
Toeppler pump + stopcock	$1\text{-}2 \times 10^{-9}$
Mass spectrometer inlet	$.1\text{-}2 \times 10^{-9}$
Total	$.8\text{-}1.1 \times 10^{-8}$
Splitting (optional)	$2\text{-}3 \times 10^{-9}$

allows simultaneous measurement of ^3He and ^4He: ^3He is collected on a Johnston 20-stage focused mesh electron multiplier (model MM-2), while ^4He is collected on a faraday cup. The primary difference between MS-1 and MS-2 flight tubes is that MS-1 has a single moveable faraday cup, while MS-2 has three faraday cups (see figure 2.6), all of which can be moved with respect to one another without breaking vacuum. When helium analyses are performed using MS-2, ^4He is collected on the center faraday cup. The resolution (approximately 1:600) is adequate to completely resolve the $^3He^+$-HD^+ peak from the ^3He peak. Figure 2.7 shows a mass scan in the vicinity of ^3He and ^4He, for an air helium standard aliquot.

The mass spectrometers were operated in the "static mode" (i.e., with the valve to the ion pump closed). Typical sensitivities for helium and argon were 1.4×10^{-4} amps/torr and 1.0×10^{-3} amps/torr, respectively. Typical source conditions were: filament current, 6 amps; emission current, 5 mA; and trap current 400 μA.

1. Helium procedure

The He-Ne fraction was toepler-pumped into the reproducible volume between the stopcock and pneumatic valve (S1 and P1, respectively, in figure 2.5). Opening P1 allowed the gas to expand in the mass spectrometer through the traps (CT3 and T1). The U-tube trap at liquid nitrogen temperature (T1) kept mercury vapor from entering the mass spectrometer, and the charcoal trap (CT3, also at liquid nitrogen temperature) allowed partial separation of He from Ne by slowing Ne relative to He. The trap characteristics and inlet timing were carefully chosen to allow inlet of 70 percent of the He and 1 percent

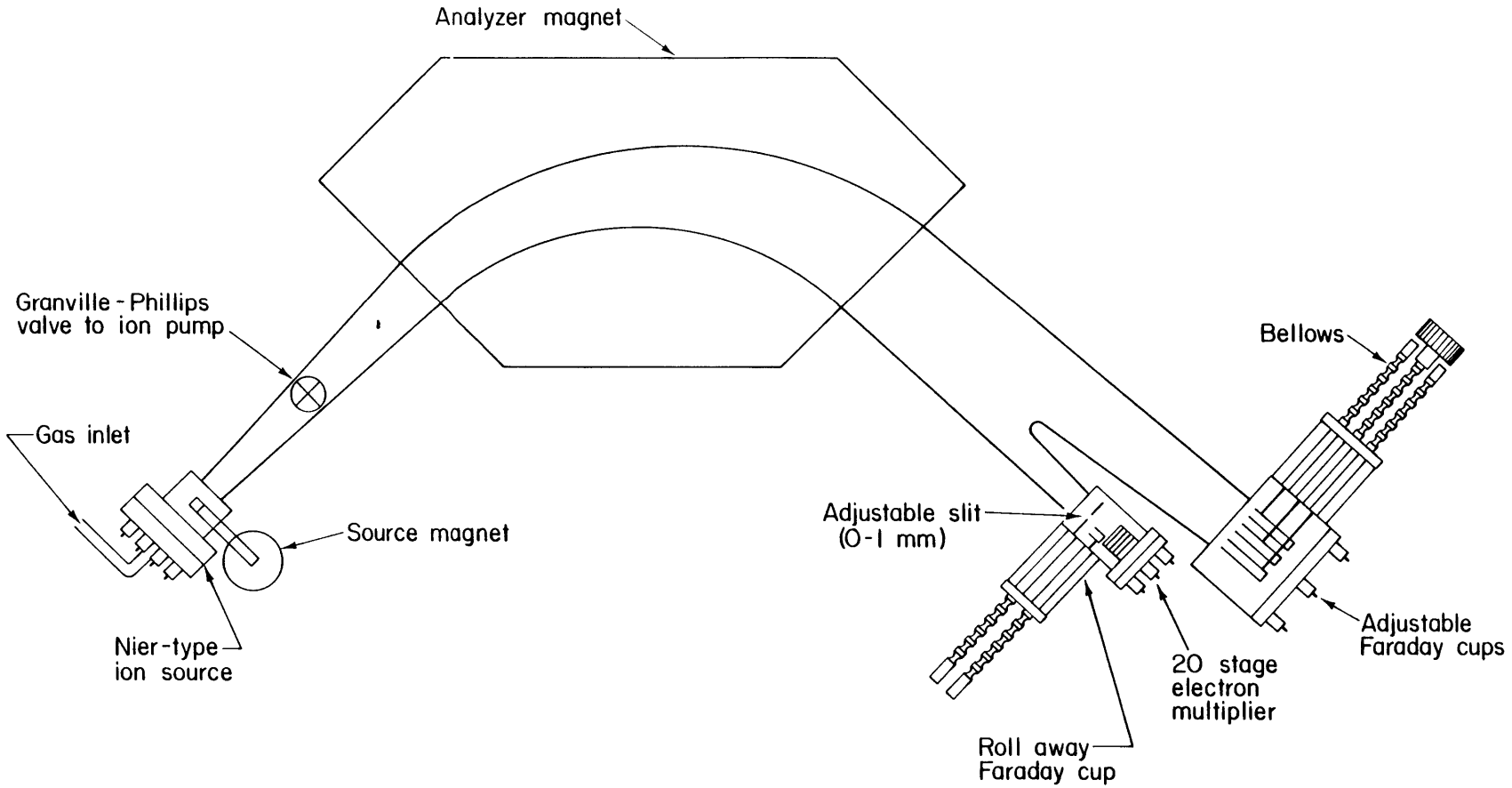


Figure 2.6: W.H.O.I branch tube mass spectrometer (MS-2).

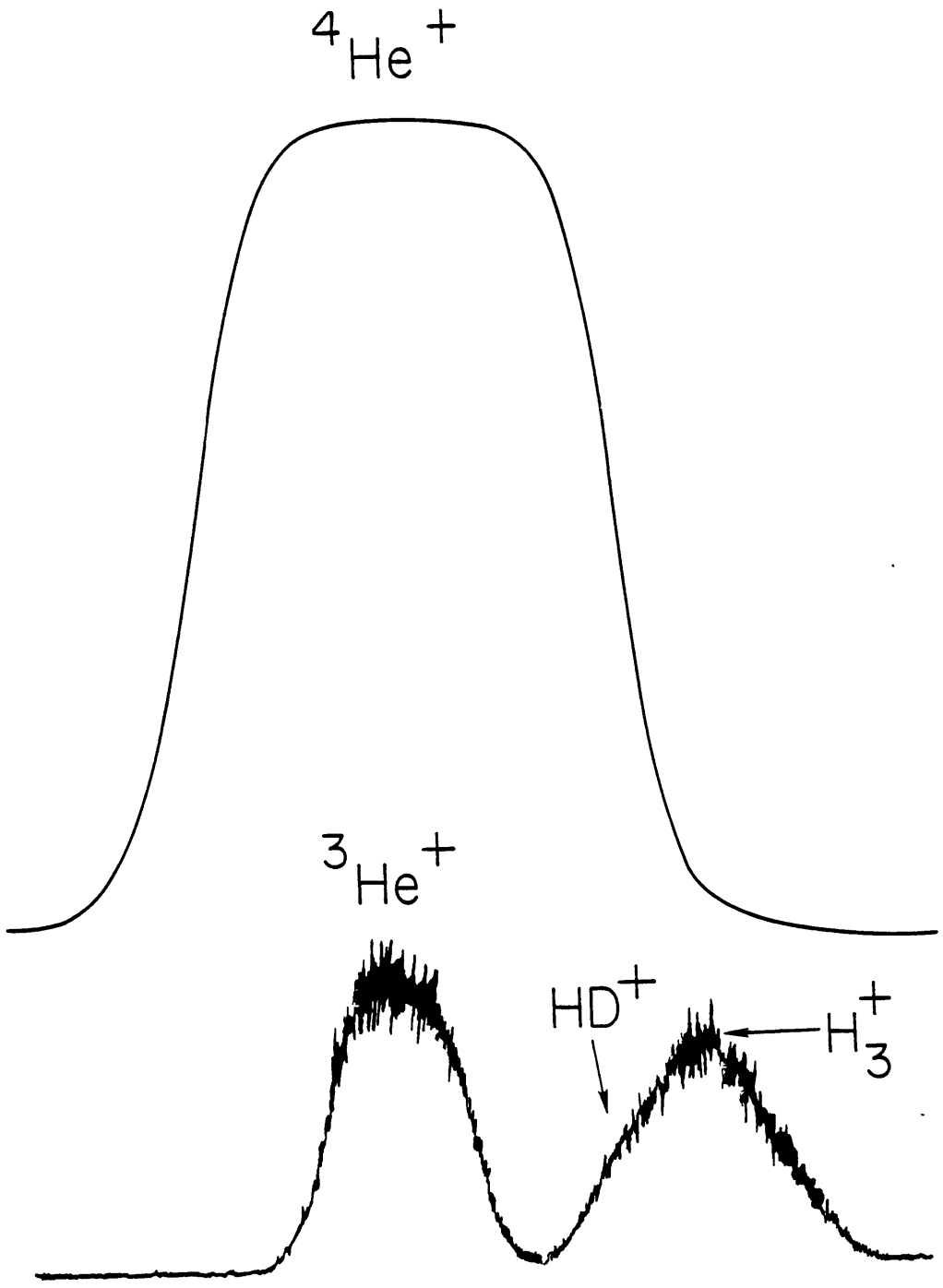


Figure 2.7: Magnet scan of air helium aliquot (1.8×10^{-6} cc ^4He), showing chart trace of ^4He (faraday cup) and ^3He plus HD-H_3 (electron multiplier) peaks.

of the Ne before closing the valve, minimizing the effect of potential variation in Ne contents. After inlet, several minutes were allowed for the titanium sponge traps (attached to the flight tube) to remove H_2, reducing the H_3^+-HD^+ peak. The magnet current was adjusted to center the ^3He beam on the collector, and the analysis was begun. The analysis typically consisted of 12 integrations on the ^3He and ^4He peaks, separated by baseline measurements (made by increasing the acceleration potential 10V). In the case of MORB glasses (~1 x 10^{-6} cc He), the baseline integrations were 10 seconds, while the peak integrations were 90 seconds. For smaller samples (<1 x 10^{-7} cc He) the baseline and peak integrations were 50 seconds. The samples were preceded and followed by air standards of equivalent size. The H_3^+-HD^+ peak height was monitored before each sample and standard to assure that conditions were identical. Due to the different isotopic ratio between the sample and air standards, it was necessary to run line blanks between them to reduce "memory" in the line. Experience has shown that memory is primarily due to the stopcock plus toepler section of the line. It could be reduced by working the stopcock and the mercury between samples, but between samples of different isotopic ratio it was necessary to run line blanks. For very small samples (see chapter 5), air is inappropriate as a standard, and aliquots of the "replicate standard" rock were used (see below).

2. Standardization

The atmospheric standards used for the helium analyses were collected in 10 liter stainless steel reservoirs. The temperature,

barometric pressure, and relative humidity were used to correct to standard temperature and pressure. All standards were collected on the balcony of the Clark laboratory by pointing the evacuated reservoir into the on-shore wind (to avoid contamination from any tank helium in the laboratory). Standard aliquots were then taken by equilibrating calibrated volumes with the standard reservoir. The aliquot volumes (see figure 2.5) were calibrated by peak height comparison with glass standard volumes that were in turn calibrated gravimetrically (with mercury). The estimated relative uncertainty for the total calibration procedure was .5 percent.

Due to the dependence of the measured $^3He/^4He$ ratio upon sample size, it was necessary to generate a standard curve for each set of samples and source configurations. It was found that the shape of the curve, and its stability as a function of time, were strongly dependent on the source settings: in particular, the repeller voltage had a large effect. Several authors have noted that high magnetic fields in the Nier type ion source can lead to mass discrimination for ions of small mass (Naidu and Westphal, 1966). It is also well known that the repeller voltage has a strong effect on the efficiency of Nier type ion sources (Naidu and Westphal, 1966; Wallington, 1971; Mark and Castleman, 1980). Experience with our ion source suggests that the gas pressure also has an effect on the mass discrimination. This can be intuitively understood as a result of changing the shape and size of the field of ions that can be extracted from the ionization region. Since the trajectories of mass 3 and 4 ions within the ionization region can be different, the mass discrimination may be a result of

different transmission efficiencies for these two trajectories. However, since the theory has not adequately described the behavior of commonly used ion sources (Ozard and Russell, 1969; Mark and Castleman, 1980), there is at present no satisfactory explanation for the pressure dependence of this mass discrimination.

A typical size vs. ratio standard curve for air standards is shown in figure 2.8. The curves were found to be stable over long periods of time, as long as there were no perturbations to the system (such as power failure, etc.). The mass discrimination was shown to be a function purely of sample size by using standards of different isotopic ratio (both higher and lower than atmospheric). Also, the shapes of the curves were shown not to be a result of electron multiplier non-linearity by reproducing them for different electron multiplier voltages, and for the different isotopic ratio standards.

At the beginning of a series of samples, a number of air standards of varying size were analyzed to determine the general nature of the size dependence, and whether it was reproducible. The air standards of different size were generated by using the splitting technique described earlier. While running samples, the curve was then periodically checked and verified for the sizes of the samples run on any particular day. The curve shown in figure 2.8 was typical for the MORB samples. With these large helium samples, it was possible to carefully gauge the concentration by inletting 1 percent of the sample, and then splitting the sample down to allow inlet of a sample size that was well calibrated. Using this technique, the uncertainty due to this correction could be minimized to roughly 1 percent. For small samples,

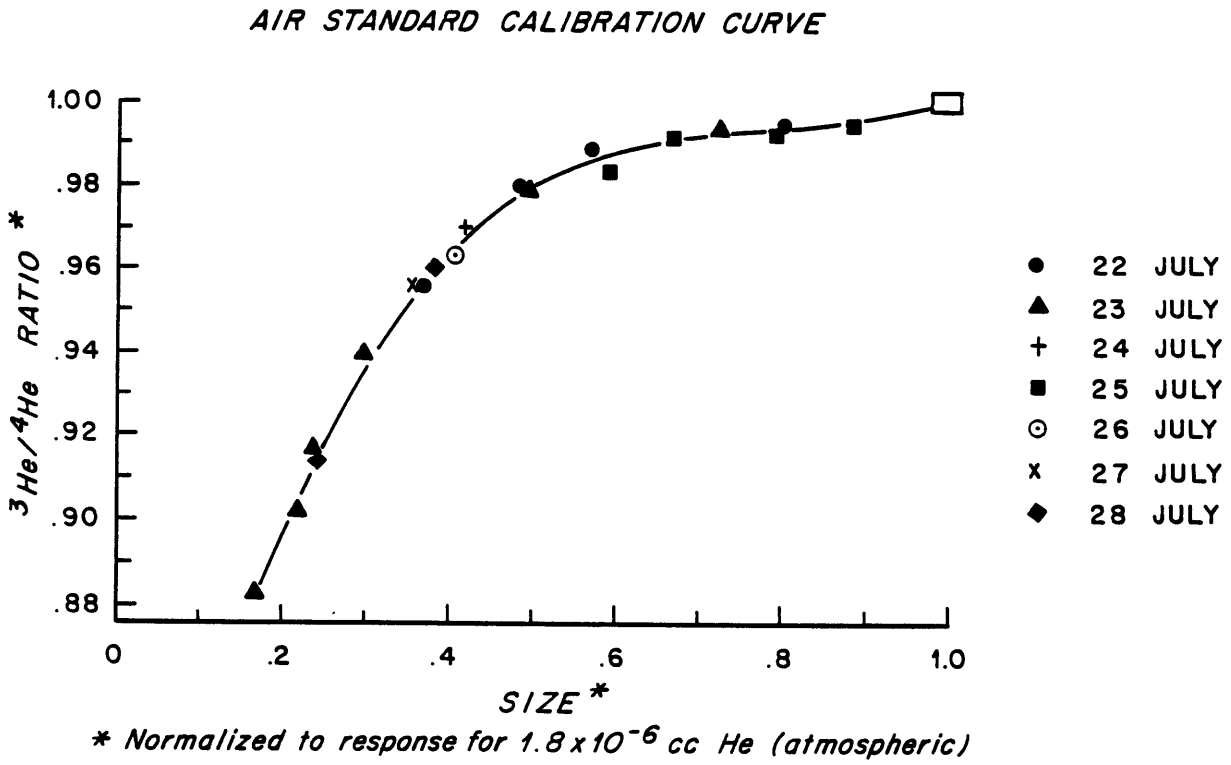


Figure 2.8: Typical calibration curve for air standards.

such as the gases contained in phenocrysts, no splitting was necessary.

3.) Precision and Reproducibility

The precision of an individual isotopic ratio analysis was calculated as the sum of the estimated uncertainties for all the steps in the analysis:

$$\sigma_T = (\sigma_b^2 + \sigma_s^2 + \sigma_l^2)^{1/2}$$

where σ_b, σ_s, and σ_l are the estimated uncertainties due to the blank, standard ratio (determined by reproducibility), and linearity curve, respectively. Typical values for the components in these estimates are shown in table 2.2. For large samples such as typical MORB glasses, the uncertainty was on the order of 1 percent. For the smaller samples the blank becomes a significant factor in calculating the isotopic ratio, and the uncertainties involved in standardization become slightly larger due to ^3He ion counting statistics. Where possible, these latter difficulties were alleviated by extracting helium from large sample sizes.

To check the reproducibility of the helium isotope ratio analysis procedure (extraction, blanks, and mass spectrometry), one MORB glass sample (Alv 519 2-1-b) was used as a "replicate standard" rock. Table 2.3 shows the results for analyses of this standard rock, which span the time period of this study. The standard deviation for the replicate analyses are quite close to the estimated uncertainties, suggesting that the estimates are valid. The analyses after 10 July 81 in table 2.2 were performed using MS-2 and illustrate that the two mass spectrometers yield similar results.

Table 2.2: Typical contributions to the uncertainty of helium isotope ratio measurements (all in percent)

	Large samples (10^{-5}–10^{-6}cc/gram)	Small samples (10^{-7}–10^{-9}cc/gram)
Blank uncertainty	< .2	.2 - 10
Standard Reproducibility	.5	.5 - 2
Size effect Correction	.7	.7 - 2
Total	.9	.9 - 10

Table 2.3: Reproducibility of the replicate standard rock Alv 519 2-1-b

Date	$^3He/^4He$ (R/R_A)
18 May 79	8.18
	8.01
	8.06
16 October 79	7.97
	7.86
30 December 79	7.95
3 January 80	7.86
6 January 80	7.76
7 January 80	7.82
11 March 80	7.79
12 March 80	7.76
29 July 80	7.97
2 November 80	8.07
	7.90
10 July 81	7.94
18 September 81	8.03
22 September 81	8.06
30 September 81	7.94
Mean =	7.94
Standard deviation =	.12 (1.5 percent)

CHAPTER 3

DISTRIBUTION OF HELIUM IN MID-OCEAN RIDGE BASALT GLASSES

A. Introduction

Mid-ocean ridge basalts (MORB) glasses provide unique samples of magmatic gases. These basalts are extruded on the ocean floor at great pressure (typically 3 km water depth) and low temperature, which results in rapid quenching, the formation of glass, and trapping of some of the original volatiles (e.g. see Fisher, 1971). Since basalts are derived by partial melting of the mantle, the trapped gases must inherit some of the mantle source characteristics.

However, before the relation between an erupted basalt and its mantle source can be studied, any potentially fractionating processes must be understood and accounted for. As an example, vesicles are present in almost all MORB glasses, and are evidence that a volatile phase is saturated at ocean floor pressures (Moore, 1979). Experimental evidence suggests that the vesicles are primarily filled with CO_2 (Moore et al., 1977). While available partitioning data suggest that all the noble gases will partition favorably into the vesicles (e.g. see Kirsten, 1968), the possible effect of vesiculation on the measurements has largely been ignored. It is conceivable that vesiculation could be mass fractionating, in which case the helium isotopic ratios in the glasses could be altered. Other processes that can possibly have an impact on the helium concentrations and isotopic ratios in the gases are diffusion and fractional crystallization, neither of which has been studied for basaltic melts. Therefore, these

potentially fractionating mechanisms are of considerable importance to the use of helium concentrations and isotopic composition in studying the mantle, and are the subject of this chapter.

As discussed in the introduction, the helium concentration in oceanic basalt glass is of interest not only in understanding mantle evolution, but also in balancing the atmospheric helium budget. If the helium resides within the vesicles, any concentration measurements will be strongly affected by the extent to which these vesicles have been opened. The experimental work of Kirsten (1968) showed that helium partitions favorably into a gas phase from a silicate melt. For example, using Kirsten's partition coefficient (for enstatite melt $K = 1.4 \times 10^{-4}$ ccSTP/ gram-atm; Kirsten, 1968) and assuming that 2 percent vesicles exist within the melt (at quenching), more than 98 percent of the helium should be in the vesicles. Several authors have noted this possibility (Lupton and Craig, 1975; Jambon and Shelby, 1979), but the systematics have never been studied. In particular, it is not clear whether enstatite partitioning experiments are applicable to oceanic basalts, since the partition coefficient may vary significantly with composition (Kirsten, 1968).

An additional problem in the interpretation of the helium results is a lack of diffusivity measurements on natural glasses. Synthetic glasses have been studied extensively (cf. Doremus, 1973), and these results are often applied to natural samples (e.g., Craig and Lupton, 1976). Since helium has significant diffusivities in glasses, even at low temperatures, this parameter is vital in evaluating the amount of post-eruptive degassing that has taken place for any given sample.

Using Craig and Lupton's estimate for the diffusion coefficient at 2°C (5×10^{-15} cm^2/sec; Craig and Lupton, 1976), we can calculate that helium will diffuse a characteristic length of 8 millimeters in five million years. Glassy rims of basalts extruded on the ocean floor are typically less than 1 cm in thickness, suggesting that diffusion may have important effects on helium measurements of older samples. Craig and Lupton developed a model to explain their measurements of lower $^3He/^4He$ ratios (~6 x atmospheric) in older samples by diffusion coupled with production of ^4He from decay of U and Th. However, this calculation is dependent upon a diffusion coefficient obtained by extrapolation from measurements on synthetic glasses, and is a parameter that has not been experimentally verified.

Another process that can potentially alter the basaltic helium concentration is fractional crystallization. While it is reasonable to assume that helium would favorably partition into the melt rather than crystal phase, there is no direct experimental evidence for this. In fact, helium has a quite small atomic radius (~1Å) and could conceivably fit into defects and voids in crystal structures.

Available helium isotopic measurements on MORB glasses do not allow an evaluation of the range of values, or of any potential fractionation mechanisms. Craig and Lupton (1976, 1981) have suggested that the $^3He/^4He$ ratio is "uniform" for mid-ocean ridge basalts. As discussed in the introduction, however, their results for tholeiites, combined with the one tholeiite glass sample reported by Krylov et al. (1974), suggest a 25 percent variation.

The objectives of this research are to 1) determine the effect of

vesiculation and crystallization on helium concentrations and isotopic ratios; 2) measure helium diffusivity in basaltic glass; and 3) search for $^3He/^4He$ variations on a global scale. To this end, we have measured ^3He and ^4He concentrations, glass-vesicle and glass-plagioclase partitioning, and some helium diffusivities in basaltic glasses from the Mid-Atlantic Ridge, the Juan de Fuca Ridge, Galapagos Spreading Center, the Mid-Cayman Rise, and the Central Indian Ocean Ridge.

B. Experimental

1. Methods

In order to evaluate partitioning, samples were both crushed and melted, using the methods described in the previous chapter. The hand-picked glass chips were divided into several splits, allowing tests of experimental reproducibility and sample heterogeneity. A portion of each sample was used to make a polished thin section for electron microprobe analysis (see table 3.1) and examination under petrographic microscope. This insured that the petrographic point counts (for vesicularity) and major element analyses were representative of the samples for helium analysis. Electron microprobe analyses for major elements were performed on the MAC (15 Kev) facility in the Department of Earth and Planetary Science at MIT (unless otherwise noted). The conditions have been described in the previous chapter.

Petrographic point counts were used to determine sizes and amounts of vesicles present, and phenocryst assemblages. Since point counts of objects smaller than the thickness of the section (such as small

Table 3.1: Major Element Chemistry of Glasses

	A11 92 31-31 (1)	KNR 54-47 24 (2)	ALV 714 6-1	ALV 735 6-1	ALV 714 6-4	ALV 892 2	ALV 519 2-1	ALV 518 3-1 (3)	JF1	JF2
SiO_2	50.68	51.02	51.45	51.49	51.34	51.50	49.18	51.26	50.37	50.88
Al_2O_3	15.73	15.83	13.43	13.51	13.59	14.57	16.47	14.93	13.89	14.01
FeO	9.96	9.89	12.40	12.56	12.64	10.49	9.16	9.65	11.92	11.82
MgO	7.52	6.99	6.60	6.59	6.55	8.11	9.19	8.18	6.77	6.71
CaO	11.01	10.15	11.08	11.04	10.94	12.24	12.70	11.39	11.62	11.11
Na_2O	2.85	3.79	2.27	2.15	2.12	1.90	1.97	2.50	2.67	2.73
K_2O	.11	.28	.08	.08	.08	.04	.08	.18	.13	.20
MnO	—	—	.23	.20	.23	.15	.17	.15	.27	.27
TiO_2	1.47	1.98	1.75	1.70	1.69	1.11	.70	1.30	1.86	1.87
P_2O_5	.15	.20	.04	.02	.04	—	—	—	.10	.12

(1) From Bryan and Sargent (1978).
(2) From Thompson et al. (1980).
(3) From Bryan and Moore (1977).

vesicles) can result in erroneously high modal analyses (Chayes, 1956), the results were corrected for this effect where necessary. Chayes (1956) has shown that for the present case, the volume percent vesicles must be multiplied by a correction factor:

$$C = 4r/(4r + 3k)$$

where r is the vesicle radius, and k is the section thickness. The modal counts were performed using a mechanical stage, with count spacing less than the size of the vesicles. When this was not possible, due to very small vesicles (see below), the volume percent vesicles was estimated by counting vesicles, measuring their diameters, and comparing their summed area to the total area of the thin section. In order to insure that the vesicle size determinations (obtained using a Leitz "stage micrometer") were representative, the sections were cut to a thickness larger than the vesicle diameter. If the section was infinitely thin with respect to the vesicle diameter, the observed diameter would depend on the place that the surface intersected the vesicles, and will generally be smaller than the true diameter. This effect was minimized by measuring 50-100 vesicle diameters, and insuring that the sections were "thick" relative to the vesicle diameter.

The diffusion experiments were performed using stepwise heating. A sieved sample (~400 mg) of glass grains was placed in a small, stainless steel, resistively heated furnace attached directly to the inlet line of the mass spectrometer. The temperature (measured using a chromel-alumel thermocouple to an accuracy within 5-10°C) was increased in a stepwise manner (from 125° to 400°C, in roughly 50° steps), and

the successive fractions were introduced into the mass spectrometer. The thermal mass of the furnace is sufficiently small to insure rapid temperature equilibration. The diffusion coefficient for each temperature can then be calculated from the fraction of helium released (F), the elapsed time (t), and the diffusion equation for spherical particles. The solution of the differential equations for diffusion from a sphere can be expressed as:

$$F = 1 - \frac{6}{\pi^2} \sum_{n=1} \frac{1}{n^2} \exp \frac{-n^2 \pi^2 Dt}{R^2}$$

where R is the spherical radius. In the present case, in which the sequential temperature steps result in significant losses, the diffusion coefficient at the i + 1 temperature step may be approximated by the following equations, for $F \leq .10$, $.10 < F < .90$, and $F > .90$, respectively (cf. Fechtig and Kalbitzer, 1966):

$$D_{i+1} = \frac{(F_{i+1}^2 - F_i^2)\ \pi R^2}{36 \cdot (t_{i+1} - t_i)}$$

$$D_{i+1} = \frac{R^2}{\pi^2 (t_{i+1} - t_i)} \left[-\frac{\pi^2}{3} (F_{i+1} - F_i) - 2\pi \left(1 - \frac{\pi}{3} F_{i+1}\right) - \left(1 - \frac{\pi}{3} F_i\right) \right]$$

$$D_{i+1} = \frac{R^2}{\pi^2 (t_{i+1} - t_i)} \ln \frac{(1 - F_i)}{(1 - F_{i+1})}$$

Where F_i is the total fraction of gas released during the i + n step. The main assumptions involved are that the gas is homogeneously distributed in the particles (at t = o), that there is no back-diffusion

into the particles during the experiment, and that the particles can be described as spheres of some known diameter (R).

2. Samples

The samples used for this study were selected because they provided adequate quantities of extremely fresh glass, from a variety of locales on the oceanic ridge system. The microprobe analyses presented in table 3.1 reveal that this small group of basalts represents a large variation in major element chemistry. All the samples were collected from mid-ocean ridge axes, which assures that their ages are less than 50,000 years, but each locale differs in spreading rate, bulk chemistry, and water depth. All are greater than 96 percent vitreous glass, with phenocrysts and microphenocrysts occurring only as minor phases.

FAMOUS Area. Alv 519 2-1-b is an olivine phyric basalt from 36°49'N, 33°16'W on the central rift valley of the Mid-Atlantic Ridge (2700 m depth). It is among the least "fractionated" basalts ever recovered from the ocean floor (Bryan and Moore, 1977), and is classified as "high Mg-Ca" according to the scheme of Melson et al. (1976). Olivine occurs as euhedral microphenocrysts, and rarely as phenocrysts with spinel inclusions. Alv 518 3-1 is also from the central rift valley, but has olivine, plagioclase, and pyroxene as phenocrysts. It would be considered more fractionated, on the basis of major element chemistry and petrography. The ridge morphology, petrography, and geochemistry of the FAMOUS area have been extensively described elsewhere (Ballard and van Andel, 1977; Bryan and Moore, 1977; White and Bryan, 1977). Geochemically, the FAMOUS basalts are

transitional between the enriched and normal ridge segments between 50° and 30° N, having slightly higher $^{87}Sr/^{86}Sr$ ratios and large-ion-lithophile concentrations than the normal ridge (White and Bryan, 1977).

Mid-Atlantic Ridge. AII 92-31-31A was dredged from the floor of the rift valley (23°01.8'N, 44°55.44'W) at a depth of 3500 meters (Bryan and Sargent, 1978). It contains olivine and plagioclase as microphenocrysts, and occasionally plagioclase phenocrysts. This sample would be classified as a normal MORB that has undergone some fractional crystallization.

TR138 811D-1 was dredged from 52.01°N on the mid-Atlantic ridge (Schilling, 1975), and is described further in chapter 4.

Juan de Fuca Ridge. The samples labeled "JF" are pillow fragments subsampled from a dredge on the southern end of the Juan de Fuca Ridge at a depth of 2220 m (USNM 111240/0, 44°40'N, 130°20'W; Melson, 1969). These samples would be classified as "high Fe-Ti" basalts. They contain phenocrysts of olivine, plagioclase, and clinopyroxene, which sometimes occur as glomerocrysts. Quench microphenocrysts were identified as plagioclase and olivine. Using the major element classification scheme of Melson et al. (1976), these samples are Fe-Ti rich basalts, which are typical of the Juan de Fuca Ridge. The isotopic composition of lead and strontium in basalts from the Juan de Fuca ridge (Church and Tatsumoto, 1975; Hedge and Peterman, 1970) is consistent with a normal (i.e., depleted) source region.

Galapagos Spreading Center. Alv 714 G-1, 714 G-4, 735 G-1, and Alv 892-2 are submersible samples from the Galapagos Spreading Center

(0°49'N, 86°08'W, depth 2750 m). The morphology of this area is distinguished from the slower spreading ridges by the presence of sheet flows (pahoehoe), and has been mapped by van Andel and Ballard (1979). Alv 714 G-1, 714 G-4, and 892-2 are pahoehoe, while Alv 735 G-1 is a pillow fragment. Alv 714 G-4 is devoid of microphenocrysts, and contains only an occasional plagioclase phenocryst. Alv 714 G-1 and Alv 735 G-1 contain plagioclase and (rarely) olivine as microphenocrysts; plagioclase phenocrysts also occur infrequently. All of these samples would be classified as Fe-Ti rich basalts, which are typical of relatively fast spreading ridges (Byerly et al., 1976). The major element chemistry of the basalts, regional topography, and the discovery of hot springs at the ridge axis are all consistent with the existence of shallow magma chambers (Byerly et al., 1976; Bryan and Sargent, 1978; Corliss et al., 1979). These samples were obtained from a section of the ridge for which Schilling et al.(1976) report La/Sm ratios similar to normal MORB.

Mid-Cayman Rise. Knr 54 47-24 was dredged from 5400 meters depth on the Mid-Cayman Rise (18°6'N, 81°47'W), which differs from the typical mid-ocean ridge because of its great depth and because it is bordered by a transform fault (Thompson et al., 1980). The major element chemistry is also quite different, having greater quantities of Na_2O, TiO_2, and K_2O. Thompson et al. (1980) showed that major element variations within the suite of samples they studied could be accounted for by moderate amounts of fractional crystallization but suggested that the source region must be different from normal MORB to account for all of the trace element results.

Central Indian Ridge. AII 93-11 54 was dredged from the Central Indian Ridge (24°59'S, 69°59'E) at 3500 m depth (Hoskins et al., 1977). It contains olivine and plagioclase as microphenocrysts, and olivine as phenocrysts. Major element analysis for this sample is not available, but on the basis of petrography, it would be classified as a typical mid-ocean ridge basalt.

C. Results

Results of the helium measurements, for both crushing and fusion extractions, are listed in table 3.2. Replicate analyses of several samples demonstrates that the reproducibility for the entire procedure (extraction and mass spectrometry) is within the estimated uncertainty (see table 3.2). For the most part, the samples that underwent replicate analyses appear to be quite homogeneous. For one sample (Alv 519 2-1), the inner 5 mm of the glassy rim yielded a slightly lower total concentration than the outer 5 mm of the rim. Although such gradients within single samples have been observed by other workers (Dymond and Hogan, 1978), the present difference in helium concentration is just slightly outside of experimental uncertainty, and must therefore be confirmed by further analysis. However, replicate analyses of the Mid-Cayman rise sample (Knr 54 47-24) yielded substantially different concentrations; we believe that this can be explained by heterogeneous vesicle distributions within the glass, which is discussed below.

1. Glass-Melt Partitioning

As mentioned earlier, experimental partitioning studies suggest that most of the helium in oceanic basalts should exist within the

vesicles. Results from melting and crushing experiments on the same samples (table 3.2) allow an evaluation of this partitioning. The percentage of helium in vesicles was calculated as the difference between total helium and helium released by crushing. For several samples, this was also determined by crushing and then melting the remaining powder (see table 3.2); the two methods yield identical results. As shown in table 3.3, in most cases a significant fraction of the helium does reside within the vesicles, but the relative amounts are a strong function of volume percent vesicles. This is to be expected from equilibrium partitioning, since the fraction of helium dissolved in the glass should be a function of the partial pressure of gas present (i.e., vesicularity). According to Henry's law, the amount of helium dissolved in the glass is directly proportional to partial pressure of helium and a solubility constant (K); i.e.:

$$C = K \times P_{He}$$

where C is the concentration in the glass (cc/g) and the units of K are cc STP/g-atm. Rearranging this expression, the fraction of the helium in the vesicles (He_v/He_g) can be calculated from:

$$\frac{He_v}{He_g} = \frac{V_v}{V_g} \left(\frac{1}{\rho K} \right)$$

Where

He_v = helium in vesicles
He_g = helium dissolved in the glass

ρ = density of the glass (3 g/cc)
K = Henry's law coefficient (cc STP/g-atm)

V_v = volume of vesicles (cc)
V_g = volume of glass (cc)

Table 3.2: Helium Concentrations and Isotopic Ratios for Basaltic Glasses

	Location	^{4}He Concentration (cc STP/gram x 10^6)	^{3}He/^{4}He x 10^5
ALV 519 2-1-b	FAMOUS		
Outer 5 mm of rim		5.7 ± .1	1.08 ± .02
		x 2.7 ± .1	1.10 ± .02
		x 2.7 ± .1	1.09 ± .01
Inner 5 mm of rim		4.5 ± .1	1.07 ± .02
		4.9 ± .1	1.08 ± .01
		x 4.0 ± .1	1.10 ± .01
ALV 518 3-1	FAMOUS	4.6 ± .1	1.13 ± .02
AII 92 31-31a	23°N M.A.R.	27.3 ± .9	1.13 ± .02
		x22.0 ± 2.0	1.13 ± .01
		* 5.4 ± .3	1.13 ± .02
JF 1	Juan de Fuca Ridge	x16.4 ± 4.0	1.08 ± .01
		* 4.8 ± .3	1.07 ± .01
JF 2		x 5.8 ± .3	1.15 ± .01
ALV 735 G-1	Galapagos Spreading Center	11.6 ± .8	1.13 ± .01
		11.5 ± .8	1.13 ± .01
		10.6 ± .4	1.10 ± .01
		x 4.7 ± .3	1.14 ± .01
		* 4.3 ± .3	1.13 ± .01
ALV 714 G-1	Galapagos Spreading Center	12.5 ± .4	1.12 ± .01
		11.9 ± .2	1.10 ± .01
		12.9 ± .8	1.13 ± .01
		x 3.9 ± .1	1.08 ± .01
ALV 714 G-4		11.2 ± .6	1.13 ± .01
		x 1.7 ± .2	1.12 ± .02
ALV 892-2		7.7 ± .2	1.14 ± .01
		x 0.3 ± .05	1.08 ± .08
KNR 54 47-24	Mid Cayman Rise	.8 ± .1	1.07 ± .02
		4.7 ± .1	1.06 ± .02
		x 0.08 ± .01	1.03 ± .25
AII 93-11 54	Central Indian Ridge	12.8 ± .2	1.07 ± .02
		x 5.0 ± .1	1.07 ± .01

x = gas released upon crushing
* = melting of powder remaining after crushing
Analyses without symbols refer to melting of 2 mm chips.

Table 3.3: Fraction of ^4He Contained in Vesicles, Volume Percent Vesicles and Mean Vesicle Sizes

Sample	Percent of ^4He in Vesicles	Volume (percent) Vesicles (1)	Mean Vesicle Size (mm)	Vesicle Size Range (mm)
Outer 5 mm (FAMOUS area)	47 ± 3	2.0 ± .4	.3	.02 - .4
ALV 519 2-1-b Inner 5 mm	85 ± 9	2.2 ± .4	.3	.02 - .4
JF 1 (Juan de Fuca Ridge)	77 ± 20	1.0 ± .3	.1	
AII 92 31-31a (M.A.R)	80 ± 8 80 ± 2	1.6 ± .3	.15	.005 -.3
AII 93 11-54 (Central Indian)	39 ± 1	.7 ± .2	.08	.02 - .22
ALV 735 G-1 (Galapagos)	42 ± 4 52 ± 4	.3 ± .05	.03	.01 - .07
ALV 714 G-1 (Galapagos)	31 ± 2	.2 ± .1	.02	.005 -.03
ALV 714 G-4 (Galapagos)	15 ± 2	.1 ± .05	.01	.005 -.03
ALV 892-2 (Galapagos)	4 ± 1	.02 ± .01	.01	.005 -.015
KNR 54 47-24 (Cayman)	3 ± 2	.3 ± .15	--	.01 -1.1

(1) As determined by petrographic point count

Therefore, from a plot of volume percent vesicles (V_v/V_g) and fraction of helium in the vesicles (He_v/He_g), and an assumed glass density, the Henry's law coefficient can be calculated (see figure 3.1).

However, when comparing the MORB glass results to Henry's law coefficients determined at standard temperature and pressure, several corrections must be made for the conditions at which the glasses formed. As noted by Poreda (1982), the glasses are "frozen" at some temperature above 273°K (ST), and according to the ideal gas law, K must be corrected by:

$$K_{STP} = K_T \left(\frac{T^*}{T_R} \right)$$

where: $T^* = 273°K$
T_R = rigid temperature of the glass

The rigid temperature for helium will be the temperature at which the vesicles and the glass stop equilibrating. Moore et al. (1977) estimated that glasses become rigid at 800–1000°C. While the helium may equilibrate until lower temperatures are reached (making the correction smaller), the rigid temperature will be assumed to be 900°C (see also Poreda, 1982).

Another correction that must be considered when comparing the MORB partitioning data to experimentally determined partitioning is the temperature dependence of Henry's law coefficient (K). For example, Kirsten's (1968) enstatite data was obtained at 1500°C, which is significantly higher than the assumed rigid temperature of 900°C. Dymond and Hogan (1978) used the temperature dependence of noble gas

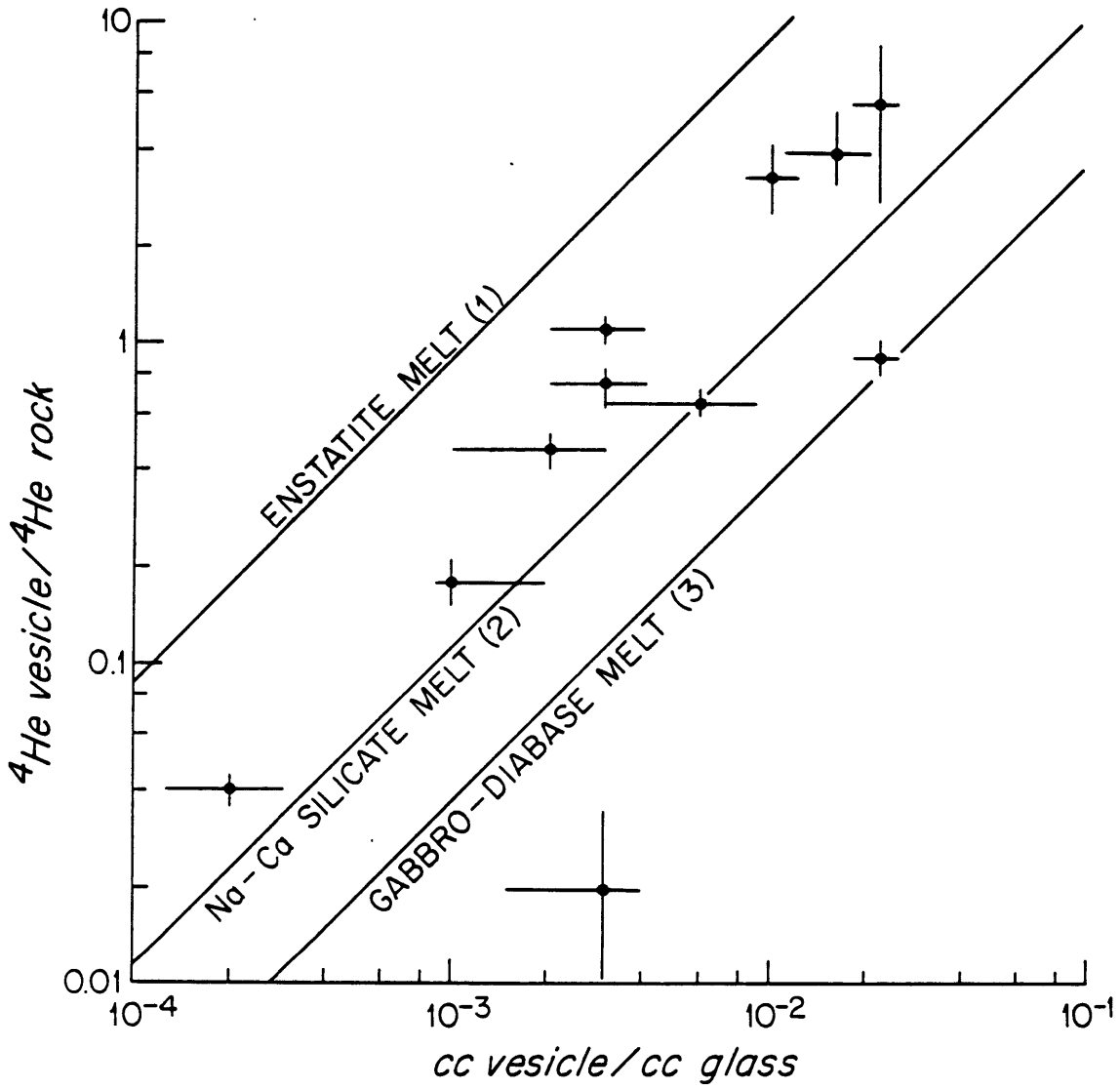


Figure 3.1: Volume fraction vesicles vs. gas-melt He partitioning. Solid lines were calculated from experimental results of (1) Kirsten (1968), (2) Mulfinger and Scholze (1962), (3) Gerling (1940), assuming a density of 3 gram/cc (see text). The points are results taken from tables 3.2 and 3.3

solubility in fluoride melts, observed by Blander et al. (1959), to derive the following relationship:

$$\frac{K_1}{K_2} = \exp \frac{-br^2}{T_2} \frac{\Delta T}{T_1}$$

where T_1 is 1173 K, T_2 is 1773 K, K_1 and K_2 are the Henry's law coefficients at these temperatures, b is a melt constant with units of $^\circ K\ Å^{-2}$, and r is the atomic radius of the gas in Å. If we follow Dymond and Hogan (1978) by using .93 Å for the helium atomic radius, and Kirsten's value of $1.15/Å^{-2}$ for b/T_2, we must correct Kirsten's Henry's law coefficient by almost a factor of two, from 1.2×10^{-4} to $.7 \times 10^{-4}$. This is in the opposite sense to the correction for the rigid temperature. There are two uncertainties in this calculation: first, the constant b may differ for basaltic melts; and second it is not clear what the appropriate atomic radius should be. Blander et al. (1959) used 1.2 Å for the atomic radius of helium, which when used in the above calculation, yields an even lower value of $.5 \times 10^{-4}$ for Kirsten's extrapolated enstatite Henry's law constant. The required correction for the Na-Ca silicate and gabbroic melts will be less extreme, since the experimental temperatures were 1200° and 1300° C respectively.

The MORB glass partitioning results are plotted in figure 3.1, and the corrected (to 900°C) experimental partitioning data are shown for comparison. From the slope of the MORB points, it would appear that equilibrium partitioning is applicable under natural conditions. However, the data suggest that helium solubility in basaltic melt is significantly higher than the value obtained by Kirsten (1968) for

enstatite melt (the value most often used in the literature). This is consistent with the hypothesis that the solubility of helium increases with the complexity of the melt, as suggested by Kirsten (1968). The value obtained from a linear regression through the points is 1.6 ± .8 x 10^{-3} cc STP/g-atm. Applying the two corrections discussed above, the MORB Henry's law constant is 3.7 x 10^{-4} cc STP/g-atm, compared to .7 x 10^{-4} for enstatite melt.

Since this value is calculated from crushing experiments, it is conceivable that the apparent solubility is raised by the loss of gas from vesicles before analysis (i.e., during preparations of the 2 mm chips). This is unlikely to affect most of our results since the vesicles are small relative to the size of the glass chips; the probability of vesicle rupture by fracturing is therefore low. The two samples that lie off the solubility trend would be most likely to be affected by this gas loss mechanism. One of them (Alv 519 2-1 outer 5 mm) has the largest vesicles and the highest vesicularity, while the other (Knr 54 47-24) has the largest size distribution (discussed below). For this reason, the low value for Knr 54 47-24 was excluded from the linear regression used to estimate the basaltic melt Henry's law coefficient. The low value for Alv 519 2-1 was included because replicate crushing experiments yielded similar partitioning results. Inclusion of either result changes the calculated solubility by less than the stated uncertainty.

These results clearly illustrate that vesicles are an important reservoir for the helium in oceanic basalt glass. The equilibrium partitioning of the heavier noble gases should favor the vesicles even

more, because of the expected lower solubilities with respect to helium (Kirsten, 1968). However, the diffusion rates of these gases will be lower, making equilibration, between vesicle and melt, slower. The vesicle size and size frequency distribution will therefore be important controls on the concentration measured in the laboratory, particularly if the glasses are crushed prior to analysis. In the case in which the vesicles are comparable in size to the grains analyzed, a significant fraction of the helium can be lost simply by sample preparation. We cannot eliminate the possibility that some gas loss by this mechanism has occurred in the present study, even though 2 mm chips were used for both the crushing and melting experiments. However, this should only have an effect upon the samples mentioned above.

Another difficulty arises when vesicle size distribution is very broad and vesicularity is low. Since volume of vesicles (and therefore gas content) will be a function of $(\text{radius})^3$, heterogeneities within single samples are possible. The Mid-Cayman Rise sample (Knr 54 47-24) represents such a case, with a vesicle size range of .01 to 1.0 mm., and a fairly low vesicularity (.3 percent). In the thin section examined, only one vesicle of 1 mm diameter was present, but this would lead to large variability in helium concentration within the sample, both due to the statistical likelihood of finding such a vesicle in a given sample, and the possibility that large vesicles will be fractured during sample preparation. Since our methods are quite reproducible for the other samples, this is the most likely explanation for the different concentrations obtained by replicate analyses in this case.

The other samples contain roughly gaussian size distributions (approximately centered about the size labelled "mean size" in table 3.2). Several samples (Alv 519 2-1-b, AII 93 11-54, and AII 92 31-31a) contain bimodal size distributions; in these cases the "mean size" reflects the size that contributes most of the volume of vesicles. Knr 54 47-24 differs in that there is a continuous size variation, and would require analysis of a very large sample to average out simple statistical variation. It is also noteworthy that this sample lies outside of the partitioning trend displayed by the other samples in figure 3.1.

These results make evident the difficulty in interpreting published concentrations. The measured value will be a function of original ^4He content of the magma, extent of pre-quenching degassing, vesicle size, and grain size analyzed. Since these last two parameters are rarely documented, published results are difficult to compare, and must often be taken as minimum values.

2. Glass-phenocryst partitioning

Varying degrees of fractional crystallization may also change apparent gas concentrations in evolved melts. While crystal-melt partition coefficients for the noble gases have not been extensively studied, it is quite reasonable to assume that helium favors the melt (and the vesicles) relative to crystalline phases. This is supported by helium analyses of olivine phenocrysts in Kilauea lavas by Kaneoka et al. (1978). They obtained quite low concentrations (4×10^{-8} ccSTP/gram), suggesting that helium is not favorably partitioned into the olivine structure. If the Kilauea phenocrysts grew in a melt with

a helium concentration typical of ocean-floor glasses (10^{-6} to 10^{-5} ccSTP/gram), the implied olivine-melt partition coefficient would be between .04 and .004. However, since sub-aerial lavas are more completely degassed relative to submarine basalt glasses, it is difficult to infer a melt concentration, so these values are somewhat speculative.

The generally incompatible behavior of helium is also supported by the analysis of handpicked plagioclase phenocrysts from TR 138 11D-1 (see table 3.4). The phenocrysts were first crushed in vacuo for extraction, and then the powder was melted in the manner described above. Comparison of the total (crushed and melted) concentrations for plagioclase ($1.2 \pm .1 \times 10^{-7}$ cc/gram) to those of glass ($11.9 \pm .3 \times 10^{-6}$ cc/gram, table 3.1) allows the calculation of an effective plagioclase/melt partition coefficient for helium of .01. This is probably an upper limit to the true partitioning value, since most of the helium (92 percent) in the plagioclase was released by crushing. Undoubtedly, the helium released by crushing is due to vesicles in melt inclusions, which are common in plagioclase, and vesicles trapped during crystal growth. Therefore, the equilibrium partition coefficient is more appropriately calculated from the helium concentration in the plagioclase powder (after crushing to < 120 μ), which yields a value of $K_D = .0008$. The actual partition coefficient may be even lower than this, if some of the helium released by melting the powder was dissolved in the melt inclusions. In either case, crystallization of plagioclase will increase the helium concentration in the melt. However, even 50 percent crystallization

Table 3.4: Plagioclase-Glass Partitioning for Sample TR 138 11D-1

	^4He (x 10^6 cc/g)	K*	$^3He/^4He$
Glass	11.9 ± .3	----	1.35 ± .01 x 10^{-5}
Plagioclase (crushed)	.11 ± .01	.01	1.31 ± .10 x 10^{-5}
Plagioclase (powder melted)	.01 ± .003	.0008	1.38 ± .35 x 10^{-5}

$$*K = \frac{\text{concentration}}{\text{concentration in glass}}$$

will not affect the concentrations as much as loss of two volume percent vesicles.

Despite the uncertainties, the currently available information strongly suggests that helium behaves as an incompatible element with respect to the phases commonly crystallizing from basalt. Additional results, described in chapter 5, support this conclusion.

3. Determination of diffusion rates by stepwise heating

Using the method of stepwise heating, diffusion coefficients were determined for a temperature range of 125° to 400°C. Alv 519 2-1-b was chosen for these experiments because it had the fewest vesicles smaller than the grain size to be heated. To confirm that the results were unaffected by the presence of small vesicles, the sample containing the smallest volume percent vesicles (Alv 892-2) was also used. Results of several different stepwise heating experiments are shown in figure 3.2, using the conventional Arrhenius plot (the data are listed in appendix 1.1). In general, fractions taken at one temperature agree within the experimental uncertainty, confirming that volume diffusion is occurring. In addition, there is quite good agreement between the different grain sizes, and between the two samples, indicating that vesicles do not affect the results.

In calculating diffusion coefficients, we have assumed that the "effective" radius is one-half the mean sieve diameter. Although there is undoubtedly a size distribution, even the maximum range (the difference between adjacent sieve sizes) will have an insignificant effect on these estimates (Gallagher, 1965). The deviation from sphericity should also have a negligible effect, as long as the

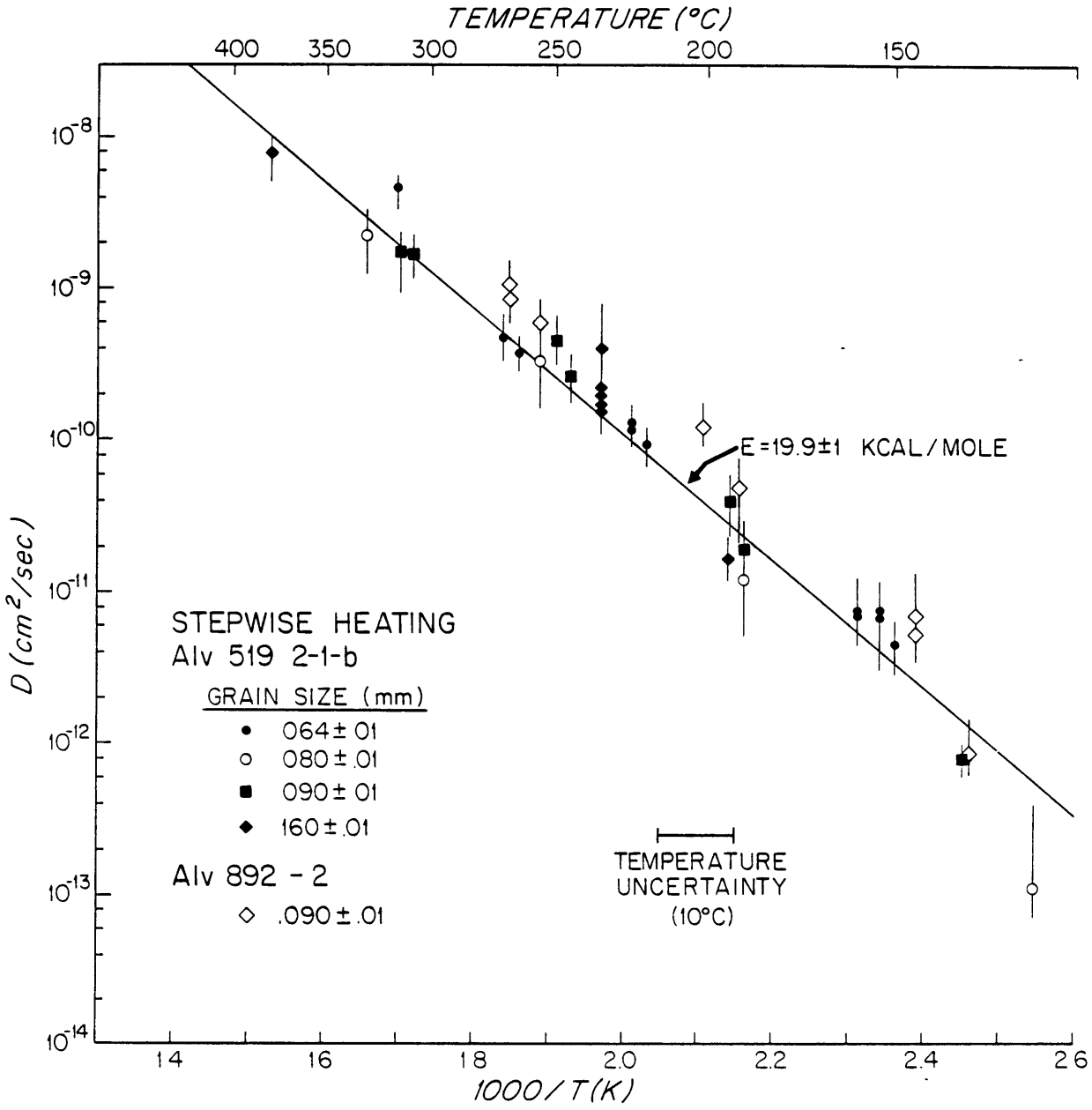


Figure 3.2: 1/T vs. log D for stepwise heating experiments on sieved samples of ALV 519-2-1-b. The grain sizes are mean sieve diameter, and the uncertainties are the difference between sieve sizes (maximum).

particles are not needle-shaped (Jain, 1958; Lin and Yund, 1972) and are not made of aggregated small particles. The absence of these conditions was confirmed by microscopic examination both before and after heating.

Assuming volume diffusion is taking place, we can fit the results to the relation:

$$D = D_0 \exp(-E/RT)$$

where D is the diffusion coefficient at a temperature T, E is the activation energy, R is the gas constant, and D_0 is the diffusivity at infinite temperature. We obtain E = -19.9 ± 1 Kcal/mole, and ln D_0 = -2.7 ± .6. These uncertainties reflect one standard deviation about the linear regression line.

Using these values, we can calculate the diffusion coefficient of helium in basaltic glass at ocean floor temperatures (0°C) to be 1.0 ± .6 x 10^{-17} cm^2/sec. This low diffusivity implies that significant diffusion will not take place in less than a hundred million years (for a .5 cm glassy rim of oceanic basalt). Clearly, weathering of the glass will be a greater problem than diffusion.

Unfortunately, there are no other experimental diffusion data for natural basalts to allow comparison, and most estimates have been based on data for synthetic glasses. Current glass structure models suggest that gas diffusion rates are primarily controlled by the mole percentage of "network formers" and "network modifiers" (cf. Doremus, 1973). The network formers (SiO_2 in this case) create the polymeric structural framework, the holes in which provide diffusion paths for small atoms such as helium. On the other hand, the network

modifiers plug up these holes and impede diffusion. A number of experimental studies have qualitatively verified this model (Norton, 1957; Altemose, 1961), leading to its use in extrapolation to basaltic composition. Jambon and Shelby (1979) estimated the diffusion parameters from permeation rate measurements on basaltic glass combined with literature values for diffusion in Na-Aluminosilicate glass. Their values for E and Do are 14 ± 2 and ~ 7 x 10^{-3}, respectively, a significant difference from those reported here. (Extrapolation to 0°C gives a diffusion coefficient of 4 x 10^{-14} cm^2/sec). However, since diffusion rates are strongly dependent upon chemical composition (Shelby, 1976), such a comparison is questionable.

Craig and Lupton (1976) used weight percent SiO_2 to scale pyrex diffusivities to basaltic composition, and estimated the activation energy using the same assumption. Their estimate of D_{He} in basaltic glass at ocean floor temperatures (0°C) is 5 x 10^{-15} cm^2/sec, which differs significantly from our value. It is more correct, however, to scale diffusivity as a function of <u>mole</u> percent SiO_2, as noted by Altemose (1961). Using this assumption (and the dependence of permeation rate on mole percent SiO_2 given by Altemose), we obtain D_{He} (at 0°C) of 4 x 10^{-17} cm^2/sec, in better agreement with our experimental results. However, this calculation assumes that the activation energies and compositional dependencies for diffusion and permeability are the same, which is not strictly valid, since solubility's dependence on both temperature and composition may be significant (permeation rate is equal to the product of solubility and diffusivity). The overall solubility dependence upon

composition (cf. Altemose, 1961; Shelby, 1976) tends to make this estimate a lower limit, but the total effect should be less than an order of magnitude (for extrapolation from pyrex to basalt compositions). It is not clear, on the basis of previous studies, what the temperature dependence of solubility for basaltic glass will be (Doremus, 1973; Shelby, 1976), and hence whether the activation energies used are too high or too low. Therefore, considering the lack of information, the estimates of D(0°C) for He in basaltic glass made on the basis of synthetic glass data, give values which are not inconsistent with our results.

Thus, the diffusion model proposed by Craig and Lupton (1976, 1981) to explain their low $^3He/^4He$ samples (6 x atmospheric, for 5 m.y. old basalt) would seem unlikely, since the diffusion rates required for their calculations are too high. It is conceivable that weathering and devitrification enhance the diffusion rates, leading to more rapid exchange with time for these older samples; but if the samples were chosen on the basis of freshness, this would be unlikely. Since typical U and Th concentrations in oceanic basalts are not high enough to account for this ratio change by production of radiogenic ^4He in such short times, it is also possible that the low ratios observed are characteristic of the source regions for these samples. The resolution of these possibilities must await further studies of old basaltic glass samples.

It is also important to note that the diffusion rates reported here indicate that significant diffusion can occur at moderate temperatures. For example, it is common practice to crush samples before analysis,

and to heat them to remove adsorbed atmospheric gases. In the case of basaltic glass, this procedure can lead to significant helium loss (in addition to helium loss from the vesicles), if the grain size is sufficiently small, and the temperatures sufficiently high. If 50 micron grains are heated for 30 minutes at 200°C, roughly 30 percent of the helium will be lost by diffusion.

4. $^{3}He/^{4}He$ Ratios

Reproducibility of ratio measurements is confirmed by complete replicate analyses of several samples, and is within the range of the estimated uncertainties. The $^{3}He/^{4}He$ ratios for this set of samples, excluding TR 138 11D-1, are remarkably constant at 1.10 ± .03 x 10^{-5} (see figure 3.3). However, the $^{3}He/^{4}He$ ratio for TR138 11D-1 is quite close to 10 x atmospheric, a value that differs from the other samples by 20 percent. This difference is well outside the experimental uncertainty, and shows that there are significant helium isotopic variations on the mid-ocean ridge. These results are compared to those of Craig and Lupton (1976) in figure 3.3. Also shown for reference are the results obtained by Jenkins et al. (1978) for the hydrothermal effluent at the Galapagos spreading center. The $^{3}He/^{4}He$ of the glass samples and the hydrothermal effluent from the same area are identical, within the uncertainty of the measurements.

The $^{3}He/^{4}He$ ratio results from the glass-vesicle and glass-phenocryst partitioning experiments illustrate that there is no significant isotopic fractionation between the vesicles, phenocrysts, and glass. This suggests equilibrium partitioning, since diffusion is expected to be mass fractionating. Further, the close agreement with

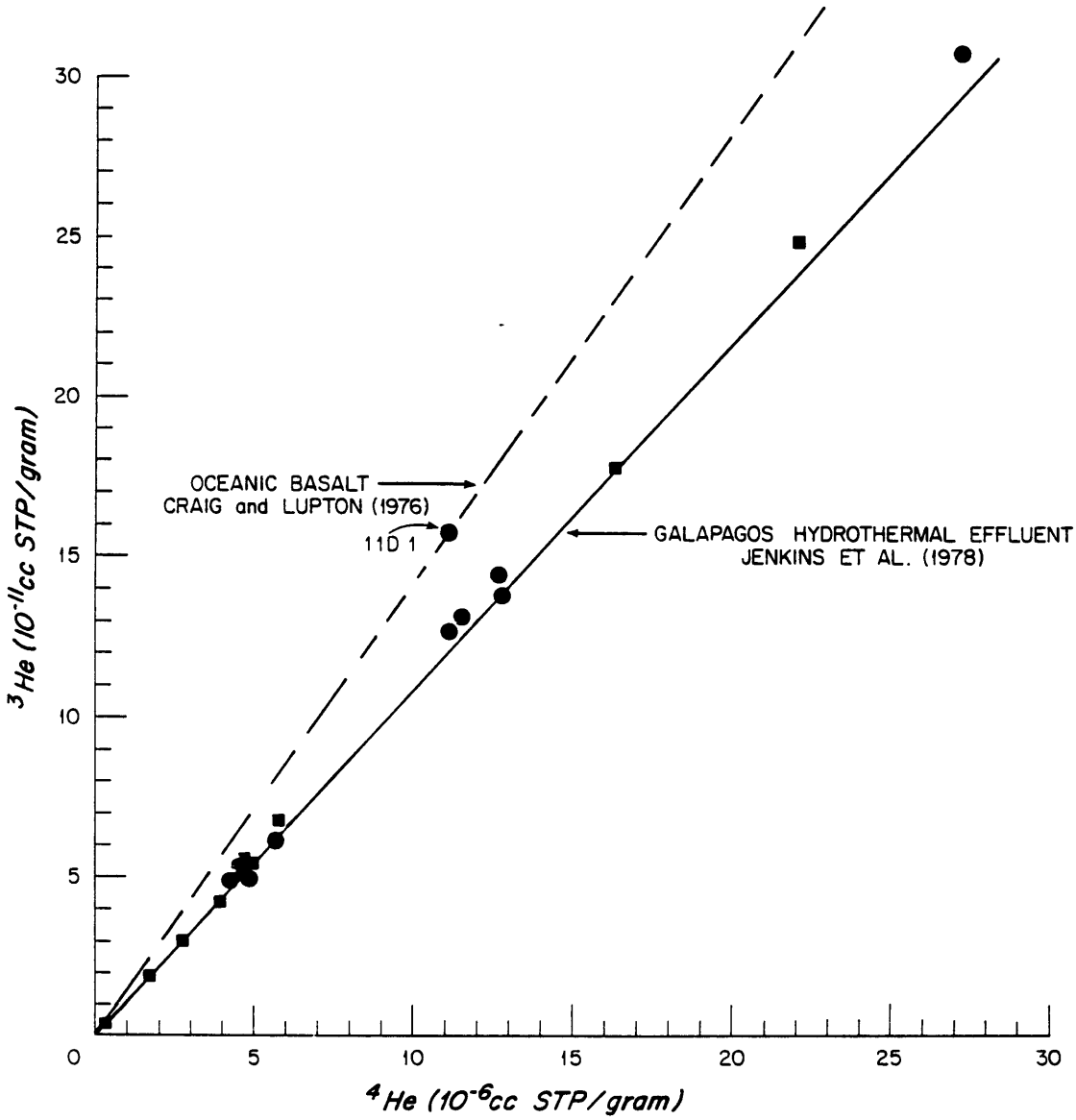


Figure 3.3: ^4He vs. ^3He for basaltic glass samples analyzed. Square symbols denote samples crushed in vacuo, round symbols are for melting. Solid line shows results obtained by Jenkins et al. (1978) for the Galapagos effluent.

the Galapagos hydrothermal effluent is consistent with the idea that the macroscopic transport of helium in these systems is only weakly mass dependent (if at all).

D. Discussion

The importance of vesicles in determining the He concentration (and potentially the concentrations of all the gases) in oceanic basalt glass is illustrated by our crushing experiments. Several authors have noted the importance of accurate concentration measurements in modeling the degassing of the crust (Lupton and Craig, 1975; Corliss et al., 1979; Hart et al., 1979). Hart et al. (1979) suggest that the least degassed melt will be that which has erupted under the greatest hydrostatic pressure (e.g. the Cayman Trough). Our results support this contention in the sense that the sample from the Cayman Trough (Knr 54 47-24) had a small amount of helium in the vesicles. However, the mere presence of vesicles in this sample suggests that pre-eruptive degassing cannot be totally ruled out, and that hydrostatic pressure may not be the only variable to be considered.

Lupton and Craig (1975) noted that their observed helium concentrations were much too low to account for the oceanic ^3He flux. The concentrations presented here are typically a factor of ten higher, and suggest that their results may have been affected by gas loss from the vesicles. Using the highest helium concentration obtained (2.7×10^{-5} cc STP/gram for AII92 31-31), degassing the oceanic crust to a thickness of only 2.5 km will produce the ^3He flux (assuming a crustal production rate of 2 km^2/yr). Therefore, the

helium results do not necessarily indicate that the whole oceanic crust is degassed.

The important parameters in controlling the extent of degassing of a melt will be depth of the magma chamber, residence time, and conditions under which CO_2 saturation occurs. If supersaturation of the major gas phase (CO_2) does occur, vesicles can escape by rising through the melt (Delaney et al., 1978). Measurements of CO_2 in basalts vary between 800 and 2300 ppm (Moore et al., 1977; Moore, 1979; Delaney et al., 1978), which would place the depth of CO_2 saturation between 1 and 2 km below the average ridge crest (3 km water depth), so that degassing may occur during residence time in a magma chamber. Clearly, vesicularity (and gas loss) would also be affected by initial CO_2 content, residence in a magma chamber, depth of the magma chamber, and ascent velocity. Thus, great care must be taken in using the noble gas content of oceanic basalt glass to estimate mantle concentrations. An important first step in unraveling a sample's magmatic history is to document the volume and the size of the vesicles, and the gas-melt partitioning.

It is interesting to note that the the vesicle sizes, size distributions, and total vesicularity seem to vary systematically between the different locales on the oceanic ridge studied here. The fast spreading ridge samples are characterized by small vesicles, small vesicle size distributions, and low vesicularity, while the slow spreading ridge samples contain larger vesicles, broader size distributions, and higher vesicularity. The deepest sample (Mid-Cayman Rise) contains the largest range of sizes. This general trend in total

vesicularity has also been observed by Moore (1979) for a much more extensive set of oceanic basalts from various ridges. While the present set of samples is much too small to allow any generalizations, these differences presumably reflect the different magma chamber depth and possibly different decompression histories for the different ridge systems.

The vesiculation process can also fractionate the relative abundances of the noble gases. Fisher (1975) used the He/Ar ratios from oceanic basalts to estimate a "minimum" K/U ratio for the oceanic mantle. As pointed out by Schwartzman (1978), however, partitioning between melt and gas phase can separate He from Ar. Our results indicate that the He concentration is a function of the magmatic processes mentioned above, the vesicle size distribution, and the grain size of the sample analyzed. Thus, unless the experimentalist documents these last two parameters, He concentrations (and possibly He/Ar ratios) are difficult to interpret.

The isotopic results show that vesiculation and crystallization do not affect the magmatic $^{3}He/^{4}He$ ratios. This, coupled with the low diffusion coefficient for helium at 0°C ($\sim 10^{-17}$ cm^2/sec), suggests that glass measurements reflect the characteristics of the mantle source regions for the basalt. Interpreted in this way, the isotopic variations show that the oceanic mantle is heterogeneous with respect to helium isotopes. However, only one sample (TR138 11D-1) differs by more than 3σ from the rest of the samples. Schilling (1975) and White and Schilling (1978) showed that the trace element and $^{87}Sr/^{86}Sr$ characteristics of this sample are quite similar to "normal" MORB. On

the other hand, the rest of the samples have diverse geochemical characteristics, but are identical with respect to $^{3}He/^{4}He$. For example, the two samples Alv 892-2 and AII 93 11-54 have $^{87}Sr/^{86}Sr$ ratios of ~.70256 and .70320, respectively (S. Hart, personal communication). Therefore, the relationship between $^{3}He/^{4}He$ and $^{87}Sr/^{86}Sr$ is not simple; this is discussed in greater detail in chapter 4.

E. Summary

To summarize the results described in this chapter:

1. Crushing and melting experiments suggest that helium in MORB glasses obeys equilibrium partitioning between vesicles and glass. The partitioning results for samples with a large range of vesicularities allows estimation of the helium solubility in basaltic melts. The calculated Henry's law coefficient is 3.7×10^{-4} cc STP/g-atm, which is significantly higher (by a factor of 5) than the value reported by Kirsten (1968) for enstatite melt. However, the comparison between these two values is dependent on two corrections: one for the "rigid" temperature of the glass, and one for the temperature dependence of the Henry's law coefficient.

2. The helium glass-vesicle partitioning can strongly affect determinations of helium concentrations, depending upon vesicularity, vesicle size, and grain size analyzed. Many of the concentration measurements in the literature must therefore be viewed as minimum values. By inference, this is also true for other noble gas concentrations and noble gas abundance patterns.

3. Plagioclase-melt partitioning, obtained by extracting helium from coexisting phenocrysts and glass, indicates that helium behaves as an incompatible element. The values obtained for K_D (.01 to .001) are probably an upper limit, since some of the helium in the phenocrysts may reside within melt inclusions.

4. Diffusion rates, determined using the method of stepwise heating (for the temperature range of 150-500°C) yielded an activation energy for helium diffusion in basalt glass of 19.9 ± 1.0 Kcal/mole. Extrapolation of these results to 0°C shows that helium diffusion will be insignificant for unaltered glasses less than 50 million years old.

5. There is no isotopic fractionation, within the uncertainty of the measurements, between glass and vesicles or glass and phenocrysts. These results, and the low helium diffusion rate suggests that the isotopic composition of the glasses reflects the isotopic composition of the mantle source.

6. Most of the samples described in this study have $^3He/^4He$ ratios remarkably close to 1.10×10^{-5} (or 8 x atmospheric). One sample from near 52°N on the mid-Atlantic ridge has a $^3He/^4He$ ratio of ~10 x atmospheric, which shows that there are significant helium isotopic variations in the oceanic mantle.

CHAPTER 4

HELIUM ISOTOPIC VARIATIONS IN MID-OCEAN RIDGE BASALTS

A. Introduction

Basalt erupted at the mid-ocean ridges is the most voluminous volcanic rock on the face of the earth. The first studies of mid-ocean ridge basalts (MORB) resulted in the hypothesis that they represent a "window" to the mantle: an indicator of the mantle composition unaffected by continental contamination (Engel et al., 1965; Gast, 1965). Although these early studies emphasized the compositional uniformity of MORB, more extensive sampling has revealed considerable compositional variability, both locally and regionally (Schilling, 1973; Frey et al., 1974; Blanchard et al., 1976; Bryan et al., 1976; White et al., 1976). In particular, there are systematic trace element and isotopic gradients along the ridge crest near islands such as Iceland and the Azores (Schilling, 1973; Hart et al., 1973; Sun et al., 1976; Schilling, 1975; White and Schilling, 1978). In general, the basalts erupted near islands are enriched in large ion lithophile elements and the radiogenic isotopes of Sr and Pb. The isotopic variations show that the mantle heterogeneities have existed for long time periods (Hofmann and Hart, 1978).

One interpretation of the geochemical gradients that occur along the mid-ocean ridge is mixing between a "plume" source and the normal depleted upper mantle (Schilling, 1973, 1975). This hypothesis requires that oceanic islands are produced by upwelling mantle plumes (Wilson, 1963; Morgan, 1972), and that these plumes consist of

geochemically undepleted material from the lower mantle. The terms "depleted" and "undepleted" are used in the manner defined by Hart and Brooks (1981): depleted refers to a system that has evolved with parent/daughter ratios that are lower than a closed (or undepleted) system. In the case of helium, an undepleted reservoir is one that has had unchanged $^{3}He/(Th+U)$ since the formation of the earth, and would have a higher present-day $^{3}He/^{4}He$ ratio. Since such mantle reservoirs may no longer exist, undepleted is used here as a relative term. As shown in this chapter, normal MORB glasses appear to have a relatively constant $^{3}He/^{4}He$ ratio of ~8.4 x atmospheric. For consistency with other geochemical studies, normal MORB will be assumed to be derived from a depleted source. Therefore, any sample with $^{3}He/^{4}He$ ratio greater than 8.4 x atmospheric is derived from a relatively undepleted source.

Normal MORB can be characterized by low abundances of incompatible trace elements (relative to alkali basalts or chondritic meteorites), as indicated by low Rb/Sr, Sm/Nd, La/Sm, and Nb/Zr ratios (Schilling, 1975b; Erlank and Kable, 1976; Kay and Hubbard, 1978; Hanson, 1977; Sun et al., 1979). Low $^{87}Sr/^{86}Sr$ and high $^{143}Nd/^{144}Nd$ ratios indicate that the depletion has existed for long time periods (DePaolo and Wasserburg, 1976; Richard et al., 1976; O'Nions et al., 1977). For the purposes of this study, normal MORB will be defined as having $^{87}Sr/^{86}Sr < .7028$, $La/Sm < 1.0$, and $Zr/Nb > 20$.

Some of the basalts erupted near islands such as Iceland and the Azores have significantly higher $^{87}Sr/^{86}Sr$ ratios and incompatible element abundances (e.g. Sun et al., 1976; White and Schilling, 1978).

These have commonly been referred to as "enriched" or "plume" type MORB to distinguish them from normal MORB. The goal of this study is to use the helium isotopic information to characterize the mantle source regions for enriched MORB. If these basalts are derived from sources that are undepleted (relative to normal MORB), then significantly higher $^3He/^4He$ ratios should be observed.

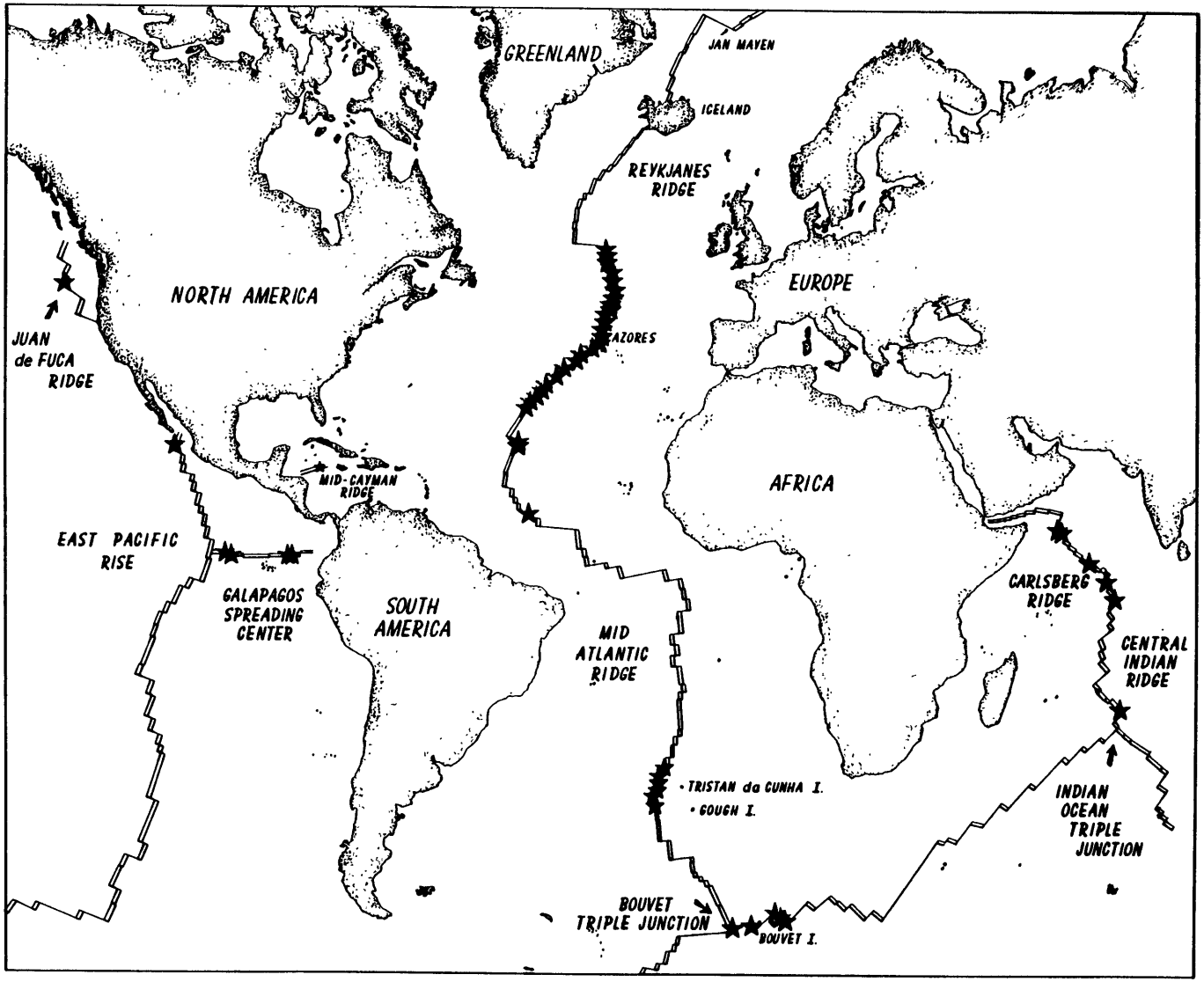
Published values of $^3He/^4He$ ratios for mid-ocean ridge basalt glasses vary from roughly 8 x atmospheric (Krylov et al., 1974; Poreda and Craig, 1979; Kurz and Jenkins, 1981) to 10 x atmospheric (Lupton and Craig, 1975; Craig and Lupton, 1976). While one of the objectives of this study is to determine what is "typical" with respect to MORB $^3He/^4He$, it is possible to contrast these values with those obtained for some oceanic islands. $^3He/^4He$ ratios reported for Icelandic hot springs (as high as 20 x atmospheric; Polak et al., 1975) and Kilauea fumaroles (15 to 18 x atmospheric; Craig and Lupton, 1976; Jenkins et al., 1978) are significantly higher than the MORB values. The $^3He/^4He$ ratio will decrease with time most rapidly for the source regions that have the lowest $^3He/(U+Th)$, since ^4He is produced by decay of U and Th. It is therefore quite reasonable to infer that the mantle tapped by Hawaii and Iceland has had a higher time integrated $^3He/(U+Th)$ ratio relative to MORB. In a general way, these results are consistent with the mantle "plume" models that have been proposed to explain other isotopic variations (e.g. Sun and Hanson, 1975; Schilling, 1973). For example, Hart et al. (1979) have suggested that the atmosphere has been formed by preferential degassing of the upper mantle, leaving the lower mantle relatively undegassed.

If so, the upper mantle source regions for oceanic basalts with lowest $^{87}Sr/^{86}Sr$ ratios correspond to the most depleted, degassed mantle, and should also have the lowest $^{3}He/^{4}He$ ratios.

The goal of this study is to determine the helium isotopic ratios of normal and enriched type MORB, and to use this information to identify those basalts derived from undepleted mantle sources. For this reason, an attempt was made to select samples that were well documented with respect to trace element and isotope geochemistry, while also providing a global representation; the locations of the samples studied are shown in figure 4.1. The ridge segment discussed in the most detail is between 27 and 52°N on the Mid-Atlantic Ridge. Dredged basalts fom this transect have been particularly well studied with respect to Sr isotopes, trace elements, and some volatile elements (Schilling, 1975; White et al., 1976; White and Schilling, 1978; Schilling et al., 1980) These data indicate large variations in the region, with high values for $^{87}Sr/^{86}Sr$, La/Sm, K, Rb, Cs, F, Br, and Cl, reaching two broad maxima at 45°N and 38°N latitude. Similar variations have been observed along the Reykjanes Ridge, with the Sr and Pb isotopes becoming more radiogenic toward Iceland (Hart et al., 1973; Sun et al., 1975). It is important to note that the maximum $^{87}Sr/^{86}Sr$ values near the Reykjanes Ridge (.70306) are much lower than those observed near the Azores Platform (up to .70359), while both of these regions are higher than normal MORB values (.7023 to .7028).

Dredged basalts from the South Atlantic, the Indian Ocean, East Pacific Rise, and the Galapagos spreading center (in addition to the samples discussed in chapter 3) allow an evaluation of global

Figure 4.1 Sketch map of the mid-ocean ridges with the locations of the basaltic glass samples described in this study (indicated by stars).


GREENLAND
JAN MAYEN
ICELAND
REYKJANES RIDGE
NORTH AMERICA
EUROPE
AZORES
JUAN de FUCA RIDGE
MID-CAYMAN RIDGE
AFRICA
EAST PACIFIC RISE
GALAPAGOS SPREADING CENTER
SOUTH AMERICA
MID ATLANTIC RIDGE
CARLSBERG RIDGE
CENTRAL INDIAN RIDGE
• TRISTAN da CUNHA I.
• GOUGH I.
INDIAN OCEAN TRIPLE JUNCTION
BOUVET TRIPLE JUNCTION
BOUVET I.

variability. Many of these samples come from ridge segments that would be considered normal, such as the East Pacific Rise and the Carlsberg Ridge, others, such as those from the Bouvet triple junction, are classified as enriched type MORB (Dickey et al., 1977). Although it is impossible to characterize the world ridges on the basis of a single study, these samples provide an opportunity to compare normal and enriched type MORB from a number of localities.

B. Results and Discussion: Global Variations

1. Overall variations

The helium concentrations and isotopic compositions of basaltic glasses analyzed in this study are listed in tables 4.1, 4.2, and 4.3. Since the intent was to document global variations, most of these analyses were performed by crushing in vacuo. As discussed earlier, there is no isotopic fractionation between vesicles and glass, and the ease of the crushing extraction allowed more analyses to be performed. Some of the North Atlantic samples were crushed and melted to confirm that there is no isotopic fractionation between vesicles and melt. In agreement with the conclusions reached in chapter 3, the partitioning experiments between glass-vesicle indicate that no isotopic fractionation is involved in these processes. For the sixteen glass samples analyzed by more than one extraction method (see table 4.1), the "crushed" and the "melt" helium are isotopically indistinguishable at the .5 percent level, which is within the experimental uncertainty.

Although the geographic sample coverage is biased in favor of those regions that have been studied in the most detail (i.e., North and South Atlantic), these data allow some qualitative statements about

Table 4.1: ^4He Concentrations (x 10^6 ccSTP/g) and $^3He/^4He$ Ratios (x 10^5) For Three Different Extraction Methods

		MELTED				CRUSHED				POWDER MELTED			
Sample	Latitude	^4He	±	$^3He/^4He$	±	^4He	±	$^3He/^4He$	±	^4He	±	$^3He/^4He$	±
CH 98 15-505	27.77					4.64	.2	1.22	.01				
CH 98 14-107	29.28					15.7	.5	1.23	.01				
CH 98 12-301	30.17					3.3	.1	1.20	.01				
CH 98 11	30.68					2.7	.1	1.19	.01				
TR 123 5D-3	32.62	7.8	.3	1.36	.02	9.1	.8	1.34	.02				
TR 123 5D-5	32.62									.77	.02	1.34	.03
TR 123 5D-6	32.62					11.2	.9	1.34	.01	1.16	.03	1.37	.02
TR 123 4D-sg	33.37					1.91	.02	.95	.01				
TR 123 4D-7	33.37					.750		.98					
TR 123 1D-5	34.23	9.0	.2	1.13	.01								
TR 123 1D-6	34.23	9.1	.2	1.10	.01								
TR 119 7D-SG	35.33	10.0		1.11	.01								
TR 119 6D-6	35.84					5.2	.1	1.12	.01	.71	.02	1.13	.02
AII 73 16-5-5	36.71					.84	.01	1.09	±.02				
TR 89 21D sg	38.43					<.005	.--	.--	.--				
TR 154 10D-3	38.70					.07	.02	1.01	.10	<.005	.--	.--	.--
TR 154 21D-4	38.89					.03	.01	.90	.10	<.01	.--	.--	.--
TR 154 8D-1	39.20	<.009	.--	.--	.--								
TR 154 8D-3	39.20					.44	.03	1.04	.05				
TR 89 30D-10	39.63	5.2	.2	1.13	.01	3.9	.1	1.13	.01	1.30	.03	1.13	.02
TR 89 30D-2	39.63	6.7	.1	1.13	.01								
TR 154 20D-3	39.76	3.1	.1	1.06	.01								
TR 154 7D-2	39.94					5.4	.1	1.10	.01	.82	.01	1.11	.03
TR 154 19D-3	40.74					3.68	.03	1.00	.01				
TR 154 18D-2	41.18					2.35	.06	1.04	.01				
TR 154 17D-2	41.67	4.6	.1	1.02	.01	1.98	.04	1.04	.02	1.01	.02	1.04	.02
TR 154 16D-3	42.39	3.4	.1	.97	.03	1.82	.03	1.00	.01	1.79	.03	1.01	.02
TR 154 15D-2	42.79					1.44	.02	1.04	.01				
TR 154 12D-1	43.37					<.01	.--	.--	.--				
TR 154 13D-2	44.00					8.8	.4	1.03	.01	.51	.01	1.04	.03
TR 154 14D-4	44.82	5.3	.1	1.08	.01	4.2	.1	1.08	.01	1.26	.03	1.08	.02
TR 138 1D-3	46.23					4.8	.1	.98	.01	.10	.01	.96	.05
TR 138 2D-3	47.05					3.6	.1	.95	.01				
TR 138 5D-2	49.52					2.39	.06	1.11	.01				
TR 138 6D-1	50.04					6.1	.1	1.19	.01	.44	.02	1.23	.03
TR 138 7D-1	50.46	9.1	.3	1.13	.01	3.8	.1	1.18	.01				
TR 138 8D-1	51.28					12.7	.8	1.17	.01	1.64	.01	1.17	.03
TR 138 9D-2	51.56					5.8	.2	1.30	.01	1.36	.03	1.31	.02
TR 138 11D-1	52.01					10.1	.3	1.37	.01	1.80	.04	1.35	.02
TR 100 13D	52.48					14.4	.7	1.54	.02	.93	.03	1.52	.02

Table 4.2: Helium results:

Dredged Glasses from the Atlantic, Indian, and Pacific Oceans

Sample	Location	^4He $x10^{-6}$ cc^{STP}/gram	σ	$^3He/^4He$ R/RA	σ
North Atlantic					
AII 20 3-2	~11°N	9.2	.2	9.20	.13
AII 96 18-1	23°31.5'N, 44°49.1'W	9.4	.3	8.40	.12
G104 25-2	23°32.0'N, 44°57.4'W	13.4	.5	8.35	.11
South Atlantic					
AII 107-7 2-38	46°12.8'S, 14°02.8'W	5.5	.6	7.75	.16
AII 107-7 4-4	42°54.9'S, 16°22.2'W	5.5	.1	8.37	.12
AII 107-7 6-20	41°14.9'S, 16°36.2'W	.75	.01	8.08	.14
AII 107-7 7-10	40°26.3'S, 16°44.9'W	9.9	.4	7.71	.11
AII 107-7 10-1	38°52.9'S, 16°14.4'W	1.76	.04	8.16	.18
AII 107-7 13-1	37°50.0'S, 17°08.5'W	12.5	.5	8.07	.10
AII 107-7 17-71	35°16.7'S, 15°44.1'W	7.6	.3	8.31	.10
Carlsberg Ridge					
NOAA M79 2-53	9°49.5'N, 57°56.7'E	.41	.01	8.58	.17
		8.11*			
M79 3-10	9°49.9'N, 57°57.6'E	.393		8.00	.16
M79 6-9	3°47.0'N, 63°52.0'E	13.3	.6	8.48	.10
M79 7-57	3°41.9'N, 63°53.5'E	11.9	.6	8.49	.1
M79 9-96	1°39.0'S, 67°46.4'E	11.6	.6	8.66	.1
		.41*	.01	8.22	.25
M79 11-5	5°21.3'S, 68°37.2'E	10.1	1.0	8.89	.18
M79 12-3	5°17.0'S, 68°31.9'E	.70	.02	8.36	.18
Pacific Ocean					
USNM 1113157-D805	Galapagos S. C. 2.60'N, 95.33°W	-----	---	6.85	.09
USNM 1113157-D557 (VG D08)	Galapagos S. C. 2.44°N, 95.62°W	2.87	.08	7.00	.08
G79-4 D1-4	East Pacific Rise 22°50'N, 108°08'W	8.5	.10	8.31	.12
G79-4 D 14	East Pacific Rise 22°26'N, 108°23'W	9.5	.1	8.49	.12
		13.4*	.5	8.35	.12
Alv 972-1	East Pacific Rise 22°55.5'N, 108°05.5'W	7.0	.1	8.24	.12
		13.4*	.6	8.31	.12

All extractions performed by crushing, except those denoted by (*), which were powders melted, after crushing.

Table 4.3: Helium results:
Dredged glasses from the Bouvet triple junction

Sample	Location*	^4He $x10^{-6}$ cc^{STP}/gram	σ	$^3He/^4He$ R/RA	σ
CH 115 37 1D-1	54°35.9'S, 00°58.2'W	.176	.007	7.11	.4
CH 115 37 1D-11	54°35.9'S, 00°58.2'W	.52	.03	7.66	.4
AII 107-6 33-1	54°38.9'S, 00°04.8'W	.70	.01	7.44	.10
AII 107-6 47-11	54°01.3'S, 03°32.0'E	.218	.004	9.98	.4
CH 115 508D-1	54°13.7'S, 04°03.1'E	.121	.002	12.9	.4
		.053	.008	11.9	2.0
AII 107-6 56-21	54°22.9'S, 05°12.0'E	1.08	.02	7.45	.13
AII 107-6 56-27	54°22.9'S, 05°12.0'E	2.22	.03	7.12	.10
AII 107-6 57-5	54°01.5'S, 07°15.4'E	3.09	.07	7.46	.19
AII 107-6 57-25	54°01.5'S, 07°15.4'E	3.49	.09	14.3	.3
		3.58	.05	14.1	.2

*Locations from Dickey et al. (1977) and Farmer and Dick (1981)

global variations in MORB (all the analyses reported in this chapter and in chapter 3 are displayed in histogram form in figure 4.2) The $^{3}He/^{4}He$ ratio varies from 6.8 to 14.2 x atmospheric. On the basis of presently available data, this appears to characterize the range of values for MORB. Slightly higher $^{3}He/^{4}He$ ratios have been reported for Reykjanes Ridge basalts (up to 15.0 x atmospheric; Poreda et al., 1980), which are clearly related to Icelandic volcanism (see chapter 5).

The histogram shows that most MORB glasses have $^{3}He/^{4}He$ ratios between 7.0 and 9.0; higher values are quite rare. It is also clear that the sample population does not form a symmetric distribution about a mean value. Based on other geochemical evidence, this could be due to the superimposition, or perhaps mixing, of several sample populations. For example, most the samples in figure 4.2 with $^{3}He/^{4}He$ ratios less than 7.8 x atmospheric are basalts with incompatible trace element enrichments and high $^{87}Sr/^{86}Sr$ ratios (i.e., samples from 33-50°N in the North Atlantic, and the South Atlantic near Bouvet Island). Several samples from the western end of the Galapagos spreading center (95°W) also have low $^{3}He/^{4}He$ ratios, but may not be enriched to the same extent. Clague et al. (1981) have described major and trace element geochemistry of samples from the same dredges; they found that these basalts are distinct from those sampled from 85°W, and are slightly enriched in light rare earths with respect to normal MORB.

2. Helium in normal MORB

Using the trace element and isotopic criteria described above, the samples that could be considered normal MORB were selected from those

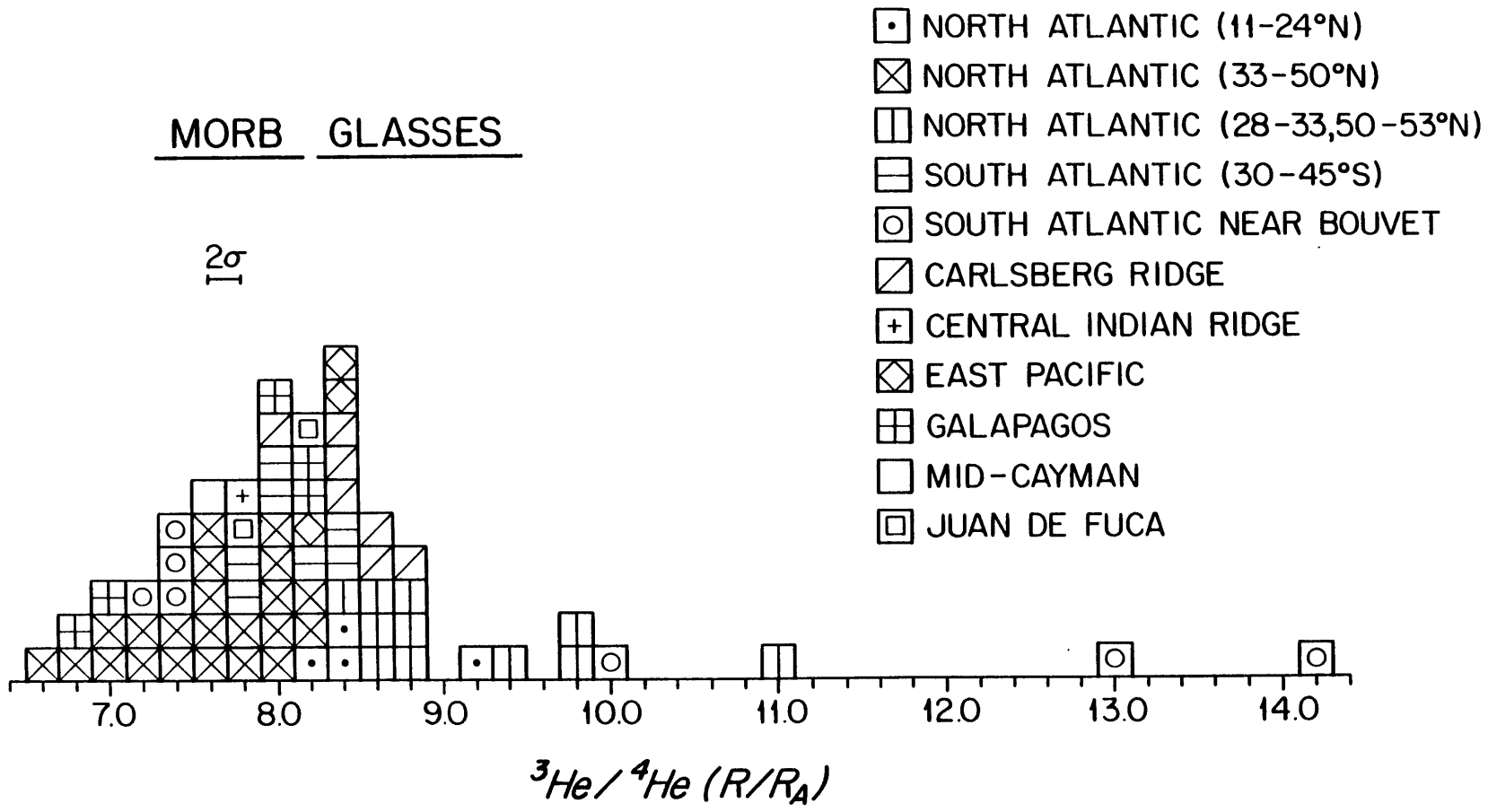


Figure 4.2: Histogram of all $^3He/^4He$ measurements on MORB glasses reported in this study.

listed tables 4.1, 4.2, and 4.3, and in chapter 3. The $^3He/^4He$ ratios from these normal MORB samples are plotted on the histogram in figure 4.3, and appear to form a normal distribution about a mean value of 8.4 x atmospheric (with $1\sigma = .3$). While trace element or isotopic data from various sources (see figure 4.3) is available for most of the samples, no data was available for the Carlsberg Ridge samples, and they were assumed to be normal MORB. It is also important to note that several samples that would be classified as normal MORB by most criteria have higher $^3He/^4He$ ratios. The most notable example is AII107-6 57-25, which is discussed in more detail below. Nevertheless, the apparent gaussian distribution shown in figure 4.3 allows the choice of a normal MORB $^3He/^4He$ ratio of 8.4 x atmospheric. Although this must be confirmed by more analyses, it provides a useful value with which we can compare the other results.

It is also important to establish the range of concentrations in MORB glasses. As discussed in chapters 1 and 3, the concentration of helium in oceanic crust has implications for the atmospheric ^3He budget. Additionally, if a "typical" pre-eruptive magmatic concentration can be estimated, it may be possible to infer concentration. The total helium concentrations for the normal MORB samples are plotted as a histogram in figure 4.4. The common occurrence of samples with He concentrations greater than 10^{-5} cc STP/gram supports the conclusions of chapter 3. While vesiculation and posteruptive degassing clearly can have important effects on these concentrations, these data suggest that typical MORB concentrations are ~1to 3 x 10^{-5} cc STP/gram. Concentrations lower than this (e.g.

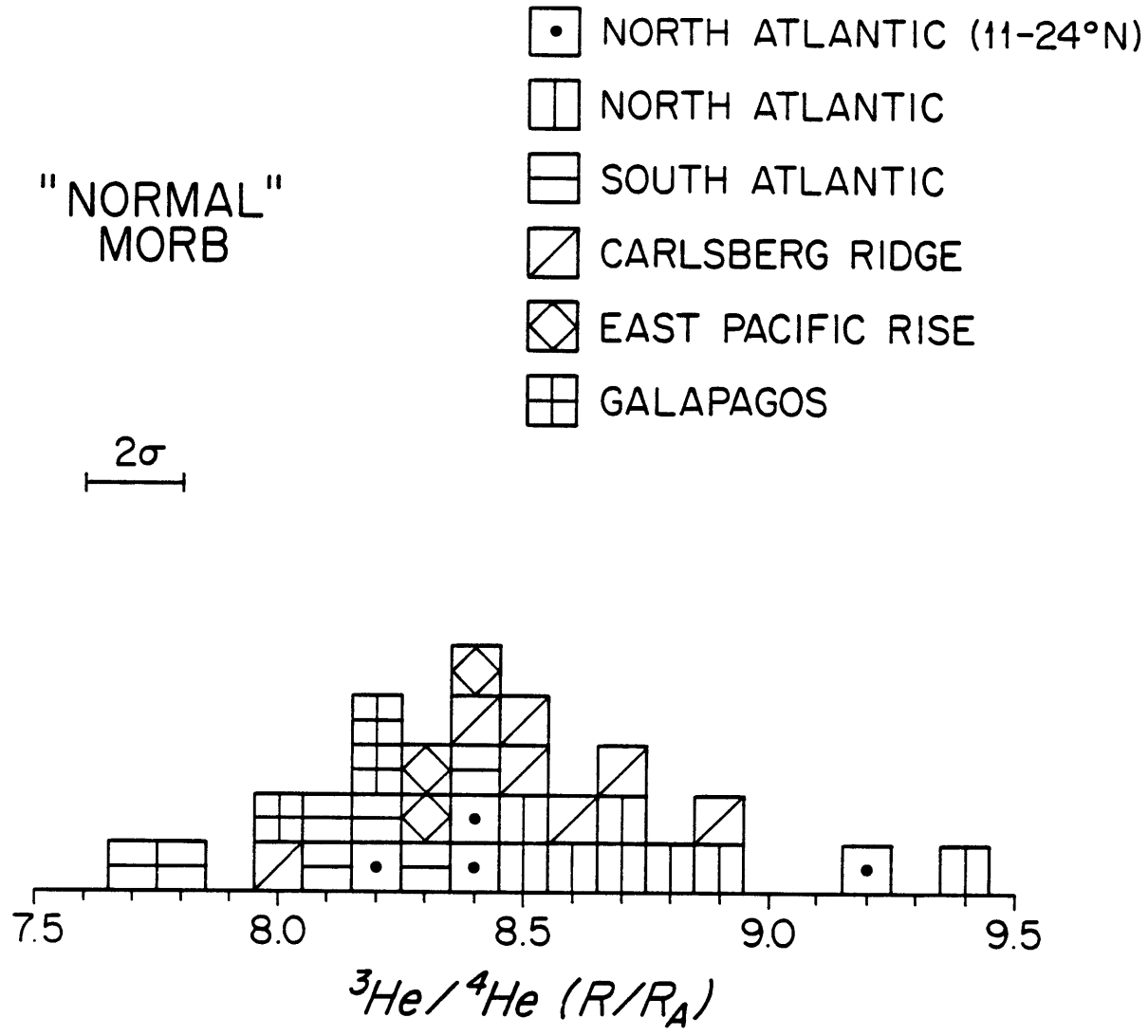


Figure 4.3: Histogram plot of $^3He/^4He$ measurements on all glasses that could be classified as normal MORB, based on trace element and isotopic criteria (see text). Trace element and isotopic date for these samples from: North Atlantic (11-24°N): Machado et al. (1982), Bryan et al., 1981; North Atlantic: White and Schilling (1978); East Pacific Rise: J. Bender (personal communication); Galapagos: S.R. Hart (personal communication).

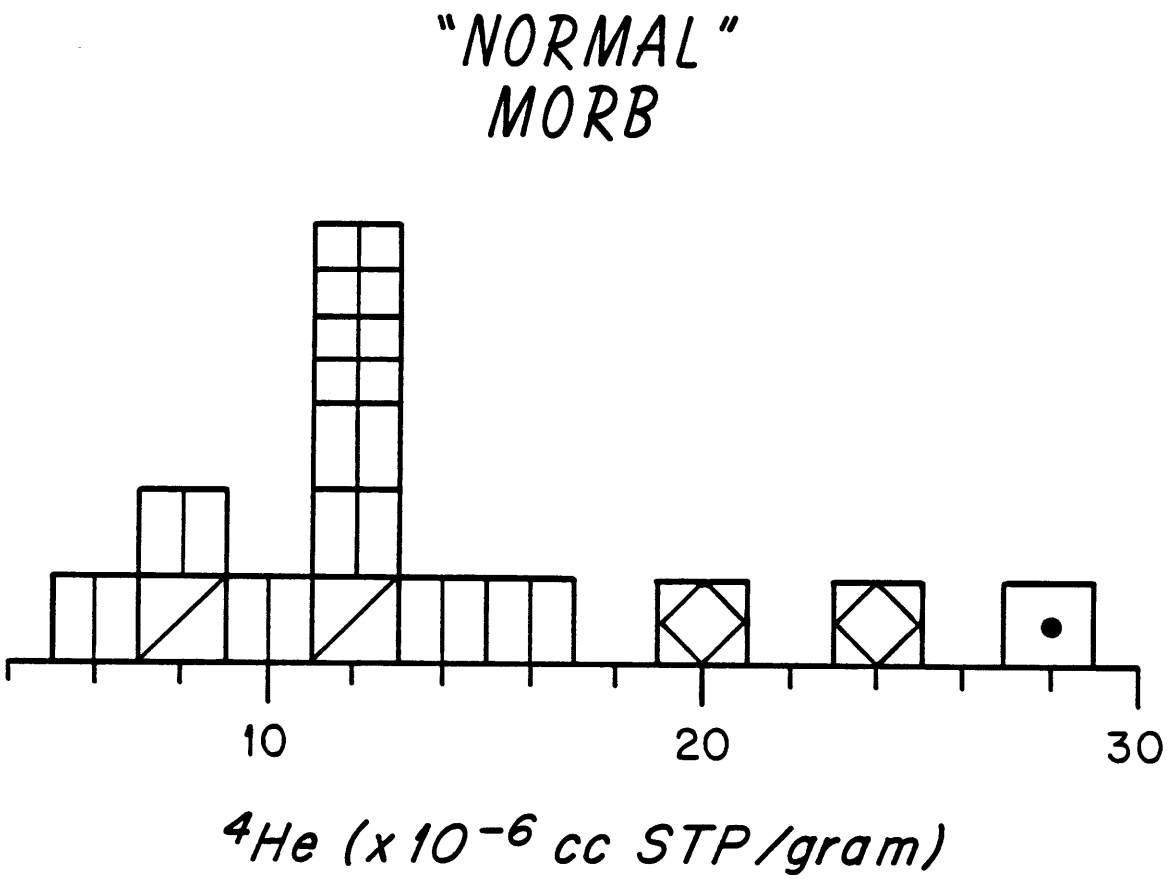


Figure 4.4: Histogram of helium concentrations for normal MORB samples (only those for which total He was determined). Symbols as in figure 4.3.

Craig and Lupton, 1976, 1981) may be a result of gas loss (see below).

C. Results and Discussion: Central North Atlantic

1. Helium isotopic variations

The dredge locations of the North Atlantic samples, from 28° to 52°N latitude, are shown with respect to the major tectonic features in figure 4.5. Helium isotopic results for these samples are listed in table 4.1 and plotted with respect to latitude in 4.6. Also shown for comparison are the published $^{87}Sr/^{86}Sr$ variations for the mid-Atlantic ridge (Hart et al., 1973; White et al., 1976), and helium isotopic results for the Reykjanes Ridge reported by Poreda et al. (1980). The maxima in $^{87}Sr/^{86}Sr$ at 45°, 39° and 35°N are also observed in La/Sm, Rb, Cs, Sr, Cl, Br, and F (Schilling, 1975; White et al., 1976; Schilling et al., 1980). These geochemical variations have been interpreted as evidence for a mantle plume (Schilling, 1975), or an upper mantle enrichment event such as metasomatism (Schilling et al., 1980). If such a mantle reservoir were less degassed, one might expect it to have had a higher time-integrated $^{3}He/(Th+U)$ ratio and hence a higher present day $^{3}He/^{4}He$ ratio. As shown in figures 4.6 and 4.7, however, there is no association between high $^{3}He/^{4}He$ and high $^{87}Sr/^{86}Sr$. In fact, there is an overall negative correlation between $^{3}He/^{4}He$ and $^{87}Sr/^{86}Sr$, in the sense that the maxima at 45° and 37°N are accompanied by relatively low values in $^{3}He/^{4}He$. Using the normal MORB value of 8.4 x atmospheric (1.16×10^{-5}) defined in the previous section, the values obtained at these locations are significantly lower; the lowest value being 9.36×10^{-6} (6.76 x atmospheric, for TR138 2D-3 at 47.05°N).

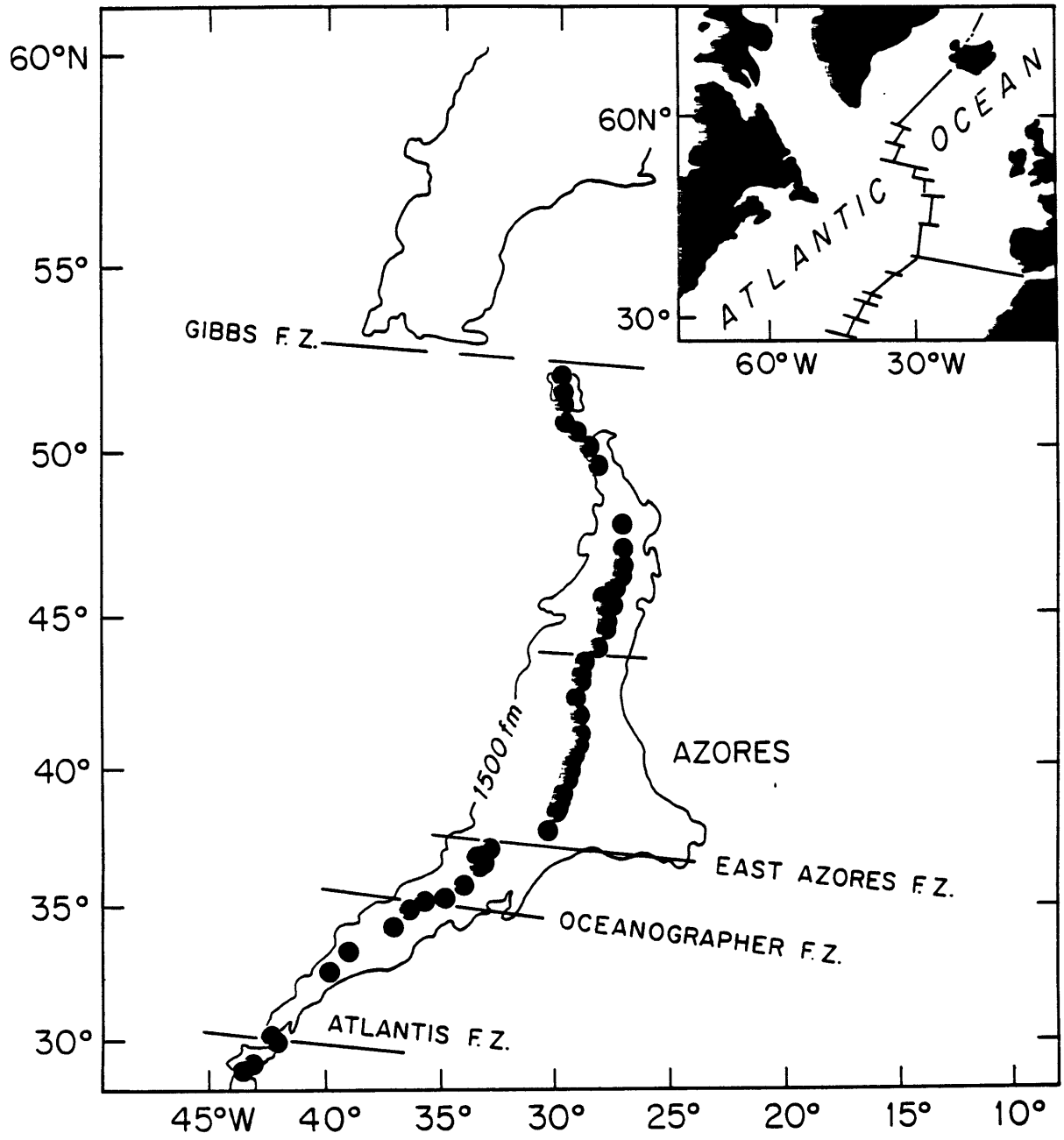
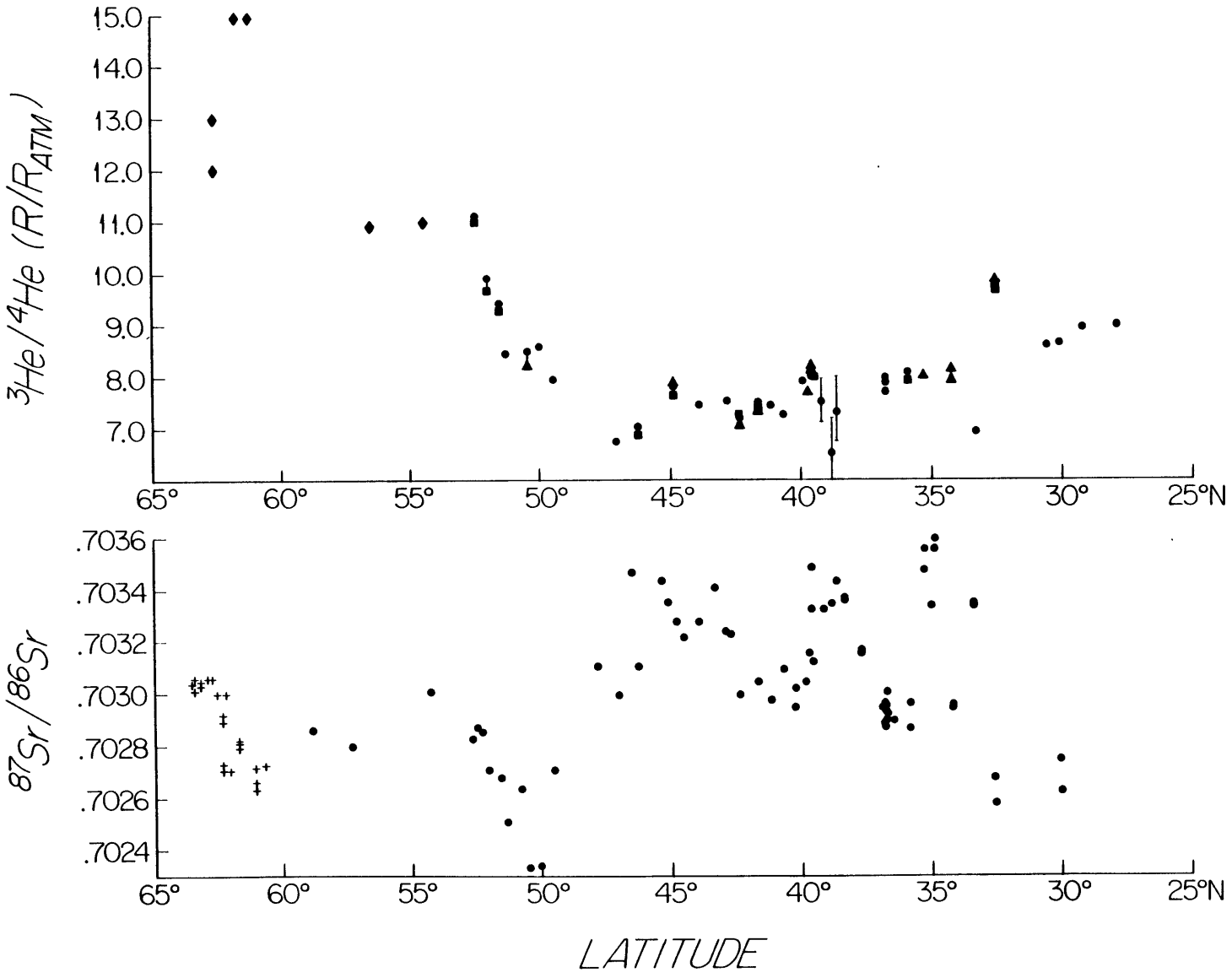


Figure 4.5: Dredge locations along the mid-Atlantic ridge (27-53°N) that are discussed in this section.

Figure 4.6: (a) Helium isotopic variations in basaltic glasses along the mid-Atlantic ridge. Different symbols denote different extraction methods used in this study: (▲) = melting in vacuo; (●) = crushing in vacuo, and (■) = melting of powder that was previously extracted by crushing (see text). Solid lines connect different extractions of the same sample. Where error bars are not shown for these $^{3}He/^{4}He$ analyses, they are within the field of the symbol. Points denoted by (◆) were taken from Poreda et al. (1981).
(b) Strontium isotopic variations along the Mid-Atlantic Ridge [from White and Schilling (1978), and Hart et al. (1973)].

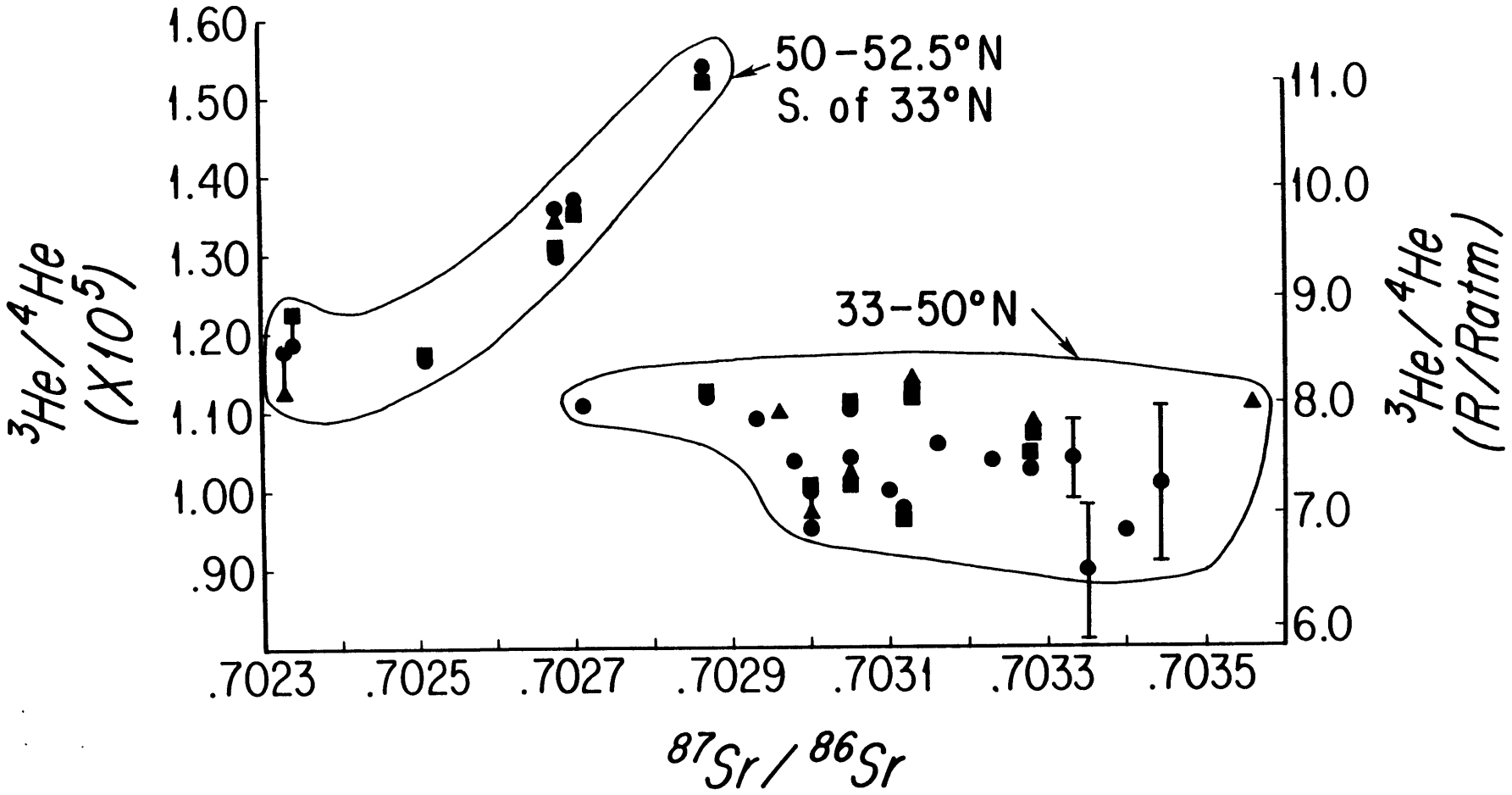

15.0
14.0
13.0
12.0
11.0
10.0
9.0
8.0
7.0
$^3He/^4He$ (R/R_{ATM})
65°
60°
55°
50°
45°
40°
35°
30°
25°N
.7036
.7034
.7032
.7030
.7028
.7026
.7024
$^{87}Sr/^{86}Sr$
65°
60°
55°
50°
45°
40°
35°
30°
25°N
LATITUDE

In detail, the geographical variability reveals two distinct provinces. The samples between 50° and 53°N show quite a good positive correlation between $^{3}He/^{4}He$ and $^{87}Sr/^{86}Sr$, in addition to an increase in $^{3}He/^{4}He$ ratio with latitude (see figure 4.7). It appears that these relatively high $^{3}He/^{4}He$ ratios (8.5-11.1 x atmospheric) extend to the entire ridge north of 50°N, as suggested by published values for Reykjanes Ridge basalts (Poreda et al., 1980) and hot springs in the neo-volcanic zone of Iceland (Polak et al., 1975). The value reported by Poreda et al. (1980) for glass from 55°N is close to our result for 52.5°N (11.1 x atmospheric, see figure 4.6).

South of 33°N, the $^{3}He/^{4}He$ ratios are also relatively high (8.6-9.0 x atmospheric) for the samples with low $^{87}Sr/^{86}Sr$ ratios. While we do not have Sr isotopic ratios for four of the five samples south of 33°N, the values reported by White and Schilling (1978; figure 4.6b) should be applicable. Sun et al. (1979) have also reported similar $^{87}Sr/^{86}Sr$ ratios from this part of the ridge. There appears to be a distinct break at 33°N rather than the gradient that is evident near 50°N (see figure 4.6a). This may, however, be an artifact of the sample distributions.

In contrast, the samples from 33-50°N do not reveal a positive correlation between Sr and He isotopes (see figure 4.7). For a fairly large range in $^{87}Sr/^{86}Sr$ for MORB (.7027 to .7035), there is a relatively small variation in $^{3}He/^{4}He$ (6.9-8.1 x atmospheric), which results in the scattered field shown in figure 4.7. This has important implications for characterization of the mantle source regions for oceanic basalts, since the two provinces require distinctly

Figure 4.7: $^{3}He/^{4}He$ vs. $^{87}Sr/^{86}Sr$ for the mid-Atlantic ridge, 30-52.5°N latitude. Symbols and error bars are the same as in figure 4.6.


50-52.5°N
S. of 33°N
33-50°N
1.60
1.50
1.40
1.30
1.20
1.10
1.00
.90
11.0
10.0
9.0
8.0
7.0
6.0
.7023
.7025
.7027
.7029
.7031
.7033
.7035
$^3He/^4He$ (X10^5)
$^3He/^4He$ (R/Ratm)
$^{87}Sr/^{86}Sr$

different sources. The larger amounts of radiogenic ^{87}Sr in the 30-50°N samples are apparently associated with low $^{3}He/^{4}He$ ratios, whereas north of 50°N and south of 33°N there is an association between radiogenic ^{87}Sr and higher $^{3}He/^{4}He$ ratios. Possible mechanisms for this are discussed below.

2. Concentration variations and glass-vesicle partitioning

Given the $^{3}He/^{4}He$ variation, and the implied He/U variation in the source regions, one might expect systematic He concentration variations for these samples. However, there are several processes that make the "mantle" concentration difficult to infer from measurements on the glasses. The most important is gas-melt partitioning, since helium is quite favorably partitioned into the vesicles that are ubiquitous in oceanic basalt glasses (see chapter 3). This process is important to the present study, because the vesicularities are quite variable and range up to 24 volume percent (Schilling et al., 1980). Following the procedure discussed earlier, the helium was extracted from relatively large grains of glass (larger than 2mm in size) to minimize the opening of vesicles before analysis. The total concentration can be determined from the helium released by melting a representative sample of the chips (column 1 of table 4.1), or melting the powder remaining after crushing (column 3 of table 4.1) and adding it to the helium released by crushing (column 2 of table 4.1). Comparison of total concentrations obtained by these two methods shows that they agree within the experimental uncertainty.

The latitudinal variation in total ^{4}He concentration and vesicularity is shown in figure 4.8a. The vesicularities shown in

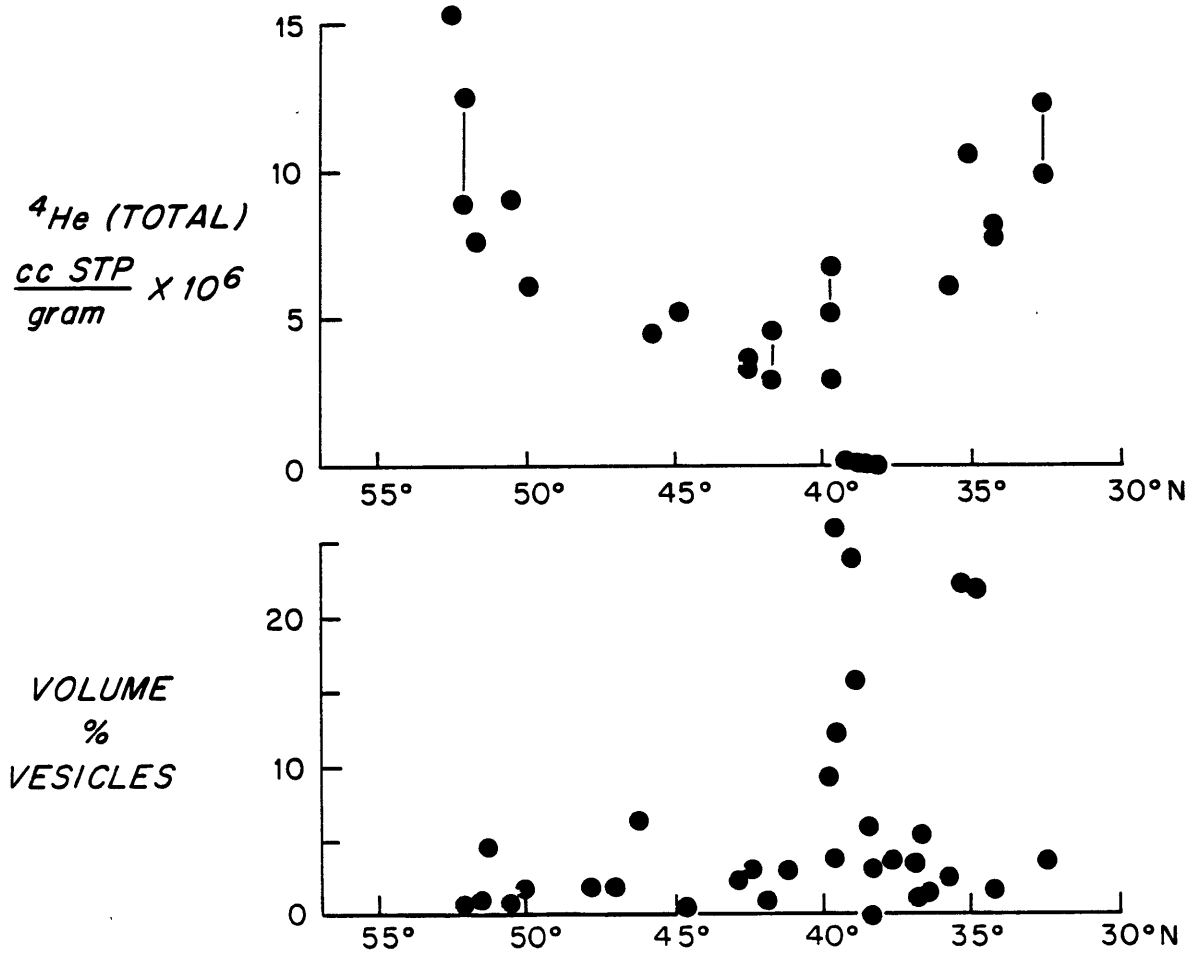


Figure 4.8: (a) Total He concentration variations (in cc STP/g) along the mid-Atlantic ridge.
(b) Vesicularity variations along the mid-Atlantic ridge [from (Schilling et al., 1980)].

figure 4.8b (from Schilling et al., 1980) were determined by point counting thin sections that included the glassy rim and variolitic zone of the samples. Although these vesicularity values were not obtained from the same sample split analyzed for He (for detailed studies of partitioning, see chapter 3), we can use these results to examine geographic variations in helium concentrations. The maximum vesicularity near the Azores Platform (35°N) is presumably due to the shallow depth of the ridge crest, and larger quantities of volatiles present in the mantle (Schilling et al., 1980). A partial explanation for low He concentrations in samples from this region may be that vesiculation has stripped the helium out of the melt. Loss of ^4He can take place either by pre-quenching degassing of the magma, or by loss during fracturing of the glass (on the sea floor, during the dredging process, or if the vesicles are large, when the glass is removed from the rock in the laboratory).

As seen from the latitudinal variations in total helium concentrations and vesicularities (figure 4.8), there is good evidence that helium has been lost from some of the samples by sea-floor degassing. This is further illustrated by the negative correlations between total He and vesicles (figure 4.9a), and total He and Cl (figure 4.9b). The negative correlation between vesicularity and ^4He is to be expected, since the samples with the most vesicles have undergone the most gas loss.

As shown by Unni and Schilling (1978), Cl and Br are not partitioned favorably into a gas phase until extremely high vesicularities are attained (~50 percent). Rowe and Schilling (1979)

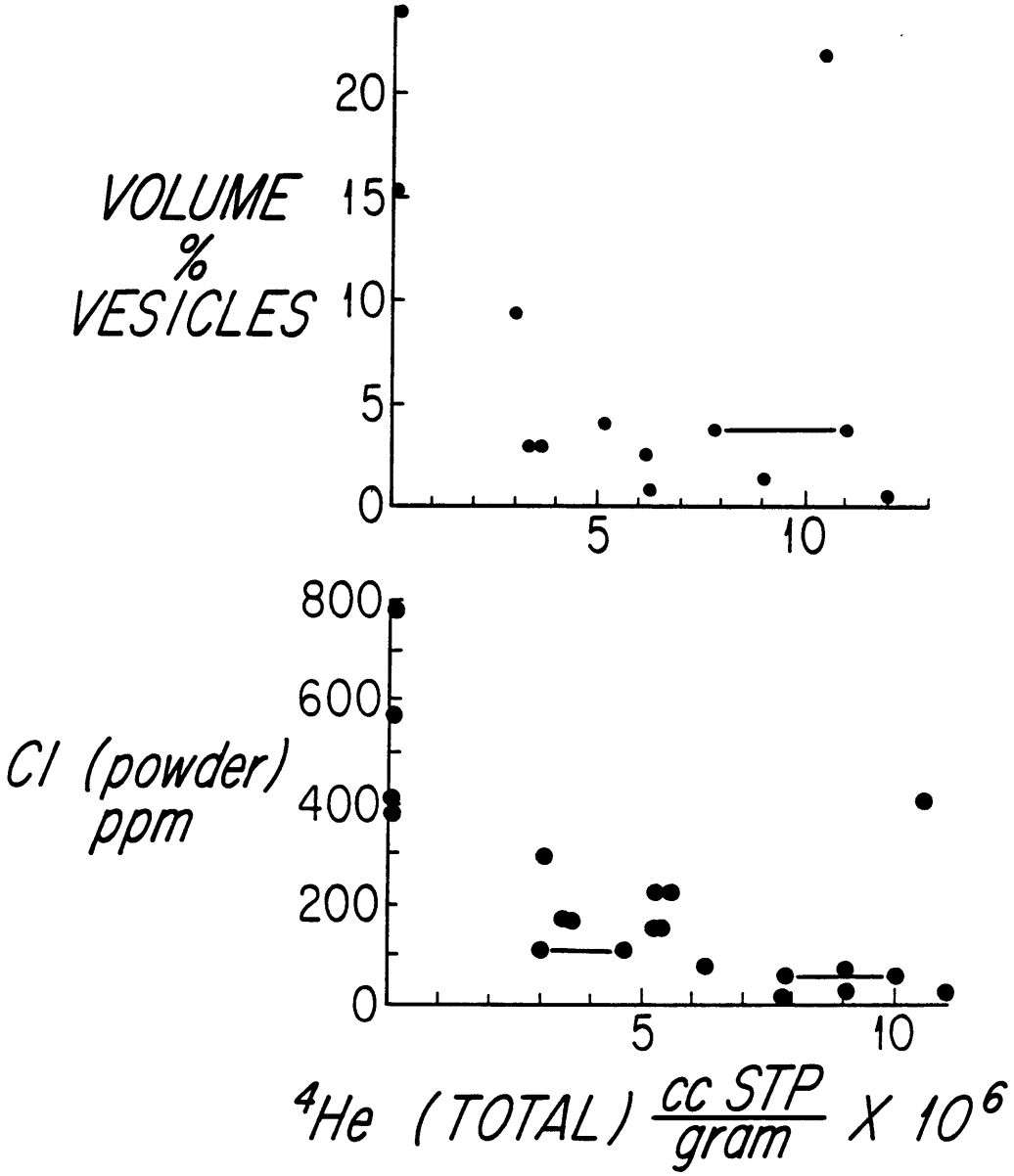


Figure 4.9: (a) Total ^4He vs. volume percent vesicles.
(b) Total ^4He vs. Cl content.

further suggested that these elements are not partitioned favorably into CO_2-rich vesicles, but do partition into H_2O-rich vesicles, thus explaining lack of degassing until extremely shallow depths on the Reykjanes Ridge. This hypothesis was supported by the study of the present samples for Cl, Br, and F by Schilling et al. (1980). The negative correlation between ^4He and Cl (figure 4.9b) can therefore be partially explained by different partitioning behavior: He is favorably partitioned into CO_2 vesicles, while Cl is not. Therefore, if the maxima in volatile concentrations (Cl, Br, and F) near the Azores Platform (Schilling et al., 1980) were accompanied by large mantle helium concentrations, sea-floor degassing has erased the evidence. Unfortunately, it is not clear how much He and Cl may covary in the mantle before being affected by vesiculation, so the negative correlation shown in figure 4.9b may simply reflect partitioning during gas loss.

Given the complications in interpreting He concentrations, it is nevertheless important to examine any possible relationship between He and $^3He/^4He$. As shown in figure 4.10, samples with higher $^3He/^4He$ ratios generally have higher total ^4He concentrations. However, there are two distinct groups that correspond to the same groupings shown in the $^3He/^4He$ vs $^{87}Sr/^{86}Sr$ diagram (figure 4.7). This relationship can be the result of several different causes. First, it is possible that the concentrations in the glasses reflect, to some extent, the mantle concentrations. In this case, the association between the high $^3He/^4He$ ratios and the higher concentrations is due to a higher time-integrated He/(Th+U) ratio in

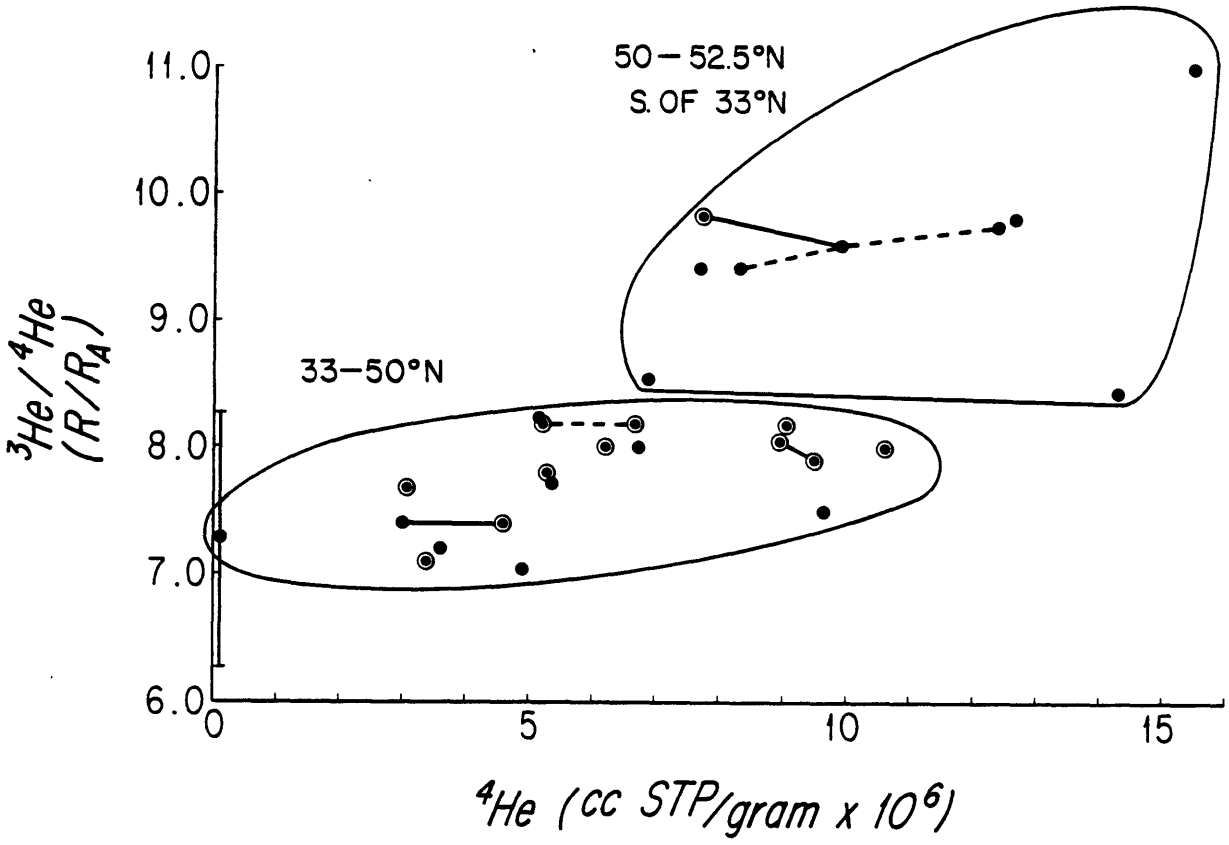


Figure 4.10: Total ^4He vs. $^3He/^4He$. (●) denotes that the total concentration was calculated as the sum of crushing and powder-melted concentrations, and (◉) denotes the total concentration obtained by the melting of chips. Solid lines connect duplicate analyses of the same sample, and dashed lines connect samples from the same dredge.

the source region. Unfortunately, we cannot ignore the effects of gas loss (by vesiculation) and fractional crystallization upon the apparent concentrations. Clearly, the samples with the lowest concentrations are also highly vesicular (see figures 4.8 and 4.9). Since these vesicular samples occur predominantly near the Azores Platform, the two groups in figure 4.10 must also reflect this effect.

3. Isotope systematics

Before discussing possible mechanisms for the helium isotopic variations, previous studies of the region should be reviewed, particularly since the isotopic variations are well documented with respect to Sr, Nd, and Pb isotopes. The general negative correlation between $^{143}Nd/^{144}Nd$ and $^{87}Sr/^{86}Sr$ observed for oceanic basalts (DePaulo and Wasserburg, 1976; Richard et al., 1976; O'Nions et al., 1977) has been shown to apply to the North Atlantic, including the region studied here (O'Nions et al., 1979). In addition, North Atlantic MORB display a striking correlation between radiogenic Sr and Pb (Cohen et al., 1980; Dupre and Allegre, 1980), lending further credence to coherent fractionations in U/Pb, R/Sr and Nd/Sm. The Nd-Sr inverse correlation has allowed the estimation of "bulk earth" values for closed system chondritic evolution (c.f. O'Nions et al., 1977; Allegre et al., 1979). If this is interpreted in the simplest manner, basalts with $^{87}Sr/^{86}Sr$ ratios closest to the bulk earth value (~.7047) are the least depleted or the most "primitive." Oceanic island basalts (OIB) fall on the same trend, but lie closest to bulk earth values, defining a field with higher $^{87}Sr/^{86}Sr$ and lower $^{143}Nd/^{144}Nd$ than MORB. In contrast to the Nd and Sr systematics,

the Pb isotopes do not display a simple relation between MORB and OIB (Allegre et al., 1980; Sun, 1980). This has recently led several authors to suggest that to explain all the isotopes, the addition of a subducted crustal component into the mantle is required (Hofmann and White, 1980; Chase, 1981; Zindler, 1981).

If the enriched MORB that lies closest to bulk earth on the Nd-Sr diagram is more primitive with repect to helium, one would expect higher $^{3}He/^{4}He$ ratios near the Azores Platform and 45°N. The helium results (figure 4.6) show that this is not the case; the observed $^{3}He/^{4}He$ ratios for these regions are among the lowest reported in the literature, suggesting a lower $^{3}He/(Th+U)$ ratio than typical MORB. On the other hand, the basalts from 50-52.5°N and 27-33°N have $^{87}/^{86}Sr$ ratios that range from low to slightly higher than normal MORB, but are characterized by higher $^{3}He/^{4}He$ ratios. These two distinct trends are illustrated by the two fields in figure 4.7, and the geographic variability shown in figure 4.6. While Poreda et al. (1980) noted that their helium results from the Reykjanes Ridge (plotted as diamonds in figure 4.6) show no local correlation with $^{87}Sr/^{86}Sr$, these data support the existence of a high $^{3}He/^{4}He$ province that extends north of the region studied here.

The helium isotopic variations for the North Atlantic illustrate that there are distinct provinces, each with unique isotopic characteristics:

Type A: The high $^{3}He/^{4}He$ regions north of 50°N which have low to slightly enriched $^{87}Sr/^{86}Sr$ [.7026-.7030, (Hart et al., 1973)].

Type B: The low $^{3}He/^{4}He$ regions near the Azores Platform and 45°N which have high $^{87}Sr/^{86}Sr$ [> .7030 (White et al., 1976)].

Type C: The samples from 27-33°N, which have $^{3}He/^{4}He$ of ~8-9 x atmospheric and $^{87}Sr/^{86}Sr$ between .7023 and .7028 (Hoffman and Hart, 1978).

The unique characteristics of these provinces, and the systematics illustrated in figure 4.10, are best explained by three-component mixing. Thus, the basalts from each of the provinces are mixtures of the different mantle sources. Based on the definition of normal MORB given earlier, and the trends in figure 4.10, one of these sources is inferred to be the depleted upper mantle. All the iostopic variations can then be explained by mixing between two other mantle sources, one with higher $^{3}He/^{4}He$, and one with lower $^{3}He/^{4}He$. For example, the type A province would be produced by mixing between the depleted upper mantle and an undepleted end-member, to generate higher $^{3}He/^{4}He$ ratios.

In this mixing model, the type B characteristics would be produced by mixing between the depleted upper mantle and a source with lower $^{3}He/^{4}He$ and higher $^{87}Sr/^{86}Sr$. This requires the presence of a mantle source region that has had lower $^{3}He/(Th+U)$ ratios for time periods long enough to lower the $^{3}He/^{4}He$ ratios while <u>also</u> having higher Rb/Sr. This component requires some mechanism to lower the $^{3}He/(Th+U)$ ratio while raising the Rb/Sr ratio. Since helium differs from U and Th in volatility, it is reasonable to assume that the mechanism for lowering $^{3}He/(Th+U)$ is degassing. Therefore, the type

B component will be referred to as recycled, since any degassed mantle reservoir has, at some point in the past, seen the earth's surface. Several specific mechanisms can produce the helium and strontium isotopic composition of this recycled reservoir; among the possibilities are 1) contamination of the melts during ascent to the surface; 2) remelting of mantle that has experienced metasomatic events; and 3) remelting of subducted oceanic crust.

O'Hara (1980) has suggested that many of the isotopic variations within oceanic basalts can be explained by contamination from the crust through which they are erupted. While oceanic crust can be expected to have low $^{3}He/(Th+U)$ ratios due to degassing, this seems unlikely to explain the low helium isotopic ratios for several reasons. The oceanic crust at mid-ocean ridges is very young, which means that there has not been much time to accumulate radiogenic ^{4}He. Even in 1 million years, only 10^{-8}ccSTP/gram of ^{4}He will accumulate in normal mid-ocean ridge basalt, which is insignificant compared to the concentrations in most glasses. In addition, the crust is very thin, making any interaction least likely at mid-ocean ridges. Finally, seawater cannot produce the variations because the He/Sr ratio in seawater is so low that a very small interaction would produce little change in the $^{3}He/^{4}He$ ratio but very large variations in the $^{87}Sr/^{86}Sr$.

Another alternative is that the isotopic variations may be caused by metasomatic events in the mantle, or similarly, multiple melting events in which the mantle is enriched by the addition of melt and later remelted (e.g. Erlank and Rickard, 1977). Both these processes

require that helium be separated from Th and U to produce the type B mantle. It is possible that He would be lost by degassing during the metasomatic or melting process, leaving a residue that is relatively enriched in Th and U. However, the precise mechanism of this degassing is unclear. Partial melting alone cannot effectively separate He from U and Th, since He behaves as an incompatible element (see chapters 3 and 5). As was shown by Gast (1968), melting is only effective for separating lithophilic elements from one another in the residue.

We prefer to explain the type B mantle characteristics by the addition of subducted crust into the mantle, which adds sediments or altered crust. This hypothesis is more attractive for several reasons. First, He and Th+U are easily separated by subduction. Helium is lost to the atmosphere, while Th and U are added by hydrothermal alteration, and by the addition of sediments or seawater. Support for this hypothesis is given by other isotopic observations, e.g. basalts from Sao Miguel Island in the Azores island group that lie off the Sr-Nd correlation trend. Hawkesworth et al. (1979) interpreted this as evidence of a recently added sediment component in the mantle. In addition, this model agrees with models suggested by several authors to account for Pb isotope variations (Hofmann and White, 1980; Chase, 1981). Details of possible recycling models are further discussed below, and in chapter 6.

In summary, the observed isotopic variations can be explained by mixing between three distinct mantle reservoirs. The high $^{3}He/^{4}He$ ratios of the type A basalts are consistent with the presence of an undepleted mantle reservoir, which mixes with the normal MORB mantle

source. The lower $^{3}He/^{4}He$ and higher $^{87}Sr/^{86}Sr$ ratios of type B discussed above are best explained by the presence of recycled oceanic crust in the mantle. The end-members for the two distinct trends that mixing produces on the $^{3}He/^{4}He$ vs. $^{87}Sr/^{86}Sr$ diagram (figure 4.7) cannot be conclusively identified on the basis of this data, and are discussed further in chapter 6.

Significantly, basalts from both the Azores Platform (type B) and the Reykjanes Ridge (type A) would be classified as enriched or plume type MORB on the basis of trace element and other isotopic data (e.g. Sun et al., 1977; White and Schilling, 1978). Therefore, the helium isotopes provide an important new way to determine the possible origins for enriched type MORB, and reveal new complexities in the mantle.

It is important to note that several other studies have also documented the existence of distinct geochemical "provinces" in the region discussed here. Schilling (1975) and Bougault and Treuil (1981) observed distinctly different trace element abundance patterns north and south of the Hayes fracture zone (~33°N). Basalts from north of 33°N were characterized by flat to light rare earth enriched abundance patterns, while those from south of 33°N displayed rare earth patterns that were predominantly light rare earth depleted. Melson and O'Hearn (1979), Morel and Hekinian (1980), Sigurdsson (1981), Schilling et al. (1982), and Bryan and Dick (1982) have used major element variations to define geographic groupings that roughly correspond to the provinces observed for the helium isotopes. Sigurdsson (1981) has shown that glasses erupted between 35-53°N have higher total silica and alkalis, while the ridge segments between 29-33°N and 54-70°N are characterized

by Fe enrichment and Al depletion. As shown in the plot of K_2O vs. $^3He/^4He$ (figure 4.11), the $^3He/^4He$ results correspond closely with these major element groups identified by Sigurdsson. Therefore, the low $^3He/^4He$, high $^{87}Sr/^{86}Sr$ province (type B or recycled mantle) is also characterized by light rare earth enrichment, and relatively high silica and alkali contents. The type A province is characterized by high $^3He/^4He$, low $^{87}Sr/^{86}Sr$, Fe enrichment, and Al depletion.

C. Results and Discussion: South Atlantic near the Bouvet Triple Junction

Given the geochemical provinces that occur in the North Atlantic, it is of considerable importance to document whether the different basalt types are globally represented, and to ascertain the origins of the variations. The MORB glass samples discussed in this section were obtained from the South Atlantic near the Bouvet triple junction, the region where the Antarctic, African, and South American plates join (see figure 4.12). Sclater et al. (1976) have discussed the geophysics of this ridge-fracture-fracture type triple junction and the surrounding area. The short ridge segments to the east and west are offset by large fracture zones (see figure 4.12).

Dickey et al. (1977) studied the geochemistry of dredged basalts from the region, and showed that their mantle sources are distinct from those of normal MORB. In particular, they observed high $^{87}Sr/^{86}Sr$ ratios, and enrichments in the light rare earth elements. Based on these parameters, basalts erupted near the Bouvet triple junction have affinities to those erupted between 33 and 50°N on the Mid-Atlantic Ridge.

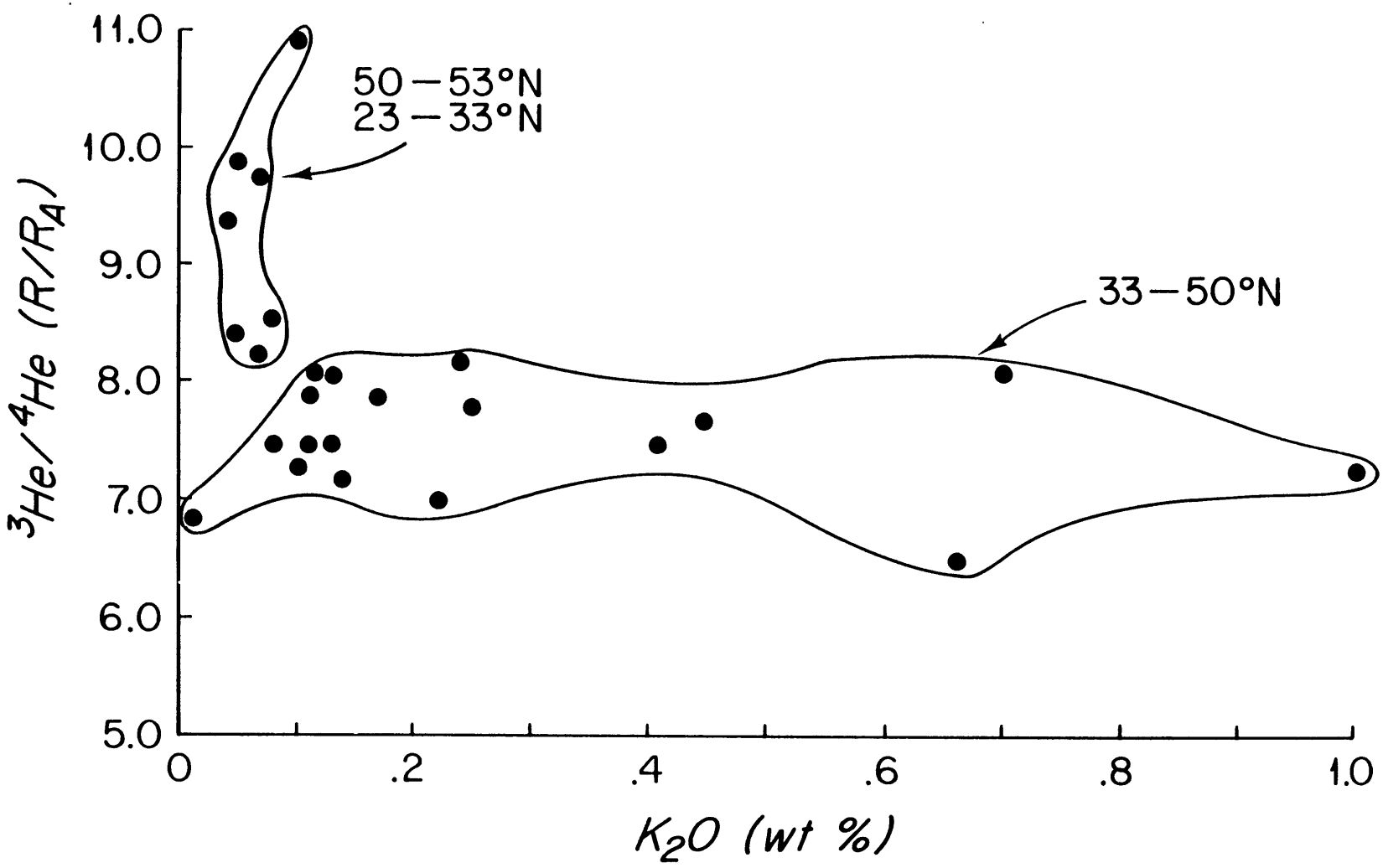


Figure 4.11: $^3He/^4He$ vs. K_2O for North Atlantic samples. Helium data from table 4.1; K_2O from Sigurdsson (1981).

The samples discussed here include several of those studied by Dickey et al. (1977, collected during cruise 115 of R/V Chain), in addition to samples recently collected during cruise 107-6 of R/V Atlantis II by Dr. H. Dick and associates. Dredge locations are shown in figure 4.12, and helium isotopic results are listed in table 4.3. Strontium isotopic analyses of several of the AII107-6 samples were performed at MIT by Dr. Anton Le Roex as part of a collaborative study; this data is presented here in graphic form only.

A cursory examination of table 4.3 reveals two important aspects of the data. First, there is a larger range of $^{3}He/^{4}He$ ratios within this small set of samples (7.1 to 14.2 x atmospheric) than in the much larger suites of samples described earlier. In addition, large variability exists within a single dredge from the Islas Orcadas-Shaka Ridge (AII 107-6 dredge 57). This is also illustrated by the $^{3}He/^{4}He$ vs. $^{87}Sr/^{86}Sr$ diagram (see figure 4.13). Most of the samples have $^{3}He/^{4}He$ ratios lower than 8.0 x atmospheric, and plot within the same field as the 33-50°N samples. The two samples from the ridge segment just north of Bouvet Island have distinctly higher $^{3}He/^{4}He$ and $^{87}Sr/^{86}Sr$ ratios. Also plotted for reference is a single analysis of plagioclase phenocrysts in a Bouvet Island Hawaiite (see chapter 5); the $^{87}Sr/^{86}Sr$ range for Bouvet was taken from O'Nions et al. (1974). In contrast, sample 57-25 has the lowest $^{87}Sr/^{86}Sr$ ratio and would be classified as normal MORB on the basis of trace elements (i.e., La/Sm, Zr/Nb; le Roex, personal communication), but has the highest $^{3}He/^{4}He$ ratio.

The high $^{3}He/^{4}He$ ratios observed for the two dredges north of

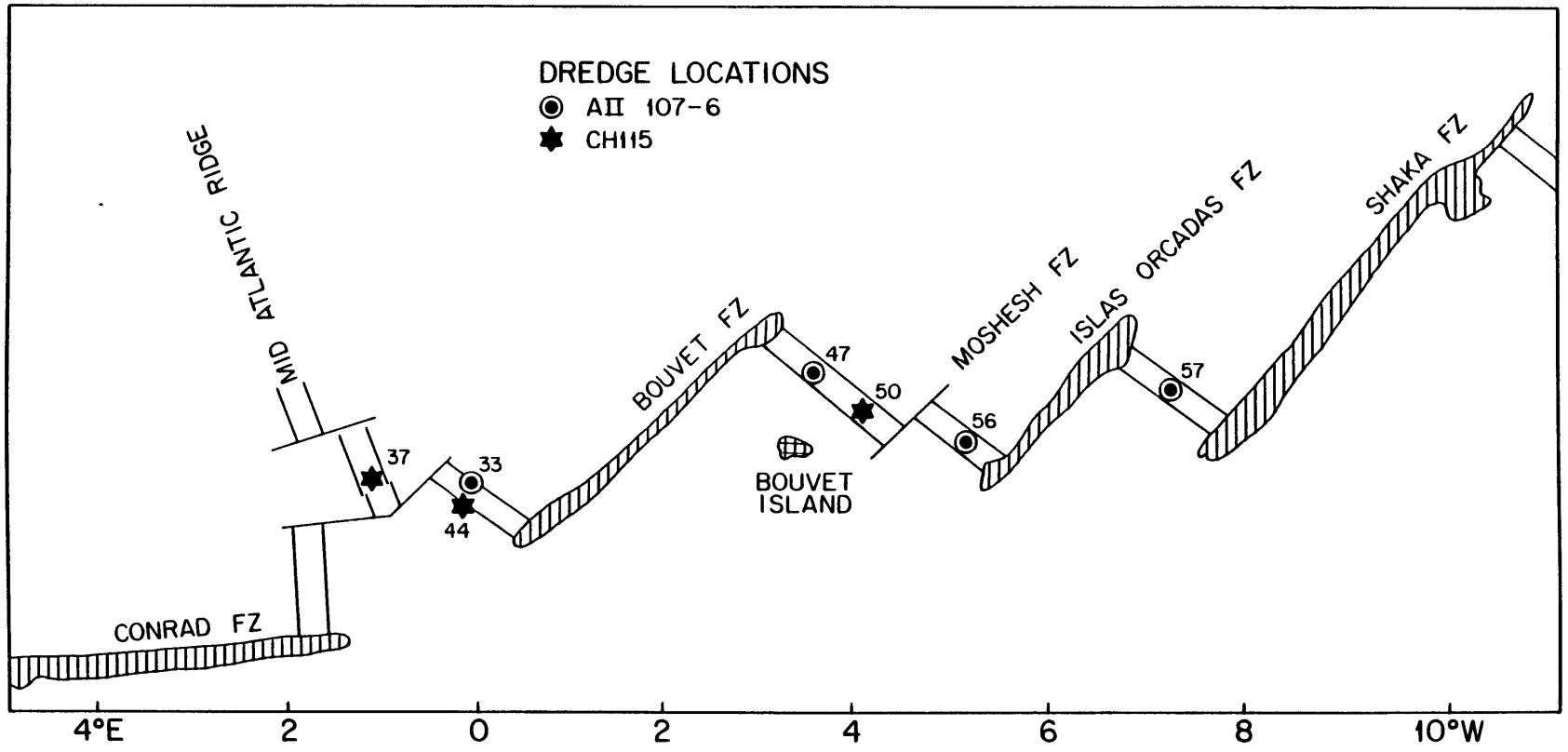


Figure 4.12: Sketch map of the ridge system near the Bouvet triple junction, with dredge locations indicated.

Bouvet Island support the hypothesis that the ridge crest eruptives are related to the Bouvet lavas, as suggested by Dickey et al. (1977). In a general way, this also supports Schilling's (1973) plume-MORB mixing model for the geochemical gradients along mid-ocean ridges near islands. In its simplest form, this model requires that the mantle source for island basalts be a rising plume of primitive mantle, which mixes with the depleted source for normal MORB. Within the present set of samples, the Bouvet Island and ridge rocks do have relatively higher $^{3}He/^{4}He$ ratios.

As shown in figure 4.13, all the South Atlantic samples, except 57-25, can be intermediate compositions caused by two-component mixing, with the two end-members most closely approximated by the Bouvet Island sample, and the sample 57-5. As discussed by Vollmer (1976) and Langmuir et al. (1978), two-component mixing on a ratio-ratio plot will result in a hyperbola with the form:

$$Ax + Bxy + Cy + D = 0$$

where:

$A = a_2b_1y - a_1b_2y$
$B = a_1b_2 - a_2b_1$
$C = a_2b_1x_1 - a_1b_2x_2$
$D = a_1b_2x_2y_1 - a_2b_1x_1y_2$

and:

a_1 = ^{4}He content in component 1
b_1 = ^{86}Sr content in component 1
y_1 = $^{3}He/^{4}He$ in component 1
x_1 = $^{87}Sr/^{86}Sr$ in component 1

The shape of the hyperbola is related to the ratio:

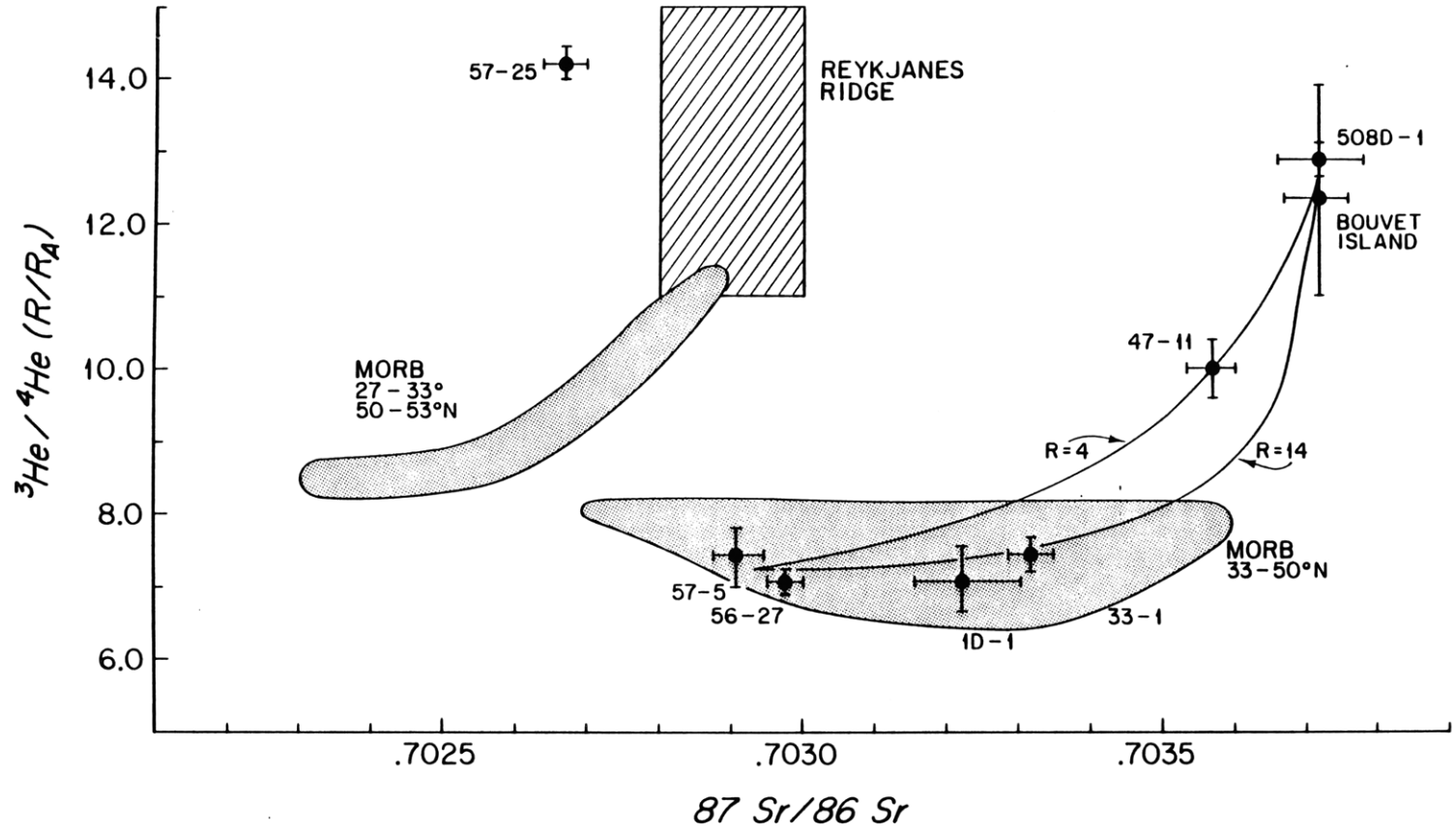


Figure 4.13: $^3He/^4He$ vs. $^{87}Sr/^{86}Sr$ for Bouvet triple junction samples. Helium analyses from table 4.6, strontium analyses from Dickey et al. (1977) and le Roex (personal communication). Fields shown for the North Atlantic MORB are from figure 4.7; Reykjanes Ridge data from Poreda et al. (1980) and Hart et al. (1973). See text for a discussion of the mixing lines (R = 4 and R = 14).

$$R = \frac{a_1 b_2}{a_2 b_1} = \frac{{}^4He_1{}^{86}Sr_2}{{}^4He_2{}^{86}Sr_1}$$

and for R = 1 the mixing curve will be a straight line (see also Langmuir et al., 1978).

If the variations in this set of samples are caused by mixing, with the end-members shown in figure 4.13, then the curvature of the mixing lines requires that R ~4-16. However, if the three mantle types described above are globally represented, these two end-members must have experienced an earlier mixing event, given their position on the diagram. For example, if there are three discrete, world-wide mantle types, the Bouvet Island sample must have been intermediate between them before mixing with 57-5. This is not entirely clear from figure 4.13, but results from oceanic islands (presented in chapter 5) support the existence of three global reservoirs, and show that Bouvet Island lies in the middle of the three-component mixing diagram. Similarly, the mantle source of 57-5 must have been intermediate between the MORB and recycled end-member before the most recent mixing event. It is clear that the mixing line shown in figure 4.13 cannot extend to the hypothetical normal MORB source ($^{86}Sr/^{87}Sr$ ~.7025, $^3He/^4He$ ~8.4 x atmospheric). The necessity for three mantle reservoirs in any mixing model is further illustrated by the position of sample 57-25 on the diagram.

The samples from the Bouvet ridge have unique He and Sr isotopic signatures that were not observed for any samples in the North

Atlantic. If the mixing hypothesis is accepted to explain the variations, then the North Atlantic basalts are the result of mixing between the normal basalt reservoir and one of the other two reservoirs, but never both. This is illustrated by the absence of samples falling in between the two fields in figure 4.7. In contrast, by the mixing hypothesis, the Bouvet ridge samples appear to have undergone mixing between all three reservoirs.

D. Isotopic Variations and Mantle Heterogeneity

The isotopic systematics of helium and strontium, taken together, require the existence of three distinct mantle reservoirs. Detailed studies of the Central North Atlantic and the South Atlantic near the Bouvet triple junction suggest that the reservoirs are spatially close enough to allow local inter-mixing. Although the overall variations, illustrated in figure 4.2, may not necessarily be an accurate representation of the world basalt population, it seems clear that the high $^{3}He/^{4}He$ basalts (referred to as type A above) are much rarer than the normal MORB or low $^{3}He/^{4}He$ basalts (type B). Given these generalizations, it is important to evaluate models for mantle structure and evolution.

As discussed in the introduction, one explanation for the geochemical variations along the ridge segments near islands is mixing between an upwelling mantle plume and the depleted upper mantle. Clearly, the helium results also show evidence for mixing near islands, but show that more than two mixing end-members are required. The samples with low $^{3}He/^{4}He$ ratios and high $^{87}Sr/^{86}Sr$ ratios are not derived from a primitive mantle source. Compared to a normal MORB

$^{3}He/^{4}He$ ratio of 8.4 x atmospheric, these low $^{3}He/^{4}He$ samples must be derived from a mantle source that has had a lower time-integrated $^{3}He/Th+U$ ratio. In general these low $^{3}He/^{4}He$ samples are characterized by enrichments in alkali elements (e.g. K) and incompatible trace elements. These geochemical properties can be attributed to a recycled component in the mantle, since lowering the $^{3}He/(Th+U)$ ratio requires either ^{3}He loss (degassing) or U and Th gain. The re-introduction of subducted crust is the favored hypothesis to generate these characteristics.

The high $^{3}He/^{4}He$ samples (i.e., > 8.4 x atmospheric) are also ovserved near islands, but are not characterized by the extreme enrichments in incompatible elements. In fact, many of these samples, such as those from 50-53°N in the Atlantic, would be classified as normal MORB. The two distinct enrichment trends are illustrated in figures 4.7, 4.11, and 4.13. Source regions for high $^{3}He/^{4}He$ samples have had a higher $^{3}He/(Th+U)$ ratio than either normal MORB or low $^{3}He/^{4}He$ MORB. Based on simple closed system evolution, this reservoir is therefore less degassed, or more primitive.

Based on the observed trends, particularly between $^{3}He/^{4}He$ and $^{87}Sr/^{86}Sr$, it would appear that these different components have interacted by mixing. Since the range of $^{3}He/^{4}He$ and $^{87}Sr/^{86}Sr$ values observed for MORB is not as large as is observed for islands (see chapter 5), possible end-members are discussed in chapter 6. However, several important constraints are implied by the MORB data. In accordance with mantle models that call for a global (and uniform) depleted upper mantle source for normal MORB (e.g., Schilling, 1975b),

$^3He/^4He$ ratios for "normal" MORB from all over the world form a roughly gaussian distribution about a mean value of 8.4 x atmospheric. The histogram plot of all the MORB analyses (figure 4.2) shows that the high and low $^3He/^4He$ basalts are also globally distributed, but that the low $^3He/^4He$ samples are more common.

If this population is representative of the parent population, the relative frequency of each basalt type must reflect the proximity of the reservoirs to one another. For example, the recycled component interacts with the normal MORB source to a greater extent than does the undepleted reservoir. If the recycled component is generated by mixing of subducted crust into the mantle, this supports the notion that the mantle is layered and that the upper layer is the source for normal MORB, which interacts with recycled crust. Similarly, the relative rarity of the high $^3He/^4He$ samples can be explained by the insulating nature of the upper layer. Of course, helium isotopes alone cannot constrain the relative depths of these reservoirs, as discussed in more detail below. However, the compelling evidence for three mantle reservoirs is more consistent with a layered mantle than one which is convecting from top to bottom.

Although the results indicate the presence of three mantle reservoirs, and indicate that they interact, the mechanism of mixing cannot be constrained by the helium data. Mixing can occur between melts derived from different sources (magma mixing) or between the sources themselves (i.e., solid state mixing). Langmuir et al. (1978) have shown that the mixing trends produced by these two processes are sometimes different, when elemental-ratio mixing diagrams are

constructed. Unfortunately, the helium concentrations are not amenable to this approach, since vesiculation clearly alters the concentrations.

E. Conclusions

The present study of helium isotopic variations confirms that the mantle is regionally heterogeneous. The different regional relationships between the $^{3}He/^{4}He$ and $^{87}Sr/^{86}Sr$ ratios add another constraint to models for the evolution of these heterogeneities, and provides another geochemical tracer for mantle processes. In detail, we can make several conclusions.

1. The crushing and melting experiments on a number of samples from the Central North Atlantic confirm that there is no isotopic fractionation between vesicles and melt for oceanic basalts. This, and the lack of any other fractionating process, allows an interpretation of the isotopic variations as reflecting the mantle source regions.
2. There are significant variations in total helium concentration in the glasses, with the lowest values observed near 45°N and the Azores Platform. Much of this variation can be attributed to near-surface processes (i.e., vesiculation), hampering estimates of the concentration variations in the mantle. This is particularly true for those samples with very high vesicularities (>5 percent by volume).
3. The MORB samples having trace element and strontium isotopic characteristics of normal MORB define a crude gaussian distribution of $^{3}He/^{4}He$ ratios, with a mean value of 8.4 x atmospheric and a standard deviation of .3. These samples

come from all over the world ridge system, suggesting that the mantle source is global in extent.

4. Based on the He and Sr isotopic variations, three distinct, globally represented basalt types can be recognized:
   - Normal MORB with $^{3}He/^{4}He$ ~8.4 x atmospheric and $^{87}Sr/^{86}Sr$ ~.7023-.7025.
   - High $^{3}He/^{4}He$ MORB with $^{3}He/^{4}He$ > 8.4 x atmospheric and $^{87}Sr/^{86}Sr$ ~.7025-.7030.
   - Low $^{3}He/^{4}He$ MORB with $^{3}He/^{4}He$ < 8.0 x atmospheric and $^{87}Sr/^{86}Sr$ > .7030.

   The variations suggest that these three basalt types are produced by mixing between three different mantle sources. The data presented here cannot distinguish between mixing of sources or mixing of melts.

5. Based on the classification scheme described above, the high $^{3}He/^{4}He$ basalts are much less common that normal MORB or the low $^{3}He/^{4}He$ MORB, within the set of samples studied. If this is representative of the parent population, the mantle sources for normal MORB and low $^{3}He/^{4}He$ MORB interact much more with one another than with the source for high $^{3}He/^{4}He$ MORB.

6. The regional distribution of the three basalt types in the North Atlantic Ocean suggests that there are distinct geochemical provinces. Basalts erupted near the Azores Platform between 33-50°N have low $^{3}He/^{4}He$ ratios. South of 33°N the basalts have the isotopic characteristics of

normal MORB, while north of 50°N (extending to Iceland) the basalts have high $^{3}He/^{4}He$ ratios. The trace element and major element differences between the provinces support these distinctions. The samples from 33-50°N are enriched in the alkali elements, in incompatible trace elements, and have high $^{87}Sr/^{86}Sr$ ratios. In contrast, samples from south of 33°N and north of 50°N are depleted to slightly enriched with respect to incompatible trace elements, have relatively high FeO contents, and have low to moderate $^{87}Sr/^{86}Sr$ ratios.

7. Isotopic variations in a suite of dredged basalts from near the Bouvet triple junction also require the presence of all three mantle types. This small group of samples has as large a range of $^{3}He/^{4}He$ ratios as the rest of the world ocean (7.0-14.2 x atmospheric). Two samples from the same dredge have $^{3}He/^{4}He$ ratios that differ by a factor of 2. In contrast to the broader geographic trends seen in the North Atlantic, the isotopic variations suggest that all three mantle types have intermixed on a local scale.

8. Constraints on the origins of the three mantle end-members can be derived from the helium and strontium isotope systematics. The low $^{3}He/^{4}He$, high $^{87}Sr/^{86}Sr$ basalts have been derived from a mantle source that has had lower $^{3}He/(Th+U)$ and higher Rb/Sr than normal MORB. The most geochemically consistent mechanism for producing this component is recycling of oceanic crust back into the mantle by subduction. The high $^{3}He/^{4}He$ basalts are partially derived from an undepleted

source that has had time integrated $^{3}He/(Th+U)$ ratios higher than MORB.

CHAPTER 5

HELIUM ISOTOPIC SYSTEMATICS OF OCEANIC ISLANDS

A. Introduction

Despite the small erupted volume of oceanic island basalt compared to ocean ridge basalt, the volcanic islands have traditionally figured prominently in models of oceanic mantle structure. Before the advent of sampling by dredging and submersible, the islands represented the only available samples of oceanic crust. Early studies used major element and petrographic data to characterize the rock types that were present; it was immediately realized that there is wide compositional diversity, and that most volcanic islands consist primarily of alkali basalt suites (e.g. Baker, 1973). Based on these studies, Kennedy (1933) suggested that tholeiites were absent from oceanic islands. Following the detailed study of Hawaiian volcanoes, which are primarily tholeiitic with a thin cap of alkali basalt, it became evident that tholeiitic basalts are also present (MacDonald, 1949). The prevailing view was that alkali basalts were derived from a tholeiitic parent by fractional crystallization (e.g. Tilley, 1950).

Although many of these major element variations can be explained by variable degrees of partial melting (Gast et al., 1964; Gast, 1968), the questions raised by these early studies have carried over to the present day. In particular, it is now clear that some of geochemical diversity in oceanic rocks is caused by primary heterogeneity within the oceanic mantle. Beginning with the pioneering work of Gast (1964, 1968), isotopes and trace elements have become powerful tools for

elucidating the mantle origins of basaltic rocks. Gast (1968) showed that the incompatible trace element ratios could not be extensively altered by different degrees of partial melting, and that there must be heterogeneities in the oceanic mantle. The isotopic differences between the mid-ocean ridge basalt (MORB) and the ocean island basalts, as well as between different islands, cannot be explained by any feasible combination of fractional crystallization, partial melting, or disequilibrium melting (Sun and Hanson, 1975; Brooks et al., 1976; Hofmann and Hart, 1978). These isotopic differences require that the heterogeneities have existed, in some cases, for time periods in excess of 1 billion years.

To some extent these heterogeneities are also reflected in the major element characteristics of the basalts. The alkali basalts from islands have typically higher and more variable $^{87}Sr/^{86}Sr$ ratios than MORB (Peterman and Hedge, 1970; O'Nions and Pankhurst, 1974; Brooks et al. 1976; Sun and Hanson, 1975). Langmuir and Hanson (1980) have shown that there are significant differences in FeO/MgO between the Azores, Hawaii and Iceland that cannot be explained by fractional crystallization or melting processes.

Plate tectonic theory has provided an important framework for interpreting the geochemical data. Noting the linearity of the Hawaiian-Emperor seamount chain, Wilson (1963) suggested that the volcanoes in the chain were formed by a stationary mantle "hot spot" beneath the moving lithospheric plate. Morgan (1971) developed this idea further by suggesting that the heat source is provided by an upwelling "deep mantle plume," and that such plumes are responsible for

the formation of most oceanic islands. Morgan also pointed out that the geochemical differences between MORB and ocean island basalts (as discussed by Gast, 1968) could be explained by this hypothesis, if the mantle is heterogeneous. This concept found wide acceptance with geochemists. Schilling and co-workers applied the plume model to the geochemical gradients observed along the mid-Atlantic ridge near Iceland and the Azores (Schilling, 1973, 1975; Hart et al., 1973; White and Scilling, 1978). In this model, a rising mantle plume beneath the Azores and Iceland, which is relatively enriched in incompatible elements, would mix with the depleted upper mantle source for MORB, producing gradients near the islands (see also chapter 4). Sun and Hanson (1975) suggested that alkali basalts erupted on oceanic islands were derived from such an undepleted mantle source that is deeper than the source for MORB.

The first Nd isotopic measurements lent credence to the two-layer model, and an observed global negative correlation between $^{87}Sr/^{86}Sr$ and $^{143}Nd/^{144}Nd$ allowed estimation of "bulk earth" values for these ratios (DePaulo and Wasserburg, 1976; O'Nions et al., 1977; Richard et al., 1976). Several authors have suggested that the upper mantle had been depleted by the formation of the continents, and used Sr and Nd mass balances to calculate the mass of the mantle that has been depleted (Jacobsen and Wasserburg, 1979; O'Nions et al., 1980). The results suggest that about one third of the mantle would be depleted in forming the continents; this would correspond to a depleted layer about 700 km thick. These calculations were based on the assumption that the lower mantle is represented by the "bulk earth"

values.

There are several problems with this simple two layer model. First, many islands that are depleted relative to bulk earth Sr and Nd isotope values have rare earth abundances that are enriched. This has led many workers to suggest that the mantle source region for these islands has experienced a recent metasomatic event (e.g. Erlank and Rickard, 1977), which has changed the trace element abundances. In addition, the Pb isotopic composition of all oceanic basalts is too radiogenic to have been derived from a chondritic bulk earth (Hofmann and White, 1980; Chase, 1981). On the basis of the Pb data, Hofmann and White (1980) proposed that oceanic islands (i.e., plumes) are derived by remelting of old subducted oceanic crust. This is qualititavely similar to the recycling models originally suggested by Armstrong (1968,1981) except that the subduction of sediments is not an assumed condition. Depending upon the timing and exact nature of the "recycling," it is possible to obtain isotopic signatures (of Sr and Nd) that are similar to bulk earth by this mechanism. Anderson (1982a; see also DePaolo and Wasserburg, 1979) has shown that the Nd-Sr correlation could be produced by mixing ancient depleted and enriched reservoirs.

The MORB helium results, discussed in chapter 4, imply the presence of three mantle reservoirs, which is of obvious importance to choosing between the various proposed models. However, the isotopic variability within MORB is quite limited compared to island basalts (Hofmann and Hart, 1978). The goal of this study is to use helium isotopes to distinguish between undepleted mantle sources and those that have some

contribution from recycled material by studying oceanic island basalts. As discussed earlier, high $^{3}He/^{4}He$ ratios indicate the presence of primordial helium from a relatively undepleted source. In contrast, any recycled component would be expected to have been partially degassed, leading to lower $^{3}He/(Th+U)$ ratios, and given enough time, lower $^{3}He/^{4}He$ ratios. The helium results for the mid-Atlantic ridge presented in chapter 4 (Kurz et al., 1982a) show that a convenient way to discriminate between these two mantle sources is to plot $^{3}He/^{4}He$ vs. $^{87}Sr/^{86}Sr$. Based on the data plotted in figure 4.7, $^{3}He/^{4}He$ ratios higher than ~ 8.4 x atmospheric are indicative of a greater proportion of primordial helium, while recycled (degassed) material has characteristically lower $^{3}He/^{4}He$ ratios. Therefore, the results from the North Atlantic provide a useful empirical scale that can be applied to the $^{3}He/^{4}He$ data from oceanic islands. In this chapter, the terms "high" and "low" $^{3}He/^{4}He$ ratios will imply values relative to the dividing line between the two groups in figure 4.7, and will be used to indicate undepleted and recycled mantle characteristics. The term undepleted will again be used in a relative sense, since the $^{3}He/^{4}He$ ratio of pristine-undepleted earth is unknown (see chapter 6).

Several studies have reported $^{3}He/^{4}He$ analyses from oceanic islands, primarily Hawaii and Iceland (Polak et al., 1976; Craig and Lupton, 1976; Kaneoka and Takaoka, 1978, 1980 Poreda et al., 1980;). The results show that the $^{3}He/^{4}He$ ratios are characteristically higher than the MORB values, which is, in a general sense, consistent with the mantle plume model. However, most of these analyses were

carried out on the gases in fumaroles and hot springs, which makes comparison to isotope work on volcanic rocks difficult. Only the work of Kaneoka et al. (1978; Kaneoka and Takaoka, 1980), on several Hawaiian rocks, involves samples of reasonably well-documented field locations. Further, prior to the initiation of this work, no helium isotopic analyses had been performed on samples from islands that are considered to represent "bulk earth" (O'Nions et al., 1977) in terms of Sr and Nd isotopic composition.

Given the small number of noble gas analyses on oceanic islands, this study represents an attempt to characterize both global and local helium isotopic variations. In order to document the global variations, samples of oceanic islands that represent the range of Sr, Nd, and Pb isotopic compositions were selected. Where possible, samples that have been analyzed for these isotopes, by other laboratories, were used. The islands discussed in this study are shown in figure 5.1. To properly interpret any global variations, it is also necessary to document and understand any local isotopic variations. To this end, a somewhat more detailed study of two islands, Hawaii and Iceland, was performed.

The discussion of the helium isotopic results presented in this chapter is divided into four parts: a survey of islands in the Atlantic and Indian Oceans; variations within the island of Iceland; variations within a single shield volcano (Loihi seamount); and variations within the island of Hawaii. It is clear from the results that there are large variations between islands, within islands, within individual volcanoes, and that helium isotopes provide new insight into

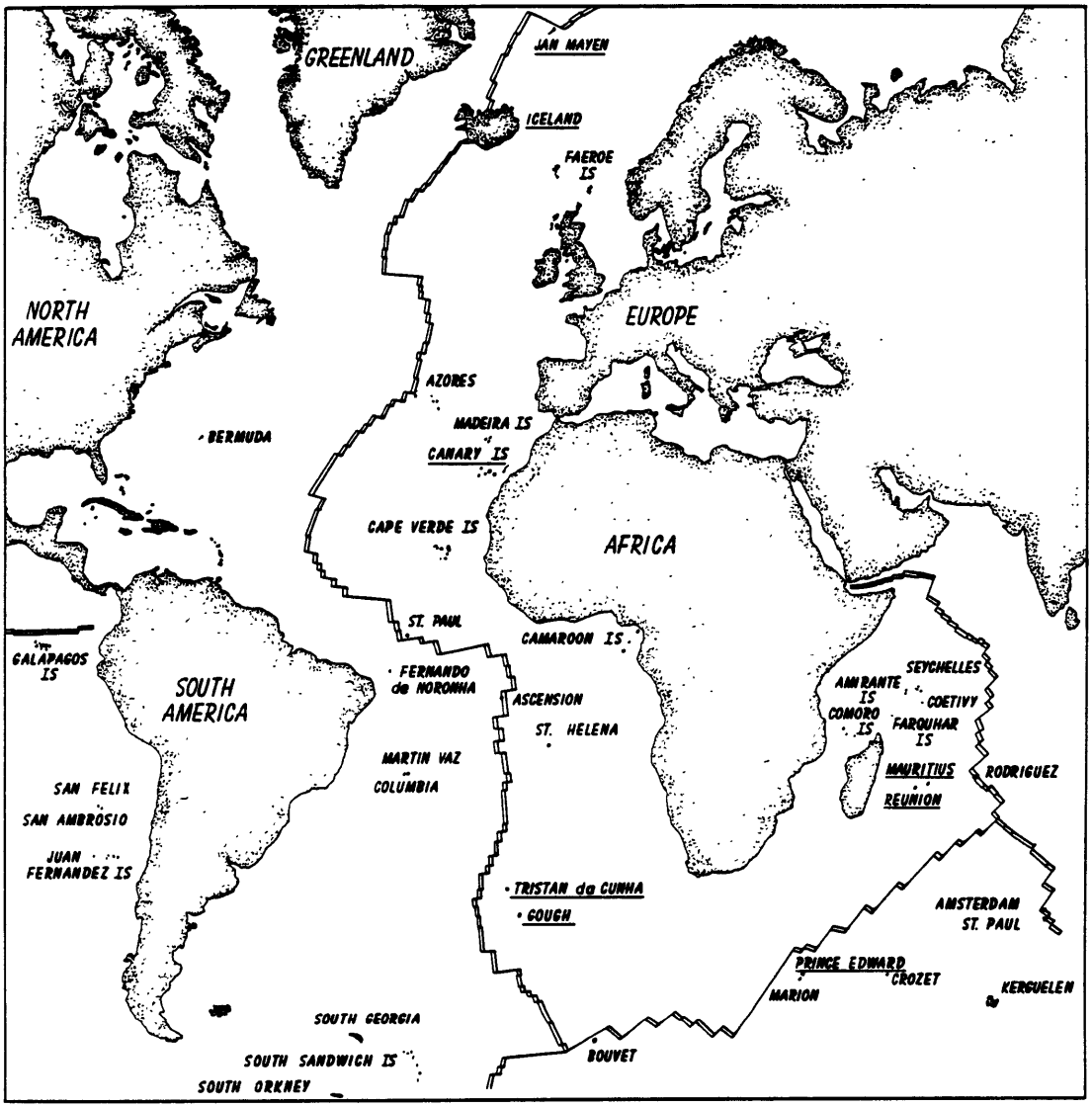


Figure 5.1: Map of the Indian and Atlantic Oceans showing the islands with respect to the mid-ocean ridges. Samples from the islands that are underlined have been studied in this chapter.

the causes of the variations.

B. Samples

Numerous studies have shown that the glassy rims of submarine basalts trap significant quantities of magmatic gases (Funkhouser et al., 1968; Fisher, 1971). Since the results discussed in chapters 3 and 4 show that vesiculation and crystallization do not change the isotopic composition of helium within the glass, such samples are ideal for noble gas analysis. Although quenched glass may exist on the submerged flanks of many oceanic islands, samples of this nature have only been observed near Hawaii (Moore and Fiske, 1969). A number of the samples from Hawaii discussed below are dredged basaltic glasses. Several of the samples from Iceland are quenched sub-glacial glasses that were erupted during the last glacial period (10-12,000 year b.p.). The ice and ice-melt cover were thick enough to cool the magma quickly, as in the submarine samples (discussed further below). However, aside from these two islands (Iceland and Hawaii), glasses were unavailable.

An alternate sampling approach, described by Anderson (1974) and Kaneoka and Takaoka (1978), is to extract the gases trapped within basaltic phenocrysts. One must assume that the gas within these phenocrysts is in equilibrium with the surrounding magma, and that there are no xenocrysts derived from other sources. Several petrographic criteria can be used to evaluate the validity of these assumptions. First, one must know the site of gas residence within the crystals to document its magmatic origin. Second, xenocrysts that are out of equilibrium with the host magma can be distinguished by optical

strain features (deformation lamellae), compositional zoning, and corrosion textures. For these reasons, a doubly polished thin section of each of the samples analyzed was examined using a petrographic microscope. Descriptions of the samples and their locations are given in Appendix II. The Loihi Seamount glasses have been described by Moore et al. (1982); relevent details of their work are discussed along with the results.

Within this set of samples, phenocrystic melt inclusions are ubiquitous, and are the probable site of residence for the gases. As discussed below, crushing experiments support this hypothesis. Although the melt inclusions may not be identical to the magmas containing the phenocrysts (due to post entrapment magmatic evolution), they should be isotopically identical as long as the crystals are not xenocrysts. Examination of the olivine phenocrysts in thin section, and also in reflected light during hand picking, often shows that the melt inclusions are aligned along crystal boundaries, implying that they are incorporated during particular episodes of crystal growth. Examples of typical inclusions within olivine phenocrysts are shown in figure AII.1

In all cases, an attempt was made to choose samples that were relatively unfractionated and also porphyritic; therefore, the samples were primarily picrites, ankaramites, and olivine rich basalts. In choosing porphyritic samples with large phenocrysts for analysis, it is always possible that one generation of crystals grew from several different magma batches. In the case of the alkali basalts (from Tristan da Cunha, Gough, Jan Mayen, La Palma, and Prince Edward

Islands), zoning within the clinopyroxene can be observed in thin section (see descriptions in Appendix II). The crystals therefore should provide an "integrated" history of the melts they have grown from. Trace element studies of the zoning in pyroxenes from alkali basalts (using the ion probe) have shown that in some cases the magma batches may have been derived from different sources (N. Shimizu, personal communication), so phenocrysts must not be viewed simplistically.

For the present set of samples, xenocrysts were identified in thin section by the following criteria:

1. Non-uniform extinction of olivine in crossed polarized light, which is indicative of a deformation history. An example of these "kink bands" is shown in figure AII-2. These structures are ubiquitous in metamorphic dunites (see section on Hawaii). The presence of kink bands in a basaltic crystal requires that it existed in a solid environment, since deformation is not possible for a crystal floating in a melt.

2. Subhedral or anhedral crystal morphology, which may indicate reaction with the surrounding melt (disequilibrium), or disaggregation from a wall rock or xenolith.

3. The presence of fluid inclusions aligned in bands and rows that appear in metamorphic dunites, but are rare in basaltic phenocrysts (Roedder, 1965).

Crystals with these characteristics were for the most part not found. However, in several Hawaiian samples some xenocrysts were present and, as discussed below, the helium within the fluid inclusions may "dominate" the helium within true phenocrysts. Since the helium contents of phenocrysts are extremely low ($< 4 \times 10^{-8}$ cc/gram), one must be particularly cautious in checking for the presence of xenocrysts. The helium concentration in dunite and gabbro xenoliths is

typically 10 to 100 times higher (see below), so even a small percentage of xenocrysts can have an important effect.

C. Results

1. Islands of the Atlantic and Indian Oceans

The concentrations and isotopic compositions of the helium contained in basaltic phenocrysts from a number of oceanic islands are given in table 5.1. In agreement with the hypothesis that helium behaves as an incompatible element (see chapter 4), the phenocryst helium concentrations are extremely low ($< 3 \times 10^{-8}$ ccSTP/gram). This leads to larger uncertainty in the $^3He/^4He$ ratio measurement, due to greater importance of the blank correction, and larger uncertainty in the standard (see chapter 2). Where large samples were available, this could be compensated for by extracting the helium out of a large quantity of phenocrysts (up to 3 grams in some cases); variable uncertainties in table 5.1 partially reflect this.

The isotopic measurements were confirmed to be reproducible within the stated uncertainty by duplicate analyses of several samples by both crushing and melting (ALR416, ALR266, JM151A, TK26). In cases in which no ratio is reported and only an upper limit to the concentration is given, the helium released was not significantly greater than the procedural blank. The large isotopic variations displayed by this data set are far outside the uncertainty introduced by the analytical procedure.

2. Iceland

The helium results for samples from the island of Iceland are presented in table 5.2. As with the phenocryst samples, these

Table 5.1: Helium results: Atlantic and Indian Ocean islands

Sample		Extraction Method	^{4}He ccSTP/gram	σ	^{3}He/^{4}He (R/Ratm)	σ
Reunion						
R43	Oliv.	Crush	1.21×10^{-8}	.03	13.3	.4
R36	Oliv.	Crush	7.1×10^{-9}	.6	13.5	.5
Bouvet						
WJ8B	Plag.	Crush	1.4×10^{-9}	.2	12.4	1.5
Mauritius						
M68	Oliv.	Crush	5.2×10^{-9}	.3	11.4	.8
Gough						
ALR26G	cpx	Crush	3.93×10^{-8}	.09	6.17	.2
	Oliv.	Crush	1.53×10^{-8}	.06	6.2	.3
ALR41G	cpx	Crush	1.3×10^{-9}		4.9	1.6
	cpx	Melt	$<7 \times 10^{-10}$		----	---
	cpx	Crush	5.8×10^{-10}	.9	5.5	.7
Tristan						
TK 46A	Oliv.	Crush	7.3×10^{-9}	.8	6.3	.7
	Oliv.	Melt	1.0×10^{-9}	.1	5.6	2.1
	cpx	Crush	3.5×10^{-8}	.2	5.1	.3
TK 26	Amph.	Crush	3.3×10^{-7}	.1	5.20	.1
	Amph.	Melt	1.3×10^{-7}	.1	4.70	.1
Prince Edward						
WJ 21E	Oliv.	Crush	2.33×10^{-8}	.05	7.4	.2
Jan Mayen						
JM 151	Oliv.	Melt			6.3	.5
	Cpx	Crush	9.7×10^{-9}	.4	6.8	.3
La Palma						
LP 249	cpx	Crush	3.4×10^{-8}	.1	7.5	.3
St Helena						
SH 13	Oliv.	Crush	$< 1.0 \times 10^{-9}$		----	

Table 5.2: Helium results* for Icelandic samples

Samples	Phase Analyzed	^{4}He ccSTP/gram	σ	^{3}He/^{4}He (R/RA)	σ
HS782	Glass	$< 1 \times 10^{-9}$	---	---	---
HS806	Glass	1.54×10^{-7}	.06	8.67	.09
HS785	Glass	3.0×10^{-8}	.2	15.2	.4
EZ274	Oliv.	1.1×10^{-8}	.1	14.0	.3
	Glass	9.3×10^{-9}	1.0	13.9	.2
EZ 149B	Glass	1.3×10^{-8}	.1	18.0	.5
EZ 125B	Glass	6.2×10^{-8}	.3	22.2	.3

* All samples crushed in vacuo.

sub-glacial glasses have quite low helium contents, making blank correction important. In this instance, the concentrations are low due to extreme vesicularity and probable gas loss by vesicle opening. Since sub-glacial glasses have not been previously analyzed for volatiles, the olivine phenocrysts from one of the samples (EZ274) were extracted for comparison with the glass analysis. The isotopic results were identical, suggesting that sub-glacial glasses can be used for helium isotopic measurements, if they are not completely degassed.

3. Loihi Seamount and the island of Hawaii

Helium analyses of basaltic glasses, phenocrysts, and xenoliths from the Loihi Seamount and four of the five volcanoes on the island of Hawaii are listed in tables 5.3, 5.4, and 5.5. In selecting samples, an attempt was made to obtain recent eruptives from each volcano. As shown in tables 5.5 (and Appendix II), the Kilauea and Mauna Loa samples are reasonably well documented in terms of age. The four Kilauea samples were collected from different places on the east rift of the volcano, and yield isotopic ratios that agree within 2σ. Since the two Puna Ridge samples were submarine glasses and the other two were phenocryst separates, this agreement confirms that phenocrysts can be used to indicate the magmatic $^3He/^4He$. Similarly, phenocrysts and glasses from Mauna Loa yield identical isotopic ratios.

In contrast, the phenocryst and glass analyses from the Hualalai dredged samples show significant isotopic variations. However, petrographic examination reveals the presence of xenocrysts among the olivines in sample KK 10-1, containing abundant fluid inclusions (see figure AII.1).

Table 5.3: Helium Analyses of Loihi Seamount Glasses

	Crushed				Powder melted			
Glasses	^4He ($\times10^{-7}$ccSTP/g)	σ	$^3He/^4He$ ($\times10^{-5}$)	σ	^4He ($\times10^{-7}$ccSTP/g)	σ	$^3He/^4He$ ($\times10^{-5}$)	σ
KK 23-3	.61	.04	3.20	.12	.65	.01	3.57	.10
29-10	6.21	.1	3.81	.08	1.03	.03	3.71	.14
18-8	2.71 2.92	.06 .05	4.41 4.47	.09 .08	.17	.03	4.84	.42
20-14	3.25	.10	3.70	.07				
16-1	8.47	.10	4.17	.07				
78 H-W2-16	3.79	.10	3.38	.07				
24-7	.21	.04	3.14	.30	.99	.05	3.02	.17
25-4	5.4	.1	3.13	.07	.41	.02	3.24	.13
20-4	5.20	.14	3.33	.10	.056	.006	3.39	.15
17-2	2.78	.08	3.33	.07	.036	.007	3.46	.28
21-2	.29	.01	.639	.03	<.02	----	----	---
27-4	4.01	.1	3.34	.07	.419	.02	3.35	.15
31-12	13.0	.5	2.89	.07	.88	.04	2.84	.08
17-5	3.64	.08	2.77	.07	<.015	---	----	---
15-4	.50 .45	.03 .01	2.93 2.81	.07 .07	<.010	---	----	---

Table 5.4: Helium Analyses of Loihi Dunite Xenoliths*

Sample	Grain Size (mm.)	^4He ($\times 10^{-7}$ ccSTP/g)	σ	$^3He/^4He$ ($\times 10^{-5}$)	σ
KK 27-9A	1-2	13.3	.5	3.31	.07
27-9B	.5-1.0	18.8	.6	3.32	.08
17-5W	.5-1.0	3.75	.07	2.93	.07
31-12W	<.5	2.12	.06	2.98	.07

* All extractions performed by crushing in vacuo.

Table 5.5: Helium analyses of glasses, phenocrysts, and xenoliths from the Hawaiian volcanoes[a]

	Location	Phase Analysed	^4He (ccSTP/gram)	σ	$^3He/^4He$ (R/Ratm)	σ
Kilauea						
1 *Puna 2	East Rift	glass	1.51×10^{-7}	.03	14.7	.5
2 *Puna 678	East Rift	glass	1.88×10^{-7}	.04	14.5	.3
3 *66055	crater wall	olivine	5.8×10^{-9}	.3	14.0	1.4
4 57370	1840 lava	olivine	1.14×10^{-8}	.06	13.4	.7
Mauna Loa						
5 ML84	1868 flow	olivine	1.39×10^{-8}	.05	8.02	.75
6 ML55	1950 lava	olivine	1.15×10^{-8}	.06	8.6	.40
7 185	Kealakekua	glass	1.08×10^{-7}	.03	8.16	.20
8 187	Kealakekua	glass	2.37×10^{-8}	.09	8.20	.15
9 203-1	Kealakekua	glass	2.56×10^{-8}	.05	8.26	.21
Hualalai						
Dredged tholeiites						
10 KK 9-14	West flank	glass	1.51×10^{-6}	.03	17.6	.5
11 KK 14-7	West flank	glass	2.60×10^{-6}	.05	15.2	.3
12 KK 10-1	West flank	olivine	5.65×10^{-9}	.11	14.4	.4
Xenoliths 1801 flow						
13 11387-107	dunite	olivine	2.85×10^{-7}	.06	8.99	.18
14 -11	dunite	olivine	3.44×10^{-7}	.14	8.91	.18
15 -104	gabbro	olivine	3.44×10^{-7}	.14	9.15	.18
16 -54	gabbro	CPX	1.88×10^{-7}	.09	8.67	.25
17 111815	dunite	olivine	1.09×10^{-7}	.09	8.60	.25
Mauna Kea						
18 48593	Oakala	olivine	6.79×10^{-9}	.3	7.90	.46

[a]All analyses performed by crushing in-vacuo.

*From Kurz et al., 1982b

4. Evaluation of the Method

From the results presented in tables 5.1-5.5, it would appear that basaltic phenocrysts can be used to indicate the magmatic $^3He/^4He$ ratio. Several different attempts were made to verify this approach, each of which gave a positive result:

i) Analyses of phenocrysts and submarine glasses from the same volcanic center, at Kilauea and Mauna Loa, yielded the same isotopic results.

ii) Analysis of phenocrysts and glasses from the same sample (EZ274 from Iceland) also yielded identical results.

iii) Analyses of different phenocrysts from the same sample (clinopyroxene and olivine from ALR26G and TK46A) yielded identical results.

However, as noted earlier, the success of this method depends critically on the absence of xenocrysts, and requires careful petrographic examination of the samples to be analyzed. In several cases, which are discussed further below, the presence of xenocrysts in thin section and the high concentration of helium in the xenoliths (table 5.4) illustrate the importance of petrographic examination.

D. Discussion

1. Crystal-melt partitioning

The low helium contents of the basaltic phenocrysts confirm that helium is not favorably partitioned into olivine, clinopyroxene, or plagioclase. Unfortunately, we cannot determine precise partitioning coefficients (K_D). First, it is impossible to know the helium content of the magma from which the crystals formed, even if it were assumed to be homogeneous during crystal growth (which is unlikely, given the common presence of zoned crystals). In addition, petrographic evidence suggests that the helium resides within melt

inclusions, rather than within the crystal lattice, so most of the gas within these crystals is not truly dissolved. Finally, most of the analyses presented in tables 5.1-5.5 were performed by crushing. It is possible, however, to set reasonable upper limits for the values of K_D for clinopyroxene, olivine, and plagioclase. In all the cases where crushing and melting extractions were performed on the same sample, more than 85 percent of the helium was released by crushing. Assuming this is true for all the samples studied here, and that the range of helium concentrations in the parental melts were 10^{-5} to 10^{-6} ccSTP/gram, it is quite reasonable to conclude that $K_D << .01$ for all the crystals. This upper limit is further validated by the fact that the helium measured resides within the melt inclusions. The petrogenetic implications of this partitioning behavior are discussed in greater detail in chapter 6.

2. Overall $^3He/^4He$ variations

The observed $^3He/^4He$ varies from ~5 x atmospheric, for Gough and Tristan da Cunha ankaramites, to 32 x atmospheric, for the tholeiites from Loihi seamount. To determine the possible causes for the large variations, it is informative to plot $^3He/^4He$ vs. $^{87}Sr/^{86}Sr$, as shown in figure 5.2. The two groups that were observed on this diagram for MORB from the North Atlantic are also observed in the data from the oceanic islands, but with a much greater range of values. Samples from Hawaii, Iceland, Bouvet, and Reunion all have $^3He/^4He$ ratios and $^{87}Sr/^{86}Sr$ ratios that are higher than MORB. The trend created by the points from MORB, Reykjanes Ridge, Iceland, and Loihi seamount are consistent with mixing between an

undepleted mantle and the depleted MORB reservoir. However, there is considerable variation within Iceland and Hawaii. In the case of Iceland, $^{87}Sr/^{86}Sr$ data for these samples are not available, so the $^{3}He/^{4}He$ values are plotted in the center of the range of published $^{87}Sr/^{86}Sr$ values. Without this information, it is impossible to properly evaluate whether the variations within Iceland are consistent with this mixing hypothesis. Several mixing lines, for different He and Sr concentrations in the end-members are shown in figure 5.2 (assuming Loihi and MORB are mixing end-members).

In contrast to these "high $^{3}He/^{4}He$ islands" Tristan da Cunha, Gough, Prince Edward, La Palma, and Jan Mayen all have $^{3}He/^{4}He$ ratios that are lower than MORB but $^{87}Sr/^{86}Sr$ ratios that are higher. These isotopic characteristics require a mantle source that has had lower time integrated $^{3}He/(Th + U)$ and higher Rb/Sr ratios than MORB. The most plausible mechanism for lowering the $^{3}He/(Th + U)$ ratio of a mantle reservoir is degassing. This component will be referred to as "recycled" because it has presumably been degassed at some time in the past. Therefore, the overall variations on this diagram could be explained by mixing of three components: MORB, undepleted mantle, and a recycled component. The recycled component could be generated by remelting of subducted oceanic crust, melting of old metasomatized mantle that has become enriched in U with respect the He, or contamination of the magmas during their passage through old crust.

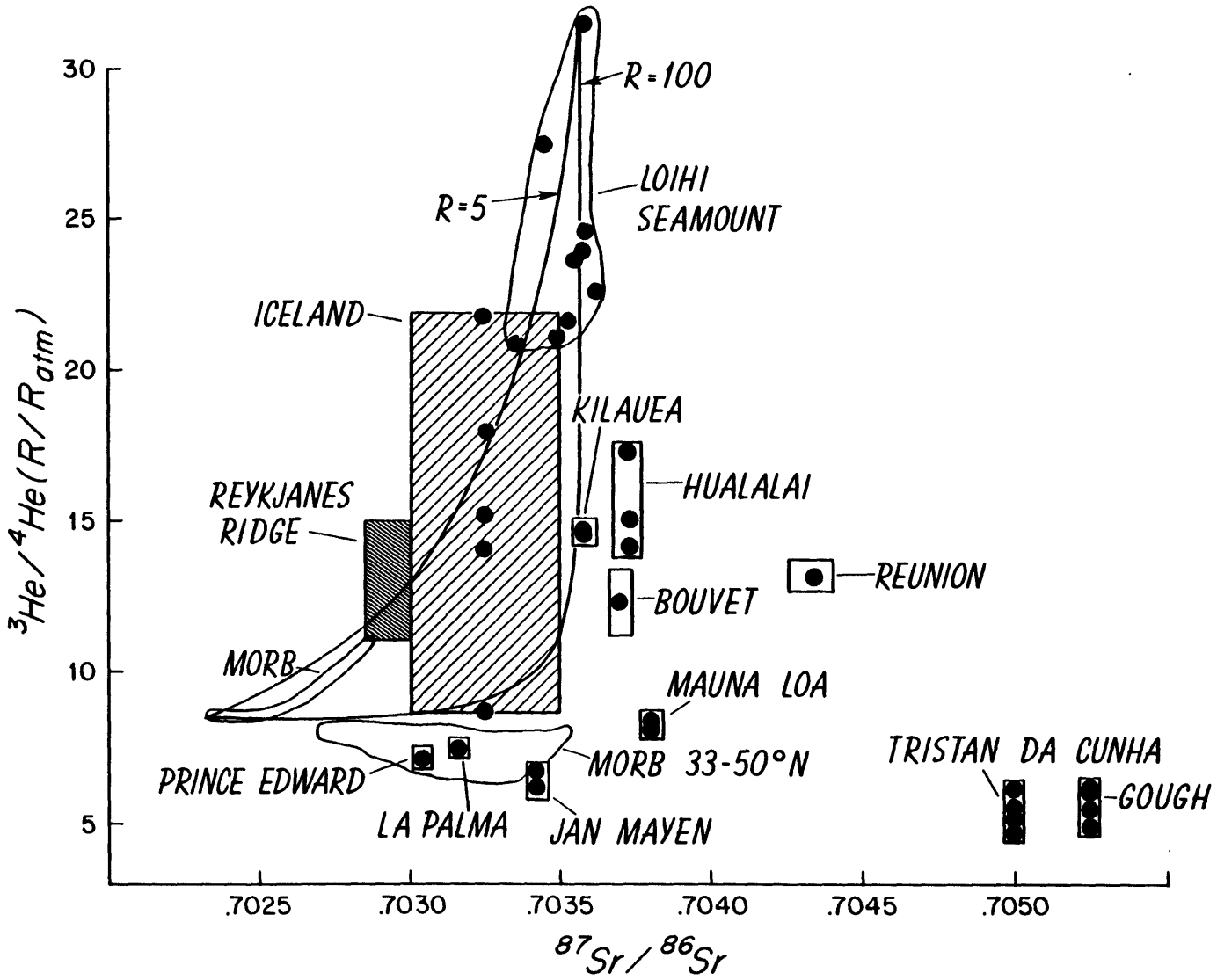
In identifying the origins of these distinctly different helium isotopic characteristics for the various islands, it is important to

Figure 5.2: $^{3}He/^{4}He$ vs $^{87}Sr/^{86}Sr$ for oceanic rocks.
Locations for which helium and strontium analyses were performed on the same sample:
MORB (see chapter 4)
Reykjanes Ridge (Poreda et al., 1980; Hart et al., 1973)
Loihi seamount (this study and Staudigel et al., 1981)
Kilauea (this study and Hart, 1973)
Hualalai (this study and D. Clague, personal communication)
Gough and Prince Edward (this study and Kurz et al., 1982)

For some of the samples, strontium analyses were taken from the literature, and the references are listed below (all helium data from this study):
Jan Mayen, La Palma, Bouvet, and Tristan da Cunha: O'Nions and Pankhurst, 1974
Mauna Loa: O'Nions et al., 1977
Reunion: Ludden, 1978
Iceland: Hart et al., 1973; O'Nions and Pankhurst, 1974; Sun and Jahn, 1975; O'Nions et al., 1976

Two mixing lines are shown for comparison, and were drawn assuming that component 1 has $^{3}He/^{4}He = 8.5 \times R_a$, $^{87}Sr/^{86}Sr = .7023$ and component 2 has $^{3}He/^{4}He = 32.0 \times R_a$, $^{87}Sr/^{86}Sr = .70358$.
The ratio R is defined as:

$$R = \frac{^{4}He_1 \; ^{86}Sr_2}{^{4}He_2 \; ^{86}Sr_1}$$


30
25
20
15
10
5
$^3He/^4He(R/R_{atm})$
R=100
R=5
LOIHI SEAMOUNT
ICELAND
KILAUEA
HUALALAI
REYKJANES RIDGE
REUNION
BOUVET
MORB
MAUNA LOA
MORB 33-50°N
TRISTAN DA CUNHA
GOUGH
PRINCE EDWARD
LA PALMA
JAN MAYEN
.7025
.7030
.7035
.7040
.7045
.7050
$^{87}Sr/^{86}Sr$

examine compositional variations. It is clear from figure 5.3 that all the low $^3He/^4He$ islands are primarily alkaline in nature. All of the exposed volcanic rocks on Tristan da Cunha, Gough, Jan Mayen, La Palma, and Prince Edward are alkali basalts, whereas Reunion, Hawaii, and Iceland are primarily tholeiitic. This is illustrated by the plot of $^3He/^4He$ weight percent K_2O (see figure 5.3). A similar trend, over a smaller compositional range is observed in the suite of dredged MORB from the North Atlantic. Although the present data set does not necessarily characterize all oceanic islands, it seems that alkali basalts have generally lower $^3He/^4He$ ratios. Bouvet and Mauritius islands are considered to have rock suites that are intermediate between alkaline and tholeiitic trends (Baker, 1973). Le Roex (1980) showed that the exposed rocks on Bouvet could have evolved from a tholeiitic parental melt by extreme fractional crystallization. In agreement with the intermediate compositional trends, the samples from these islands also have intermediate $^3He/^4He$ (see figures 5.2 and 5.3).

These results have important implications for models of the origin of alkali basalt and the structure of the oceanic mantle. The low $^3He/^4He$ ratios observed for some alkali basalts shows that they cannot be derived from undepleted mantle. The terms "undepleted" and "undegassed" will be used interchangeably here, which implicitly assumes that the degassing history and hence the helium isotopic evolution is related to the fractionation mechanisms for the Rb-Sr, U-Pb, and Sr-Nd isotopic systems. The isotopic characteristics of truly undepleted mantle would be $^{87}Sr/^{86}Sr$, $^{143}Nd/^{144}Nd$, and

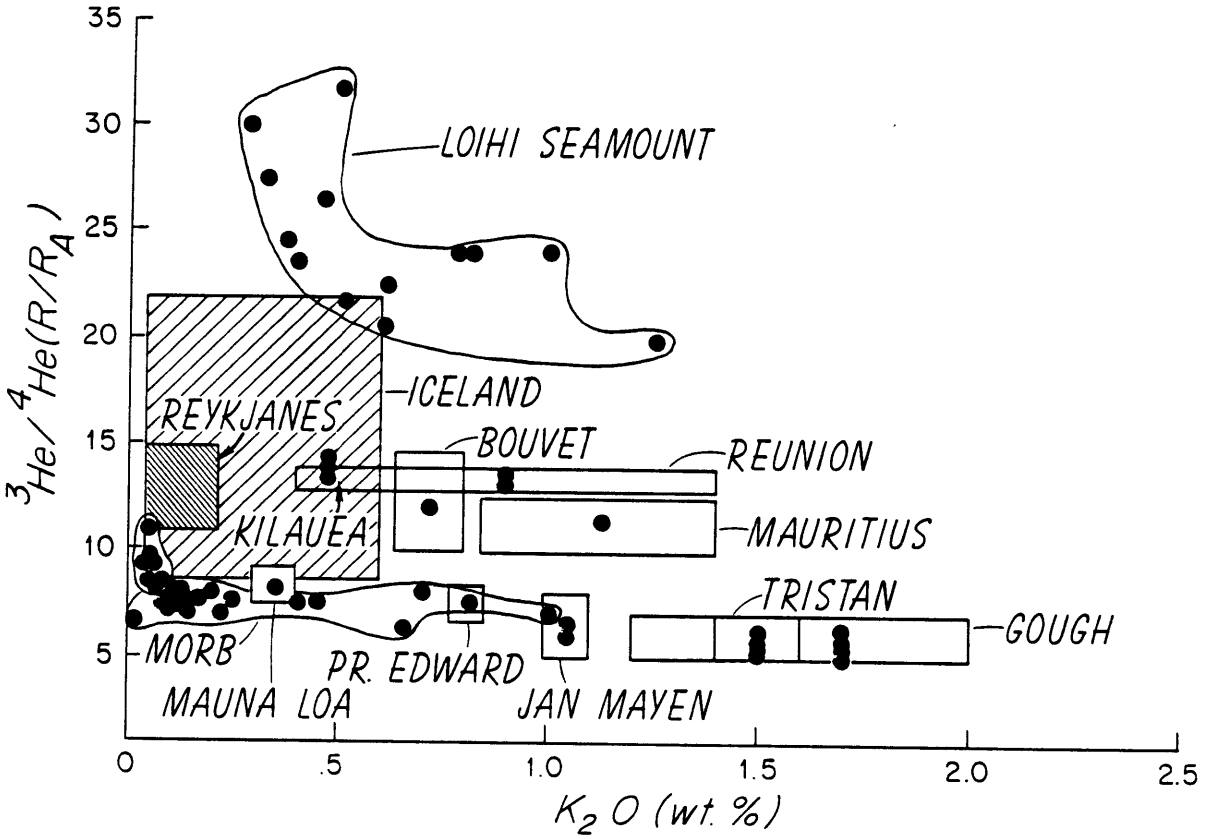


Figure 5.3: $^3He/^4He$ vs. K_2O for oceanic rocks. Localities for which K_2O and helium analyses were performed on the same samples:

MORB: see chapter 4
Loihi seamount: this study and Moore et al., 1982
Mauna Loa: this study and Fornari et al., 1980
Kilauea: this study and Moore, 1965
Prince Edward: this study and Voerwoerd, 197L
Bouvet: this study and le Roex, 1980
Reykjanes Ridge: Poreda et al., 1980; Schilling, 1973
Jan Mayen: this study and S. Maaloe (personal communication)

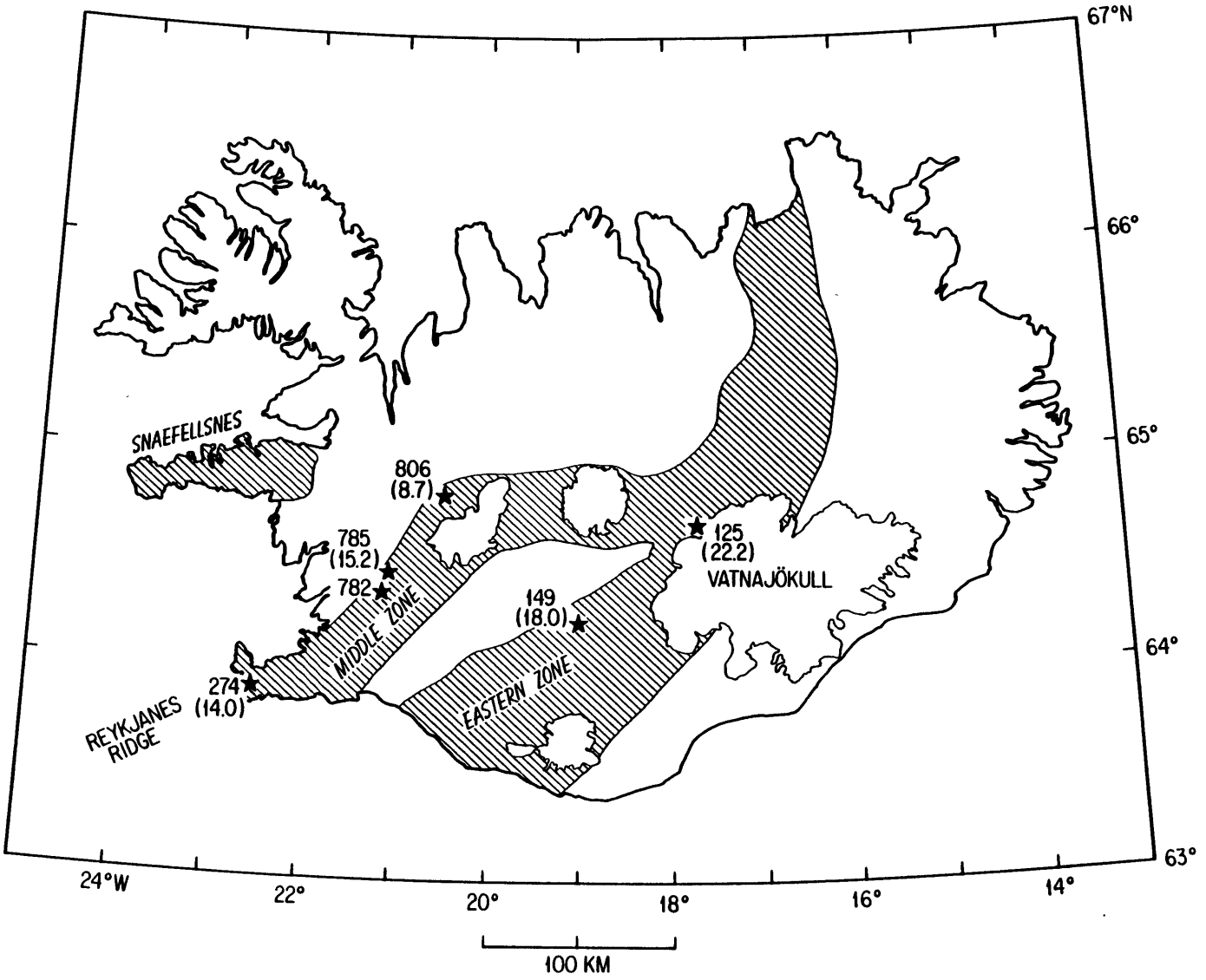
Where K_2O analyses were not available for the same samples, data for similar rock types from the same locality were taken from the literature:
Gough: Le Maitre, 1962
Tristan da Cunha: Baker et al., 1964
Iceland: this study Jakobbson, 1972; Sigurdsson et al.
1978; Sigvaldason et al., 1974

$^3He/^4He$ ratios close to those expected for closed system evolution. Unfortunately, it is at present impossible to specify what the $^3He/^4He$ for such a mantle reservoir would be, since the details of early earth history are unknown (a discussion of the possibilities is given in chapter 6). However, the highest $^3He/^4He$ ratio identifies the volcanism that is derived from the most undepleted source. Therefore, the tholeiites from the Loihi seamount are derived from the most undepleted mantle presently sampled by terrestrial volcanism, in agreement with the Wilson-Morgan hot spot hypothesis. In contrast, the alkaline islands are not derived from an undegassed source.

3. Iceland

Although the number of samples analyzed from Iceland is quite small (see table 5.2), the large isotopic variations correlate with other geochemical information, and therefore merit a detailed discussion. Iceland is a volcanic island situated directly on the mid-Atlantic ridge (see figure 5.1), and has been vigorously studied in the past decade. Although the volcanic rocks are as old as tertiary, most of the work has focussed on the well-defined zones of recent activity, which are in a general sense extensions of mid-ocean ridge volcanism (see figure 5.4). Geophysical studies have shown that Iceland differs from the adjacent ridge segments in several respects: thicker crust, anomalous topography, higher heat flow to the base of the crust, anomalous seismic velocities associated with partial melting, and larger eruptive volume (Palmason, 1971; Vogt, 1974; Saemundsson, 1979). Schilling (1973) proposed that these geophysical anomalies, and

PAGES (S) MISSING FROM ORIGINAL


67°N
66°
65°
64°
63°
24°W
22°
20°
18°
16°
14°
SNAEFELLSNES
806
(8.7)
785
(15.2)
782
125
(22.2)
VATNAJÖKULL
149
(18.0)
MIDDLE ZONE
EASTERN ZONE
274
(14.0)
REYKJANES
RIDGE
100 KM

the geochemistry of the basalts erupted along the Reykjanes Ridge could be explained by the presence of a mantle plume beneath Iceland. A number of isotopic studies have confirmed that the mantle beneath Iceland is heterogeneous (Hart et al., 1973; Sun et al., 1975; O'Nions and Pankhurst, 1974; O'Nions et al., 1976), but suggest that Schilling's (1973) two end-member mixing model is somewhat oversimplified (Langmuir et al., 1978; Zindler et al., 1979).

There are also definite major element and petrographic variations within the rift zones of Iceland (Jakobsson, 1972, 1979; Sigvaldason, 1969; Sigvaldason et al., 1974). Jakobsson (1972) showed that basalts erupted along the eastern and middle volcanic zones are primarily tholeiitic, while the Snaefellses zone and southern part of the eastern zone are primarily alkali basalt. Sigvaldason et al.(1974) showed that are significant alkali element variations within the tholeiite suites, with central Iceland having the most K rich basalts. Jakobsson (1979) has shown that Icelands' active rift zones are divided into discreet dike swarms, whose orientations define the rift direction; each swarm is geochemically and geologically distinct from its neighbors. Several studies have also shown that there are isotopic variations within a single swarm (Zindler et al. 1979; Wood et al., 1979)

Given these important geochemical variations, the helium isotope measurements were intended to help determine the location and nature of any mantle plume beneath Iceland. Poreda et al. (1981) have reported high $^{3}He/^{4}He$ ratios from dredged basalts from the Reykjanes Ridge (11-14 x atmospheric). Even higher $^{3}He/^{4}He$ ratios have been reported from the helium in hot springs on the island itself (20-22 x

atmospheric; Polak et al., 1975; Poreda et al., 1980). However, the highest values were obtained from hot springs between the eastern and middle zones, making any connection to the geochemistry of the rift zones tenuous. The only helium analyses of Icelandic rift rocks yielded ratios much lower than the hot springs (.1-10 x atmospheric; Mamyrin et al., 1974). However, these analyses were of bulk rock samples, rather than phenocrysts or subglacial glasses, and the low helium concentrations (10^{-9} to 10^{-8} cc/gram) strongly suggest that any initially trapped mantle helium has been "swamped out" by atmospheric or radiogenic helium.

The results reported in table 5.2 and displayed in figure 5.4 show that there are isotopic differences between the eastern and middle volcanic zones, and within each zone. The use of subglacial glasses to indicate magmatic isotopic ratios appears to be valid; the results for olivine and glass from the same sample confirm this, and allow the isotopic variations to be interpreted as the result of mantle heterogeneity. Therefore, the high $^{3}He/^{4}He$ ratios observed for the two samples near the central eastern zone (18 and 22 x atmospheric) imply the presence of an undepleted mantle source beneath this part of Iceland. The results from the middle volcanic zone also indicate $^{3}He/^{4}He$ ratios primarily higher than MORB, but significantly different from the eastern zone. Based on this limited data set, there is no apparent "gradient" along the middle zone, which suggests that simple mixing between the highest eastern zone source and some MORB type source does not necessarily explain the difference.

The one sample with a lower $^{3}He/^{4}He$ ratio (8.67 x R_A,

HS806), indicates the presence of MORB type mantle beneath Iceland, near Langjokull, and should be characterized by depleted rare earth element patterns and $^{87}Sr/^{86}Sr$ ratios <.7030. This particular sample is, in fact, depleted in the light rare earth elements (La/Sm < 1; P. Meyer, personal communication), and reported $^{87}Sr/^{86}Sr$ values from Langjokull are among the lowest on Iceland (~.7030; Hart et al., 1973). Therefore, based upon the classification system delineated in chapter 4, normal MORB type mantle is present beneath Iceland.

In contrast, the samples from the central part of the eastern volcanic zone have $^{3}He/^{4}He$ ratios up to a factor of 2.5 times higher than the Langjokull sample. It is therefore important to compare other geochemical studies of this region, to determine the characteristics of plume-type basalts. In this connection, it is important to note that the basaltic eruption rate near the central eastern zone has been higher than the rest of Iceland during recent times (Jakobsson, 1972; Saemundsson, 1979). These basalts are quartz normative tholeiites, which differ from the olivine tholeiites erupted on the middle volcanic zone (Jakobsson, 1972), and also have higher K contents (Sigvaldason et al. 1974). The sample with the highest $^{3}He/^{4}He$ is slightly enriched in the light rare earth elements (La/Sm > 1.5, P. Meyer personal communication). A number of laboratories have also reported that the $^{87}Sr/^{86}Sr$ ratios of the tholeiites from central Iceland are higher than those from the other zones (Hart et al. 1973; O'Nions and Gronvold, 1973; Wood et al., 1979). However, Wood et al. (1979) has showed that the $^{87}Sr/^{86}Sr$ ratio can vary significantly over a very small geographic area, so

these values cannot necessarily be applied to the samples analyzed in this study.

Despite the uncertainties, several generalizations can be made with regard to the overall geochemical variations. First, the trace element and isotopic geochemistry of the Langjokull region is consistent with the presence of normal MORB type mantle beneath Iceland. The higher $^{3}He/^{4}He$ ratios, enrichments in incompatible trace elements (i.e., La), and higher $^{87}Sr/^{87}Sr$ ratios from central Iceland are consistent with the presence of more undepleted mantle beneath this region. The overall trends are consistent with the classification scheme discussed in chapter 4, and illustrated in figures 4.7 and 5.2.

Muehlenbachs et al. (1974) have reported $\delta^{18}O$ measurements from the central eastern zone that are lower than MORB (~3 permil as compared to 5.5-6.00 permil). Condomines et al. (1981) showed that the samples with low $\delta^{18}O$ values also have higher $^{230}Th/^{232}Th$ than other parts of Iceland. They suggested that these results could either be explained by primary mantle heterogeneity (i.e., differences in Th/U ratio), or by differences in transit time to the surface. In the latter case, the residence times would have to be on the order of 10,000 years, and could explain the low $\delta^{18}O$ by the consequently increased probability of interaction with groundwater. The helium isotope results are more consistent with mantle heterogeneity, since one would expect groundwater interaction to lower the $^{3}He/^{4}He$ ratio. However, the low helium content of groundwater, with respect to most igneous rocks, implies that it would be possible to alter the magmatic $\delta^{18}O$ without altering $^{3}He/^{4}He$, so this evidence is not

conclusive. It should be noted that the $\delta^{18}O$ values for the Loihi seamount samples that have the highest $^{3}He/^{4}He$ ratios are also somewhat low ($\delta^{18}O$ 4.5-5.0 per mil; Kyzer and Javoy, 1981); data from Hawaii and Iceland suggest a relationship between low $\delta^{18}O$ and $^{3}He/^{4}He$. Confirmation of this will require further analyses of the central eastern volcanic zone of Iceland.

It is also of interest to note that Jan Mayen has distinctly different isotopic characteristics, but is geographically quite close to Iceland.

4. Loihi Seamount and the island of Hawaii

a. Background

As discussed in the introduction, the Hawaiian-Emperor seamount chain is the classic hot spot locality that led to the Wilson-Morgan plume model. The hypothesis that mantle plumes near Hawaii and other linear volcanic chains are fixed in space and time has given plate tectonics an absolute reference frame (Morgan, 1972). The best evidence for this model of the Hawaiian Islands is the systematic increase in age to the northwestern end of the chain (Dana, 1890; MacDougall, 1964; Jarrard and Clague, 1977), and the geochemical affinities of the basalts along the chain (Jackson et al., 1980). Unfortunately, detailed geochemical studies of the Hawaiian rocks have not helped constrain the details of models. For example, an alternative theory is that the melting and volcanism along the Hawaiian chain are caused by linear lithospheric fractures (Turcotte and Oxburgh, 1978). While isotopic and trace element studies have shown that each volcano on the island of Hawaii is chemically distinct

(O'Nions et al., 1977; Tatsumoto, 1978; Leeman et al., 1980), the variation cannot be simply related to the age of the volcano, or to the plume model. The purpose of this study is to use helium isotopes to trace the contribution of deep mantle material to the volcanic rocks on the island of Hawaii, and to provide a further test of the plume model.

The age trend on the island is similar to the rest of the chain, with the ages of the volcanoes increasing to the north (see figure 5.5) in this order: Loihi seamount, Kilauea, Mauna Loa, Hualalai, Mauna Kea and Kohala. As the youngest island in one of the most well studied island chains, Hawaii provides a unique opportunity to study the isotopic variations between volcanoes in an age sequence, as well as during the evolution of a single volcano.

Field studies of the exposed (subaerial) areas of the Hawaiian islands led to a general model for the evolutionary stages that each Hawaiian volcano passes through (Macdonald and Katsura, 1964; Macdonald, 1968). In this model, the bulk of the volcano is contructed during a "shield building" stage, which is characterized by voluminous (non-explosive) eruption of tholeiitic basalt. It is generally agreed that this requires less than 10^6 years (Jackson et al., 1972). In the final stages of the shield building phase, when the eruptive volume is decreasing, the central caldera collapses and is filled with eruptives of interbedded tholeiitic and alkalic compositions. Following caldera filling, the volcano erupts primarily alkali basalts. Finally, in the "post erosional stages" after significant time has passed, the volcano may intermittently erupt nephelinitic basalts. Gabbroic and ultramafic xenoliths are primarily found in

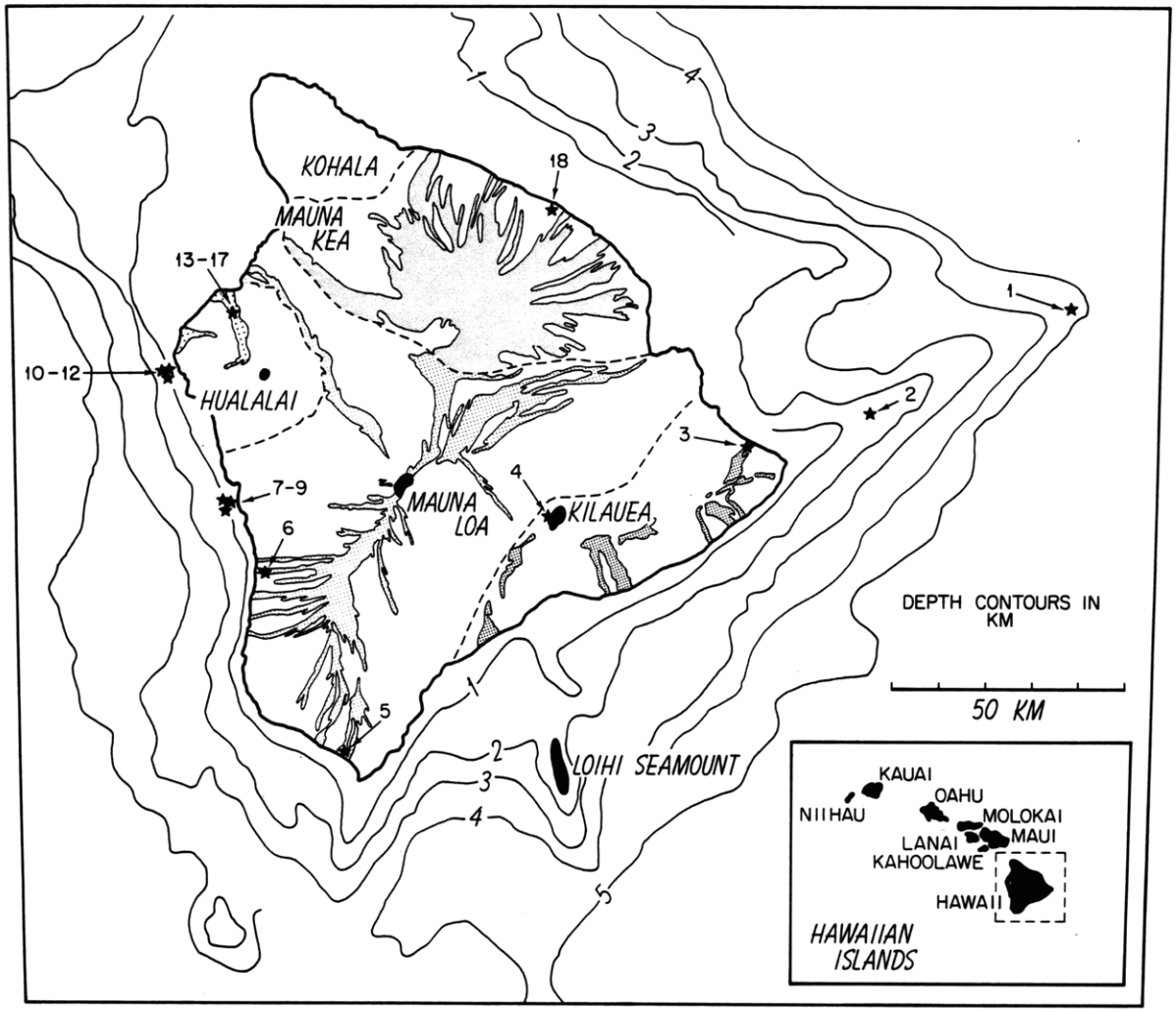


Figure 5.5: Map of Hawaii with sample locations. Numbers refer to the sample key in table 5.5.

these last alkalic and nephelinitic stages (Jackson and Fiske, 1972). Citing the timing of this sequence and the field relationships, Macdonald (1968) suggested that the alkali basalts were derived from a tholeiitic parent by fractional crystallization..

Recent studies of the youngest Hawaiian volcano, the Loihi seamount, have added a complication to this model (Moore et al., 1982). The summit of the Loihi seamount lies 1 km below sea level, and dredging has provided the first opportunity to sample the early stages of Hawaiian volcanism. Moore et al. (1982) have shown that both tholeiitic and alkali basalts are present.

Helium isotopic analyses of fumarole gases from Kilauea showed that $^{3}He/^{4}He$ was higher than that observed for most mid-ocean ridge basalts (Craig and Lupton, 1976). This has now been confirmed by analyses of phenocrysts from subaerial flows on Kilauea as well as dredged submarine glasses from the east rift (Kaneoka et al., 1978; Kurz et al., 1982b). As noted earlier, this conforms with the plume hypothesis since higher $^{3}He/^{4}He$ ratios should be observed for volcanic rocks derived from a deeper, more primitive mantle source. Kaneoka and Takaoka (1980) reported even higher $^{3}He/^{4}He$ ratios in megacrysts from Haleakala volcano (Maui), which showed that there are helium isotopic variations within the Hawaiian islands. In addition, two different flows from Haleakala had significantly different $^{3}He/^{4}He$ ratios (Kaneoka and Takaoka, 1980), which implies that there are variations within a single volcano. The present study was intended to characterize the helium isotopic variability both between and within the most recent Hawaiian volcanic eruptives.

In selecting samples, emphasis was placed on the most recent tholeiitic eruptions of each volcano (where possible), allowing the comparison of volcanoes which represent the different stages. In addition, a more detailed survey was performed on dredged glasses from the Loihi seamount in order to help understand variations within a single volcano. The results presented here confirm that there are variations between the volcanoes on Hawaii. The variations can be interpreted in terms of changing mantle source chemistry during evolution of the volcano, and provide strong confirmation of the mantle plume hypothesis. The results from the Loihi seamount and Hualalai show that there are also variations within a single volcano that can be related to rock type and petrography.

b. Loihi Seamount - partitioning

The remarkable diversity of basalt types dredged from the Loihi seamount, ranging from differentiated alkali basalts to tholeiites, has been described by Moore et al. (1982). The concentration and isotopic composition of the helium within 15 of the Loihi glasses, selected to span this compositional range, are presented in table 5.3. Since the vesicularities range from .1 to 41 volume percent (see table 5.6), the helium was extracted both by crushing and by melting in vacuo, to (1) compare the glass-melt partitioning with mid-ocean ridge basalts, (2) determine whether any isotopic fractionation occurs, and (3) determine the extent to which the highly vesicular samples have degassed.

Kurz and Jenkins (1981) showed that MORB glasses obey equilibrium glass-melt partitioning between .01 and 3 volume percent vesicles. The helium partitioning results for Loihi glasses (from tables 5.3 and 5.6)

Table 5.6: Partitioning values and vesicularities (from Moore et al., 1982) for Loihi Seamount glasses

Sample	Rock Type	volume $^{o}/o$ vesicles	Total He^4	$\frac{^4He \text{ vesicles}}{^4He \text{ glass}}$
KK 23-3	tholeiite	1.3	1.25	.938
29-10	tholeiite	4.2	7.24	6.03
18-8	tholeiite	6.0	2.88	15.94
20-14	tholeiite	5.8	4.1[a]	
16-1	tholeiite	2.5	5.0[a]	
78 HW 2-16	tholeiite	<.5	6.0[a]	
24-7	transitional	.1	1.22	.21
25-4	transitional	2.1	5.78	13.19
20-4	alkali basalt	5.6	5.16	91.1
17-2	differentiated alkali basalt	5.7	2.81	81.8
21-2	differentiated	24.9	.29	>14.5
27-4 *	alkali basalt	27.0	4.42	9.57
31-12 *	alkali basalt	27.9	14.8	7.18
17-5 *	basanite	41.4	3.64	>243.0
14-4	alkali basalt	18	.50 .45	>48

*sample from a xenolith bearing flow (see table 5.4).

[a]Total helium calculated from vesicularity, crushed concentration, and the equilibrium partitioning curve.

are compared to the MORB results in figure 5.6. Loihi samples with vesicularities in the range .1 to 5 volume percent lie within the MORB partitioning field, while there is considerably more scatter for the samples with higher vesicle contents. Assuming that the partitioning is not strongly composition dependant, the samples that lie below the MORB field in figure 5.6 (KK31-12, KK27-4) have probably experienced gas loss, an explanation that is consistent with the high vesicularities.

Similarly, samples that lie above the MORB field must have gained gas by some mechanism. It is quite possible that the glasses are heterogeneous on a small scale, leading to different vesicularites between the sub-samples that are used for this section (point counts) and for gas extraction. Petrographic evidence supports this hypothesis for at least one sample (KK 15-4), in which the vesicles are elongated, indicating active volatile movement before quenching of the glass.

Vesicle heterogeneities on the scale of a single sample cannot, however, explain the high parititioning value for sample 17-5. First, this sample had 41 percent vesicles, both in thin section and in the sample analyzed, which shows that it would be difficult for any part of the sample to have more vesicles without disaggregating. In addition, visual examination (under the binocular microscope) shows that the vesicles are quite large (up to 1 mm), and that most of them are open, implying that substantial gas loss <u>has</u> taken place. If so, the partitioning value should plot below the MORB field in figure 5.6.

In this case, it is likely that fluid inclusions within olivine xenocrysts contribute significant quantities of helium to crushing

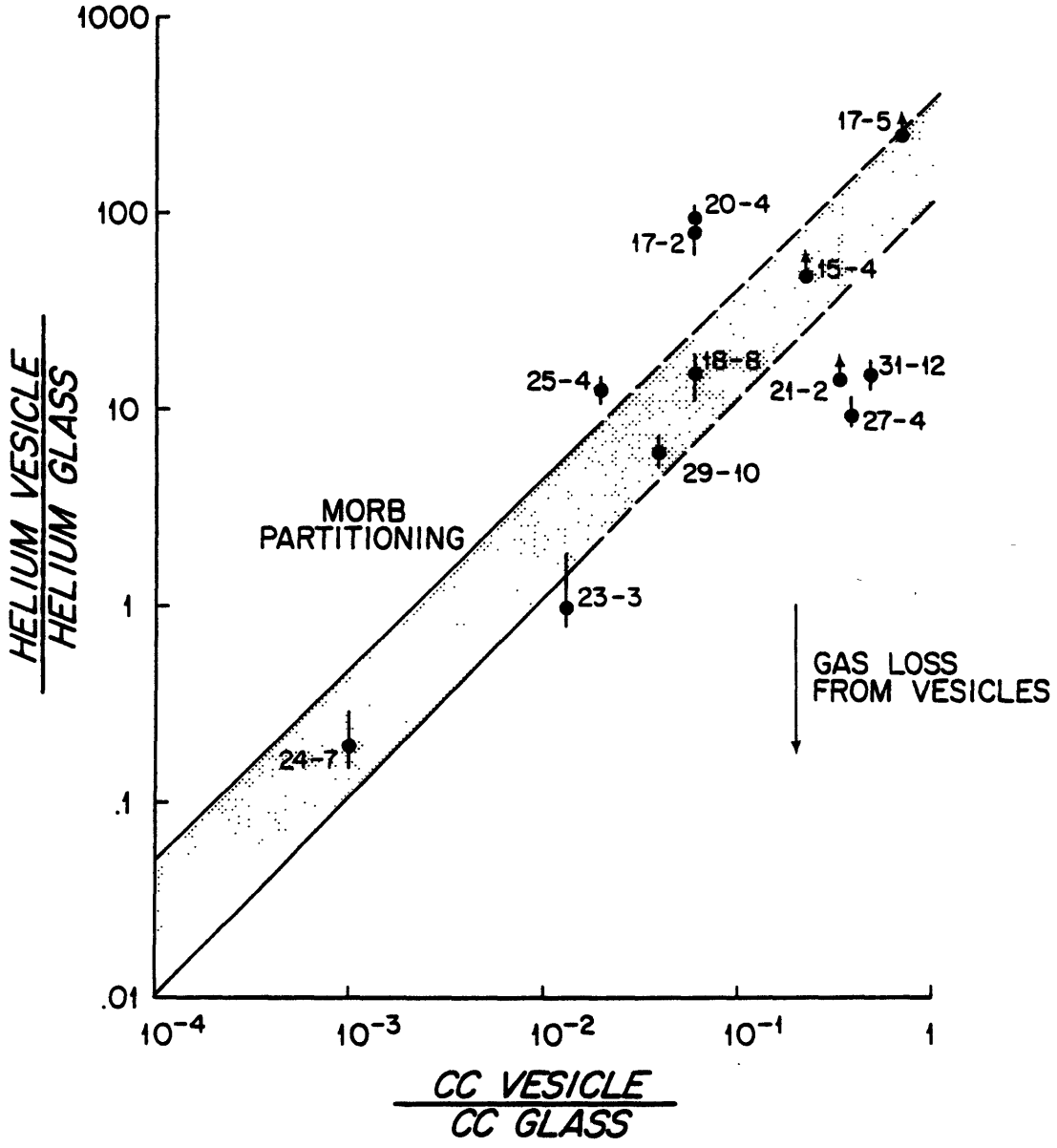


Figure 5.6: Partitioning plot for Loihi seamount glasses. Partitioning points with an arrow attached are lower limits due to low helium contents in the glass (see text). All data from table 5.6, MORB field from chapter 3.

extraction, elevating the apparent gas-melt partitioning. Petrographic examination of KK 17-5 supports this conclusion, since many of the olivines within the glass have kink bands and rows of fluid inclusions, and show evidence of dissolution, suggesting that they are xenocrysts.

The helium analyses of several Loihi dunite xenoliths illustrate the potential importance of xenocrysts to glass measurements, since the observed concentrations are higher than the total concentrations in many of the glasses (see table 5.4). This result is clearly related to the high abundance of fluid inclusions within the dunite, as is illustrated in the photomicrographs (see Appendix II). Using phase equilibria, Roedder (1981) has shown that these fluid inclusions consist primarily of CO_2 that has been trapped at pressures of 3-5 kbar. Given the high trapping pressure, and high abundance of the inclusions within the xenoliths, it is not surprising that they contain signficant quantities of helium. In their petrographic point counts of the xenolith bearing glasses (KK17-5, 31-12, and 27-4), Moore et al. (1982) found between 18-22 volume percent olivine phenocrysts within the glass. Examination of sample 17-5 in thin section (see Appendix II) shows that many of these olivines within the glass contain kink bands and fluid inclusions, and are probably xenocrysts formed by disaggregation of the xenoliths. Therefore, the analysis of 17-5 probably reflects the helium in the xenocrysts rather than the glass. Further, the xenoliths must be considered as a source of gas (to the glasses) that is not necessarily related to the mantle source region.

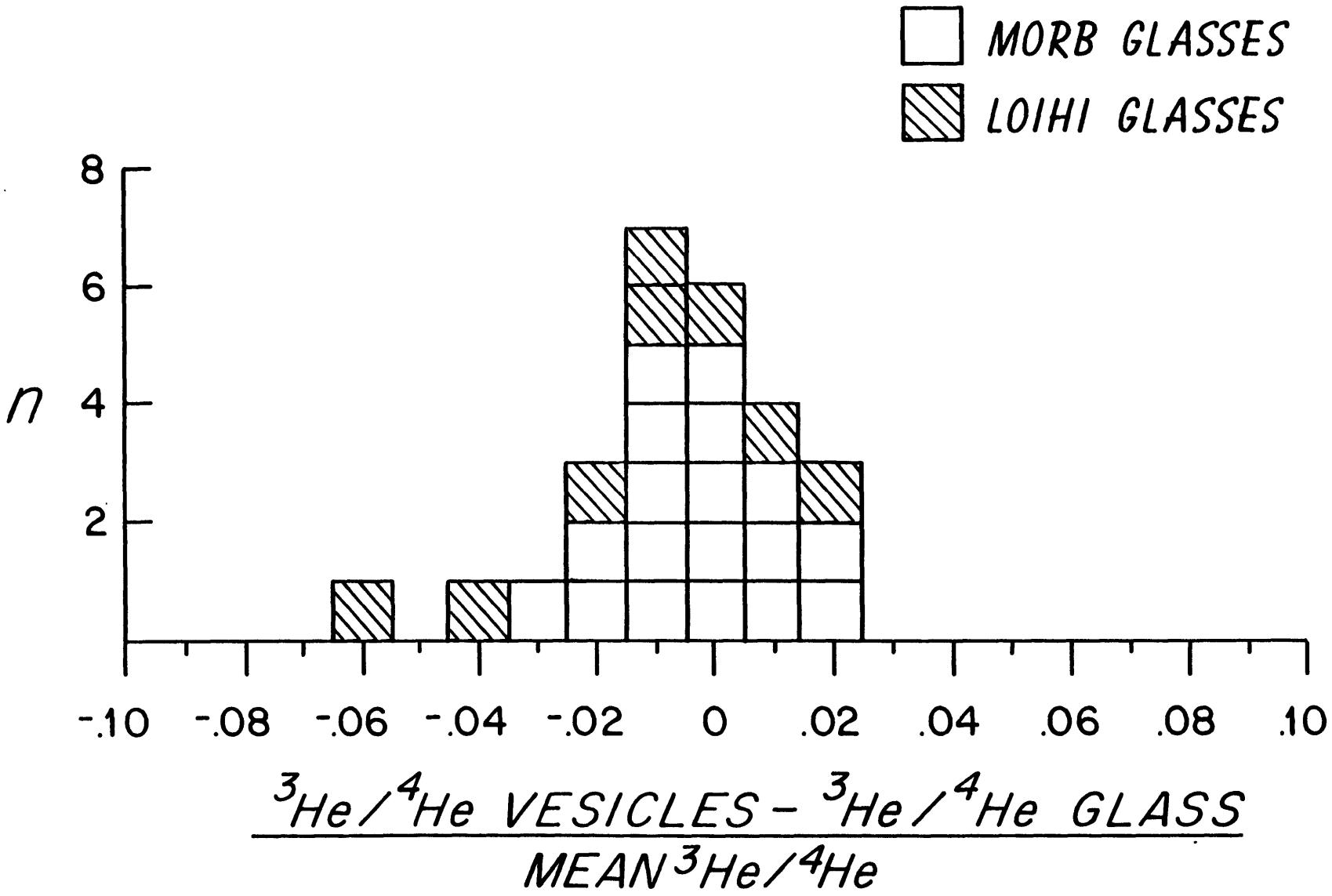
It is also important to note that the concentration of helium in the xenoliths is to some extent a function of grain size (see table

5.4), with higher concentrations observed in the larger grains. This is consistent with the petrography of the samples, since most of these xenoliths have porphyroclastic texture. The larger olivine grains have a greater abundance of fluid inclusions than the small grains, making them appear darker (see Appendix II). One model for the origin of this texture is that the original coarse grained rock has been partially recrystallized, resulting in large grains surrounded by the younger recrystallized grains. The distribution of helium in these xenoliths is consistent with this scenario, if the gas was present before the recrystallization, and hence is more abundant in the original grains.

c. Loihi - isotopic variations

For the samples where it was possible to analyze the helium by crushing and by melting (of the same sample), there appears to be no significant isotopic fractionation between vesicles and glass, in agreement with earlier partitioning studies (Kurz and Jenkins, 1981; Kurz et al., 1982a). This is illustrated by the histogram plot of the difference between $^{3}He/^{4}He$ ratio in glass and vesicles (figure 5.7). For comparision, the MORB samples, for which crushing and melting extractions were performed on the same sub-sample (see chapters 3 and 4), are also plotted. The data forms a normal distribution about zero, with a range of roughly ±3 percent. Since the uncertainty of the $^{3}He/^{4}He$ measurement for MORB glasses is roughly 1-2 percent, and the uncertainty of the Loihi measurements is 1-3 percent (see table 5.3), this range is within two standard deviations of the uncertainty. Several of the vesiculated samples (KK 21-2, 17-5, 15-4) had no detectable helium left in the glass, due to efficient degassing, and

Figure 5.7: Histogram plot of the difference between $^{3}He/^{4}He$ ratio in glass and in vesicles, for Loihi and MORB glasses. Loihi data from table 5.3, MORB data from chapters 3 and 4.


MORB GLASSES
LOIHI GLASSES
n
8
6
4
2
-.10
-.08
-.06
-.04
-.02
0
.02
.04
.06
.08
.10
3He/4He VESICLES - 3He/4He GLASS
MEAN 3He/4He

could not be plotted on this diagram.

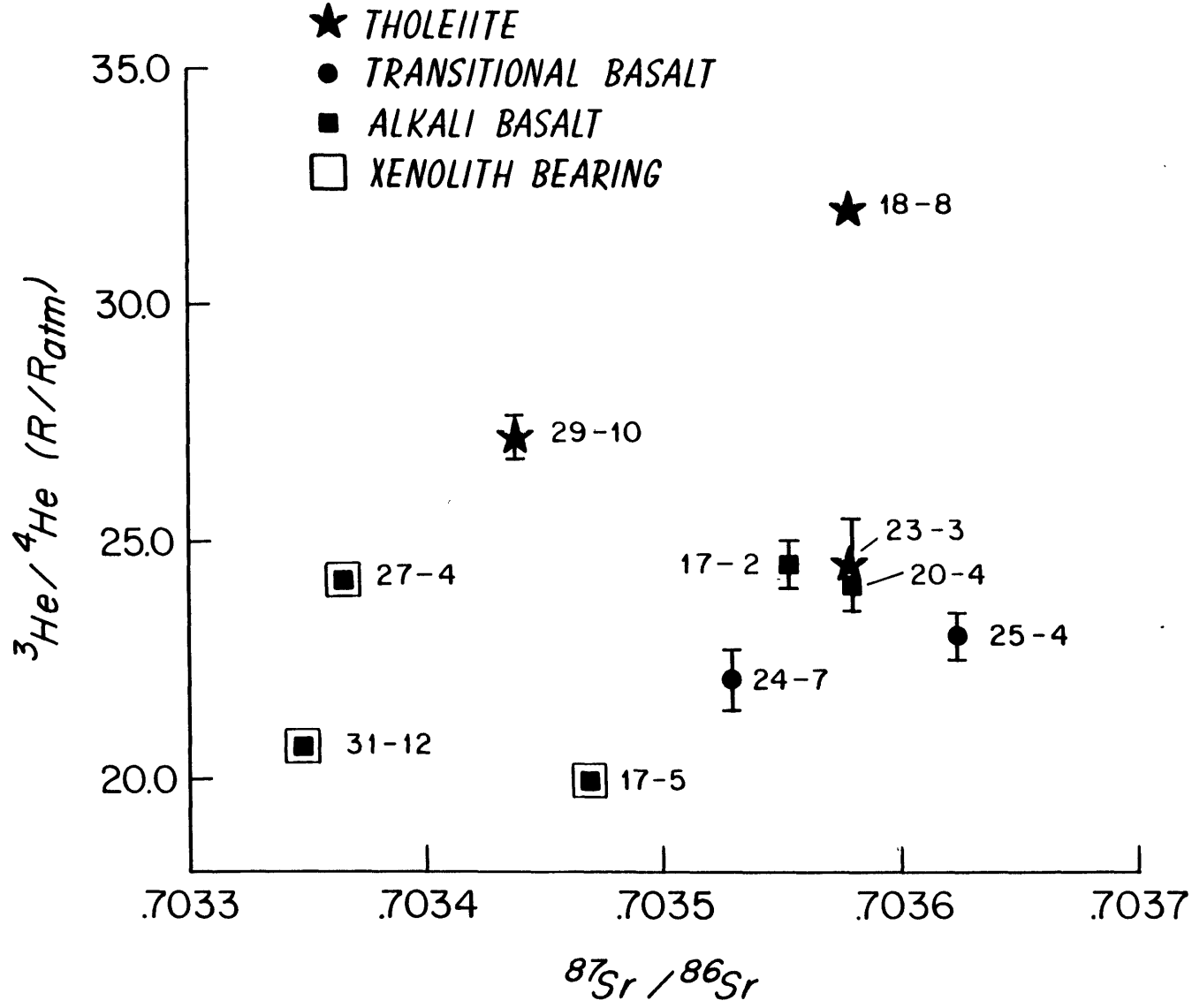
As discussed by Kurz et al (1982b), the $^3He/^4He$ ratios in the Loihi seamount glasses are among the highest reported for any presently erupting terrestrial volcano. However, the three analyses reported earlier (KK20-4, KK23-3, KK18-8) did not span the compositional range of erupted basalts, and as shown in Table 5.3, do not characterize the variation in $^3He/^4He$ ratio. The $^3He/^4He$ ranges from 2.77×10^{-5} (20.0 x atmospheric) for an alkali basalt (KK 17-5) to 4.41×10^{-5} (31.9 x atmospheric) for a tholeiite (KK 18-8). One sample (KK21-2, a differentiated alkali basalt) has a $^3He/^4He$ ratio significantly lower than this range (4.6 x atmospheric). However, there is petrographic evidence that KK 21-2 has interacted with seawater or atmosphere, rendering the isotopic ratio unrepresentative of the mantle source. Although the glass is fresh and unaltered, this sample's extreme vesicularity (25 percent by volume), coupled with small cracks that permeate the glass, suggest that any gas remaining is no longer representative of the pre-eruptive magma. Since there is good evidence that vesiculation is not isotopically fractionating (figure 5.7), the low ratio observed for this sample must be a result of contamination by the atmosphere. The narrow boundary between adjoining vesicles (typically less than .1 mm) and cracks provide effective pathways both for gas loss from the vesicles and diffusive atmospheric contamination. Cracks are lined with clay minerals, which shows that they were formed during quenching on the ocean floor. The efficiency of the degassing is illustrated by the small helium content of the glass ($<1 \times 10^{-9}$ cc/g) and the small quantity of gas relased

by crushing in vacuo (2.9×10^{-8} cc/g). Given the small boundary between adjoining vesicles,and the presence of cracks, it therefore seems likely that this sample has been contaminated.

It is noteworthy that among the other fourteen samples, the tholeiites have significantly higher $^{3}He/^{4}He$ ratios. This is clearly illustrated in the plot of $^{87}Sr/^{86}Sr$ vs. $^{3}He/^{4}He$ (figure 5.8). The strontium isotopic analyses for these samples have been taken from Staudigel et al. (1981); the Sr, Nd and Pb isotopic variations will be discussed in detail elsewhere. It is also important to note that the xenolith-bearing alkali basalts define a separate field in this diagram. As discussed earlier, the extremely high helium concentrations within the dunite xenoliths, and the high abundance of xenocrysts within the glass, suggest that the mantle source of the xenoliths must be considered as a possible mixing end-member. The samples KK 18-8 and KK 31-12 define the extremes not only on the $^{87}Sr/^{86}Sr$ vs. $^{3}He/^{4}He$ plot, but also on the Sr vs. Nd and Sr. vs. Pb isotope plots, which lends credence to this argument. However, it is not clear to what extent the xenolith helium has contributed to the helium in the glass.

If we assume that all of the modal olivine in these three glasses are xenocrysts (~20 percent for KK 31-12, 27-4, 17-5) and that the helium concentration in the xenocrysts was originally similar to the highest observed for the xenoliths (KK 27-9A and B: 1.5×10^{-6} cc/gm), a maximum of 3×10^{-7} cc STP/gram helium in these samples would be xenolith-derived. In all three cases, this could account for a significant percentage of the observed helium

Figure 5.8: $^{3}He/^{4}He$ vs $^{87}Sr/^{86}Sr$ for the Loihi seamount samples. Helium data is from table 5.3 and the strontium data is from Staudigel et al., 1981.


THOLEIITE
TRANSITIONAL BASALT
ALKALI BASALT
XENOLITH BEARING
35.0
30.0
25.0
20.0
$^3He/^4He$ (R/R_{atm})
18-8
29-10
23-3
17-2
20-4
27-4
25-4
24-7
31-12
17-5
.7033
.7034
.7035
.7036
.7037
$^{87}Sr/^{86}Sr$

content (20 percent for 31-12, 68 percent for 27-4, and 82 percent for 17-5). Since the xenocrysts are typically .1 to 1 mm in size, it is impossible to separate them from the glass without crushing the glass and hence opening the vesicles. However, we cannot assess the relative contribution this would make to magmatic helium because all three samples have greater than 27 percent vesicles, and have therefore lost much of this original helium. In addition, there appears to be considerable variation, in concentration and isotopic ratio, within the xenoliths themselves (see table 5.4).

Finally, it is possible that the mantle source for the xenoliths has contributed gas to the magma before eruption by interaction in a magma chamber, or during ascent. Since the xenoliths contain liquid CO_2 inclusions trapped at 3-5 kbar pressure (Roedder, 1981), the parental source for the xenoliths can provide significant quantities of CO_2 to account for the extreme vesicularities of these samples. Therefore, the xenoliths represent a plausible explanation for the anomalous vesicularity in addition to the distinct $^3He/^4He$ ratios.

It can also be argued that the xenoliths are in isotopic equilibrium with their hosts because they are genetically related, and the mantle source for the alkali basalts is isotopically distinct from that of the thoeliites. Given the equivocal nature of the evidence described above, we cannot discount this hypothesis. If the tholeiites and alkali basalts were derived from the same source, very special conditions are required to generate the observed $^3He/^4He$ variations. In particular, the alkali basalts must have interacted with another source of helium, perhaps represented by the xenoliths.

In the case of the helium isotopes, the possiblity that "xenolithic helium" has been added to the Loihi samples and/or magmas cannot be ruled out.

It is also noteworthy that there are significant variations among the tholeiites, which could also be explained by interaction with "xenolithic" helium. Since xenocrysts and xenoliths are not present within the tholeiites, any such interaction must have taken place in the magma chamber, or during melting. The isotopic variations require that the tholeiites are derived from different sources, or that they have interacted with another source; it is impossible at present to distinguish between these possibilities.

d. Helium results for Hawaiian volcanoes

The helium measurements on glasses, phenocrysts, and xenoliths from Kilauea, Mauna Loa, Hualalai and Mauna Kea are presented in table 5.5 and are plotted with the Loihi results in figure 5.9. Since significant differences between alkali basalts and tholeiites were observed for the Loihi Seamount and the goal of this study was to compare the different volcanoes, tholeiites from each volcano were analyzed wherever possible. In the case of Mauna Kea, this was not possible, so the helium was extracted from the phenocrysts within alkali olivine basalt. As shown in figure 5.9, the $^{3}He/^{4}He$ ratio roughly decreases with age of the volcano. Possible explanations for these variations are:

1. Mantle heterogeneity beneath Hawaii, with each volcano tapping a different source (or combination of sources) at different stages of evolution.

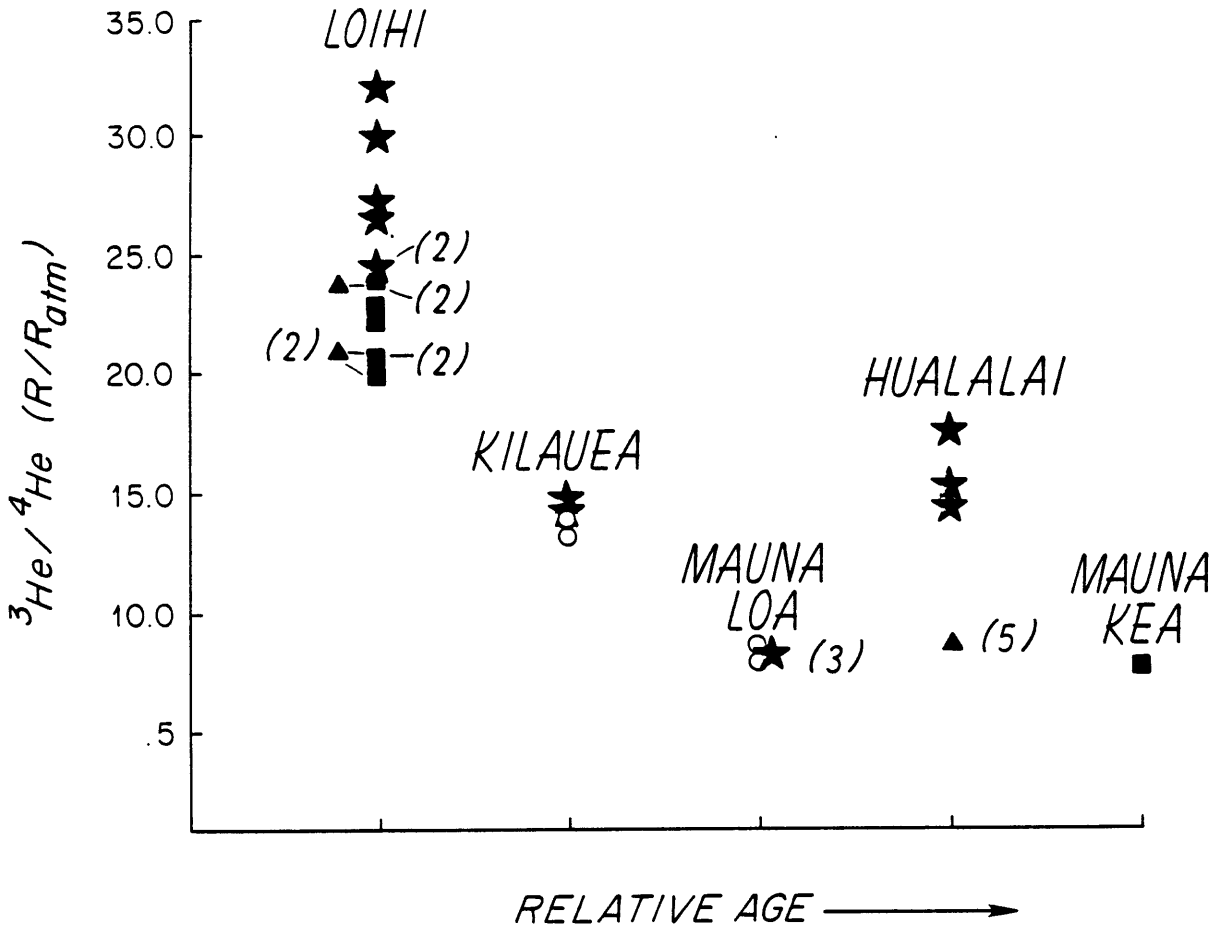


Figure 5.9: $^3He/^4He$ vs. volcano age for the Hawaiian volcanoes. The volcano age scale is relative age since initiation of volcanism, on the basis of field and K-Ar studies (e.g. Macdonald, 1968). Numbers in parentheses refere to number of analyses; symbols:

★ SUBMARINE THOLEIITE

○ SUBAERIAL THOLEIITE

■ ALKALI BASALT

▲ XENOLITH IN ALKALI BASALT

2. Production of radiogenic ^4He during the life of a single magma chamber, resulting in lower $^3He/^4$ ratios with time.

3. Disequilibrium melting, with the earlier stages of volcanism representing melting of the helium rich phases.

4. Interaction with seawater, resulting in lower $^3He/^4He$ ratios with time.

We can immediately eliminate recent production of ^4He (point 2 above), since the tholeiites contain so little U and Th, and all of the rocks discussed here are very young ($< 10^5$ years). Using Tatsumoto's (1978) U and Th contents for Hawaiian tholeiites (~ 200 ppb), only 2×10^{-9} cc/gram radiogenic ^4He would be produced in 10^5 years. Even for this maximum time, radiogenic production of helium in a magma chamber (or in situ) will be insignificant compared to the helium contents in the glasses.

As has been discussed by Hofmann and Hart (1978), disequilibrium melting is unlikely as long as enough time is available for local diffusive equilibrium, and that diffusion rates of cations insure equilibrium. Given the rapid diffusion rate of helium in silicate melts, any disequilibrium process is least likely for helium.

Finally, interaction with seawater is unlikely because there is so little helium in seawater (~ 4×10^{-8}cc/gram). In order to slightly modify the magmatic $^3He/^4He$ ratio, such a large volume would be required that drastic increases in $^{87}Sr/^{86}Sr$ would be observed.

Therefore, the most reasonable explanation for the helium isotopic variations must involve mantle heterogeneities beneath Hawaii. Since the Loihi samples have the highest $^3He/^4He$ ratios, we may infer

that its mantle source has the highest proportion of primordial helium. The decrease in $^{3}He/^{4}He$ with the relative age of the volcano implies that the relative contribution of primordial helium decreases as the volcano evolves. This is consistent with the idea that the heat source for the Hawaiian melting anomaly is derived from a primordial mantle plume, and that high $^{3}He/^{4}He$ ratios are associated with this mantle source. The $^{3}He/^{4}He$ ratios are also related to plate motions since once the volcano moves off the "hot spot," the source of primoridal helium is removed and therefore the source changes.

A clue to the physical nature of the change in source chemistry with time may be derived from the vertical trend, defined by the Hawaiian basalts, on the $^{87}Sr/^{86}Sr$-$^{3}He/^{4}He$ diagram. The trend indicates that the later stages involve mantle sources with $^{3}He/^{4}He$ ratios close to, or lower than MORB (8-9 x atmospheric), with $^{87}Sr/^{86}Sr$ ratios similar to the earlier stages. The $^{87}Sr/^{86}Sr$ ratio of Mauna Loa (.7038; O'Nions et al., 1977) makes it difficult to explain the variations by mixing between a Loihi-type source and a normal MORB source. If this evolution were due to greater involvement (by melting) of typical upper mantle, the $^{87}Sr/^{86}Sr$ would be expected to <u>decrease</u> due to the depleted nature of the MORB source.

e. <u>A model for the Hawaiian Islands</u>

Any plausible model for the helium and strontium isotopic variations shown in figures 5.2 and 5.9 must also incorporate the field observations (e.g. MacDonald, 1968), and the geophysical studies of the area. The sea floor near Hawaii is characterized by a broad region of

unusually shallow depths associated with heat flow and gravity anomalies (Watts and Cochran, 1974; Detrick and Crough, 1978; Detrick et al. 1981). Detrick and Crough (1978) and Crough (1979) have suggested that this "Hawaiian swell" is produced by heating of the lithosphere from below. In their model, the cool lithosphere is uplifted by the heating near Hawaii, and as it moves away the sea floor subsides according to the normal crustal thickness-age relation. Detrick and Crough (1978) also suggest that the lithosphere is thinnest beneath Hawaii, and that heat conduction rates suggest that heat must be delivered by magma transport.

Feigenson et al.(1981) performed a detailed geochemical study of Kohala volcano on Hawaii, and showed that the eruption rate, and degree of partial melting decrease with time. They suggested that this could best be explained by stress induced melting coupled with viscous dissipation (i.e., melt removal). However, this model does not account for the geophysical observations, and cannot explain the $^{3}He/^{4}He$ variations in figure 5.9. However, their observations are of fundamental importance.

In light of the helium data, and the geophysical evidence for an asthenospheric heat source, a hot spot model which involves melting of the lithosphere is most feasible. In this model, melting is induced within an upwelling mantle diapir by adiabatic expansion. The plume becomes partially molten, and the heat is transferred into the overlying oceanic lithosphere by melt migration, which in turn produces melting within the lithosphere. During the initial stages of Hawaiian volcanism, the volcano is directly over the plume, there is a high

input of heat, a high degree of partial melting, and high $^3He/^4He$ ratios. The magma that is erupted at the surface is a hybrid produced by melting within the lithosphere and asthenosphere (plume) type melts. After the volcano moves off the plume, the lithosphere is still removing the heat by producing melt, but the material transfer from below is decreased. At this stage, the degree of partial melting, eruption rate, and $^3He/^4He$ ratio all begin to decrease.

An additional constraint is the decrease in $^3He/^4He$ with increasing volcano volume shown in figure 5.10. The model described above can explain this relationship, if the samples from the smaller volume volcanoes are the product of higher degrees of partial melting. The higher degree of partial melting would then be the result of a greater involvement of melt from the plume, and would consequently have higher $^3He/^4He$ ratios. This is in qualitative agreement with a decrease in extent of partial melting with volcano evolution (Feigenson et al., 1981).

In addition to accounting for the time dependence of the helium and strontium isotopic variations on Hawaii, this model can also explain the variations within Hualalai and Loihi seamount, since the variations in helium and strontium isotopes require the presence of mantle heterogeneity beneath a single volcano. It is quite reasonable to expect that the lithosphere and upwelling asthenosphere should have different $^3He/^4He$ ratios, and therefore could expain this variation.

Several important problems arise from this model. First, since Hualalai has a low volume, is now quiescent, and has a high $^3He/^4He$ ratio (in the tholeiites), extinction must not occur at the same

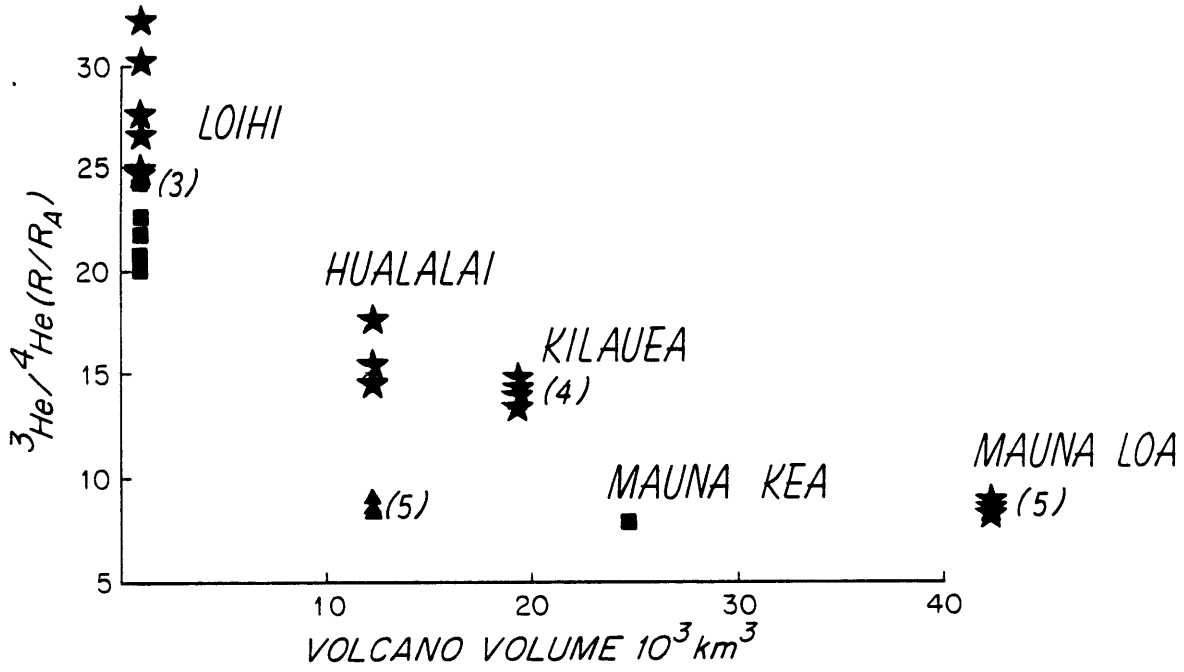


Figure 5.10: $^3He/^4He$ vs. volcano volume for the Hawaiian volcanoes. Volcano volumes are taken from Bargar and Jackson, 1974. Numbers in parentheses refer to the number of analyses; symbols:

★ THOLEIITES

■ ALKALI BASALTS

▲ XENOLITH

evolutionary stage for all Hawaiian volcanoes. This possibility has previously been implied by Shaw et al. (1980), who showed that there has been episodicity along the Hawaiian chain, both in eruption rates and erupted volumes. There is, at present, no physical mechanism to explain this episodicity. An additional problem is that the chemical and isotopic composition of the lithosphere is unknown, and depends to a great extent on the details of oceanic crustal formation. For example, it is not clear if the lithosphere (below the crust) is made of lherzolite that has been depleted by extraction of basalt at the mid-ocean ridge. If it were, it would be doubly depleted, due to the initially depleted nature of the upper mantle before melt extraction. This doubly depleted material would not necessarily yield basalt upon melting, and would not necessarily have any helium left. However, the higher $^{87}Sr/^{86}Sr$ ratio in the Mauna Loa basalts would argue against involvement of normal MORB type mantle.

Finally, the results from Haleakala volcano (Kaneoka and Takaoka, 1980) do not necessarily conform to the simple model, since extremely high $^{3}He/^{4}He$ ratios (up to 37 x atmospheric) were observed in phenocrysts from alkali basalts. Although the younger of the two samples analyzed by Kaneoka and Takaoka (1980) had a lower $^{3}He/^{4}He$ ratio (C. Chen, F. Frey, personal communication) as predicted, the alkali basalts were erupted late in the volcanoe's evolution and have $^{3}He/^{4}He$ ratios higher than the Loihi tholeiites.

5. Implications for mantle heterogeneity

a. The mantle plume model

The mantle plume model as envisioned by Wilson (1963) and Morgan

(1971), is a dynamical explanation for linear island chains. It only requires that the heat source for the island basalt volcanism be derived from a mantle upwelling phenomenon. The association with primitive undepleted mantle has primarily been inferred by geochemists (Schilling, 1973, 1975; Sun and Hanson, 1975). However, as pointed out by Hofmann and White (1980), the dynamic aspects of mantle plumes need not imply the presence of undepleted mantle. They suggest that subducted oceanic crust that remains within the mantle for long time periods (1 b.y.) can produce both the heat necessary for upwelling and the isotopic anomalies.

The helium isotopic results presented in this chapter show that there are two groups of islands: low $^3He/^4He$ and high $^3He/^4He$ islands. The low $^3He/^4He$ samples are primarily from islands with alkaline compositional affinity: Tristan da Cunha, Gough, Jan Mayen, La Palma, and Prince Edward. The low $^3He/^4He$ ratios for these samples (< 8 x atmospheric) are clearly inconsistent with their derivation from undepleted mantle, which is a strong argument against the presence of geochemically primitive mantle plumes beneath these islands. These results are not necessarily inconsistent with the dynamic aspects of mantle plumes. However, if mantle plumes are present beneath the low $^3He/^4He$ islands, they must derive their heat from non-primitive sources (i.e., low $^3He/(Th+U)$.

It should also be noted that the subaerial part of each volcano comprises a small fraction of the total erupted volume. For example, in the case of Tristan da Cunha, only 4 percent of the volcano lies above sea level. It is conceivable that the alkali basalts are

underlain by tholeiitic shields. The results from Hawaii show that the $^3He/^4He$ decreases as the age of the volcano increases, and that the alkali basalts have lower $^3He/^4He$ ratios. However, it is not clear how these relationships apply to other islands or whether all islands have tholeiitic shields. Regardless of these uncertainties, the alkali basalts are <u>not</u> derived from a undepleted source.

The islands with high $^3He/^4He$ ratios are tholeiitic in composition. Hawaii and Iceland display the highest $^3He/^4He$ ratios, and in these two cases, there is good evidence for the presence of primitive, undepleted mantle. Further, there are significant variations on a local scale (~30 km) that imply helium isotopes can be used to trace undepleted mantle. In both Hawaiian and Icelandic samples, the locally highest $^3He/^4He$ ratios are associated with the youngest, most active volcanism. These results are entirely consistent with the presence of primitive undepleted mantle beneath these two islands, and therefore with the plume model.

The helium isotopic variations within the island of Hawaii provide the most convincing evidence for the plume model. The highest $^3He/^4He$ ratios are observed for tholeiite samples of the youngest volcano (Loihi seamount) and decrease in the older volcanoes (Kilauea and Mauna Loa; see figure 5.9). Using high $^3He/^4He$ ratios as a tracer of primitive mantle, this variation can be readily explained by the plume model. The plume location is fixed (Morgan, 1981), and is at present directly below the Loihi Seamount. As the Pacific plate moves, the volcano slowly moves farther away from the hot spot, in a pattern that has been occurring for at least 70 million years (Jarrard and

Clague, 1977). As the volcano moves away, the helium isotope ratio decreases due to the waning influence of the primordial helium from the hot spot. As this occurs, the volcano nears extinction, because the heat source is also removed. Since the samples analyzed in this study are, for the most part, recent eruptives of each volcano, the observed variations reflect the aging process that any Hawaiian volcano passes through. In this model, the Hawaiian volcanoes each represent these different stages:

1. In the early stages of volcanism, the plume influence is strong, which leads to high $^3He/^4He$ ratios (Loihi seamount).

2. At the intermediate stages, the $^3He/^4He$ ratios are slightly lower than the early stages, due to increased involvement of "normal" upper mantle helium (Kilauea).

3. At the end of shield building, the $^3He/^4He$ ratios are more typical of upper mantle helium (~8 x atmospheric); Mauna Loa).

4. The final stages of volcanism also have low $^3He/^4He$ ratios, characteristic of the normal upper mantle (Mauna Kea).

b. The layered mantle

The isotopic variations in oceanic basalts are of fundamental importance to structural models of the earth's mantle. In particular, the proven presence of heterogeneities helps to constrain possible modes of mantle convection. Although it is generally agreed that convection is the major mechanism of terrestrial heat loss geophysicists are presently debating whether convection is mantle-wide (Elsasser et al., 1979) or layered (Richter and McKenzie, 1981). An example of the interrelation between geochemistry and convection models has been presented by Richter and Ribe (1979), who modeled the effect

of shallow mantle convection on Sr isotopic variations in the south Pacific islands. Clearly, to evaluate the geochemical constraints on these convection models, it is necessary to understand the origin of the chemical heterogeneities. The helium isotope variations offer new clues regarding both the nature and the origin of the chemical heterogeneities.

One of the most important results obtained in this study is that basalts from Tristan da Cunha and Gough islands have low $^{3}He/^{4}He$ ratios. Samples from both these islands have Sr and Nd isotopic compositions close to "bulk earth" (O'Nions et al., 1977). The low $^{3}He/^{4}He$ ratios show that these islands cannot be derived from primitive undepleted mantle, and that the negative $^{143}Nd/^{144}Nd$ - $^{87}Sr/^{86}Sr$ correlation must not be viewed simplistically. The helium results suggest that these islands are derived from a recycled mantle source, that is, one which has had the $^{3}He/Th+U$ lowered by degassing in the past. If this recycled source is old oceanic crust, the Nd-Sr anti-correlation may be partially produced by mixing. This has been suggested independently by Anderson (1982a), who also points out that a third mantle reservoir can explain the "Pb paradox" and the trace element variations.

In contrast to the low $^{3}He/^{4}He$ - high $^{87}Sr/^{86}Sr$ islands, Iceland and Hawaii have somewhat lower $^{87}Sr/^{86}Sr$ ratios and up to four times higher $^{3}He/^{4}He$ ratios. Thus the most primitive islands, in terms of helium isotopic composition, are depleted with respect to "bulk earth" Sr and Nd isotopic compositions. This also suggests a mixing origin for the Nd-Sr correlation.

These distinct isotopic trends (illustrated in figure 5.2) are reflected in the major and trace element compositions of the basalts. The samples with lower $^3He/^4He$ ratios in general have higher K_2O contents (see figure 5.3). This is true within individual suites of samples (from Loihi seamount and MORB from the North Atlantic), and in the global variations. Since the $^3He/^4He$ islands are tholeiitic in character, they generally have higher FeO/MgO ratios. The islands with intermediate $^3He/^4He$ ratios (Bouvet, Reunion, and Mauritius) have overall major element chemistry that is transitional between tholeiitic and alkalic (Upton and Wadsworth, 1972; Baker, 1973; le Roex, 1980). As has been discussed by Langmuir and Hanson (1980), not all the differences in FeO/MgO between islands can be explained by fractionation processes, and mantle heterogeneity must also explain some of the major element differences. The correlations between $^3He/^4He$ and major elements lend support to this argument.

In view of these data, any mantle model must contain three different reservoirs having distinct isotopic, trace element, and major element characteristics. In agreement with the classifications based on the MORB data (chapter 4), these three types can be summarized as follows:

1. Undepleted mantle has $^3He/^4He$ ratios >9.0 x atmospheric, low alkali abundances, relatively high iron contents, $^{87}Sr/^{86}Sr$ ratios >.7030, and rare earth patterns that are depleted to enriched in light rare earths.

2. Depleted mantle has $^3He/^4He$ ratios between 8.0 - 9.0 x atmospheric, low alkali abundances, high iron contents, $^{87}Sr/^{86}Sr$ ratios <.7030, rare earth patterns that are depleted in light rare earths.

3. Recycled mantle has $^{3}He/^{4}He$ ratios <8.0 x atmospheric, low FeO/MgO ratios, $^{87}Sr/^{86}Sr$ ratios >.7030, high alkali abundances, and light rare earth enriched abundance patterns. The geographic distributions suggest that all three mantle reservoirs are global in extent, but must be able to interact with one another. This is consistent with, but does not prove the existence of, a layered mantle. The helium data cannot allow a distinction between mixing of melts of of mantle sources (see also chapter 4). The origins of the three mantle types will be further discussed, in conjunction with geophysical data, in chapter 6.

E. Conclusions

The principal conclusions that can be derived from this study of oceanic islands are summarized below. A more detailed discussion of the implications to mantle geochemistry and degassing is given in chapter 6.

1. The use of the helium trapped within phenocrysts to indicate magmatic $^{3}He/^{4}He$ ratios is valid, as long as the petrography is carefully examined. In particular, xenocrysts must not be present, since they can contain significant quantities of helium that is unrelated to the host magma.

2. Extractions performed on phenocrysts confirm that helium behaves as an incompatible element. Although it is impossible to quantitatively calculate the partitioning value, we can estimate an extreme upper limit ($K_D << .01$).

3. The glass-vesicle helium partitioning can be used to identify samples that have gained or lost gas. When the Loihi seamount samples are compared to the MORB equilibrium partitioning, several

samples lie above or below the trend. The samples that lie below the trend have lost gas by vesicle-opening. Those that lie above the trend have gained gas, either by pre-quenching migration, or by the addition of gas-rich xenocrysts.

4. Within the experimental uncertainty of the measurements, there is no isotopic difference between the glass and the vesicles for the Loihi samples, in agreement with MORB results (see chapters 3 and 4).

5. There are significant global variations in mantle $^{3}He/^{4}He$ ratios that require the presence of at least three different reservoirs within the oceanic mantle. The variations observed for ocean island basalts can be explained if island basalts are mixtures of the different sources. While the range of $^{3}He/^{4}He$ values for ocean island basalts is much larger than for MORB, this explanation can apply to both basalt populations (see chapter 4).

6. The most undepleted sources (i.e., highest $^{3}He/^{4}He$ ratios) are sampled by volcanism on Iceland and Hawaii, which suggests that the Nd-Sr correlation alone cannot be used to judge which source regions are primitive. All of the islands that have high $^{3}He/^{4}He$ ratios consist primarily of basalts with tholeiitic affinities: Hawaii, Iceland, Bouvet, Reunion, and Mauritius.

7. There are significant variations within Hawaii and Iceland that must be explained by local mantle heterogeneities. On Hawaii, the $^{3}He/^{4}He$ decreases with the age of the volcano, and with with increasing volcano volume. These variations are consistent with the plume model, if the plume is at present directly below Loihi

Seamount and if the lithosphere is involved in producing Hawaiian magmatism. On Iceland, the helium isotopic variations are also consistent with the plume model, since the highest $^3He/^4He$ ratio is observed for central Iceland, where the eruptive rate is presently the highest.

8. The lowest $^3He/^4He$ samples are alkali basalts from Tristan da Cunha and Gough, which shows that these islands are not representative of primitive mantle. The lowest $^3He/^4He$ samples are the most enriched in alkalis; this is true for the overall global variations as well as within individual rock suites (Loihi and North Atlantic MORB). Within the Loihi suite, the alkali basalts have the lowest $^3He/^4He$ ratios, but are still significantly higher than alkali basalts from Gough and Tristan.

CHAPTER 6

IMPLICATIONS FOR MANTLE HETEROGENEITY AND DEGASSING

A. Introduction

Theories describing the origin of the atmosphere and the geochemical evolution of the mantle are inextricably linked to the earth's thermal history. Since the influential papers by Brown (1949) and Suess (1949), it has generally been recognized that the atmosphere was formed by degassing of the solid earth. Delivery of heat and gases to the earth's surface is, at present, accomplished by mantle convection and ultimately volcanism. It is therefore reasonable to assume that the histories of both processes have been related; however, there is little agreement as to the time dependence of either mantle convection or geochemical evolution. The approach taken in the preceding chapters has been to study the present-day state of the mantle, and to ascertain the origins of geochemical heterogeneities in the mantle. In this chapter, I attempt to relate the helium isotopic results to models of the structure and evolution of the mantle, and hence the degassing history of the earth. As discussed in previous chapters, the helium data suggest the existence of three different mantle reservoirs, and can therefore provide important constraints on mantle models.

While it is generally agreed that the mantle is convecting (Stevenson and Turner, 1979), there is no consensus as to the details of the convection. One set of models calls for convection cells extending throughout the whole mantle (Davies, 1977; O'Connell, 1977;

Elsasser, 1979), while another set of models calls for layered convection, with each layer containing cells of a different scale (Richter, 1973; McKenzie and Weiss, 1975; Richter and McKenzie, 1981). The mode of convection is criticially dependent upon the depth variation of density, viscosity, and temperature, which are in turn controlled by the chemical composition and initial thermal state of the earth. At present, it is impossible to unequivocally choose a single model, but we can use available geochemical and geophysical observations to choose a viable working hypothesis. As discussed below, the model that seems most consistent with all the evidence is one with a two layer mantle.

The most convincing evidence for a layered mantle comes from isotope geochemistry. The Sr, Nd and Pb variations show that different mantle reservoirs must have been separated for long periods of time (O'Nions et al., 1977; Hofmann and Hart, 1978; Sun, 1980). Mass balance calculations (using Nd) have shown that if the continents were derived from an undepleted reservoir (resulting in MORB type depeleted mantle), 30-50 percent of the mantle is required (O'Nions et al., 1979; Jacobsen and Wasserburg, 1979). While the He and Pb isotopic variations show that this is somewhat oversimplified, and that more than two mantle types are required, this calculation is useful with regard to mantle models: it suggests that a significant part of the mantle could be undepleted. This conclusion is supported by the high $^{3}He/^{4}He$ ratios (compared to normal MORB) observed for Hawaii and Iceland (see chapter 5). However, the low $^{3}He/^{4}He$ samples obtained from other islands show that the continents are not the only enriched

reservoir. This may affect the Nd mass balance calculations, depending on the volume of recycled material stored in the mantle.

To keep large parts of the mantle separate for long periods of time in the presence of convection, requires either a layered mantle or one which has large lump-like heterogeneities (Hofmann et al., 1978). A lumpy mantle model, which involves whole mantle convection, has been proposed by Davies (1981). One important problem with such a model is that convection tends to homogenize and distort any lumps (McKenzie, 1979). Further, the lumps must account for the ocean island volcanism, which is undepleted, long lived, and spatially fixed. For example, the Hawaiian-Emperor seamount chain has been erupting lavas of similar composition for the last 70 m.y. (Jackson et al., 1981), and, as shown by the helium data, is tapping a undepleted source. If this type of volcanism is to be explained by a lumpy mantle, the advection velocities must be much lower than recent estimates (Elsasser et al., 1979) and some means of accounting for the uniform eruptive compositions must be found (see also Hofmann et al., 1978).

A good deal of geophysical evidence for a layered mantle exists. Seismic studies have revealed a prominent velocity discontinuity at 650 km depth that was initially attributed to the effect of higher iron content and density below this depth (Birch, 1961; Anderson, 1967; Press, 1972). Recent work has shown that this discontinuity does not necessitate compositional differences, but can also be explained by phase changes due to increasing pressure (Anderson, 1976; Lieberman, 1978; Liu, 1978). Richter and McKenzie (1981) have pointed out that either compositional differences or phase changes can inhibit

convection through this discontinuity, depending on the thermodynamics of the phase change, and the magnitude of the density contrast. Some evidence for a barrier to convection comes from the lack of subduction zone earthquakes below 700 km (Isacks and Molnar, 1971; Richter, 1979), which suggests that the downgoing slab does not penetrate the discontinuity.

A particularly important and promising geophysical observation involves the use of gravity anomalies. When long wavelength gravity anomalies are correlated with long wavelength bathymetry, isostatic causes can be ruled out, and the most likely explanation is convection in the upper mantle (McKenzie, 1977; McKenzie et al., 1980; Watts and Daly, 1981). McKenzie et al. (1980), using this approach in the Pacific, found good correlation between long wavelength gravity and bathymetry, and observed a characteristic wavelength of 1500-2000 km that was consistent with convection cells aligned parallel to the plate motion. This type of convection has been observed in experiments involving two layer convection (Richter and Parsons, 1975; Richter, 1978). While this observation does not prove the existence of two-layer convection, such a small wavelength would be very difficult to produce with whole mantle convection (i.e., extending to 2900 km depth).

Another argument concerns the earth's thermal budget. The abundance of K, U, and Th in most oceanic basalts suggests that their mantle source regions do not contain enough of these heat producing elements to generate the observed surface heat flow (Clark and Turekian, 1979; O'Nions et al., 1979). One possible explanation is

that the lower mantle contains more heat, and that there is a thermal boundary layer between the upper and lower mantle. This arrangement could lead to layered convection cells (e.g. Richter and Parsons, 1975).

The effects that layered convection would have on the terrestrial heat budget have been discussed by McKenzie and Weiss (1975) and McKenzie and Richter (1982). McKenzie and Richter (1982) have performed model calculations showing that the present day heat flow/heat production ratio (roughly 2) can best be attained by a mantle that is layered, with each layer having its own convection scale. If the convection extended from the core to the surface, the heat flow/heat produced ratio would be closer to 1. The primary uncertainty in this argument is the estimate of heat production in the earth, which is strongly composition dependent. If current estimates of the mantle K content are correct (~200-400 ppm; Hurley, 1968; O'Nions et al., 1979), then this is reasonable. However, it should be noted that a chondritic earth would have a K content of 800 ppm.

In summary, the weight of evidence seems to favor a layered mantle, although none of the arguments discussed above can alone prove the layered mantle hypothesis. Since the helium data are more consistent with a layered mantle, this will be a starting assumption for constructing a model.

The helium data presented in chapters 4 and 5 strongly suggest the presence of three distinct mantle reservoirs, which must be included in any mantle model. The basaltic isotopic variations were interpreted to be the result of mixing between three "end-members," but aside from the depleted reservoir, the end-members are not uniquely defined by the

data. Before constructing a model, it is therefore necessary to describe potential end-members.

B. Mantle Models: Constraints from the Helium Isotopes

1. Identification of the undepleted end-member

Helium isotopes are useful in identifying which mantle sources are undepleted (or undegassed) relative to one another. However, the question naturally arises as to the identity of the most primitive mantle reservoir, i.e., the one that has remained most unfractionated (i.e., undegassed) since the earth's formation. Given the three-component mixing diagram described above, it is important to constrain the possibilities for this potential end-member. It should be noted at the outset that such a "closed" reservoir may no longer exist. Since a chondritic, bulk earth, reference model is often used to discuss Sr and Nd isotopic evolution (DePaulo and Wasserburg, 1976; Richard et al., 1976; O'Nions et al., 1977), the helium isotopic evolution will be evaluated in such a case. This exercise assumes that the material that formed the earth was somehow related to the meteorites that are now available for study.

Three noble gas components are generally recognized in stony meteorites: trapped, radiogenic, and cosmogenic (Heymann, 1972). In gas rich meteorites that allow the relative characterization of these components (by stepwise heating), the trapped gases have been divided into "solar" and "planetary" (see for example Pepin, 1968; Black, 1972a, 1972b). The He/(Th+U) ratio of gas rich meteorites is high enough that it is not necessary to correct for radiogenic ^4He. The solar gases have $^3He/^4He$ ratios of ~4 x 10^{-4}, which is very

similar to the present day solar wind (Geiss et al., 1972; Warasila and Schaeffer, 1974), and are generally thought to result from solar wind implantation in space (Heymann, 1972). The planetary gases have $^3He/^4He$ ratios near 1.4×10^{-4} and have noble gas abundance patterns similar to earth's atmosphere (hence the name "planetary"). The present day solar wind $^3He/^4He$ ratio is probably not representative of the initial value for the earth since deuterium burning in the sun has been increasing the solar $^3He/^4He$. Using estimates for primordial He/H and D/H, Trimble (1975) suggested that the early sun had a $^3He/^4He$ ratio $<2 \times 10^{-4}$. Therefore, for the present discussion, the planetary $^3He/^4He$ of 1.4×10^{-4} will be adopted as an initial value for the earth.

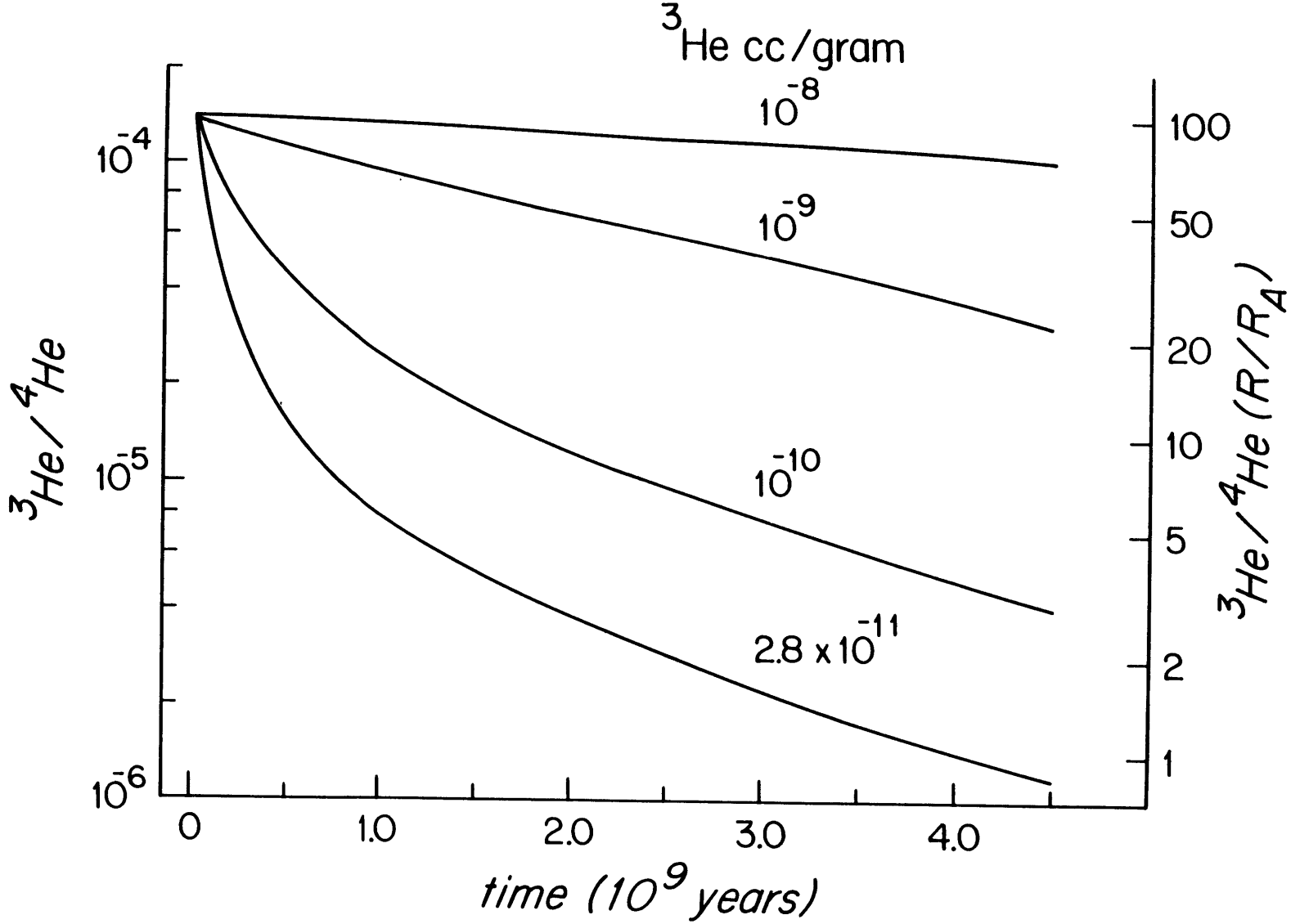
Given the assumed initial $^3He/^4He$ ratio, it is now necessary to choose initial U, Th, and ^3He contents for the earth. Chondritic meteorites have relatively constant present day U and Th contents: 15 and 45 ppb, respectively (Morgan, 1971). These values are somewhat lower than, but not totally inconsistent with estimates based on terrestrial rocks and heat flow (Hurley, 1968a,b; Jacobsen and Wasserburg, 1979; O'Nions et al, 1979). Unfortunately, choosing an initial ^3He content is not as straightforward because of the large observed range and the often dominating effect of spallation and solar helium. Nevertheless, a reasonable range for planetary chondritic ^3He concentration is 10^{-10} to 10^{-7} cc STP/g (Mazor et al., 1970). However, gas rich meteorites often have ^3He concentrations in excess of 10^{-7} cc STP/gram, and several authors have shown that most of the planetary trapped gases are contained in minor mineral phases

(Reynolds et al., 1978; Srinivason et al., 1978). With these uncertainties in mind, when one attempts to calculate $^3He/^4He$ evolution for a closed system chondritic earth, the results depend primarily upon the initial ^3He content. Several evolution lines for the assumed initial $^3He/^4He$, U, and Th and various initial ^3He contents are displayed in figure 6.1.

Clearly, if the earth had ^3He contents $> 10^{-8}$ cc/gram, any unfractionated reservoir would retain its initial $^3He/^4He$ ratio (assumed to be 1.4×10^{-4} or 100 x atmospheric). This suggests that mantle reservoirs with $^3He/^4He$ ratios higher than those observed to date are theoretically possible (i.e., > 37 x atmospheric; Kaneoka and Takaoka, 1980). On the other hand, this calculation illustrates why helium isotopes alone cannot constrain the extent to which the earth is degassed: if the earth originated with a ^3He content of $\sim 10^{-8}$ cc/gram, it could be 90 percent degassed and would still have reservoirs with $^3He/^4He$ ratios higher than 20 x atmospheric. Therefore, since the initial ^3He content is unknown, the presence of high $^3He/^4He$ ratios or present day outgassing (e.g. Jenkins et al., 1977) does <u>not</u> prove the existence of "pristine" mantle.

Assuming a normal MORB concentration of 1.2×10^{-5} cc ^4He/gram (see chapter 4) and that MORB is generated by 20 percent partial melting, the ^3He content of "normal" oceanic mantle is 2.8×10^{-11} cc STP/g. At this concentration, it would only take 700 million years for the initial $^3He/^4He$ of 1.4×10^{-4} to change to the MORB $^3He/^4He$ (see figure 6.1). In a qualitative sense this confirms that the mantle source for MORB is depleted with respect to ^3He. In

Figure 6.1: Closed system $^{3}He/^{4}He$ evolution for an assumed chondritic earth with U = 15 ppb, Th = 45 ppb, and initial $^{3}He/^{4}He = 1.4 \times 10^{-4}$. The curves are calculated with these conditions and different initial ^{3}He concentrations.


^{3}He cc/gram
10^{-8}
10^{-9}
10^{-10}
2.8×10^{-11}
10^{-4}
10^{-5}
10^{-6}
$^3He/^4He$
100
50
20
10
5
2
1
$^3He/^4He\ (R/R_A)$
0
1.0
2.0
3.0
4.0
time (10^9 years)

contrast, the highest observed $^3He/^4He$ ratios (Loihi Seamount for example) show that the mantle source regions for these samples must have had a time integrated ^3He content greater than 10^{-9} cc STP/gram (see figure 6.1). These concentration estimates have important implications for the earth's helium budget, and are discussed in greater detail below.

Another way of evaluating the potential end-member is to see if the observed $^3He/^4He$ and $^{87}Sr/^{86}Sr$ variations can be explained by mixing. Figure 6.2 shows the range of terrestrial $^3He/^4He$ and $^{87}Sr/^{86}Sr$ values for comparison (on a semi-log scale). The bulk earth Sr isotopic value has been derived from the Sr-Nd anti-correlation by a number of authors (e.g., O'Nions et al., 1977). It is assumed, for the purposes of this discussion, that this hypothetical bulk earth also had planetary $^3He/^4He$ ratios. As illustrated in figure 6.3, much of the observed variation (in the high $^3He/^4He$ islands) could be explained by mixing between a normal MORB reservoir and this undepleted bulk earth reservoir. This does not prove the existence of such a reservoir, but only shows that it could explain observed variations. Indeed, this bulk earth reservoir is not necessary since many of the observed variations can be explained by mixing between observed isotopic extremes, as described earlier (see chapter 5).

2. Identification of the recycled end-member

The $^3He/^4He$ and $^{87}Sr/^{86}Sr$ data presented in chapters 4 and 5 argue strongly for a recycled component within the mantle. The question at hand is to ascertain the origin of this recycled mantle

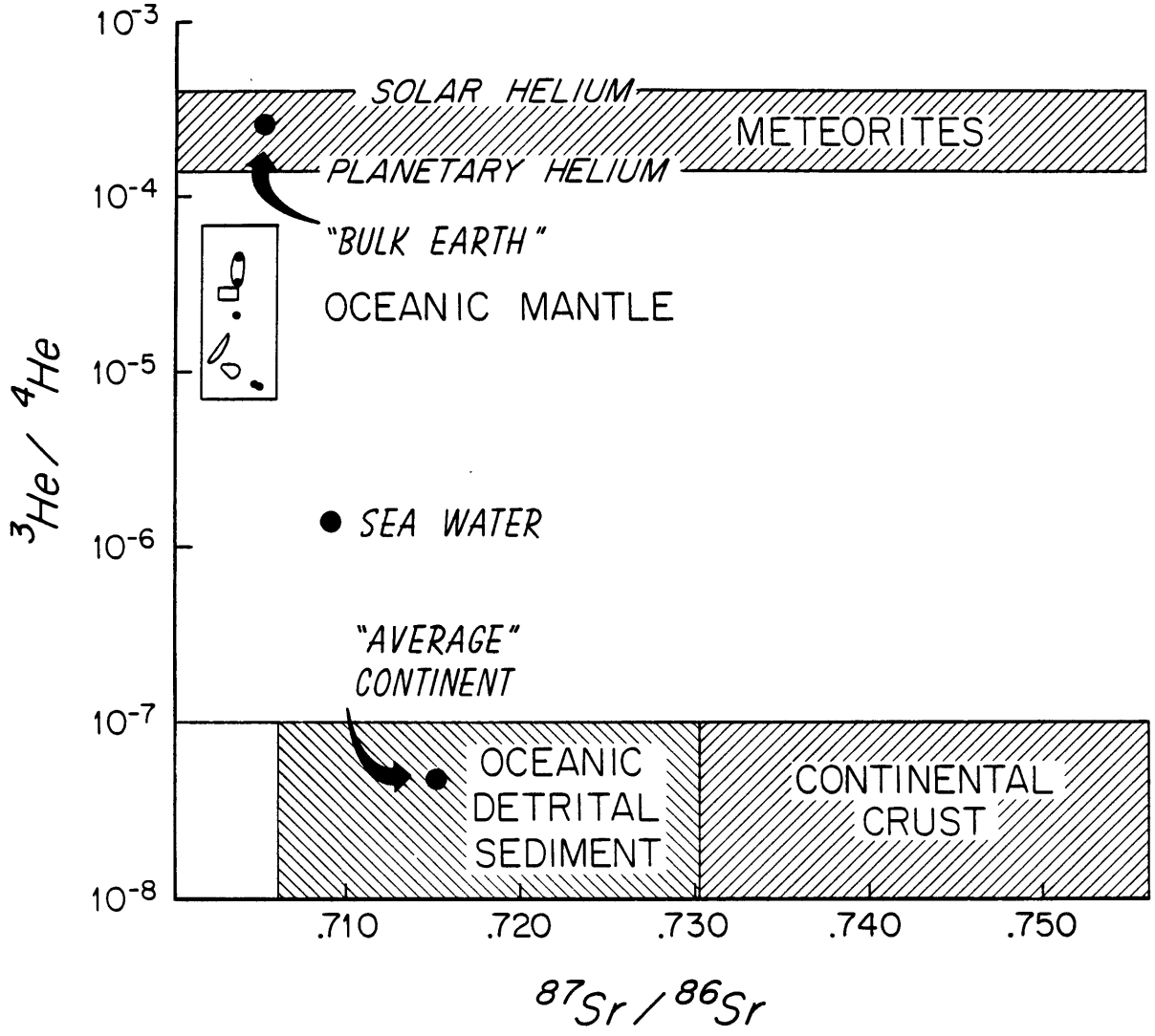


Figure 6.2: $^3He/^4He$ plotted against $^{87}Sr/^{86}Sr$ for terrestrial materials and meteorites.
Data sources:
-chondrites: Mittlefehld and Wetherill (1979); Heymann (1971)
-bulk earth: O'Nions et al. (1977)
-seawater: Clarke et al. (1976); Faure and Powell (1972)
-continental shield: Tolstikhin (1978); McColloch and Wasserburg (1978)
-oceanic detrital sediments: Dasch (1969)
-average crust: O'Nions et al., 1979; Hart and Allegre (1980)

Oceanic detrital sediments are assumed to have the same range of $^3He/^4He$ ratios as continental gases. Bulk earth $^3He/^4He$ values are plotted between planetary and solar meteoritic gases (see text). Meteorite spallation helium, which can have $^3He/^4He > 10^{-4}$, has been ignored.

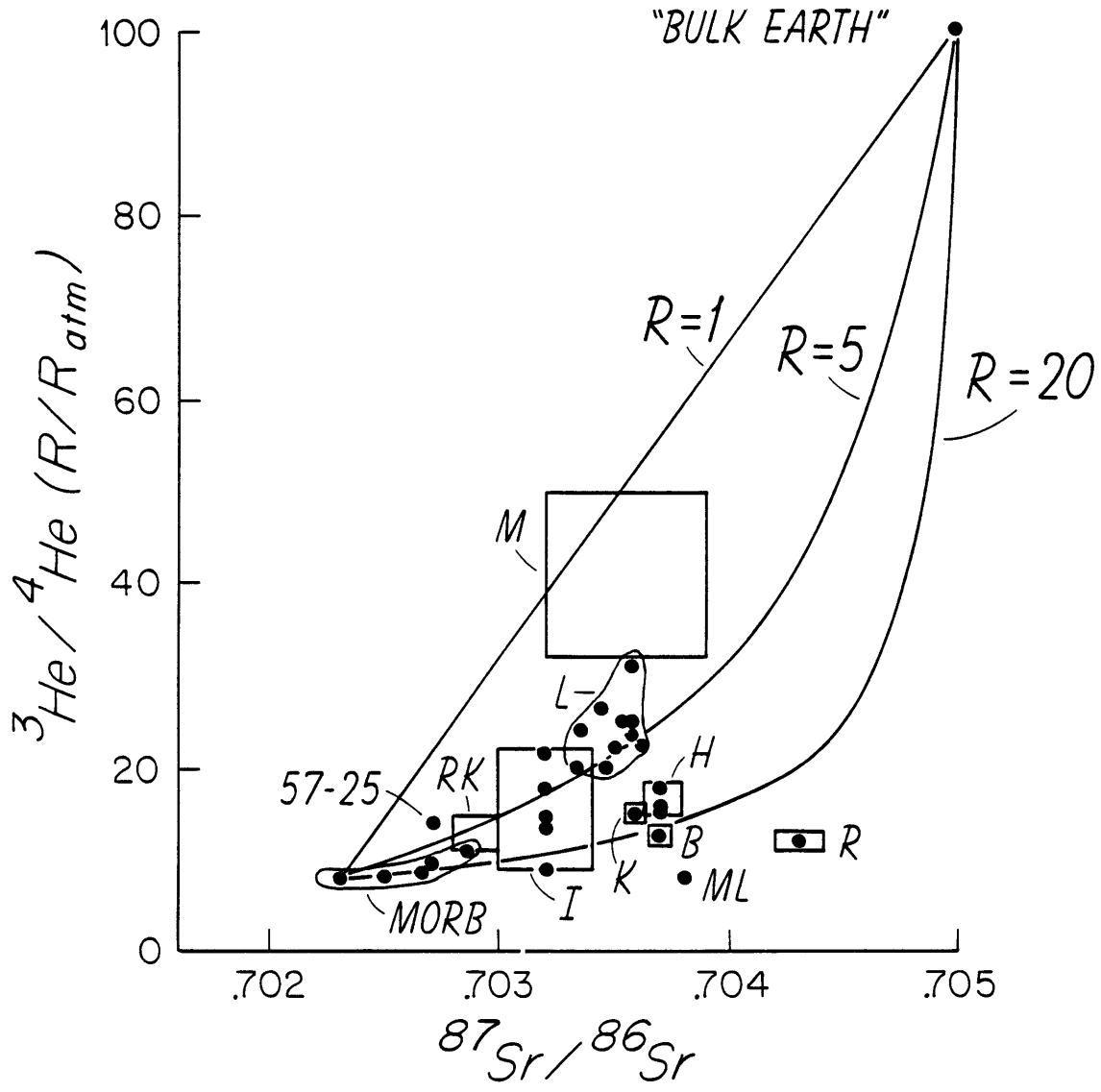


Figure 6.3: Two-component mixing lines on the $^3He/^4He$ vs. $^{87}Sr/^{86}Sr$ diagram. Data fields are from figure 5.2 (only islands with $^3He/^4He$ ratios greater than 8 x atmospheric). The mixing curves were calculated assuming that component 1 has $^3He/^4He$ = 8.4 x atmospheric, $^{87}Sr/^{86}Sr$ = .7023 (MORB) and component 2 has $^3He/^4He$ = 100 x atmospheric, $^{87}Sr/^{86}Sr$ = .705 ("bulk earth," see text).

type, an endeavor necessarily somewhat speculative. As discussed earlier, possibilities for lowering the $^{3}He/^{4}He$ while raising the $^{87}Sr/^{86}Sr$ of the basalts are:

1) Contamination of the magmas by seawater addition near the surface.

2) Contamination of the magmas by interaction with the crust through which they must pass.

3) Metasomatism in the mantle, involving separation of He from U and Th.

4) Recycling of oceanic crust into the mantle via subduction.

Since seawater's He/Sr ratio is much lower than that of the basalts, possibility No. 1 can be eliminated; addition of seawater would have little effect on the $^{3}He/^{4}He$ but would drastically increase the $^{87}Sr/^{86}Sr$. Contamination by interaction with the crust (No. 2) is unlikely in light of the MORB results. The oceanic crust at spreading centers is young and also thin, making any decrease in $^{3}He/^{4}He$ ratio very unlikely, yet low $^{3}He/^{4}He$ are also observed in some MORB. Therefore, the low $^{3}He/^{4}He$ ratios probably reflect the characteristics of the mantle.

On the basis of presently available data it is not possible to completely rule out metasomatism as a mechanism for lowering $^{3}He/^{4}He$. However, the crystal-melt partitioning results (see chapters 3 and 5) suggest that helium behaves as an incompatible element with respect to plagioclase, clinopyroxene, and olivine. This implies that melting processes alone are not effective at altering the $^{3}He/(Th+U)$ ratio, since Th and U are also incompatible elements (Tatsumoto, 1978). It is possible to change this ratio by selective

retention of Th and U in minerals such as apatite, but phases such as this have not been identified in the oceanic mantle. Given the ad-hoc nature of this fractionating mechanism, metasomatism cannot be even qualitatively evaluated.

The most feasible source of the recycled component is subducted oceanic crust that is mixed back into the mantle. A simple mass balance calculation illustrates the volumetric importance of this process. Assuming the subduction rate is equal to the crustal production rate (3 km^2/yr, Williams and von Herzen, 1974), and that the subducted oceanic crust is 7 km thick, roughly 6.3×10^{16}grams/year is subducted at present. Only 3 percent of this rate is sufficient to produce the total present day accretion rate of island arcs (using the estimate of Karig and Kay, 1981). If we extrapolate this subduction rate back through the age of the earth, 2.8×10^{26} grams will have been added to the mantle, which is ~30 percent of the mass of the upper mantle (shallower than 650 km). This should be a minimum value since the subduction rate may have been much faster in the past, due to greater heat production and faster mantle convection (Dickinson and Luth, 1971; Bickle, 1978).

The $^3He/^4He$ of the subducted material, and its effect upon mantle geochemistry, depends to a great extent upon the composition and fate of the downgoing slab. Armstrong (1968) was the first to point out the potential importance of subducted material to geochemical mantle evolution. He emphasized the role of recycled continental material as sediments (see also Armstrong, 1981), although the amount of sediment actually subducted is a controversial issue (Karig and Kay,

1981). Dickinson and Luth (1971) showed that the large volume of subducted material could have an important effect on mantle geochemistry regardless of the amount of recycled sediment.

Until recently, geochemists could not distinguish the isotopic signature of recycled mantle from that of undepleted mantle. Based primarily on Pb isotopes, Hofmann and White (1980) and Chase (1981) have shown the need for a third mantle reservoir, aside from the depleted and undepleted ones. Hofmann and White (1980) suggest that mantle plumes (i.e., oceanic islands) are produced by remelting of old subducted crust that has been stored at the core-mantle boundary. Ringwood (1975) also suggested that subducted material penetrates to the base of the mantle, but implies that it is never re-enters the convecting system. However, Hofmann and White (1980) pointed out that the oceanic crust can contain enough K, U, and Th to produce thermal anomalies, and thereby induce density instability. Anderson (1979a,b) suggested that the recycled oceanic crust is restricted to the upper 700 km of the mantle.

The possible effects of recycling on the mantle $^{3}He/^{4}He$ ratios depend critically on the extent to which the slab is degassed. For example, assuming a mean helium content for the oceanic crust is 1.2×10^{-5} cc STP/gram (see chapter 4), then to generate the oceanic ^{3}He flux (4 atoms/cm^2/sec; Craig et al., 1975; Jenkins et al., 1978) requires degassing of 5 km of the crust. If we take the highest observed MORB concentration as the crustal helium content (2.5×10^{-5} cc/g), only 2.5 km of degassed crust is required. This degassing is an efficient way to separate He from Th and U in the

crust, since neither Th or U will be lost, and U may be added by interaction with seawater (Mitchell and Aumento, 1976; MacDougal, 1977). The helium isotopic evolution of the slab depends on the extent of the degassing. The change in $^3He/^4He$ with time is shown in figure 6.5 for several different cases, all starting with normal MORB $^3He/^4He$, using minimum U and Th concentrations, and assuming that the 7 km thick crust attains internal equilibrium (i.e., the oceanic crust is not heterogeneous). If the crust is 90 percent degassed (case D in figure 6.5), the $^3He/^4He$ decreases to 10^{-6} in less than 300 million years. On the other hand, if the crust is degassed to 2.5 km or 5 km depth, the $^3He/^4He$ will decrease much more slowly.

An additional uncertainty in evaluating the rate at which $^3He/^4He$ will decrease is the fate of the oceanic crust in the subduction zone (see figure 6.4). Many models for the initiation of island arc volcanism have been proposed, among them are melting of the oceanic crust on the downgoing slab (Marsh and Carmichael, 1974), melting on the mantle just above the slab (Kushiro, 1973), and a mixture of the two (e.g Kay, 1980). The choice of melting mechanism can affect the subseqent helium isotopic evolution. Taking an extreme example, if the entire downgoing oceanic crust is melted, most of the U and Th in the crust will be removed with the melt. Therefore, the slab will have lost the source of radiogenic ^4He. The small volume of island arc volcanic rocks relative to the volume of subducted oceanic crust (~3 percent) shows that this is unrealistic, but melting at the subduction zone can result in some loss of Th and U. Studies of Pb, Sr and Nd isotopes in some island arc volcanics strongly suggest the

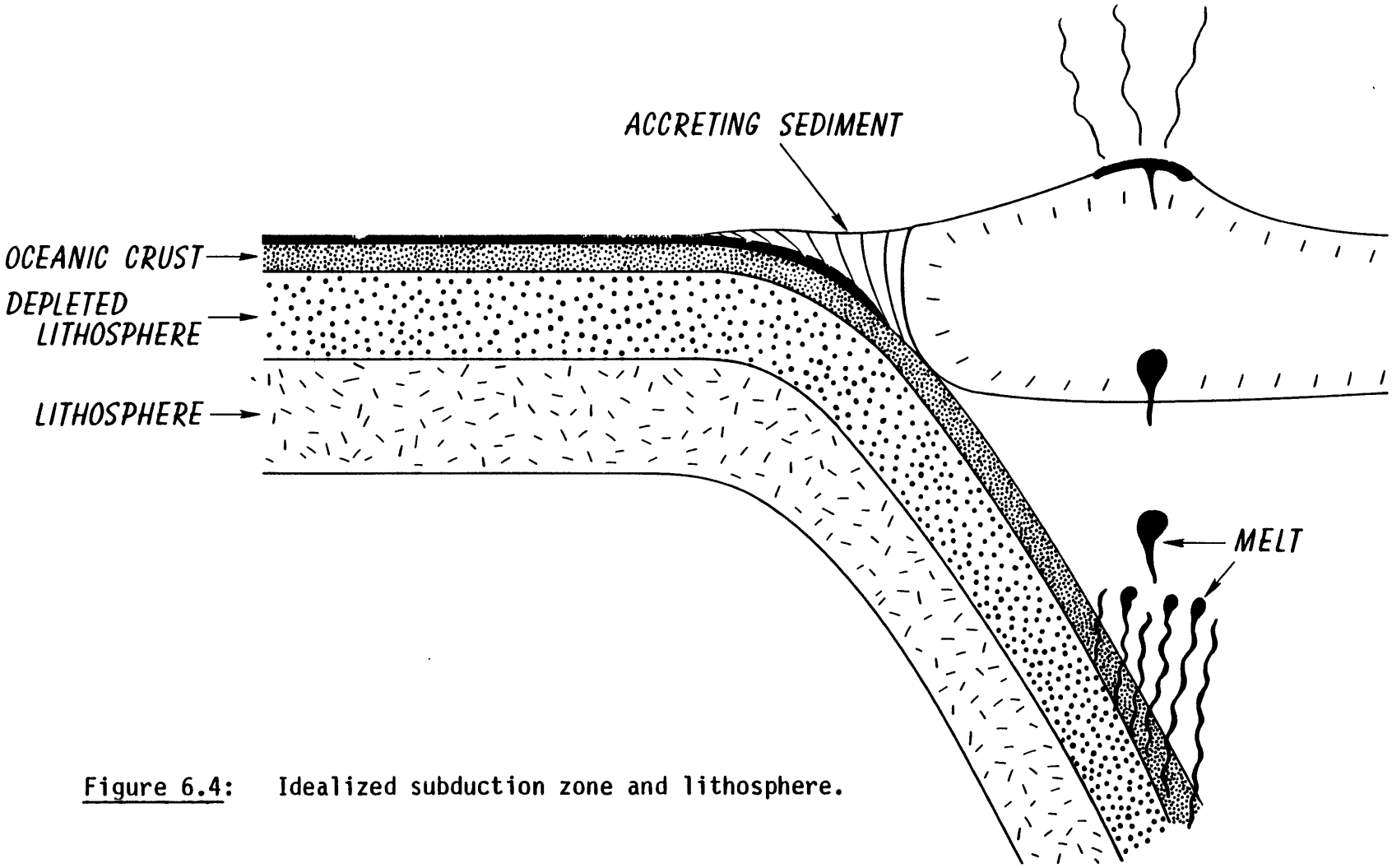
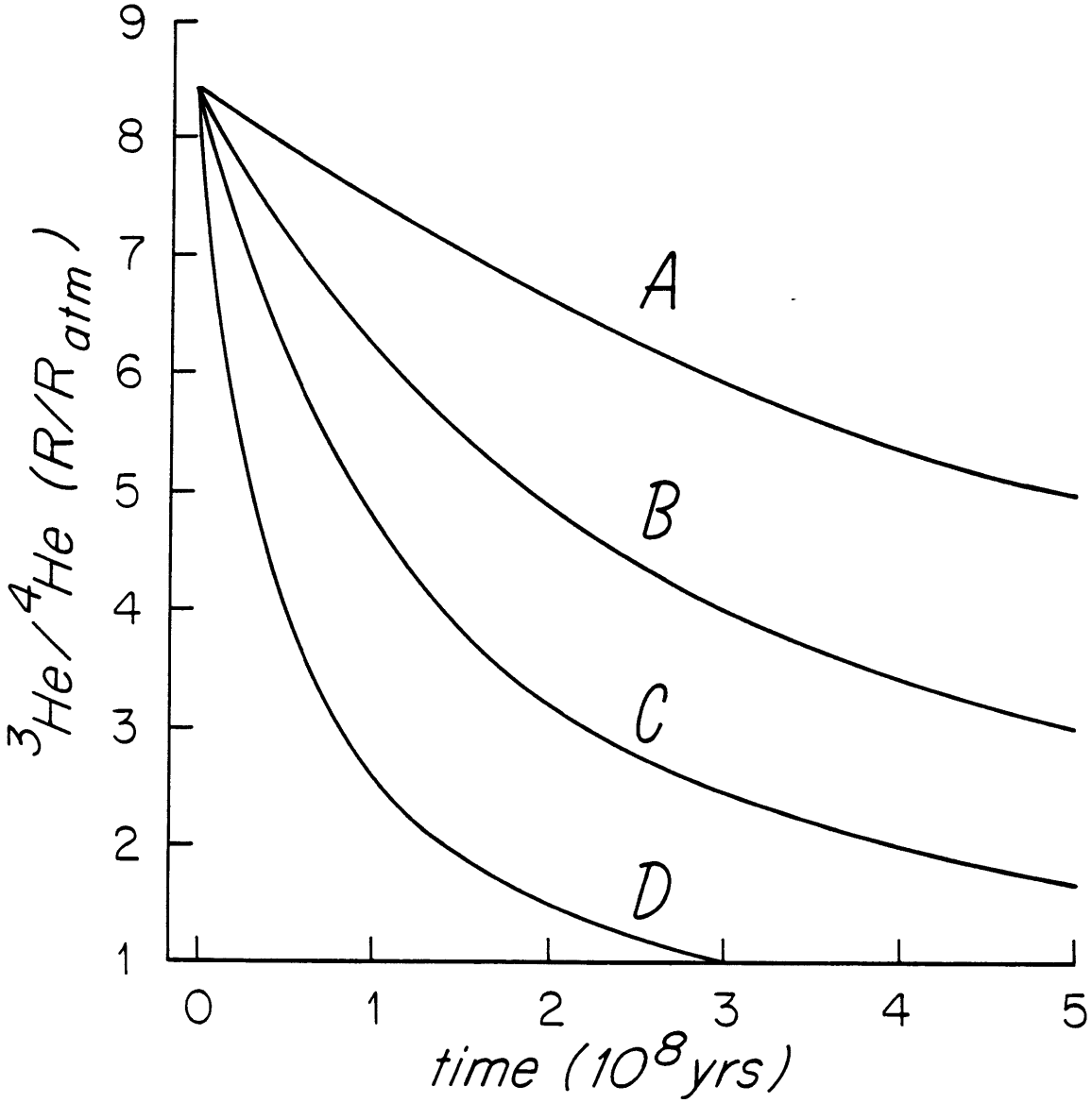


Figure 6.4: Idealized subduction zone and lithosphere.

Figure 6.5: Helium isotopic evolution for oceanic crust as a function of time, assuming initial $^3He/^4He$ = 8.4 x atmospheric, U = .1 ppm, and Th = .3 ppm. Each curve assumes different ^4He concentration in the oceanic crust. MORB concentrations taken from figure 4.4.

	^4He concentration (10^{-5} cc STP/gram)	
case A	2.5	(highest MORB concentration, undegassed)
case B	.75	("normal" MORB, degassed to 2.5 km)
case C	.34	("normal" MORB, degassed to 5.0 km
case D	.12	("normal" MORB, degassed to 6.3 km)


9
8
7
6
5
4
3
2
1
0
1
2
3
4
5
A
B
C
D
$^3He/^4He\ (R/R_{atm})$
time (10^8 yrs)

involvement of a seawater altered oceanic crust component (DePaulo and Wasserburg, 1977; Hawkesworth et al., 1977; Kay et al., 1978). However, the extent of mass transfer cannot be inferred from these studies, and not all island arc volcanics have the isotopic "fingerprint" of oceanic crust.

Several helium isotopic studies of island arc systems have been performed (Kamenskii et al., 1974; Craig et al., 1978; Poreda et al., 1981; Torgerson et al., 1982). Craig et al. (1978) measured $^3He/^4He$ ratios of 5.3 to 8.1 in hot springs from Hakone (Japan), Marianas, and Mt. Lassen. From these results, they concluded that oceanic crust is not extensively involved in arc volcanism, or that the helium content of the subducted oceanic crust is higher than their measurements on MORB (i.e., $> 1 \times 10^{-6}$ cc/gram). The measurements presented in chapter 4, show that MORB concentrations are significantly higher. Therefore it is quite possible that the helium in several of the hot springs was actually derived from melting of the slab. Torgerson et al. (1982) reported $^3He/^4He$ ratios of 3.6 to 8.2 x atmospheric from New Zealand hot springs. Although both Craig et al. (1978) and Torgerson et al. (1982) used measured He/Ne ratios to eliminate the effects of atmospheric contamination in lowering the $^3He/^4He$ ratios, Torgerson et al. (1982) concluded that near-surface "crustal" gases were important to the results. If such near-surface gases are negligible, the low $^3He/^4He$ ratios (i.e., < 8.0 x atmospheric) from a number of arc hot springs do suggest some involvement of the downgoing slab. However, some of the observed $^3He/^4He$ ratios are quite close to MORB measurements and may reflect

mixing between radiogenic slab helium and helium from the overlying mantle.

In summary, the uncertainties regarding the recycled end-member primarily relate to oceanic crust formation and degassing. If the crust is extensively degassed during formation, the resultant low $^3He/(Th+U)$ will yield a rapid decrease in the $^3He/^4He$ of this material. Further studies of the gases island arc rocks are required to constrain the actual conditions within the downgoing slab. However, consideration of the oceanic ^3He budget and the $^3He/^4He$ results from island arc hot springs suggests that the subducted slab can feasibly provide the low $^3He/^4He$ component required by the MORB and oceanic island results.

3. Possible mantle models

Any plausible model for the mantle must accomodate the three reservoirs that have been identified using the helium isotope systematics. Previous attempts to use geochemistry as a constraint on mantle structure have generally been limited to two reservoirs. One model consists of a depleted layer (source of MORB) underlain by an undepleted layer (Schilling, 1973; Sun and Hanson, 1974; Wasserburg and DePaulo, 1979). The opposite geometry, with the undepleted (or enriched) layer on top, has also been advocated by a number of workers (Dickinson and Luth, 1971; Green and Lieberman, 1976; Tatsumoto, 1978; Anderson, 1981). Davies (1981) suggested a two-reservoir lumpy model, where the lumps of undepleted mantle are suspended in depleted mantle. In their recycling model, Hofmann and White (1980) also implicitly assume two layers; in this case the recycled oceanic crust (i.e.,

enriched mantle) collects at the base of the (depleted) mantle.

This diversity is partially the result of the inability to distinguish between undepleted and recycled mantle reservoirs. As pointed out by Anderson (1982) and Kurz et al. (1982b), the basalts that appear to be most "primitive" in terms of Sr/Nd isotopic composition could also be a mixture of ancient depleted and enriched (i.e., recycled) reservoirs. Results presented in chapters 4 and 5 show that helium isotopic information quite effectively distinguishes undepleted from recycled mantle sources. Armed with this new data, the models for mantle structure will now be re-evaluated. It should be emphasized that our knowledge of mantle chemistry is not advanced enough to allow definitive answers and that such models should be viewed as working hypotheses or targets for criticism.

As discussed in the introduction to this chapter, the geophysical and geochemical evidence favor a layered mantle, and this will be an assumed condition. The first question is the relative position of the depleted and undepleted reservoirs. The highest terrestrial $^{3}He/^{4}He$ ratios are observed for basalts from the islands of Hawaii and Iceland (see chapter 5), which therefore are the most representative of the undepleted reservoir. An important constraint on mantle structure is the rarity of such volcanics relative to MORB. Additionally, undepleted $^{3}He/^{4}He$ isotopic signatures are observed in localities far removed from one another: Hawaii, Iceland, Yellowstone, Reunion, and Bouvet (in order of decreasing $^{3}He/^{4}He$). A model that has the undepleted reservoir below the depleted reservoir best explains these observations for several reasons. First, the

depleted MORB source is most commonly sampled because it is most accessible. The rarity of volcanism representative of the deeper undepleted source can then be explained by the "insulation" provided by the depleted layer. Secondly, the higher $^{3}He/(Th+U)$ of the undepleted layer requires that it be undegassed, which is also best explained by its long term isolation from the surface. As discussed earler, a lumpy mantle does not account for the long lived volcanism in places such as Hawaii.

An additional advantage of such a layered mantle model is that it can readily explain the relative abundance of the different types of MORB. It was found (see chapter 4) that samples with $^{3}He/^{4}He$ ratios lower than normal MORB (i.e., < 8.4 x atmospheric) were more common that those with higher ratios (>8.4 x atmospheric). Since we have just argued that the MORB reservoir is in the upper mantle, this suggests that the recycled reservoir is also in the upper mantle. Assuming that the subducted slab does not penetrate into the lower mantle (Richter, 1979), the recycled oceanic crust will interact more extensively with the upper mantle than with the lower mantle.

The recycled reservoir can either exist as a discrete layer at the base of the depleted reservoir, or as "sheets" of oceanic crust that are re-incorporated into the upper mantle. The validity of either, or both, of these cases depends on the style of mantle convection, and the ultimate fate of the subducted slab. McKenzie (1979) has shown that the deformation effect of mantle convection will effectively stir chemical heterogeneities; for reasonable Rayleigh numbers, a spherical heterogeneity will deform into an elongated ellipse after only one

convective overturn. If the subducted slab is returned to the mantle circulation system, it will tend to mix (or stir) with the ambient mantle. The helium results do not necessarily rule out such a case, since melting of a small percentage of the recycled crust plus the ambient mantle can produce the low $^3He/^4He$ ratio samples (depending upon the $^3He/(Th+U)$ ratio of the slab). However, a consequence of effective mixing for the recycled material is that most of the upper mantle could have been through one cycle. If we lump the oceanic crust with the residual mantle (from which the oceanic crust was derived), then a 50 km layer of degassed material is presently subducted (assuming 20 percent partial melting). Using the present-day crustal production rate (3 km^2/yr), and assuming it has been constant through time, 25 percent of the mantle has been recyled over the age of earth. If the subduction rate was faster in the past, due to greater heat production (Dickinson and Luth, 1971), then more than 50 percent of the mantle may have been recycled. This would amount to the entire mantle above the 700 km boundary.

The alternative to continuous recycling is to store the oceanic crust somewhere in the mantle out of the convective region. One possible storage site is at the 700 km boundary (Anderson, 1979a); other possibilities include the core-mantle boundary (Hofmann and White, 1980) or the shallow mantle above 220 km (Anderson, 1982). Storage of the crust alone presumes that there is a mechanism for separation from the adjacent slab and mantle. Although Hofmann and White (1982) point out that oceanic crust may be slightly denser, it is not clear that such a mechanism exists. Regardless of the exact

storage site or recycling mechanism, the large volume of material presently subducted is clearly an important means of degassing and "processing" large portions of the mantle.

Another constraint that must be placed on a mantle model is the existence and geochemistry of mantle plumes. The best example is the Hawaiian-Emperor seamount chain, although most of the islands in the oceans have been attributed to plumes or hot spots (Crough, 1978). Hawaii is characterized by gravity and bathymetry anomalies that would be expected from upwelling mantle (Watt and Daly, 1981) and also has $^{3}He/^{4}He$ ratios characteristic of the most undepleted mantle (see chapter 5). However, the Azores Platform also has correlated gravity and bathymetry anomalies (Sclater et al., 1975), but is characterized by lower $^{3}He/^{4}He$ ratios (i.e., recycled material). Tristan da Cunha also has the gravity anomaly expected of a mantle upwelling region (D. McKenzie, personal communication), but is associated with low $^{3}He/^{4}He$ ratios. If we accept the geophysical evidence for upwelling (see McKenzie, 1977) and the premise that the basaltic isotopic results represent their mantle source, then both undepleted and recycled material must be contained in plumes. As discussed earlier, localities with undepleted helium isotopic signatures are tholeiitic islands such as Hawaii, Iceland, and Reunion, whereas the alkali islands have the generally lower isotopic ratios classified here as recyled.

A model that seems most consistent with the geochemical and geophysical constraints is presented in figure 6.6. In accordance with the assumption of a layered mantle, there are two separate convecting

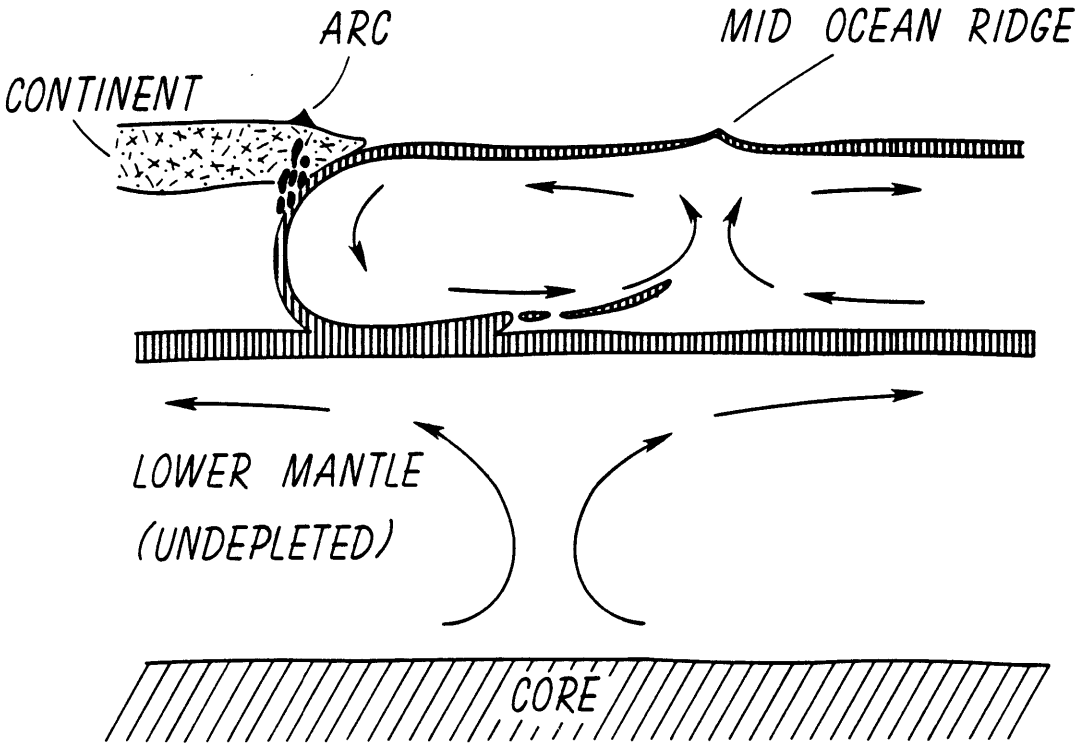
regions: the upper and lower mantle. The boundary is assumed to be the 700 km seismic discontinuity, with the upper layer consisting of the depleted MORB reservoir plus recycled oceanic crust. As discussed above, the recycled crust in figure 6.5 is stored in a layer at 700 km and/or mixed into the upper mantle convection cell. The model accounts for plumes (of both recycled and undepleted chemistry) by upwelling from, and through, the 700 km boundary. This is consistent with the experimental and observational evidence for two scales of convection within the upper mantle (Richter and Parsons, 1975; McKenzie et al., 1980). As shown in figure 6.5b, the convection cells at right angles to the plate motion can thus allow upwelling mantle to reach the surface from the boundary, despite the overall circulation.

The overall geometry in figure 6.6a is similar to previous models (Schilling, 1973; Sun and Hanson, 1975; Wasserburg and DePaolo, 1979) in having the undepleted mantle below the depleted MORB source region. The subducted slab is assumed to stop at the 700 km boundary, and accumulate or re-mix. Anderson (1979b) has suggested that the basalt would convert to eclogite faster than the surrounding mantle due to its lower temperature, and would therefore sink faster. When this material reaches the 700 Km discontinuity, its greater Al_2O_3 content inhibits the phase transition to perovskite, thus stopping it at this level. The density contrast between eclogite and peridotite (~ .1 g/cc; Anderson, 1982) may also provide a mechanism for separating a layer of eclogite.

The helium data presented in chapters 4 and 5 cannot distinguish between mixing of melts, and mixing of mantle sources. Therefore,

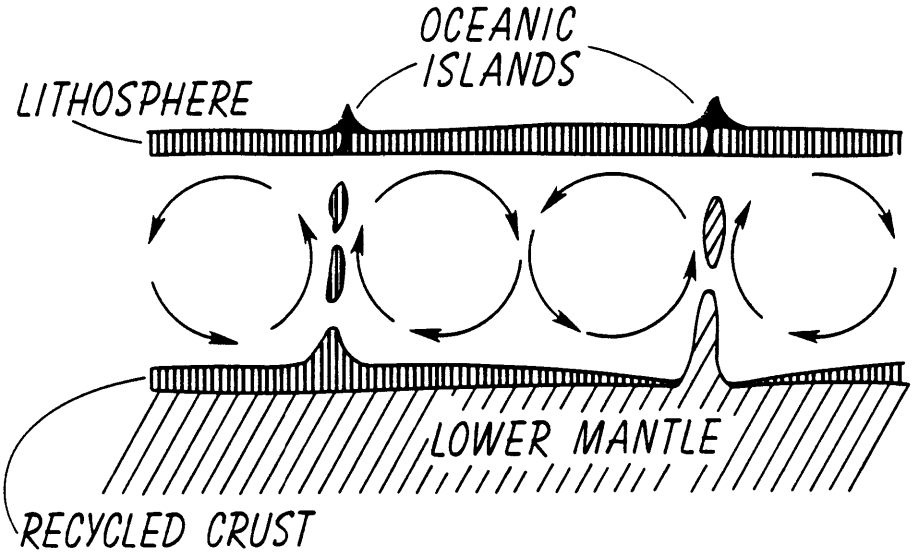
Figure 6.6: Cartoon showing the proposed mantle structure.

A



B

CROSS SECTION PEPENDICULAR TO SPREADING DIRECTION



although the mixing of mantle sources is implicitly included in figure 6.6, the role of magma mixing is difficult to evaluate, and could alter the proposed model. For example, Anderson (1982b) has suggested that the enriched reservoir is shallower than ~200 km, and has formed by metasomatism. If this region has had lower $^{3}He/(Th+U)$ ratios than MORB, then it could also produce the "recycled" isotopic characteristics. Such a situation cannot be ruled out, but the large volume of material presently subducted makes the model shown in figure 6.6 more likely, and less ad hoc.

4. Geochemical consistency of the model

The proposed model must also explain trace element and other isotopic evidence. A key question is whether Pb isotopic variations are consistent with the recycling model, since Pb isotopes provide independent evidence for a third component in the mantle (Sun, 1980; Anderson, 1982a; Zindler et al., 1982). Although Pb isotopic measurements were not performed on the samples presented in this thesis (with the exception of the Loihi Seamount samples), it is possible to construct a $^{3}He/^{4}He$ vs. $^{206}Pb/^{204}Pb$ diagram using data from the literature (see figure 6.7). The resultant plot bears some resemblance to the $^{3}He/^{4}He$ vs. $^{87}Sr/^{86}Sr$ plot in that the most radiogenic Pb samples also have the most radiogenic (i.e., lower) $^{3}He/^{4}He$ ratio. The Loihi Seamount samples have relatively low $^{206}Pb/^{204}Pb$ and $^{87}Sr/^{86}Sr$, but high $^{3}He/^{4}He$. The relative positions of many islands on the two diagrams are also quite similar. Two notable exceptions are Gough and Tristan da Cunha, which have relatively unradiogenic Pb but radiogenic $^{3}He/^{4}He$ and $^{87}Sr/^{86}Sr$ ratios.

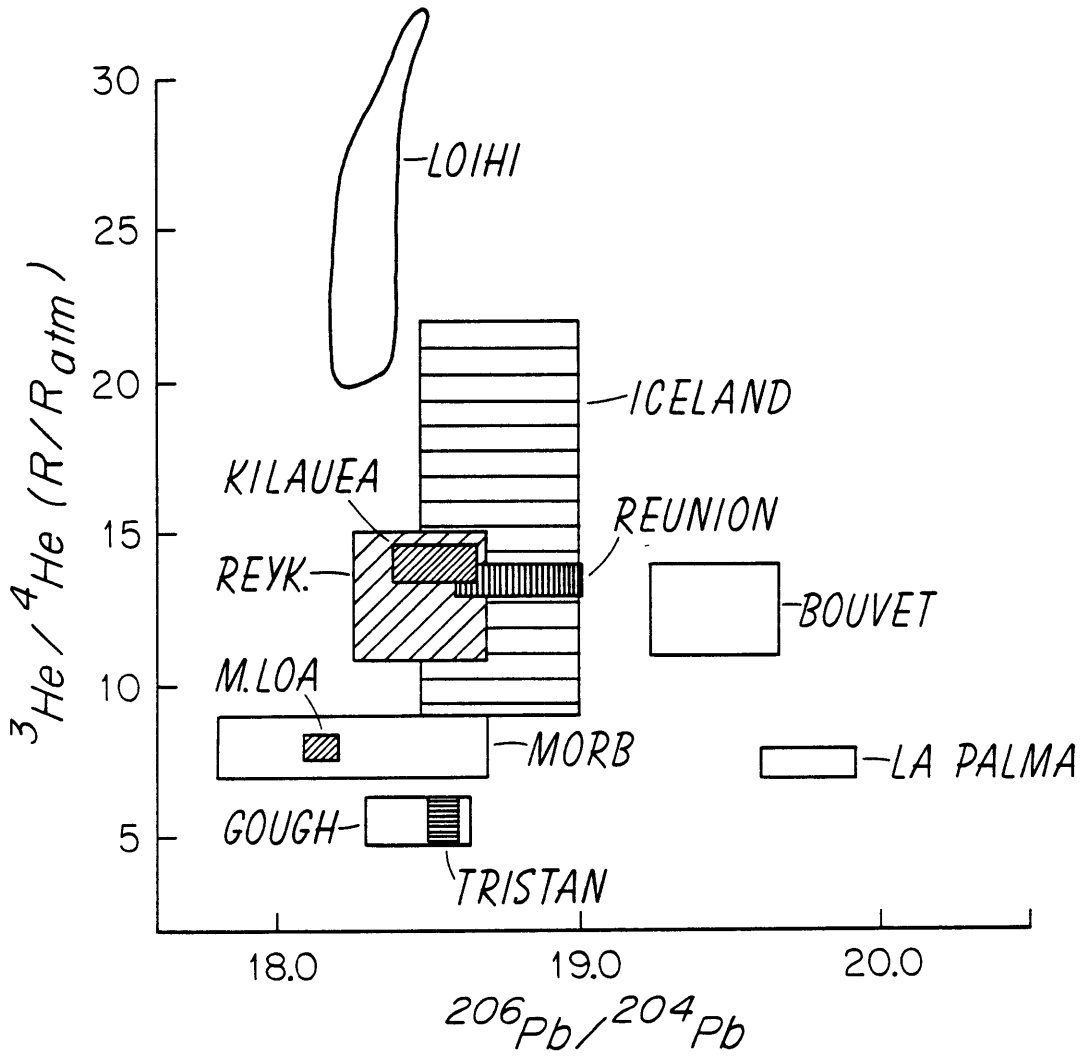


Figure 6.7: $^3He/^4He$ vs. $^{206}Pb/^{204}Pb$ for oceanic volcanic rocks. Helium data is from chapter 5, and lead data is from the recent compilation of Sun (1980), except Loihi Seamount, which is from S. Hart (personal communication). Only Loihi had lead and helium run on the same samples.

This is not simply explained by the recycling hypothesis. For example, if the higher $^{206}Pb/^{204}Pb$ of the Canary Island source were generated by a longer "isolation" (i.e., it was subducted earlier) than the Tristan and Gough sources, then it should also have lower $^{3}He/^{4}He$. It therefore seems that $^{3}He/(Th+U)$ is not necessarily related to U/Pb. However, the presently available Pb and He data are not inconsistent with the mixing hypothesis.

Recycled oceanic crust can generate the enrichments in K, Rb, Cs, Cr, Br, and F that have been observed in the Azores Platform samples (White, 1977; Schilling et al., 1980) by the presence of small amounts of seawater alteration or sediments. In this regard, it is interesting to note that the Cl/Br and Cl/F ratios are quite similar to seawater values. The low Zr/Nb ratios associated with low $^{3}He/^{4}He$ ratios (see chapter 4) can also be explained, since the high water content in the slab may stabilize Ti rich minerals (e.g., sphene, ilmenite), which concentrate Nb relative to Zr (Wood et al., 1979). This is supported by the low Ti contents of many island arc volcanics (Kay, 1980).

The major element $^{3}He/^{4}He$ correlations can also be explained by the subduction-recycling hypothesis. Since there are a number of processes that alter basaltic major element chemistry, these correlations are the most difficult to constrain. Therefore, discussion of the major element correlations is best restricted to suites of samples that have been well studied. The best cases, for which there is helium data, are tholeiite samples from Iceland, Hawaii, and the Azores Platform. Langmuir and Hanson (1980) studied the major element variations between these suites and concluded that they could

not be explained by partial melting or fractional crystallization. On the Reykjanes Ridge, they found a positive correlation between FeO and La/Sm, whereas in the Azores Platform samples, the reverse is true. Further, Iceland and Hawaii have systematically higher FeO contents than the Azores Platform. They suggested that these differences could best be explained by major element heterogeneity in the mantle. As illustrated by figures 4.3 and 5.2, the "Fe rich provinces" (see also chapter 4) are also characterized by higher $^{3}He/^{4}He$ ratios. These observations are consistent with the model, since melting of eclogite should yield more Mg rich liquids than melting of an olivine rich mantle (Yoder, 1976). If the subducted slab consists of eclogite that collects in the base of the upper mantle, melting may yield Mg rich liquids, as observed in Azores Platform basalts. In the context of the mixing model, the erupted basalt could then be a mixture of this eclogite source plus the normal (peridotite) mantle; as discussed earlier, it not possible to distinguish between mixing of mantle (solid state) or of melts.

C. Implications for mantle degassing

1. Catastrophic or continuous degassing

Models for mantle degassing have traditionally attempted to explain atmospheric evolution in terms of either continuous or catastrophic processes. Catastrophic models hold that the atmosphere was formed very early in earth history, while continuous models hold that the outgassing has been continuous and perhaps incomplete. The first efforts to evaluate these two possibilities were primarily based on gas abundances in the atmosphere. Brown (1949) and Suess (1949) compared

the terrestrial atmospheric noble gas inventories to cosmic abundances, and showed that the earth was deficient. They concluded that the earth's atmosphere was secondary, having evolved after formation. In his classic paper, Rubey (1952) compared contemporary volcanic effluent to "excess volatiles" (volatiles that could not be accounted for by rock weathering), and concluded that the compositional similarity was good evidence for continuous degassing. He was unaware of plate tectonics, or the possibility that many of the volcanic gases were recycled atmospheric gases, but this became the foundation for continuous degassing models. Turekian (1959) used the ^{40}Ar abundance in the atmosphere to construct a first order continuous degassing model. The results were dependent upon the K content of the earth (a controversial issue to the present day): if the earth originally had a chondritic K content, only 10 percent degassing could produce all the atmospheric ^{40}Ar. Holland (1962) assumed that the earth was formed by cold accretion and also constructed a model in which the atmosphere subsequently evolved with time. However, cold accretion seems inconsistent with the evidence for early formation of the core (Allegre et al., 1980).

Fanale (1971) reviewed these studies and concluded that the evidence for continuous degassing was circumstantial; in his view, the atmosphere was formed early and the noble gas abundances were explained by solubility equilibrium with a molten earth. Ringwood (1966, 1975) also favored catastrophic degassing, but suggested that the early dense atmosphere was "blown away" by the T-tauri phase of the sun. In a recent review of these conflicting opinions, Bernatowicz and Podosek

(1978) concluded that it was not possible to rule out either catastrophic or continuous degassing, and that a combination of the two may be more reasonable.

Isotopic evidence provides better constraints than the abundance arguments because, in general, it requires fewer assumptions regarding initial conditions. Argon is of interest because it is retained by the atmosphere (unlike helium) and has a primordial (^{36}Ar) as well as a radiogenic (^{40}Ar) isotope. A number of studies have used $^{40}Ar/^{36}Ar$ ratios to study possible degassing histories (e.g. Ozima, 1975; Fisher, 1978; Hamano and Ozima, 1978). Since primordial $^{40}Ar/^{36}Ar$ ratios are $< 10^{-3}$, and the half life of ^{40}K is short relative to the age of the earth, this ratio can place strong constraints on the timing and magnitude of degassing. If the whole mantle has $^{40}Ar/^{36}Ar > 10^4$, then for terrestrial K contents less than 400 ppm., catastrophic degassing is most likely. Based on argon measurements on MORB glasses, this view was adopted by Fisher (1978) and Hamano and Ozima (1978). However, Tolstikhin (1978) and Hart et al. (1979) have pointed out that the measurements, on which their conclusions are based, are not necessarily representative of the whole mantle, and that $^{40}Ar/^{36}Ar$ ratios of < 400 in volcanic rocks have been commonly observed. In many cases, the low $^{40}Ar/^{36}Ar$ ratios were obtained for samples with high $^{3}He/^{4}He$ ratios (Hart et al., 1979). However, there are several insidious sources of contamination that must be remembered. First, the atmosphere contains ~ 1 percent argon, with $^{40}Ar/^{36}Ar$ of 296, which can lower the observed ratio, and have little effect on $^{3}He/^{4}He$ (air has 5.24 ppm He). Even

worse than this, a common contaminant of terrestrial samples (which are analyzed on mass spectrometers previously used for meteorites) is "memory" of meteoritic solar or planetary noble gas, which can have low $^{40}Ar/^{36}Ar$ and high $^{3}He/^{4}He$ (see Craig et al., 1979; Rison, 1980; Smith, 1981). Therefore, the argon results are not yet unambiguous, and require careful analysis of samples that have well documented $^{3}He/^{4}He$ ratios, using mass spectrometers that have not been used for meteorites.

Perhaps the best evidence now available comes from the xenon isotopes. ^{129}Xe is the daughter of extinct ^{129}I (half life = 17 m.y.), which was present in the early solar system (Butler et al., 1963; Reynolds, 1963). Due to the short half life of ^{129}I, any differences between terrestrial samples must have been produced very early in earth history. Excess ^{129}Xe (over atmospheric) has been observed in Hawaiian xenoliths (Kaneoka et al., 1978), MORB glasses (Staudacher and Allegre, 1980), and CO_2 gas wells (Boulos and Manuel, 1971; Smith, 1981). As pointed out by Thomsen (1980), these data strongly suggest early (i.e., >4.0 b.y. ago) separation between the mantle sources (of these samples) and the atmosphere, and provide a strong argument for early formation of the atmosphere. However, Thomsen (1980) used a single $^{129}Xe/^{130}Xe$ ratio for the earth's "interior," a clearly oversimplified assumption, particularly in light of the data presented here. Therefore, the xenon results must be viewed with the same caution as the argon data: the constraints are only as valid as the data are representative of the mantle.

One way of reconciling the evidence for incomplete degassing (i.e.,

the noble gas and the ^3He flux) with the evidence for catastrophic degassing is to assume that the mantle is heterogeneous. Hart et al. (1979) have proposed such a case, in which the upper mantle is preferentially degassed, leaving the lower mantle relatively undegassed. The helium results, and the cartoon model shown in figure 6.5, are entirely consistent with this notion. This would predict that the lower mantle has high $^3He/^4He$ and low $^{40}Ar/^{36}Ar$ (< 1000). Available argon data support this: Kaneoka and Takaoka (1978, 1980) reported $^{40}Ar/^{36}Ar$ lower than 700 for Hawaii samples that had $^3He/^4He$ higher than 20 x atmospheric. Fisher (1975) has measured $^{40}Ar/^{36}Ar$ ratios greater than 10,000 in MORB glasses. The $^{129}Xe/^{130}Xe$ ratio of the lower mantle could be either close to, or quite different from the atmosphere, depending on a) the $^{129}I/^{129}Xe$ ratio of the earth, b) the age of the "separation" between the two reservoirs, and c) the extent of Xe recycling into the mantle.

2. Origin of the ^3He flux

If the upper mantle has been extensively degassed (see figure 6.6 and Hart et al., 1979), then an important problem is the origin of the ^3He in MORB glasses. If the convective overturn has ventilated this reservoir, the $^3He/^4He$ ratio should be close to 10^{-7}, the production ratio of ^3He to ^4He by U, Th decay and ^6Li $(n\alpha)^3H \rightarrow$ ^3He, respectively (Morrison and Pine, 1955). This ratio was calculated by Morrison and Pine (1955) for granitic rocks, which have much higher Li, but should be similar for basaltic sources, wiich have more Mg (the [α,n] target element). According to the model, the lower mantle can supply ^3He to the upper mantle, since it is relatively

gas-rich. Using the closed system $^3He/^4He$ evolution described earlier, a minimum ^3He content of 10^{-9} cc STP/gram was estimated for the lower mantle. If we take the highest ^4He concentration observed for MORB glass (2.7×10^{-5} cc STP/gram), and assume 20 percent partial melting, the maximum ^3He content of the MORB mantle source is 6.3×10^{-11} cc STP/gram. The large concentration difference between these two reservoirs suggests that the lower mantle can serve as a source of ^3He.

Diffusive transport alone is decidedly too slow to allow communication between upper and lower mantle: for a D of 10^{-5} cm^2/sec, helium will only diffuse 6 km in 10^9 years. However, for mantle viscosity of 10^{20} to 10^{22} poise (Cathles, 1975), the advective velocity is on the order of centimeters per year, which yields mantle overturn in ~ 2-3 x 10^8 years (see Davies, 1977; Elsasser et al., 1979). This suggests that transport from the lower layer can produce the ^3He in the upper mantle, depending on the scale of convection. For example, assuming that the mantle is in steady state, and the concentrations described above, to produce the oceanic ^3He flux (4 atoms/cm^2 sec; Craig et al., 1975; Jenkins et al., 1978) requires degassing of the lower mantle at 2.4×10^{16}g/year. This is equivalent to a global layer of less than .1 mm thickness (at 700 km depth).

If the upper and lower mantle are both convecting and there is a layer of stagnant recycled oceanic crust at the boundary, as shown in figure 6.5, then diffusion across the layer becomes the rate limiting step. The physical situation of two well-mixed layers separated by a

stagnant film resembles that of gas exchange between the air-sea boundary (Broecker and Peng, 1974). To a first approximation the flux (F) is described by

$$F = \frac{D(C_2 - C_1)}{Z}$$

where D is the diffusion coefficient in the film, Z is the depth of the stagnant film, and C_2 and C_1 are the concentrations in the two layers. Assuming a D of 10^{-5} cm^2/sec and 4 atoms/cm^2 sec for the flux, the mean film thickness is 2 kilometers. This shows that even with a stagnant layer, transport is feasible <u>if</u> the the upper mantle is convecting on rapid time scale. Most of the transport would occur in places where the film is very thin.

By this reasoning, mantle plume volcanism could also account for a significant ^3He flux, since the source is theoretically within the lower mantle. It is possible to crudely evaluate the ^3He flux from this process, using estimates of island basalt eruption rates. Only those islands or hot spots that are tholeiitic, or have been shown to have high $^3He/^4He$ ratios will be considered, since the results reported in chapter 5 suggest that alkali island basalts are derived from recycled sources. For Hawaii and Iceland, the eruption rates of .11 and .06 km^3/year, respectively, will be used (Swanson, 1973; Schilling et al., 1978). For the remaining hot spots (Reunion, Bouvet, Galapagos, Yellowstone), a mean rate of .1 km^3/year will be assumed (in the absence of better estimates), yielding a total of ~ .6 km^3/year. This is a factor of 2 lower than the rate used by Schilling et al. (1978) for the tholeiitic hot spots. If we assume

that these basalts were produced by 20 percent partial melting, and that the mantle source had 10^{-9} cc STP/gram ^3He, then hot-spot volcanism will produce a present-day flux equivalent to ~ 1.5 atoms/cm^2 sec, or roughly 40 percent of the observed oceanic flux. Clearly, if these assumptions are valid, the plume ^3He flux is a significant portion of the terrestrial budget.

The major uncertainties in these feasibility calculations are the estimates of the mantle ^3He concentrations. The observed ^3He concentrations in the Loihi Seamount glasses are always less than 5 x 10^{-11} cc STP/gram, which corresponds to a lower mantle concentration of 1 x 10^{-11} cc/gram (for 20 percent partial melting). This is a factor of 100 lower than the estimate based on closed system evolution. However, given the abundant evidence for gas loss by vesiculation, it would be unreasonable to expect the Loihi glasses to reflect their source concentrations. Even at the greater depth (i.e., higher quenching pressure) of the mid-ocean ridges, the glasses display ^3He concentrations varying from 3.6 x 10^{-10} to 2 x 10^{-13} cc STP/gram. For this reason, the highest MORB concentration was used to estimate a mantle ^3He content for the calculations.

The closed system evolution estimate for the minimum ^3He mantle concentrations is valid even if the earth had an initial $^3He/^4He$ ratio closer to solar gas (~ 4.0 x 10^{-4}) and does not depend on an assumed initial ^3He concentration. If the earth's initial $^3He/^4He$ was much greater than 10^{-3}, as would be produced by spallation helium, then the minimum ^3He concentration could be much lower than 10^{-9} cc STP/gram. However, most classes of meteorites

have a small proportion of spallation helium relative to solar and planetary helium. If the lower mantle has higher concentrations of U and Th (higher than 15 and 45 ppb), as has been suggested on the basis of heat budget considerations (Clark and Turekian, 1979; O'Nions et al., 1979), the minimum mantle ^3He concentration will be even higher than 10^{-9} cc STP/gram. Therefore, the concentrations used above seem entirely reasonable, and strongly suggest that the lower mantle is the ultimate source of ^3He observed in MORB type glasses, and in the submarine hydrothermal emanations.

Similar conclusions have been reached by several authors with respect to the earth's heat budget (Clark and Turekian, 1978; O'Nions et al., 1978). The mantle source of oceanic basalts is too depleted in heat producing elements to generate the heat flux observed at mid-ocean ridges. O'Nions et al. (1978) have suggested that the required heat source resides in the lower mantle, and that the heat flux is not necessarily accompanied by a chemical flux. This hypothesis is entirely consistent with the proposed model, and with estimated ^3He abundances in the mantle.

3. Implications for degassing history

The proposed mantle structure, with the lower mantle relatively rich in ^3He (and presumably other primordial gases), has important implications for degassing models. If the upper mantle is, in fact, depleted, it serves as an insulating layer, inhibiting the deeper gas-rich layer from releasing volatiles. Therefore, the extent of terrestrial degassing is a strong function of mantle convection. At present, the most obvious expression of mantle convection is plate

motion. However, the validity of extrapolating plate tectonic principles back in time is a controversial issue, and like degassing history, has fueled a debate between uniformitarians and catastrophists (c.f. Glikson, 1981).

Since the geological record is the best evidence regarding the history of convection and therefore deassing, some important aspects of continental geology must be mentioned. The oldest known rocks are 3.8 billion years old (Moorbath et al., 1975) and are metasediments, which strongly suggests the presence of liquid water at this time. The lack of older rocks makes statements regarding the first 800 m.y. of earth history speculative and dependent on the accretion mechanism (Smith, 1980). Tarling (1980) has suggested that during that time the earth was covered by a thin lithosphere, similar to oceanic crust, which could not be subducted, due to the high temperature and ease of dehydration. By this reasoning, continental crust could not be formed, since andesitic rocks and their differentiates could not be produced.

In contrast, the archaean (3.6 to 2.5 billion years ago) was a time of rapid continental growth (Windley, 1977; Dewey and Windley, 1981). Dewey and Windley (1981) estimated that 70 percent of the present continental mass was formed during this time. During the Proterozoic (2.6 to .7 billion years ago), continental growth was much slower, and while tectonics may have operated, continental crust was primarily remobilized and differentiated. The apparent change at the Archaean-Proterozoic boundary has been interpreted as a change in the scale of mantle convection (Kroner, 1981; Windley, 1981), and also as the beginning of subduction (Hargraves, 1981).

Due to the half lives of the heat producing elements (K, U, Th), heat production in the past was much greater than today. McKenzie and Weiss (1975) and Bickle (1978) have suggested that the higher heat production would also imply more rapid plate production and movement. The notion of rapid crustal formation is consistent with the observed abundance of archaean crust. Viscosity of mantle materials is strongly temperature dependent, which is another argument for more rapid convection in times of greater heat flux.

The geological record can readily be interpreted in terms of the plate tectonic processes of today, but it is clear that the rates and specifics of these processes were quite different (this has been termed "liberal uniformitarianism" by Hargraves, 1981). If convection were more vigorous in the past, it is also reasonable to expect that degassing was more rapid. The degassing processes may have been similar, differing only in rate. A period of particularly rapid crustal production, such as the archaean, may have been accompanied by rapid degassing. However, if archaean convection involved the whole mantle rather than the layered convection that has been assumed for the present, the degassing rate may have been disproportionately higher.

Since the present day helium flux from the mantle is reasonably well known, it is possible to test the feasibility of producing the atmosphere by extrapolation of this rate through time. Due to the fact that helium escapes from the atmosphere, this cannot be accomplished using a total helium atmospheric inventory. However, if the helium flux is used to calculate the flux of another noble gas, which does not escape (such as argon), the atmospheric abundance can then be used.

This requires that the $^3He/^{36}Ar$ ratio of the mantle gas be known. For example, if we assume that the ^3He flux has been constant over the age of the earth, 4.35×10^{36} atoms of ^3He have been lost from the mantle. If this escaping gas had $^3He/^{36}Ar$ ratios similar to the planetary gas in meteorites (~ .01; Bernatowitz and Podosek, 1978), roughly 4.2×10^{38} atoms of ^{36}Ar would have accumulated, which is only 12 percent of today's atmospheric ^{36}Ar inventory.

However, as discussed above, the degassing rate should be scaled to the greater heat production by U, Th, and K in the past. This can be accomplished by using an exponential of the form:

$$K(t) = K_p \exp(t/tm)$$

where K_p is the degassing rate today, tm is a constant depending upon the assumed abundance of U, Th, and K, and t is the time in years before the present. If we assume that the earth has a chondritic composition,

tm = 2.05 b.y., whereas if the earth has a somewhat lower heat production, as suggested by Wasserburg et al. (1964) and O'Nions et al. (1968), tm = 3.05 b.y. (see also Dickinson and Luth, 1971; McKenzie and Weiss, 1975). Integrating over 4.5 b.y., and using a chondritic earth as an upper limit, roughly four times more ^{36}Ar will have escaped. This is still only ~ 50 percent of the atmospheric inventory.

Unfortunately, the $^3He/^{36}Ar$ ratios of the escaping mantle gases are not well determined. If most of the helium flux is derived from the normal MORB type mantle, then the $^3He/^{36}Ar$ of MORB glasses should be the best approximation. Kyzer (1980) and Rison (1980) have reported helium and argon measurements on a suite of glasses. The

$^{3}He/^{36}Ar$ ratios of their samples range from .03 to .3, and the $^{40}Ar/^{36}Ar$ ratios vary from 300 to 5,000. The $^{40}Ar/^{36}Ar$ variability suggests that there may be atmospheric or seawater contamination, which would make these values lower limits. Even so, these values are significantly higher than .01, and when used in the inventory calculation, result in an even greater discrepancy, i.e. suggesting that present degassing rates are too slow. Similar conclusions are reached by using the $^{3}He/^{36}Ar$ values from Kaneoka and Takaoka (1978: Hawaiian xenoliths with $^{3}He/^{4}He$ of 8 x Ratm) or Fisher (1975: assuming $^{3}He/^{4}He$ of 8 x Ratm).

There is some evidence that samples derived from undepleted sources have significantly lower $^{3}He/^{36}Ar$ ratios, which would affect the result of the calculation if the escaping gas were derived from the lower mantle. Measurements on submarine glasses from the east rift of Kilauea reported by Rison (1980) and Kyser (1980) yield $^{3}He/^{36}Ar$ ratios of .0001 to .025. However, their $^{3}He/^{4}He$ ratios vary from 3.7 to 25 x atmospheric, while the results reported from Kilauea reported in chapter 5 (some of which were from the same dredges), yielded no variation ($^{3}He/^{4}He$ of 14 x atmospheric).

Phenocryst samples from Haleakala (Maui) studied by Kaneoka and Takaoka (1980) had $^{3}He/^{36}Ar$ of .0015 to .00317, and $^{3}He/^{4}He$ ratios from 17 to 50 x atmospheric. However, these $^{3}He/^{36}Ar$ ratios are a factor of 5 lower than the meteorite values, and may have been affected by some fractionation process. Since the gases in these phenocrysts most likely reside within melt inclusions (see chapter 5), the relative abundances may have been altered during incorporation.

Melt inclusions are formed at the crystal-melt interface, and since this zone contains all of the volatiles excluded from the crystal during growth, the $^{3}He/^{36}Ar$ ratio is particularly suspect. For example, since He diffuses faster than Ar, the He may rapidly equilibrate with surrounding melt, while the Ar is slower, leaving a low $^{3}He/^{36}Ar$ at the interface. Additional measurements will be required to ascertain the cause of the variability, and to what extent the measured $^{3}He/^{36}Ar$ ratios reflect the source.

With these uncertainties in mind, it would appear that samples derived from undepleted mantle sources have lower $^{3}He/^{36}Ar$ ratios. The proposed model suggests that $^{3}He/^{36}Ar$ may be fractionated (in the upper mantle) due to the diffusivity limited transport across the boundary between the upper and lower mantle. ^{3}He would diffuse more rapidly, leading to higher $^{3}He/^{36}Ar$ in the upper mantle, in agreement with the available measurements.

In summary, the $^{3}He/^{36}Ar$ ratio, coupled with the global ^{3}He flux can provide important constraints on the degassing rates of the past. Available MORB glass measurements suggest that the present rate is too slow to account for the atmospheric ^{36}Ar inventory, even if the rate is scaled to increased heat production in the past. Therefore, a period of more rapid degassing in the past seems necessary, which can either be viewed as a catastrophic "event" or a period when the degassing mechanism was facilitated. The latter is quite possible in the context of the layered mantle model shown in figure 6.6. If at some time in the past, the lower gas-rich layer was exposed at the surface, the degassing rate would be significantly

higher; at present, the upper mantle serves as an insulating layer. An appropriate analogy is gas exchange between the atmosphere and the sea surface. Most of the gas exchange occurs when the stagnant film at the sea surface is very thin, and the rate is a strong function of the wind speed. Exposure of the lower mantle could have a similar effect on the mantle degassing rate, and as discussed above, the geological record shows that such an episode is quite feasible.

D. Conclusions

The helium isotopic systematics indicate the existence of three distinct mantle reservoirs that have been referred to here as depleted, undepleted and recycled. The correlations between $^{3}He/^{4}He$ and $^{87}Sr/^{86}Sr$ place important constraints on the origins of these mantle reservoirs. In light of these data, and other geophysical and geochemical information, the following conclusions have been drawn.

1. The highest $^{3}He/^{4}He$ ratios are observed for tholeiitic islands such as Hawaii and Iceland. The source regions of these samples have evolved with higher time-integrated $^{3}He/(Th + U)$ than the source for MORB. Using a closed system evolution model, a minimum ^{3}He content of 10^{-9} cc STP/gram can be estimated for the undepleted reservoir. This is significantly higher than the value estimated for the MORB source (2.8×10^{-11} cc STP/gram).
2. The low $^{3}He/^{4}He$, high $^{87}Sr/^{86}Sr$ samples are derived from a source with time integrated $^{3}He/(Th + U)$ lower than MORB. These source regions can be generated by subducted oceanic crust that is mixed back into the mantle. The time necessary to lower the $^{3}He/^{4}He$ of the slab depends critically upon the nature of the

oceanic crust, the extent to which it is degassed, and the fate of the subducted material in the mantle.

3. Based on the available geophysical and geochemical information, in addition to the data presented here, a layered mantle model has been chosen as most feasible. The relative abundances of basalts derived from the three mantle types suggests that the undepleted reservoir is in the lower mantle, and that the depleted plus recycled reservoirs coexist in the upper mantle. A model is proposed which accounts for the existence of mantle plumes in the context of a three reservoir mantle. The model assumes that convection in the upper mantle is characterized by two different convective scales (e.g. Richter and Parsons, 1975). The different chemistry of the plumes is thus accounted for by derivation from the boundary between the upper and lower mantle (presumed to be at 700 km.).

4. Assuming that the upper mantle is the source for MORB, and that recycling primarily involves the upper mantle, the present day ^{3}He content and $^{3}He/^{4}He$ of the upper mantle require a source of ^{3}He. In the absence of such a source, MORB would have much lower $^{3}He/^{4}He$. Using the inferred closed-system evolution concentrations for the undepleted reservoir, the lower mantle can readily supply the ^{3}He. The implication is that most of the observed oceanic ^{3}He flux is ultimately derived from the lower mantle. Further, a significant proportion of the earth's atmospheric helium escape rate may be balanced by ^{3}He flux from hot spot volcanism (i.e., Hawaii, Iceland, Reunion, Bouvet,

Yellowstone).

5. In order to explain the atmospheric abundance of ^{36}Ar, degassing rates in the past must have been significantly greater than the rate inferred from the ^{3}He escape rate, measured $^{3}He/^{36}Ar$, and the half lives of the heat producing elements. Such a period of rapid degassing is easily reconciled with the layered mantle model, since the upper mantle is presently insulating the gas-rich lower mantle. Geological evidence shows that this may not always have been the case. Therefore, it is reasonable to attribute the rapid degassing in the past to exposure of the gas rich layer at the surface.

APPENDIX I

Table AI.1: Stepwise Heating of Alv 519 2-1-b

(Grain size =.064 ± .02 mm)

Temperature (°C)	Total Elapsed Time (seconds)	Fraction of Helium Released	Diffusion* Coefficient (cm^2/sec)
150	4,500	.146 ± .002	$4.6 \pm 2. \times 10^{-12}$
155	8,400	.220 ± .002	$7.2 \pm 3. \times 10^{-12}$
155	12,120	.267 ± .003	$6.9 \pm 4. \times 10^{-12}$
160	19,320	.340 ± .003	$7.3 \pm 3. \times 10^{-12}$
160	26,520	.396 ± .004	$7.3 \pm 3. \times 10^{-12}$
220	29,520	.583 ± .006	$9.4 \pm 3. \times 10^{-11}$
225	32,520	.729 ± .007	$1.3 \pm .4 \times 10^{-10}$
225	35,220	.80 ± .01	$1.2 \pm .4 \times 10^{-10}$
265	37,620	.92 ± .01	$3.9 \pm 1. \times 10^{-10}$
270	40,020	.97 ± .01	$4.7 \pm 2. \times 10^{-10}$
310	42,420	1.000	

*Calculated for spherical geometry

Table AI.2: Stepwise Heating of Alv 519 2-1-b

(Grain Size = .160 ± .02 mm)

Temperature (°C)	Total Elapsed Time (seconds)	Fraction of Helium Released	Diffusion* Coefficient (cm^2/sec)
200	1,200	.061	$1.8 \pm .4 \times 10^{-11}$
235	3,300	.256	$2.0 \pm .3 \times 10^{-10}$
235	4,800	.325	$2.0 \pm .6 \times 10^{-10}$
235	6,300	.378	$2.0 \pm .6 \times 10^{-10}$
235	7,800	.417	$1.8 \pm .7 \times 10^{-10}$
235	8,300	.451	$5.2 \pm 2. \times 10^{-10}$
235	9,800	.478	$1.6 \pm .9 \times 10^{-10}$
235	11,800	.537	$3.0 \pm .8 \times 10^{-10}$
315	12,300	.691	$4.6 \pm .8 \times 10^{-9}$
380	13,800	.951	$8.2 \pm 1. \times 10^{-9}$
540	------	1.000	--------

Table AI.3: Stepwise Heating of Alv 519 2-1

(Grain Size = .090 ± .01 mm)

Temperature (°C)	Total Elapsed Time (seconds)	Fraction of Helium Released	Diffusion* Coefficient (cm^2/sec)
140	3,600	.041	$8.2 \pm 5. \times 10^{-13}$
190	5,700	.151	$1.9 \pm 1. \times 10^{-11}$
195	7,500	.239	$4.0 \pm .2 \times 10^{-10}$
245	9,420	.514	$2.8 \pm .6 \times 10^{-10}$
250	11,100	.695	$4.8 \pm .7 \times 10^{-10}$
310	12,900	.934	$1.7 \pm 2. \times 10^{-9}$
315	14,820	.987	$1.7 \pm .9 \times 10^{-9}$
400	------	1.000	-----

Table AI.4: Stepwise Heating of Alv 892-2

(Grain Size = .090 ± .01 mm)

Temperature (°C)	Total Elapsed Time (seconds)	Fraction of Helium Released	Diffusion* Coefficient (cm^2/sec)
135	1,800	.030	8.9×10^{-13}
145	3,600	.082	5.7×10^{-12}
145	5,400	.116	7.1×10^{-12}
190	7,200	.244	5.4×10^{-11}
200	9,000	.392	1.3×10^{-10}
255	10,800	.699	6.4×10^{-10}
265	12,600	.886	1.1×10^{-9}
265	14,460	.949	8.8×10^{-10}
325	------	1.000	-----

Table AI.5: Stepwise Heating of Alv 519 2-1-b

(Grain size = .080 ± .01 mm)

Temperature (°C)	Total Elapsed Time (seconds)	Fraction of Helium Released	Diffusion* Coefficient (cm^2/sec)
125	1,500	.011	1.2×10^{-13}
190	3,000	.111	1.2×10^{-11}
260	4,500	.516	3.4×10^{-10}
330	6,000	.942	2.3×10^{-9}
400	------	1.000	-----

APPENDIX II

Table AII.1: Petrographic Descriptions: Atlantic and Indian Ocean Samples

Sample	Rock Type and Location	Description
R43	Picrite: Piton de la Fournaise Reunion Island	Extremely porphyritic basalt, with 4 percent vesicles and 40 percent olivine phenocrysts (1-10 mm in size) in an aphanitic ground mass. The olivines contain devitrified melt inclusions and euhedral spinels. Source: Dr. C.J. Allegre.
R36	Olivine Basalt: Piton de la Fournaise, Reunion Island	Olivine-rich basalt with euhedral olivine phenocrysts (1-3 mm in size, ~ 15 percent by volume in a fine-grained groundmass. Olivines have abundant melt inclusions, but no fluid inclusions or deformation lamellae. Source: Dr. C.J. Allegre.
WJ8B	Hawaiite: Westwind Beach, Bouvet Island	Porphyritic basalt with 40 percent plagioclase phenocrysts (2-5 mm) in a fine-grained groundmass that contains some opaque minerals. Plagioclase phenocrysts often contain up to 10 percent melt inclusions. Source: Dr. W. J. Voerwoerd. References: A. le Roex, 1980.
M68	Ankaramite: Mt. Deux Mamelles, Mauritius Island	Porphyritic basalt with 15 percent olivine phenocrysts (1-2 mm) and 15 percent clinopyroxene phenocrysts in an aphanitic groundmass that also includes blebs of opaque oxides. Source: Dr. B. Upton.
ALR26G	Ankaramite: Mt. Powett Gough Island	Ankaramite that contains 1-3 mm phenocrysts of clinopyroxene (10 percent) and olivine (15 percent) in a hyalopilitic ground mass. The clinopyroxenes are euhedral, zoned and often have corroded textures, possibly indicating disequilibrium. Source: Dr. A. le Roex.

Table II.1: Petrographic Descriptions: Atlantic and Indian Ocean Samples (continued)

Sample	Rock Type and Location	Description
ALR41G	Pyroxene Phyric Basalt: Mt. Powett, Gough Island	Porphyritic basalt containing 30 percent clinopyroxenes (3-10 mm) and smaller (~ 1 mm) olivines in an intergranular groundmass. The pyroxenes often have corroded appearance, are zoned, and have rows of melt inclusions parallel to the zoning. Source: Dr. A. le Roex.
TK46A	Ankaramite: Big Point, Tristan da Cunha Island	Basalt with 15 percent clinopyroxene (2-8 mm) and 10 percent olivine (1-3 mm) in an aphanitic groundmass that also contains large (.5 mm) blebs of magnetite. Zoning is evident in the smaller clinopyroxene grains, whereas the largest ones have a corroded texture, suggesting two generations. Source: Dr. S. Humphris.
TK26	Amphibole Gabbro Xenolith in Pyroclastics: Buff Gulch, Tristan da Cunha	Amphibole gabbro consisting of 40 percent pyroxene, 25 percent pleochroic kaersutite, 15 percent plagioclase, 10 percent opaque minerals and 5 percent olivine. Fluid inclusions are abundant throughout and are primarily aligned along healed cracks. Source: Dr. S. Humphris.
WJ21E	Ankaramite: Top of Western Escarpment : Prince Edward Island	Basalt with 15 percent euhedral to subhedral clinopyroxene crystals (1-3 mm) and 5 percent olivine (1 mm). Clinopyroxene is zoned in several cases, and some grains contain rows of fluid inclusions, which are also present in the olivines. The olivines do not display deformation lamellae. Source: Dr. W. J. Voerwoerd. Reference: Voerwoerd, 1971.
LP249	Ankaramite: La Palma	Vesicular basalt that contains 20 percent black clinopyroxenes, 5 percent vesicles, and 3 percent olivine phenocrysts in a fine-grained groundmass. Source: Dr. H. Staudigel.

Table II.1: Petrographic Descriptions: Atlantic and Indian Ocean Samples (continued)

Sample	Rock Type and Location	Description
Icelandic samples (source: Dr. H. Sigurdsson)		
HS782	Sub-Glacial Basalt: Botnsheidi, Iceland 64°22.3'N, 21°10.8'W	Glass contains 1 percent (.5 to 1 mm.) vesicles and 1 percent plagioclase phenocrysts. Many vesicles (~ 30 percent) are filled with clay minerals, and the glass often has a dull appearance, suggesting some post-eruptive alteration.
HS806	Sub-Glacial Basalt: Eiriksjokuii, Iceland 64°48.4'N, 20°26.75'W	Vitreous to spherulitic glass containing 1-2 percent vesicles (.2-.5mm) and abundant plagioclase phenocrysts (~ 1 mm.)
HS785	Sub-Glacial Basalt: Botnsheidi, Iceland 64°27.2'N, 21°05.5'W	Fresh, vitreous, aphyric glass, containing 1-2 percent vesicles (.5-1.0 mm in size).
EZ274	Sub-Glacial Basalt: Stapafell, Reykjanes Iceland 63°54.4'N, 22°31.9'W	Porphyritic olivine basalt with 10 percent vesicles and 4-5 percent olivine phenocryts in an intergranular groundmass. Olivines are 1mm. in size, and contain devitrified melt inclusions and spinel. The glass present on the outer rim has ~35 percent (1-2 mm.) and has fewer olivines than the interior.
EZ149B	Sub-Glacial Basalt: Grasatangi, Iceland 64°13.6'N, 18°59.7'W	Vitreous to spherulitic glass with olivine (~ 5 percent) and plagioclase (~1 percent) phenocrysts. Vesicles are .5 mm. in size ~ 1 percent by volume.
EZ125	Sub-Glacial Basalt: Innsta-Bakafell, Iceland 64°41.0'N, 17°39.1'W	Vitreous glass with 10 percent vesicles (1-2mm in size) and numerous plag. phenocrysts. Roughly 10 percent of the vesicles are filled with an orange red mineral.

Table II.2: Petrographic Descriptions: Hawaiian Samples

Sample	Rock Type and Location	Description
Puna No. 2	Submarine Tholeiite Glass: dredged from 1400 m, east rift of Kilauea, Hawaii	Glassy basalt with 10 percent vesicles, and containing olivine (9 percent), pyroxene (1 percent) and plagioclase (1 percent) phenocrysts. Source: Dr. J. Moore. References: Moore, 1965; Hart, 1973.
Puna No. 6	Submarine Tholeiite Glass: dredged from 4680 m, east rift of Kilauea, Hawaii	Glassy basalt with 1 percent vesicles, 14 percent olivine, 2 percent clinopyroxene, and 2 percent plagioclase. Source: Dr. J. Moore. References: Moore, 1965; Hart, 1972.
66055	Picrite Basalt: Crater wall of Kilauea (below volcano observatory) Hawaii	Vesicular (10 percent by volume picrite basalt with 7–8 percent euhedral olivine (1–2 mm) that contain numerous melt inclusions. Groundmass has an intergranular texture of interlocking plagioclase, cpx olivines and opaques. Source: Dr. S. O. Agrell.
57370	Olivine Basalt: 1840 lava near Nanowale Bay, Kilauea, Hawaii	Olivine-rich basalt with ~ 4 percent vesicles and 10 percent olivine phenocrysts in a fine-grained groundmass. Olivines are 1–2 mm in size, are euhedral to subhedral and contain abundant melt inclusions. Source: Dr. S. O. Agrell.
ML84	Olivine-rich Basalt: 1868 flow of Mauna Loa, near Pun Hoo on the coast, Hawaii	Highly vesicular basalts with 20 percent vesicles, and 10–15 percent olivine phenocrysts (1–3 mm in cross-section) in a fine-grained ground mass. Source: Dr. M. Rhodes.
ML55	Olivine Basalt: 1950 lava of Mauna Loa, near Routell at 93-mile marker, Hawaii	Highly vesicular basalt, with 15 percent vesicles (1–5 mm in size), 3–4 percent olivine phenocrysts (1 mm) in a pilotaxic groundmass. Source: Dr. M. Rhodes.
185	Submarine Pillow Basalt: from 1017 m depth, Kealakekua Bay, Hawaii	Glassy basalt with ~ 3 percent vesicles (.2–.5 mm) in a glassy intersertal matrix. In reflected light, the glass has crystallized-vitreous appearance. Source: Dr. D. Fornari.

Table II.2 (continued)

Sample	Rock Type and Location	Description
187	Submarine Pillow Basalt: from 710 m depth, Kealakekua Bay, Hawaii	Glassy basalt with ~ 15 percent vesicles (.5 -1.0 mm), similar in appearance to 185. Source: Dr. D. Fornari.
203-1	Submarine Pillow Basalt, from 1017 m depth, Kealakekua Bay, Hawaii	Glassy basalt with 4-5 percent vesicles (.3-.9 mm) in a glassy intersertal groundmass. Elongate laths of plagioclase make up ~ 30 percent of the glassy groundmass. Source: Dr. D. Fornari. Reference: Fornari et al., 1980.
KK 9-14	Glassy Basalt: Submarine part of northwest rift zone Hualalai	Glassy basalt with thick glasssy rim (~ 1 mm) associated with flow structure. Vesicles are .2 -.6 mm and constitute ~ 6 percent of the glass. Olivine phenocrysts are 1 mm in size and comprise 1 percent of the rock. Source: Dr. D. Claque.
KK14-7	Glassy Basalt: submarine part of northwest rift, Hualalai	Basalt with glassy margin that contains 2-3 percent vesicles (.1 - .3 mm in size) and large (1 mm) olivine phenocrysts. Source: Dr. D. Claque
KK10-1	Glassy Olivine Basalt: submarine part of northwest rift, Hualalai	Extremely olivine-rich basalt, that contains 50 percent olivine phenocrysts (that range in size from 1-5 mm) in a glassy spherulitic groundmass. Several of the olivines have prominent kink bands and rows of fluid inclusions. Source: Dr. D. Claque.
USNM 113987 -107	Dunite Xenolith: in alkali basalt of 1801 flow, Hualalai Hawaii	Dunite with porphyroclastic texture. Porphyroblasts are 2-4 mm in size, and contain numerous kink bands and fluid inclusions. Smaller neoblasts (< 1 mm) rarely contain as many inclusions or kink bands, and surround the larger olivines. Spinel is present as a trace constituent.

Table II.2 (continued)

Sample	Rock Type and Location	Description
USNM 113987 -11	Dunite Xenolith: in alkali basalt of 1801 flow, Hualalai, Hawaii	Dunite with large (2-4 mm) olivines surrounded by smaller neoblastic olivines, giving the rock a porphyroclastic texture. There is a significant quanity of melt and spinel that forms a vein through the thin section, and is intergranular to the smaller olivines.
USNM 113987 -104	Gabbroic Xenolith: in alkali basalt of 1801 flow, Hualalai, Hawaii	Wehrlite xenolith that contains 113987 65 percent clinopyroxene, 30 percent -104 olivine, and 5 percent plagioclase. Clinopyroxene is large and of uniform size (~ 3 mm); olivine and plagioclase are much smaller (~ 1 mm) giving the rock a porphyroclastic texture. Clinopyroxenes contain the most fluid inclusions, but they are also present in the olivines.
USNM 113987 -54	Gabbroic Xenolith: from 1081 flow, Hualalai, Hawaii	Wehrlite xenolith containing 60 percent large (4-10 mm) clinopyroxene, 25 percent olivine (~ 1 mm), and 15 percent plagioclase (~ 1 mm). The texture is porphyroclastic; clinopyroxenes contain the most fluid inclusions.
USNM 111815	Dunite Xenolith: from 1801 flow Hualalai, Hawaii	Dunite with large (3-4 mm) grains of olivine set in a groundmass of smaller olivines (< 1 mm) giving the rock a porphyroclastic texture. The texture varies within the thin section, having a layer of finer-grained olivine intermixed with melt. Source: Dr. W. Melson.
48593	Olivine-Pyroxene Phyric Basalt: Oakala, Mauna Kea, Hawaii	Olivine-rich basalt with 20 percent euhedral olivine phenocrysts (1-4 mm), and 2 percent zoned clinopyroxene opaque minerals and clinopyroxene. Source: Dr. S. O. Agrell.

Figure AII.1: Photomicrographs of porphyritic samples.

a. Photograph (in crossed polars) of thin section of sample R43 (Reunion picrite).

b. Photograph (in crossed polars) of TK 46A (Tristan da Cunha, ankaramite).

c. Photomicrograph (in plane light) of olivine crystal in sample H66055 (picrite basalt from Kilauea). Round melt inclusions are evident in the crystal.

d. Photomicrograph (in crossed polars) of plagioclase crystal in sample WJ8B (Hawaiite from Bouvet Island). Rows of dark blobs in the center of the field are melt inclusions, some of which have devitrified.

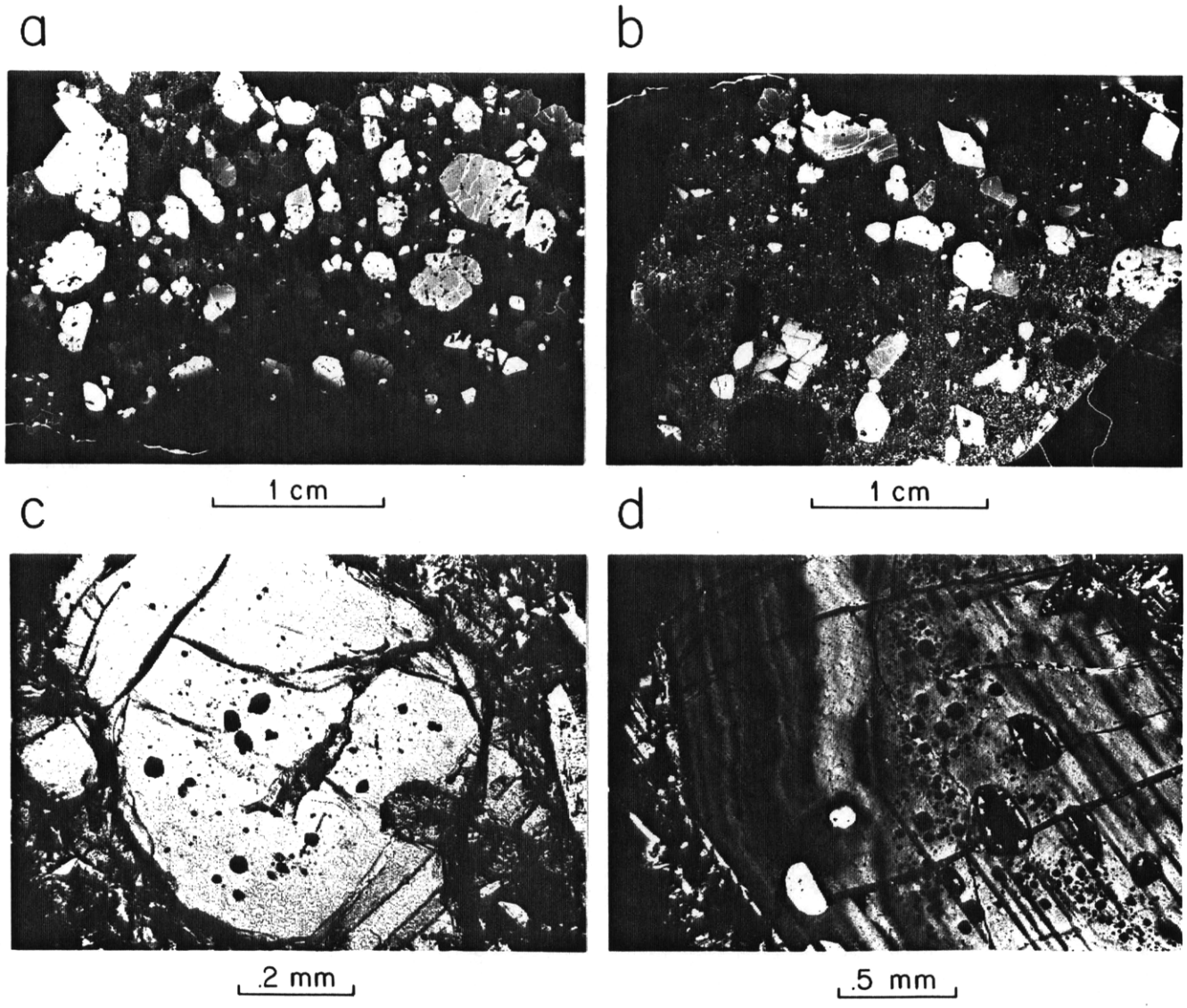

a
b
1 cm
1 cm
c
d
.2 mm
.5 mm

Figure AII.2: Photomicrographs of dunite xenoliths and olivine xenocrysts (all in cross polarized light).

a. Photograph of sample KK 27-9A, a xenolith within an alkali basalt from Loihi Seamount. Note the porphyroclastic texture, which is typical of the dunite xenoliths from Loihi and Hualalai. Host basalt is present near top of thin section.

b. Photomicrograph of olivine porphyroblast in sample KK 27-9A. Note the deformation lamellae at angles to the rows of fuid inclusions.

c. Photomicrograph of same olivine porphyroblast as in b., under higher magnification. Note the bands of fluid inclusions, which are aligned along old fractures (i.e., healed cracks), and the negative crystal morphology of some of the fluid inclusions.

d. Photomicrograph of xenocryst within tholeiite sample KK10-1 (Hualalai). The round inclusions are filled with liquid CO_2, and enclose a smaller vapor bubble. Note the similarity to c. in overall inclusion alignment.

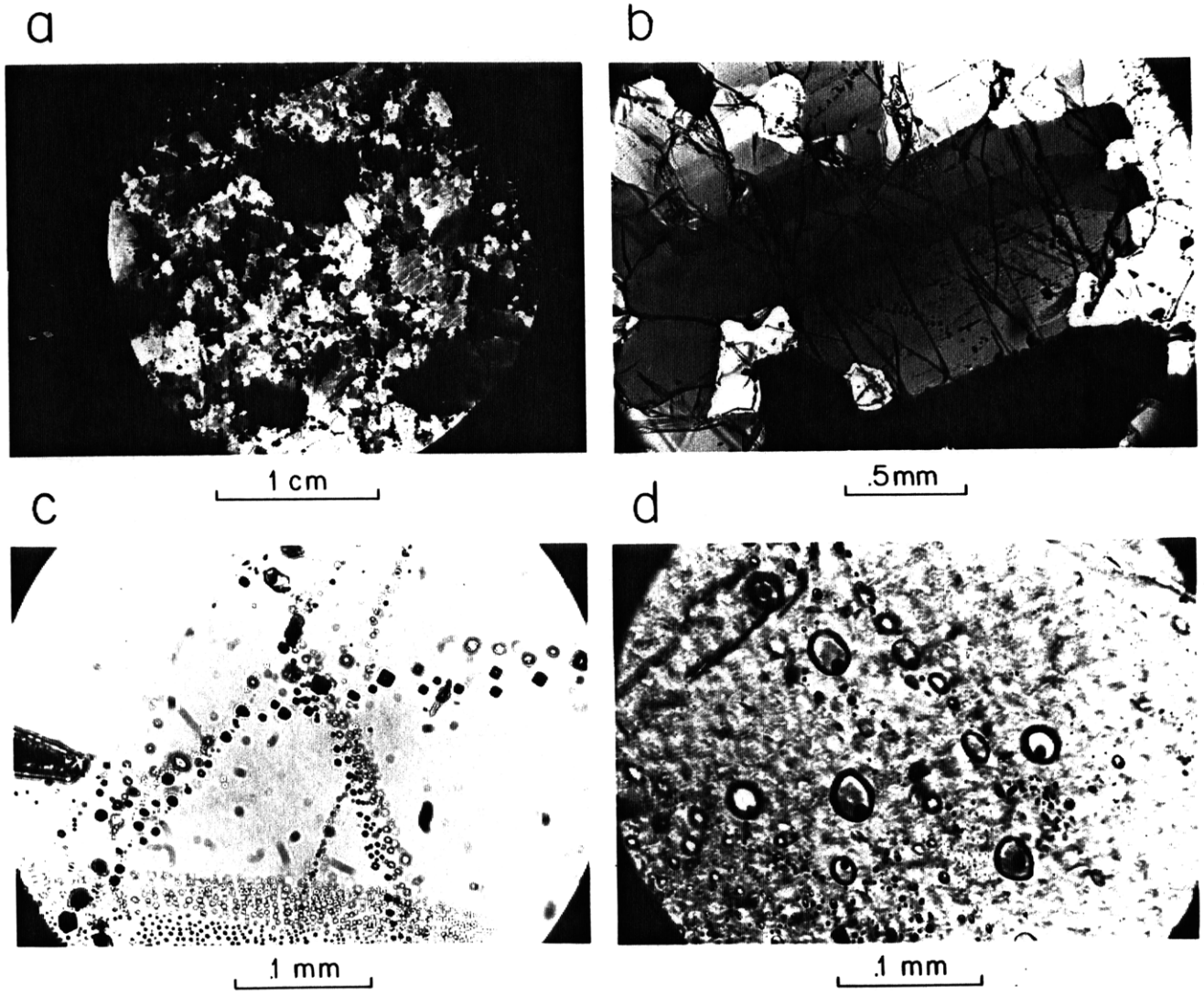

a
1 cm
b
.5mm
c
.1 mm
d
.1 mm

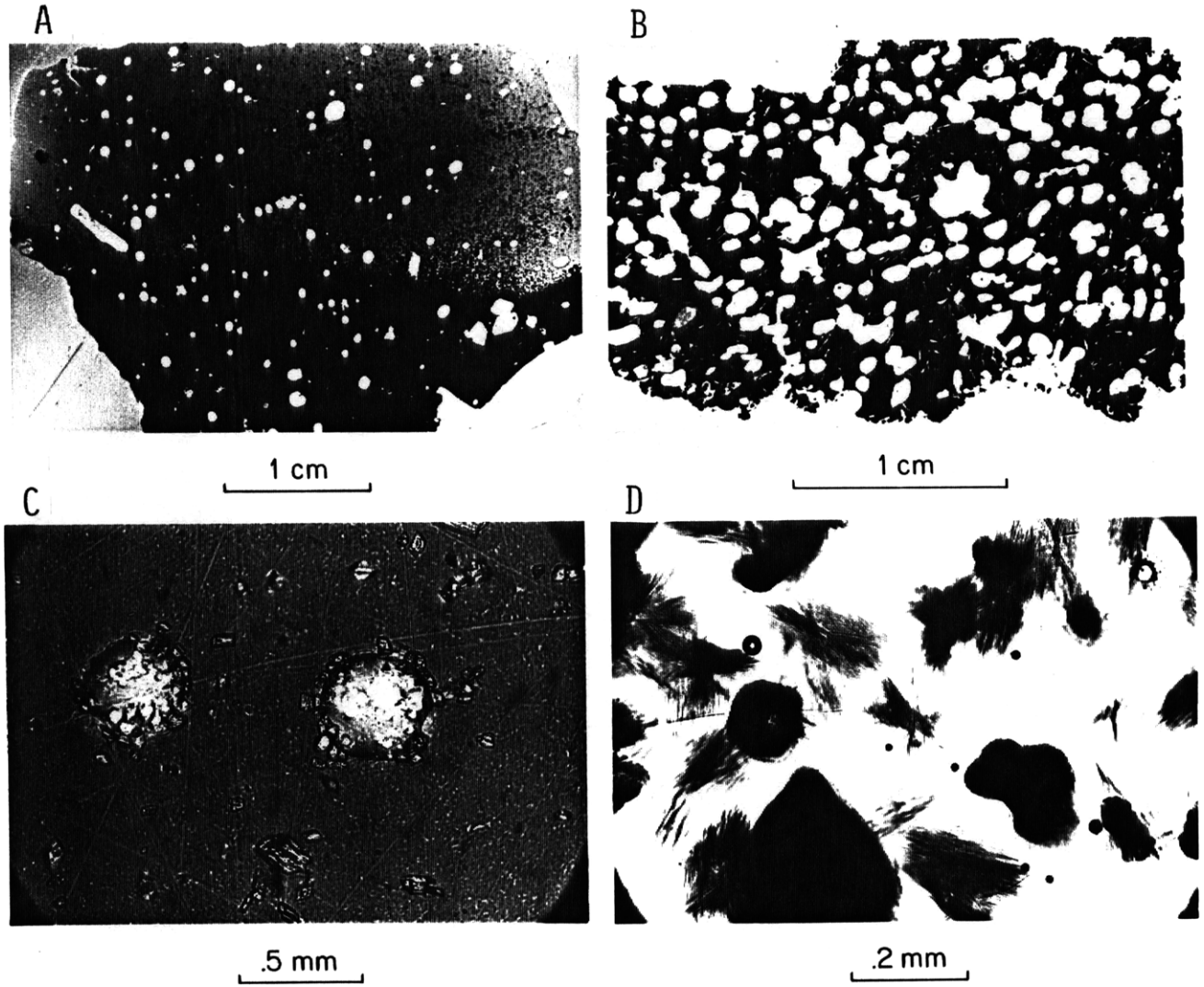
Figure AII.3: Photomicrographs of basaltic glasses (all in plane light)

a. Photograph of sample Hualalai tholeiite KK9-14 (thin section). The thin section was cut perpendicular to the chilled surface (top) to illustrate gradation from glassy exterior to holocrystalline interior.

b. Photograph of Loihi alkali basalt KK21-2 (thin section). The vesicles in this sample are unusually large and abundant. Note that in many cases the vesicles connect, suggesting that this sample has lost substantial quantities of gas.

c. Photomicrograph of FAMOUS sample Alv 519 2-1-b. The thin section was cut to a thickness of ~.15 mm to allow examination of the unusually large vesicles. Microphenocrysts of olivine can be seen suspended in the glass and attached to the vesicle surfaces.

d. Photomicrographs of Galapagos MORB sample Alv 714 G-1, showing small vesicles suspended in a glassy-spherulitic groundmass.


A
1 cm
B
1 cm
C
.5 mm
D
.2 mm

REFERENCES

Aldrich, L.T. and A.O. Nier (1946) The abundance of ^3He in atmospheric and well helium. Phys. Rev. 70:983.

Aldrich, L.T. and A.O. Nier (1948) The occurrence of ^3He in natural sources of helium. Phys. Rev. 74:1590.

Allegre, C.J., D. Ben Othman, M. Polve, and P. Richard (1979) The Nd-Sr isotopic correlation in mantle materials. Phys. Earth. Planet. Interiors 19:293-306.

Allegre, C.J., O. Brevart, B. Dupre, and J. F. Minster (1980) Isotopic and chemical effects produced in a continuously differentiating convecting Earth mantle. Phil. Trans. Roy. Soc. London A237:311.

Allmendinger, R.W. and F. Riis (1979) The Galapagos rift at 86°W: I. regional morphological and structural analysis. J. Geophys. Res. 84:5379.

Altemose, V.O. (1961) Helium diffusion through glass. J. Appl. Phys. 32:1309-1316.

Alvarez, L.W. and R. Cornog (1939a) ^3He in helium. Phys. Rev. 56:379.

Alvarez, L.W. and R. Cornog (1939b) Helium and hydrogen of mass 3. Phys. Rev. 56:613.

Anderson, A.T. (1974) Chlorine, sulfur and water in magmas and oceans. Geol. Soc. Am. Bull. 85:1485-1492.

Anderson, D.L. (1967) A seismic equation of state. Geophys. J. Royal Ast. Soc. 13:9.

Anderson, D.L. (1976) The 650 km mantle discontinuity. Geophys. Res. Lett. 3:347-349.

Anderson, D.L. (1979) Chemical stratification of the mantle. J. Geophys. Res. 84:6297-6298. ch5

Anderson, D.L. (1979) The upper mantle transition region: eclogite. Geophys. Res. Lett. 6:433-436.

Anderson, D.L. (1982a) Isotopic evolution of the mantle: the role of magma mixing. Earth Planet. Sci. Lett. 57:1-12.

Anderson, D.L. (1982b) Isotopic evolution of the mantle: a model. Earth Planet. Sci. Lett. 57:13-24.

Armstrong, R.L. (1968) A model for the evolution of strontium and lead isotopes in a dynamic earth. Rev. Geophys. Space Phys. 6:175-199.

Armstrong, R.L. (1981) Radiogenic isotopes: the case for crustal recycling on a near-steady-state no-continental growth earth. Phil. Trans. Royal Soc. London A301:443-472.

Axford, W.I. (1968) The polar wind and the terrestrial helium budget. J. Geophys. Res. 73:6855.

Baker, P.E., I.G. Gass, P.G. Harris, and R.W. Le Maitre (1964) The volcanological report of the Royal Society expedition to Tristan da Cunha, 1962. Phil. Trans. Royal Soc. London A256:439-575.

Baker, P.E. (1973) Islands of the South Atlantic. In: The Ocean Basins and Margins, vol. 1, The South Atlantic, A.E. Nairn and F.G. Stehli, eds., Plenum, New York

Ballard, R.D. and T.H. van Andel (1977) Morphology of the inner rift valley at lat 36˚50'N on the Mid-Atlantic Ridge. G.S.A. Bull. 88:507-530.

Bargar, K.E. and E.D. Jackson (1974) Calculated volumes of individual shield volcanoes along the Hawaiian-Emperor chain. U.S. Geol. Survey J. Res. 2:545-550.

Bernatowicz, T.J. and F.A. Podosek (1978) Nuclear components in the atmosphere. In: Terrestrial Rare Gases, E.C. Alexander and M. Oxima, eds., Japan Scientific Society Press, Tokyo.

Bernatowicz, T.J., K.A. Goettel, C.M. Hohenberg, and F.A. Podosek (1979) Anomalous noble gases in josephinite and associated rocks. Earth Planet. Sci. Lett. 43:368.

Bickle, M.J. (1978) Heat loss from the earth: a constraint on archaean tectonics. Earth Planet. Sci. Lett. 40:301-315.

Birch, F. (1961) Composition of the earth's mantle. Geophys. J. Royal Ast. Soc. 48:295.

Black, D.C. (1972a) On the origins of trapped helium, neon, and argon isotopic variations in meteorites. I. Gas rich meteorites, lunar soil, and breccia. Geochima. Cosmochim. Acta 36:347-375.

Black, D.C. (1972b) On the origins of trapped helium, neon, and argon isotopic variations in meteorites. II. Carbonaceous meteorites. Geochim. Cosmochim. Acta 36:377-394.

Blanchard, D.P., J.M. Rhodes, M.A. Dungan, K.V. Rogers, C.H. Donaldson, J.C. Brannon, J.W. Jacobs, and E.K. Gibson (1976) The chemistry and petrology of basalts from leg 37 of the deep sea drilling project. J. Geophys. Res. 81:4231-4246.

Blander, M., W.R. Grimes, N.V. Smith, and G.M. Watson (1959) Solubility of noble gases in molten fluorides. 2, In the LiF-NaF-Kf eutedtic mixture, J. Phys. Chem. 63:1164.

Bochsler, P., A. Stetler, J.M. Bird, and M.S. Weathers (1976) Excess ^{3}He and ^{21}Ne in josephinite. Earth Planet. Sci. Lett 39:67.

Bougault, H. and M. Treuil (1981) Mid-Atlantic Ridge: zero-age geochemical variations between Azores and 22°N. Nature 286:209-212.

Broecker, W.S. and T.H. Peng (1974) Gas exchange rates between air and sea. Tellus 26:21-35.

Brooks, C., S.R. Hart, A.W. Hofmann, and D. James (1976) Rb-Sr mantle isochrons from oceanic regions. Earth Planet. Sci. Lett. 32:51.

Brown, H. (1949) Rare gases and the formation of the earth's atmosphere. In: The Atmospheres of the Earth and Planets, G.P. Kuiper, ed., U. Chicago.

Bryan, W.B. and J. Moore (1977) Compositional variations of young basalts in the Mid-Atlantic Ridge rift valley near 37°N. G.S.A. Bull. 88:556-570.

Bryan, W.B. and D. Sargent (1978) Basalt from 22°-23°N, Mid-Atlantic Ridge median valley. Initial Reports DSDP, Vol. 45.

Bryan, W.B., G. Thompson, F.A. Frey, and J.S. Dickey (1976) Inferred geologic settings and differentiation in basalts from D.S.D.P. J. Geophys. Res. 81:4285-4304.

Bryan, W.B., G. Thompson, and J.N. Ludden (1981) Compositional variation in normal MORB from 22°-25°N: mid-Atlantic ridge and Kane fracture zone. J. Geophys. Res. 86:11, 815-11, 836.

Bryan, W.B. and H. Dick (1982) Contrasted abyssal basalt liquidus trends: evidence for mantle major element heterogeneity. Earth Planet. Sci. Lett. (in press).

Burke, K. and W. Kidd (1978) Were Archaean continental geothermal gradients steeper than those of today. Nature 272:240-241.

Butler, W.A., P.M. Jeffrey, J.H. Reynolds, and G.J. Wasserburg (1963) Isotopic variations in terrestrial xenon. J. Geophys. Res. 68:3283-3291.

Byerly G., W. Melson, and P. Vogt (1976) Rhyodacites, andesites, ferro-basalts and ocean tholeiites from the Galapagos Spreading Center. Earth Planet. Sci. Lett. 30:215-221.

Cathles, L.M. (1975) The Viscosity of the Earth's Mantle, Princeton U. Press

Chase, C.G. (1981) Oceanic Pb: two stage histories and mantle evolution. Earth Planet. Sci. Lett. 52:277-284.

Chayes, F. (1956) The Holmes effect and the lower limit to modal analyses. Min. Mag. 31:276-281.

Chayes, F. (1963) Relative abundance of intermediate members of the oceanic basalt-trachyte association. J. Geophys. Res. 68:1519-1534.

Christensen, N.I. and H.H. Salisbury (1975) Structure and constitution of the lower oceanic crust. Rev. Geophys. Space Phys. 13:57-86.

Church, S.E. and M. Tatsumoto (1975) Lead isotope relations in oceanic ridge basalts from the Juan de Fuca-Gorda Ridge area. C. Min. Pet. 53:253-279.

Clague, D. and T. Bunch (1976) Formation of ferrobasalt at East Pacific mid-ocean spreading centers. J. Geophys. Res. 81:4247.

Clague, D.A., F.A. Frey, G. Thompson, and S. Rindge (1981) Minor and trace element geochemistry of volcanic rocks dredged from the Galapagos spreading center: role of crystal fractionation and mantle heterogeneity. J. Geophys. Res. 86:9469-9482.

Clarke, W.B., M.A. Beg, and H. Craig (1969) Excess ^{3}He in the sea: evidence for terrestrial primordial helium. Earth Planet. Sci. Lett. 6:213.

Clarke, W. B., W.J. Jenkins, and Z. Top (1976) Determination of tritium by mass spectrometric measurement of ^{3}He. Int. J. App. Rad. Isotopes 27:515-522.

Clarke, S.P., and K.K. Turekian (1979) Thermal constraints on the distribution of long-lived radioactive elements in the earth. Phil. Trans. Royal Soc. London A291:269-275.

Coggeshall, H.D. (1962) Initial kinetic energy discrimination effects in crossed-field ion sources. J. Chem. Phys. 36:1640-1647.

Cohen, R.S., N.M. Evensen, P.J. Hamilton, and R.K. O'Nions (1980) U-Pb, Sm-Nd and Rb-Sr systematics of mid-ocean ridge basalt glasses. Nature 283:149-153.

Condomines M., M. Bernat, and C. Allegre (1976) Evidence for contamination of recent Hawaiian lavas from Th-U data. Earth Planet. Sci. Lett. 33:122-125.

Condomines M., P. Morand, C. Allegre, and G. Sigvaldason (1981) Th-U disequilibria in historical lavas from Iceland. Earth Planet. Sci. Lett. 55:393-406.

Corliss, J., L.I. Gordon, and J.M. Edmond (1979) Some implications of heat/mass ratios in Galapagos Rift hydrothermal fluids. In: Deep Drilling Results in the Atlantic: Ocean Crust, M. Talwani, ed., Am. Geophys. Union, Washington, D.C.

Craig, H. and D. Lal (1961) The production rate of natural tritium. Tellus 13:85.

Craig, H. and W.B. Clarke (1970) Oceanic ^{3}He: contribution from cosmogenic tritium. Earth Planet. Sci. Lett. 9:45.

Craig, H., W.B. Clarke, and M.A. Beg (1975) Excess ^{3}He in deep water on the East Pacific Rise. Earth Planet. Sci. Lett. 26:125-132.

Craig, H. and J. Lupton (1976) Primordial neon, helium, and hydrogen in oceanic basalts. Earth Planet. Sci. Lett. 31:369-385.

Craig, H., J.E. Lupton, J.A. Welhan, and R. Poreda (1978a) Helium isotope ratios in Yellowstone and Lassen Park volcanic gases. Geophys. Res. Lett. 5:987-899.

Craig, H., J.E. Lupton, and Y. Horibe (1978b) A mantle helium component in circum-Pacific volcanic gases: Hakone, the Marianas, and Mt. Lassen. In: Terrestrial Rare Gases, E.C. Alexander and M. Ozima, eds., Center for Academic Publications, Tokyo.

Craig, H., R. Poreda, J. Lupton, K. Marti, and S. Regnier (1979) Rare gases and hydrogen in josephitite. EOS Trans. Am. Geophys. Union 60:970.

Craig, H. and J. Lupton (1981) Helium-3 and mantle volatiles in the ocean and the oceanic crust. The Sea, Volume 7, C. Emiliani, ed., Wiley, New York

Crough, S. T. (1978) Thermal origin of mid-plate hot-spot swells. Geophys. J. R. Astr. Soc. 55: 451-469.

Crough, S.T. (1979) Hotspot epeirogeny. Tectonophysics 61:321-333.

Dalrymple, D.B. and J.G. Moore (1968) Argon-40: excess in submarine pillow basalts from Kilauea volcano, Hawaii. Science 161:1132.

Daly, R.A. (1925) The geology of Ascension Island. Proc. Am. Acad. Arts Sci. 60:1.

Dana, J.D. (1890) Characteristics of volcanoes. Dodd, Mead, New York.

Dasch, E.J. (1969) Strontium isotopes in weathering profiles, deep-sea sediments, and sedimentary rocks. Geochim. Cosmochim. Acta 33:1521-1552.

Davies, G.F. (1977) Whole-mantle convection and plate tectonics. Geophys. J. Royal Ast. Soc. 49:459-486.

Davies, G.F. (1981) Earth's neodymium budget and structure and evolution of the mantle. Nature 290:208-213.

Delaney, J.R., D.W. Muenow, and D.G. Graham (1978) The abundance and distribution of water, carbon and sulfur in the glassy rims of submarine pillow basalts. Geochim. Cosmochim. Acta 42:581-594.

DePaolo, D.J. and G.J. Wasserburg (1976) Inferences about magma sources and mantle structure from variations of $^{143}Nd/^{144}Nd$. Geophys. Res. Lett. 3:743-746.

DePaolo, D.J. and G. J. Wasserburg (1976) Nd isotopic variations and petrogenic models. Geophys. Res. Lett. 3:249.

DePaolo, D.J. and G.J. Wasserburg (1977) The sources of island arcs as indicated by Nd and Sr isotopic studies. Geophys. Res. Lett. 4:465-468.

DePaolo, D. J. and G. J. Wasserburg (1979) Petrogenetic mixing models and Nd-Sr isotopic patterns. Geochim. Cosmochim. Acta 43:615-627.

DePaolo, D.J. (1980) Crustal growth and mantle evolution: inferences from models of element transport of Nd and Sr isotopes. Geochim. Cosmochim. Acta 44:1185-1196.

Detrick, R.S. and S.T. Crough (1978) Island subsidence, hot spots and lithospheric thinning. J. Geophys. Res. 83:1236-1244.

Detrick, R.S., R.P. Von Herzen, S.T. Crough, D. Epp, and U. Fehn (1981) Heat flow on the Hawaiian swell and lithospheric reheating. Nature 292:142-143.

Dewey, J.F. and B.F. Windley (1981) Growth and differentiation of the continental crust. Phil. Trans. Royal Soc. London A301:189-206.

Dickey, J.S., F.A. Frey, S.R. Hart, E.B. Watson, and G. Thompson (1977) Geochemistry and petrology of dredged basalts from the Bouvet triple junction, South Atlantic. Geochim. Cosmochim. Acta 41:1105-1118.

Dickinson, W.R. and W.C. Luth (1971) A model for the plate tectonic evolution of mantle layers. Science 174:401-404.

Doremus, R.H. (1973) Glass Science. John Wiley and Sons.

Downing, R.G., E.W. Hemecke, and D.K. Manuel (1977) Josephinite: a a terrestrial alloy with radiogenic xenon-129 and the noble gas imprint of iron meteorites. Geochem. J. 11:219.

Dupre, B. and C.J. Allegre (1980) Pb-Sr-Nd isotopic correlation and the chemistry of the North Atlantic mantle. Nature 286:17-22.

Dymond, J. and L. Hogan (1973) Noble gas abundance patterns in deep sea basalts - primordial gases from the mantle. Earth Planet. Sci. Lett. 20:131.

Dymond, J. and L. Hogan (1978) Factors controlling the noble gas abundance patterns in deep sea basalt. Earth Planet Sci. Lett. 38:68.

Elsasser, W., P. Olsen, and B. Marsh (1979) The depth of mantle convection. J. Geophys. Res. 84:147-155.

Engel, A.E.J., C.G. Engel, and R.R. Havens (1965) Chemical characteristics of oceanic basalts and the upper mantle. Bull. Geol. Soc. Am. 76:719-734.

Erlank, A.J. and E.J.O. Kable (1976) The significance of incompatible elements in mid-Atlantic ridge basalts from 45°N, with reference to Zr/Nb. Cont. Min. Petrol. 54:281-291.

Erlank, A. J., and R.S. Rickard (1977) In: Extended abstracts. Second International Kimberlite Conference, F. R. Boyd and H.O. Meyer, eds., Santa Fe, New Mexico.

Fairhall, A.W. (1969) Concerning the source of the excess ^{3}He in the sea. Earth Planet. Sci. Lett. 26:125.

Fanale, F. (1971) A case for catastrophic early degassing of the earth. Chem. Geol. 8;70-105/

Farmer, H.G. and H.J.B. Dick (1981) Description of W.H.O.I. rock dredge samples. Volume 3 WHOI Technical Report WHOI-81-48.

Faure, G. and J.L. Powell (1972) Strontium Isotope Geology. Springer, Berlin.

Fechtig, H. and S. Kalbitzer (1966) Diffusion of argon in potassium bearing solids. In: Potassium Argon Dating, O. Schaeffer, ed.

Feigenson, M.D., F.J. Spera, and A.W. Hofmann (1981) The relationship between partial melting and eruption rate of Kohala volcano. Carnegie Inst. Washington Year Book 80:472-475.

Fisher, D.E. (1971) Incorporation of Ar in east Pacific basalts. Earth Planet. Sci. Lett. 12:321-324.

Fisher, D.E. (1973) Primordial rare gases in the deep earth. Nature 244:344-345.

Fisher, D. E. (1974) The planetary component of rare gases in the deep earth. Geophys. Res. Lett. 1:161.

Fisher, D.E. (1975) Trapped helium and argon and the formation of the atmosphere by degassing. Nature 256:113-114.

Fisher, D.E. (1978) Terrestrial potassium and argon abundances as limits to models of atmospheric evolution. In: Terrestrial Rare Gases, E.C. Alexander and M. Ozima, eds., Japan Scientific Society Press, Tokyo.

Fornari, D.J., A. Malahoff, and B.C. Heezen (1979) Submarine slope micromorphology and volcanic substructure of the island of Hawaii inferred from visual observations made from U.S. Navy DSV Sea Cliff. Marine Geol. 32:1-20.

Fornari, D.J., J.P. Lockwood, P. W. Lipman, M. Rawson, and A. Malahoff (1980) Submarine volcanic features west of Kealakekua Bay, Hawaii. J. Volc. Geoth. Res. 7:323-337.

Frey, F.A., W.B. Bryan, and G. Thompson (1974) Atlantic Ocean floor: geochemistry and petrology of basalts from legs 2 and 3 of the Deep Sea Drilling Project. J. Geophys. Res. 79:5567-5527.

Funkhouser, J.G. and J.J. Naughton (1968) Radiogenic helium and argon in ultramafic xenoliths from Hawaii. J. Geophys. Res. 73:4601.

Funkhouser, J.G., D. E. Fisher, and E. Bonatti (1968) Excess argon in deep sea rocks. Earth Planet. Sci. Lett. 5: 95-100.

Gallagher, K.J. (1965) The effect of particle size distribution on the kinetics of diffusion reactions in powders. In: Reactivity of Solids, G. M. Schwab, ed., Proc. 5th Intern. Symp. Reactivity of Solids, 192-203.

Gast, P.W. (1960) Limitations on the composition of the upper mantle. J. Geophys. Res. 65:1287-1297.

Gast, P.W., G. Tilton, and C. Hedge (1964) Isotopic composition of lead and strontium from Ascension and Gough islands. Science 145:1081-1085.

Gast, P.W. (1965) Terrestrial ratio of potassium to rubidium and the composition of the earth's mantle. Science 147:858-860.

Gast, P.W. (1968) Trace element fractionation and the origin of tholeiitic and alkaline magma types. Geochim. Cosmochim. Acta 32:1057-1086.

Geiss, J., F. Buhler, H. Cerutti, P. Eberhardt, and Ch. Filleux (1972) The solar wind composition experiment. Sect. 15 of Apollo 15 Preliminary Science Report, NASA SP-272 and Sect. 14 of Apollo 16 Preliminary Science Report, NASA SP-315, 14-1.

Gerling, E.K. (1940) On the solubility of helium in melts. Compt. Rend. Doklady Acad. Sci., USSR 27:22.

Glikson, A.Y. (1981) Uniformitarian assumptions, plate tectonics and the Precambrian earth. In: Precambrian Plate Tectonics, A. Kroner, ed., Elsevier.

Gramlich, J.W. and J.J. Naughton (1972) Nature of source material for ultramafic minerals from Salt Lake crater, Hawaii, from measurement of helium and argon diffusion. J. Geophys. Res. 77:3032-3042.

Green, H.W. (1979) Trace elements in the fluid phase of the Earth's mantle. Nature 277: 465-467.

Green, D.H. and R.C. Liebermann (1976) Phase equilibrium and elastic properties of a pyrolite model for the oceanic upper mantle. Tectonophysics 32:61-92.

Green, D.H., W.O. Hibberson, and A.L. Jaques (1979) Petrogenesis of mid-ocean ridge basalts. In: The Earth: Its Origin, Structure and Evolution. M. W. McElhinny (ed.) Academic Press

Hamano, Y. and M. Ozima (1978) Earth atmosphere evolution model based on Ar isotopic data. In: Terrestrial Rare Gases, E.C. Alexander and M. Ozima, eds., Japan Scientific Societies Press, Tokyo.

Hanson, G.N. (1977) Geochemical evolution of the suboceanic mantle. J. Geol. Soc. London 134:235-253.

Hargraves, R.B. (1981) Precambrian tectonic style: a liberal uniformitarian interpretation. In: Precambrian Plate Tectonics, A. Kroner, ed., Elsevier.

Hart, R., J. Dymond, and L. Hogan (1979) Preferential formation of the atmosphere-sialic crust system from the upper mantle. Nature 278:156-159.

Hart, S.R. (1973) Submarine basalts from Kilauea rift, Hawaii: non-dependence of trace element composition on extrusion depth. Earth Planet. Sci. Lett. 20:201-203.

Hart, S.R., J.G. Schilling, and J.L. Powell (1973) Basalts from Iceland and along the Reykjanes Ridge: Sr isotope geochemistry. Nature 246:104-107.

Hart, S.R. and C. J. Allegre (1980) Trace element constraints on magma genesis. In : Physics of Magmatic Processes, R. B. Hargraves, ed. Princeton University Press.

Hart, S.R. and C. Brooks (1982) Sources of terrestrial basalts: an isotopic viewpoint. In: Basaltic Volcanism of the Terrestrial Planets, Lunar and Planetary Institute, Houston (in press).

Hawkesworth, C., R.K. O'Nions, R. Pankhurst, P. Hamilton, and N. Evensen (1977) A geochemical study of island-arc and back-arc tholeiites from the Scotia Sea. Earth Planet. Sci. Lett. 36:253-262.

Hawkesworth, C.J., M.J. Norry, J.C. Roddick, and R. Volmer (1979) $^{143}Nd/^{144}Nd$ and $^{87}Sr/^{86}Sr$ ratios from the Azores and their significance in LIL-element enriched mantle. Nature 280:28.

Hedge, C.E. and Z.E. Peterman (1970) Strontium isotopic composition of basalts from the Gordo and Juan de Fuca Rises. C. Min. Pet. 27:114-120.

Hennecke, E.W. and O.K. Manuel (1975) Noble gases in an Hawaiian xenolith. Nature 257:778-780.

Heymann, D. (1971) The noble gases. In: Handbook of Elemental Abundances in Meteorites, B. Mason, ed., Gordon and Breach.

Hill, R.D. (1941) Production of ^{3}He. Phys. Rev. 59:103.

Hofmann, A.W. and S.R. Hart (1978) An assessment of local and regional isotopic equilibrium in the mantle. Earth Planet. Sci. Lett. 38:44-62.

Hofmann, A., W.M. White, and D.J. Whitford (1978) Geochemical constraints on mantle models: the case for a layered mantle. Carnegie Inst. Washington Yearbook 77:548-562.

Hofmann, A.W. and W.M. White (1980) The role of subducted oceanic crust in mantle evolution. Carnegie Inst. Washington Yearbook 477-483.

Hofmann, A.W. and W.M. White (1982) Mantle plumes from ancient oceanic crust. Earth Planet. Sci. Lett. 57:421-436.

Holland, H.D. (1962) Model for the evolution of the earth's atmosphere. In: Petrologic Studies: A Volume to Honor A.F. Buddington, Geol. Soc. Am., New York.

Hoskins, H., S. R. Gegg, and C. R. Tapscott (1977) Cruise Report R/V Atlantis II 93, Legs 5 and 6. Woods Hole Oceanographic Institution Technical Report α77-74

Hurley, P.M. (1968a) Absolute abundance and distribution of Rb, K and Sr in the earth. Geochim. Cosmochim. Acta 32:273-283.

Hurley, P.M. (1968b) Correction to: absolute abundance and distribution of Rb, K and Sr in the earth. Geochim. Cosmochim. Acta 32:1025-1030.

Hutchison, R. (1976) Strontium and lead isotopic ratios, heterogenous accretion of the earth, and mantle plumes. Geochim. Cosmochim. Acta 40: 482-485.

Isacks, B. and P. Molnar (1971) Distribution of stresses in the descending lithosphere from a global survey of focal mechanism solution of mantle earthquakes. Rev. Geophys. Space Phys. 9:103.

Jackson, E.D. (1968) The character of the lower crust and upper mantle beneath the Hawaiian Islands. Proc. 23d Internat. Geol. Congress, Prague, Sec. 1, Academica, Prague, pp 135-150.

Jackson, E.D. and T. L. Wright (1970) Xenoliths in the Honolulu volcanic series, Hawaii. J. Petrol. 11:405-30.

Jackson E.D., E. Silver, and G.B. Dalrymple (1972) Hawaiian-Emperor chain and its relation to Cenozoic circum-pacific tectionics. GSA Bull. 83:601-617.

Jackson, E.D., I. Koizumi, G.B. Dalrymple, D.A. Clague, R.J. Kirkpatrick, and H.G. Green (1980) Introduction and summary of results from DSDP leg 55: the Hawaiian-Emperor hot-spot experiment. Init. Rept. DSDP 55:5-31.

Jacobsen, S.B. and G.J. Wasserburg (1979) The mean age of mantle and crustal reservoirs. J. Geophys. Res. 84:7411-7427.

Jakobsson, S.P. (1972) Chemistry and distribution pattern of recent basaltic rocks in Iceland. Lithos 5:365-386.

Jakobsson, S.P. (1979a) Petrology of recent basalts of the eastern volcanic zone, Iceland. Acta Nat. Islandica 26:103p.

Jakobsson, S.P. (1979b) Outline of the petrology of Iceland. Jokull 29:57-73.

Jain, S.C. (1958) Simple solutions of the partial differential equation for diffusion. Proc. Royal Soc. London 243A:359-374.

Jambon, A. and J. E. Shelby (1979) Helium diffusion and solubility in obsidians and basaltic glass in the range 200-300°C. Carnegie Institution Yearbook.

Jarrard, R.D. and D. Clague (1977) Implications of Pacific Island and seamount ages for the origin of volcanic chains. Rev. Geophys. Space Phys. 15:57-76.

Jenkins, W.J. (1974) Helium isotope and rare gas oceanology. Ph.D. Thesis, McMaster U.

Jenkins, W.J., J.M. Edmond, and J. Corliss (1978) Excess ^{3}He and ^{4}He in Galapagos submarine hydrothermal waters. Nature 272:156-158.

Jenkins, W.J., M.D. Kurz, J.G. Schilling, and S.R. Hart (1980) Helium isotopic variations in the North Atlantic mantle. EOS 61:1158.

Johnson, H.E. and W.I. Axford (1969) Production and loss of ^{3}He in the earth's atmosphere. J. Geophys. Res. 74:2433.

Kamenskiy, I.L., V.A. Lobkov, E.M. Prasolov, N.S. Besrovny, E.I. Kudryartseva, G.S. Anufriev, and V.P. Pavlov (1974) Components of the upper mantle in the volcanic gases of Kamchatka. Geoch. Int. 13,3:35-48.

Kaneoka, I. and N. Takaoka (1978) Rare gases in mantle derived rocks and minerals. Earth Planet. Sci. Lett. 39:382.

Kaneoka, I., N. Takaoka, and K. Aoki (1978) Rare gases in mantle derived rocks and minerals. In: Terrestrial Rare Gases, E.C. Alexander, ed., Japan Sci. Soc. Press, Tokyo.

Kaneoka, I. and N. Takaoka (1980) Rare gas isotopes in Hawaiian ultramafic nodules and volcanic rocks. Science 208:1366-1368.

Karig, D.E. and R.W. Kay (1981) Fate of sediments on the descending plate at convergent margins. Phil. Trans. Royal Soc. London A301:233-251.

Kay, R.W. and N. Hubbard (1978)Trace elements in ocean ridge basalts. Earth Planet. Sci. Lett 38:95-116.

Kay, R.W., S.S. Sun, and C.N. Lee-Hu (1978) Pb and Sr isotopes in volcanic rocks from the Aleutian Islands and Pribilof Islands, Alaska. Geochim. Cosmochim. Acta 42:263-273.

Kay, R.W. (1980) Volcanic arc magmas: implications of a melting-mixing model for element recycling in the crust-upper mantle system. J. Geol. 88:497-522.

Kennedy, W. (1933) Trends of differentiation in basaltic magmas. Am. J. Sci. 25:239-56.

Kirby, S.H. and H.W. Green (1980) Dunite xenoliths from Hualalai volcano: evidence for mantle diapiric flow beneath the island of Hawaii. Am. J. Sci. 280A:550-575.

Kirsten, T. (1968) Incorporation of rare gases in solidifying enstatite melts. J. Geophys. Res. 73:2807-2810.

Klein, F.W. and R. Koyanagi (1981) Earthquakes at Loihi submarine volcano. EOS 62:1082.

Kockarts, G. and M. Nicolet (1962) Le probleme aeronomique de l'helium et de l'hydrogene neutres. Ann. Geophys. 18:269-290.

Kroner, A. (1981) Precambrian plate tectonics. In: Precambrian Plate Tectonics, A. Kroner, ed., Elsevier.

Krylov, A.Ya, B.A. Mamyrin, L.A. Khabarin, T.I. Mazina, and Y.I. Silin, (1974) Helium isotopes in ocean floor bedrock. Geokhimiya 8:1220.

Krylov, A.Ya, B.A. Mamyrin, Y.I. Silin, and L.V. Khabarin (1973) Helium isotopes in ocean sediments. Geochchem. Int. 10:202.

Kurz, M.D. and W.J. Jenkins (1981) The distribution of helium in oceanic basalt glasses. Earth Planet. Sci. Lett. 53:41-54.

Kurz, M.D. and W.J. Jenkins (1982) Reply to comment by R. Poreda. Earth Planet Sci. Lett. (in press).

Kurz, M.D., W. J. Jenkins, S. Hart, and J. G. Schilling (1982a) Helium isotopic variations in the mantle beneath the central North Atlantic Ocean. Earth Planet. Sci. Lett. (in press).

Kurz, M.D., W.J. Jenkins, and S.R. Hart (1982b) Helium isotopic systematics of oceanic islands: implications for mantle heterogeneity. Nature (in press).

Kushiro, I. (1973) Origin of some magmas in oceanic and circumoceanic regions. Tectonophys. 17:211-222.

Kyser, T.K. (1980) Stable and rare gas isotopes and the genesis of basic lavas and mantle xenoliths. Ph.D. Thesis, U. California, Berkeley.

Kyser, T.K. and M. Javoy (1981) Stable isotope relations in the Loihi Seamount. EOS Trans. Am. Geophys. Union 62:1083.

Langmuir, C.H., R.D. Vocke, G.N. Hanson, and S.R. Hart (1978) A general mixing equation with applications to Icelandic basalts. Earth Planet. Sci. Lett. 37:380-392.

Langmuir, C.H. and G.H. Hanson (1980) An evaluation of major element heterogeneity in mantle sources of basalts. Phil. Trans. Royal Soc. London A297:383-407.

Leeman, W.P., J.R. Budahn, D.C. Gerlach, D.R. Smith, and B.N. Powell (1980) Origin of Hawaiian tholeiites: trace element constraints. Am. J. Sci. 280A:794-819.

Le Maitre, R.W. (1962) Petrology of volcanic rocks, Gough Island, South Atlantic. Bull. Geol. Soc. Am. 73:1309-1340.

le Roex, A.P. (1980) Geochemistry and mineralogy of selected Atlantic ocean basalts. Ph.D. Thesis, U. Cape Town.

Liebermann, R.C. (1978) Elasticity of the mantle. In: The Earth: Its Origin, Structure and Evolution, M.W. McElhinny, ed., Academic Press, New York.

Lin, T.H. and R.A. Yund (1972) Potassium and sodium self diffusion in alkali feldspar. Cont. Min. Petrol. 34:177-184.

Lipman, P. (1980) The southwest rift zone at Mauna Loa: implications for structural evolution of Hawaiian volcanoes. Am. J. Sci. 280A:794-819.

Liu, L. (1979) On the 650-km seismic discontinuity. Earth Planet. Sci. Lett. 42:202-208.

Ludden, J. (1978) Magmatic evolution of the basaltic shield volcanoes of Reunion Island. J. Volc. Geoth. Res. 4:171-198.

Lupton, J.G. and H. Craig (1975) Excess ^{3}He in oceanic basalts: evidence for terrestrial primordial helium. Earth Planet. Sci. Lett. 26:133.

Lupton, J.E., R.F. Weiss, and H. Craig (1976) Mantle helium in the Red Sea brines. Nature 266:244.

Lupton, J.E., R.F. Weiss, and H. Craig (1977) Mantle helium in hydrothermal plumes in the Galapagos Rift. Nature 267:603.

Lupton, J.E., G.P. Klinkhammer, W. Normark, R. Haymon, K.C. MacDonald, R.F. Weiss, and H. Craig (1980) Helium-3 and manganese at the 21°N East Pacific Rise hydrothermal site. Earth Planet. Sci. Lett. 50:115-127.

Macdonald, G.A (1949) Hawaiian petrographic province. Geol. Soc. Am. Bull. 60:1541-1596.

Macdonald, G.A. and T. Katsura (1964) Chemical composition of Hawaiian lavas. J. Petrol. 5:82-133.

Macdonald, G.A. (1968) Composition and origin of Hawaiian lavas. Geol. Soc. Am. Memoir 16:477-522.

MacDonald, G.J.F. (1963) The escape of helium from the earth's atmosphere. Rev. Geophys. 1:305-349.

MacDougall, J.D. (1977) Uranium in marine basalts: concentrations, distribution, and implications. Earth Planet. Sci. Lett. 35:65-70.

Mamyrin, B.A., I.N. Tolstikhin, G.S. Anufriev, and I.L. Kamenskii (1969) Isotopic analysis of terrestrial helium on a magnetic resonance mass spectrometer. Geochem. Int. 6:517-524.

Mamyrin, B.A., G.S. Anufriev, I.L. Kamenskii, and I.N. Tolstikhin (1970) Determination of the isotopic composition of atmospheric helium. Geochem. Int. 7:498-505.

Mamyrin, B.A., V.I. Gerasimouskiy, and L.V. Khabarin (1974) Helium isotopes in the rift rocks of East Africa and Iceland. Geochem. Int. 11:488-494 (α3).

Mark, T.D. and A.W. Castleman (1980) Comment on the interpretation of repeller curves obtained with Nier type ion sources. J. Phys. E. __:1121-1124.

Marsh, B.D. and I.S.E. Carmichael (1974) Benioff zone magmatism. J. Geophys. Res. 79:1196-1206 OR 81:975-984.

Mazor, E., D. Heymann, and E. Anders (1970) Noble gases in carbonaceous chondrites. Geochim. Cosmochim. Acta 34:781.

McCulloch, M. T., and G. J. Wasserburg (1978). Sm-Nd and Rb-Sr chronology of continental crust formation. Science 200: 1003-1011.

McDougall, I. (1964) Potassium-argon ages from lavas of the Hawaiian Islands. GSA Bull. 75:107-128.

McDougall, I. and C. D. Ollier (1982) Potassium argon ages from Tristan da Cunha, South Atlantic Geological Magazine 119: 87-93.

McKenzie, D. and N. Weiss (1975) Speculations on the thermal and tectonic history of the earth. Geophys. J. Royal Ast. Soc. 42:131-174.

McKenzie, D.P. (1977) Surface deformation, gravity anomalies and convection. Geophys. J. Royal Ast. Soc. 48:211-238.

McKenzie, D.P. (1979) Finite deformation during fluid flow. Geophys. J. Royal Ast. Soc. 58:689-715.

McKenzie, D.P., A. Watts, B. Parsons, and M. Roufosse (1980) Planform of convection beneath the Pacific Ocean. Nature 288L442-446.

McKenzie, D.P. and F.M. Richter (1982) Parameterized thermal convection in a layered region and the thermal history of the earth (preprint)

Melson, W.G. (1969) Preliminary results of a geophysical study of portions of the Juan de Fuca Ridge. U. S. Dept. of Comm. Tech. Report ESSA C and GSTM 6.

Melson, W., T. Vallier, T. Wright, G. Byerly, and J. Helen (1976) Chemical diversity of abyssal volcanic glass erupted along Pacific, Atlantic, and Indian Ocean spreading centers. In: Geophysics of the Pacific Ocean Basin and its margin, AGU Monograph 19.

Melson, W.G. and T. O'Hearn (1979) Basaltic glass erupted along the mid-Atlantic ridge between 0-37°N: relationships between composition and latitude. In: Deep Drilling Results in the Atlantic Ocean: Ocean Crust, M. Talwani et al., eds., Am. Geophys. Union, Washington, D.C.

Middlefehldt, D.W. and G.W. Wetherill (1979) Rb-Sr studies of CI and CM chondrites. Geochim. Cosmochim. Acta 43:201.

Mitchell, W.S. and F.A. Aumento (1976) The distribution of uranium in oceanic rocks from the mid-Atlantic ridge at 36°N. Init. Rept. D.S.D.P. 37:547-559.

Moorbath, S., R.K O'Nions, and R.J. Pankhurst (1975) The evolution of early Precambrian crustal rocks at Isua, West Greenland: geochemical and isotopic evidence. Earth Planet. Sci. Lett. 27:229-239.

Moore, J.G. (1965) Petrology of deep-sea basalt near Hawaii. Am. J. Sci. 263:40-52.

Moore, J.G. and R.S. Fiske (1969) Vocanic substructure inferred from dredge samples and ocean bottom photographs, Hawaii. GSA Bull. 80:1191-1202.

Moore, J.G., J. Batchelder, and C. Cunningham (1977) CO_2 filled vesicles in mid-ocean ridge basalt. J. Volc. Geoth. Res. 2:309-329.

Moore, J.G. (1979) Vesicularity and CO_2 in mid-ocean ridge basalt. Nature 282:250-252.

Moore, J.G., D. A. Clague, and W. R. Normark (1982) Diverse basalt types from Loihi Seamount, Hawaii. Geology (in press).

Morel, J.M. and R. Hekinian (1980) Compositional variations of volcanics along segments of recent spreading ridges. Cont. Min. Petrol. 72:425-436.

Morgan, J.H. (1971) Thorium and uranium. In: Handbook of Elemental Abundances in Meteorites, B. Mason, ed., Gordon and Breach.

Morgan, W.J. (1971) Convection plumes in the lower mantle. Nature 230:42-43.

Morgan, W.J. (1972) Deep mantle convection and plate motion. AAPG Bull. 56: 203-13.

Morgan, W.J. (1981) Hot spot tracks and the opening of the Atlantic and Indian Oceans. In: The Sea, vol. 7., C. Emiliani, ed., Wiley, New York.

Morrison, P. and J. Pine (1955) Radiogenic origin of the helium isotopes in rock. Ann. N.Y. Acad. Sci. 62:71-92.

Muehlenbachs, K., A.T. Anderson and G.E. Sigvaldason (1974) Low ^{18}O basalts from Iceland. Geochim. Cosmochim. Acta 38:577.

Mulfinger, H.O. and H. Scholze (1962) Loslichkeit und Diffusion von Helium in Glasschmelzen, 1, Loslichkeit. Glastechn. Ber. 35:466.

Murck, B.W., R.C. Burruss, and L.S. Hollister (1978) Phase equilibria in fluid inclusions in ultrafic xenoliths. Am. Min. 63:40-46.

Naidu, P.S. and K.O. Westphal (1966) Some theoretical considerations of ion optics of the mass-spectrometer ion source. Brit. J. Appl. Phys. 17:645-651.

Nicolet, M. (1957) The aeronomic problem of helium. Ann. Geophys. 13:1-21.

Noble, C.S. and J.J. Haughton (1968) Deep ocean basalts: inert gas content and uncertainties in age dating. Science 162:265.

Norton, F.J. (1957) Permeation of gases through solids. J. Appl. Phys. 28:34-39.

O'Connell, R.J. (1977) On the scale of mantle convection. Tectonophys. 38:119-136.

O'Hara, M.J. (1980) Nonlinfear nature of the unavoidable long-lived isotopic, trace and major element contamination of a developing magma chamber. Phil. Trans. Royal Soc. London A297:215-227.

O'Hara, M. J. and R. E. Mathews (1981) Geochemical evolution in an advancing, periodically replenished, periodically tapped, continuously fractionated magma chamber. J. Geol. Soc. Lond. 138: 237-277.

O'Nions, R.K. and K. Gronvold (1973) Petrogenetic relationships of acid and basic rocks in Iceland: Sr-isotopes and rare earth elements in late and post-glacial volcanics. Earth Planet. Sci. Lett. 19:397-409.

O'Nions, R.K. and R.J. Pankhurst (1974) Petrogenetic significance of isotope and trace element variations in volcanic rocks from the mid-Atlantic. J. Petrol. 15:603-634.

O'Nions, R.K., R.J. Pankhurst, and K. Gronvold (1976) Nature and development of basalt magma sources beneath Iceland and the Reykjanes Ridge. J. Petrol. 17:315-338.

O'Nions, R.K., P.J. Hamilton, and N.M. Evensen (1977) Variations in $^{143}Nd/^{144}Nd$ and $^{87}Sr/^{86}Sr$ ratios in oceanic basalts. Earth Planet. Sci. Lett. 34:13.

O'Nions, N.M. Evensen, P.J. Hamilton, and S.R. Carter (1978) Melting of the mantle past and present: isotope and trace element evidence. Phil. Trans. Royal Soc. London A258:547-559.

O'Nions, R.K., N.M. Evensen, S.R. Carter, and P.J. Hamilton (1979a) Isotope geochemical studies of North Atlantic basalts and their implications for mantle evolution. In: Deep Drilling in the Atlantic Ocean: Ocean Crust, M. Talwani et al., eds., Am. Geophys. Union, Washington, D.C.

O'Nions, R.K., N.M. Evensen, and P.J. Hamilton (1979b) Geochemical modeling of mantle differentiation and crustal growth. J. Geophys. Res. 84:6091-6101.

O'Nions, R.K., N.M. Evensen, and P.J. Hamilton (1980) Differentiation and evolution of the mantle. Phil. Trans. Royal Soc. London A297:479-493.

Oskarsson, N., G. E. Sigvaldason, and S. Steinthorsson (1982) A dynamic model of rift zone petrogenesis and the regional petrology of Iceland. J. Petrol. 23: 28-71.

Oversby, V. M., and A. E. Ringwood (1971) Time of formation of the Earth's core. Nature 234: 463-465.

Ozard, J.M. and R.D. Russell (1969) Efficiency of an electrostatically focussed ion source. Appl. Scie. Res. 20:55-60.

Ozima, M. (1975) Ar isotopes and earth atmosphere evolution models. Geochim. Cosmochim. Acta 39:1127-1134.

Ozima, M. and E. Alexander (1976) Rare gas fractionation patterns in terrestrial samples and the earth atmosphere evolution model. Rev. Geophys. Space Phys. 14:385-390.

Palmason, G. (1971) Crustal structure of Iceland from explosion seismology. Soc. Sci. Islandica 40:187 p.

Parsons, B. and D. McKenzie (1978) Mantle convection and the thermal structure of the plates. J. Geophys. Res. 83:4485-4496.

Pepin, R.O. and P. Signer (1965) Primordial rare gases in meteorites. Science 149:253-265.

Peterman, Z. and C. Hedge (1971 OR 1970) Related strontium isotopic and chemical variations in oceanic basalts. Bull. Geol. Soc. Am. 82:493-499.

Phinney, D., J. Tennyson, and U. Frick (1978) Xenon in CO_2 well gas revisited. J. Geophys. Res. 83:2313-2319.

Polak, B.G., V.I. Kononov, I.N. Tolstikhin, B.A. Mamyrin, and L. Khabarin (1976) The helium isotopes in thermal fluids. In: Thermal and Chemical Problems of Thermal Waters, A.I. Johnson, ed., Publ. 119, Int. Assoc. Hydrological Sci. pp.15-29.

Poreda, R. and H. Craig (1979) Helium and neon in oceanic volcanic rocks. EOS 60:969.

Poreda, R., H. Craig, and J. G. Schilling (1980) $^3He/^4He$ variations along the Reykjanes Ridge. EOS 61:1158.

Poreda, R., H. Craig, and R. Motyka (1981) Helium isotope variations along the Alaskan-Aleutian arc. Eos Trans. Am. Geophys. Union 62:1092.

Poreda, R. (1982) Helium partitioning in basaltic glass: comments on the paper by Kurz and Jenkins. Earth Planet. Sci. Lett. (in press).

Press, F. (1972) The earth's interior as inferred from a family of models. In: The Nature of the Solid Earth, E.C. Robertson, ed., McGraw Hill, New York.

Raitt, W.J., R.W. Schunk, and P.M. Banks (1978) Quantitative calculations of helium ion escape fluxes from the polar ionospheres. J. Geophys. Res. 83:5617-5623.

Ramsay, W. (1895) On a gas showing the spectrum of helium, the reputed cause of D_3, one of the lines in the coronal spectrum. Proc. Royal Soc. London 58:65-67.

Reynolds, J.H. (1963) Xenology. J. Geophys. Res. 68:2939-2956.

Reynolds, J.H., U. Frick, J.M. Neil, and D.L. Phinney (1978) Rare gas rich separates from carbonaceous chondrites. Geochim. Cosmochim. Acta 42:1775-1797.

Richard, P., N. Shimizu, and C.J. Allegre (1976) $^{143}Nd/^{144}Nd$, a natural tracer: an application to oceanic basalts. Earth Planet. Sci. Lett. 31:269.

Richter, F.M. and C.E. Johnson (1974) Stability of a chemically layered mantle. J. Geophys. Res. 79:1635-1639.

Richter, F.M. and B. Parsons (1975) On the interaction of two scales of convection in the mantle. J. Geophys. Res. 80:2529-2541.

Richter, F.M. (1978) Mantle convection models. Ann. Rev. Earth Planet. Sci. 6:9-19.

Richter, F.M. (1979) Focal mechanisms and seismic energy release of deep and intermediate earthquakes and their bearing on the depth extent of mantle flow. J. Geophys. Res. 84:6783-6795.

Richter, F.M. and N.M. Ribe (1979) On the importance of advection in determining the local isotopic composition of the mantle. Earth Planet. Sci. Lett. 43:212-222.

Richter, F.M. and D.P. McKenzie (1981) On some consequences and possible causes of layered mantle convection. J. Geophys. Res. 86:6133-6142.

Ringwood, A.E. (1975) Composition and Petrology of the Earth's Mantle. McGraw Hill, New York.

Rison, W. (1980) Isotopic studies of the rare gases in igneous rocks: implications for the mantle and atmosphere. Ph.D. Thesis, U. California, Berkeley.

Roedder, E. (1965) Liquid CO_2 inclusions in olivine bearing nodules and phenocrysts from basalts. Am. Min. 50:1746-1782.

Roedder, E. (1981) CO_2, sulfide-melt, and silicate melt inclusions in olivine nodules from Loihi Seamount, Hawaii. EOS 62:1083.

Rowe, E.C. and J.G. Schilling (1979) Fluorine in Iceland and Reykjanes Ridge basalts. Nature 279:33-37.

Rubey, W.W. (1951) Geologic history of seawater. Bull. Geol. Soc. Am. 62:1111-1148.

Saemundsson, K. (1979) Outline of the geology of Iceland. Jokull 29:7-26.

Saito, K., A.R. Baso, and E.C. Alexander (1978) Planetary-type rare gases in an upper mantle derived amphibole. Earth Planet. Sci. Lett. 39:274-280.

Schilling, J.G. (1973) Iceland mantle plume: geochemical evidence along the Reykjanes Ridge. Nature 242:565-579.

Schilling, J.G. (1975a) Azores mantle blob: rare earth evidence. Earth Planet. Sci. Lett. 25:103-115.

Schilling, J.G. (1975b) Rare earth variations across "normal segments" of the Reykjanes Ridge, 60-65°N, mid-Atlantic ridge, 29°S, and east Pacific rise, 2-19°S, and evidence on the composition of the underlying low-velocity layer. J. Geophys. Res. 80:1459-1473.

Schilling, J.-G., R.N. Anderson, and P. Vogt (1976) Rare earth, Fe and Ti variations along the galapagos spreading centre, and their relationship to the Galapagos mantle plume. Nature 261:108-113.

Schilling, J.G., M. Bender, and C.K. Unni (1978) Origin of chlorine and bromine in the oceans. Nature 273:631-636.

Schilling, J.G., M.B. Beryeson, and R. Evans (1980) Halogens in the mantle beneath the North Atlantic. Phil. Trans. Royal Soc. London A297:147-178.

Schilling, J.G., H. Sigurdsson, and R. Kingsley (1980) Skagi and western neovolcanic zones in Iceland. J. Geophys. Res. 83:3971.

Schilling, J.G., M. Zajac, R. Evans, T. Johnston, W. White, J. D. Devine, and R. Kingsley (1982) Petrologic and geochemical variation along the Mid-Atlantic Ridge from 29° to 73°N. Am. J. Sci. (submitted).

Schwartzman, D.W. (1978) On the ambient $^{4}He/^{40}Ar$ ratio and the coherent model of degassing of the earth. In: Terrestrial Rare Gases, E.C. Alexander and M. Ozima, eds., Center for Academic Publications, Japan.

Sclater, J.G., L.A. Lawver, and B. Parsons (1975) Comparison of long wavelength residual elevation and free-air gravity anomalies in the North Atlantic and possible implications for the thickness of the lithospheric plate. J. Geophys. Res. 80:1031-1052.

Sclater, J.G., C. Bowin, R. Hey, H. Hoskins, J. Peirce, J. Phillips, and C. Tapscott (1976) The Bouvet triple junction. J. Geophys. Res. 81:1857-1869.

Sclater, J. G., C. Jaupart, and D. Galson (1980) The heat flow through oceanic and continental crust and the heat loss of the earth. Rev. Geophys. Space Phys. 18: 269-311.

Shaw, H.R., E.D. Jackson, and K.E. Bargar (1980) Volcanic periodicity along the Hawaiian-Emperor chain. Am. J. Sci. 280A:667.

Sheldon, W.R. and J.W. Kern (1972) Atmospheric helium and geomagnetic field reversals. J. Geophys. Res. 77:6194-6202.

Sharpe, H.N. and W.R. Peltier (1979) A thermal history model for the earth with parameterized convection. Geophys. J. Royal Ast. Soc. 59:171-203.

Shelby, J.E. (1976) Helium migration in sodium aluminosilicate glasses. J. Am. Ceram. Soc. 59:420.

Sigurdsson, H., J.G. Schilling, and P.S. Meyer (1978) Skagi and Langjokull volcanic zones in Iceland, I. Petrology and structure. J. Geophys. Res. 83:3971-3983.

Sigurdsson, H. (1981) First-order major element variation in basalt glasses from the mid-ocean ridge: 29˚N to 73˚N. J. Geophys. Res. 86:9483-9502.

Sigvaldason, G. (1969) Chemistry of basalts from the Icelandic rift zone. C. Min. Pet. 20:357-370.

Sigvaldason, G. (1974) Basalts from the center of the assumed Icelandic plume. J. Petrol. 15:497-524.

Sigvaldason, G.E., S. Steinthorsson, N. Oskarsson, and P. Imsland (1974) Compositional variation in recent Icelandic tholeiites and the Kverkjoll hot spot. Nature 251:579-582.

Sleep, H. H., and B. R. Rosendahl (1979) Topography and tectonics of mid-oceanic ridge axes, J. Geophys. Res. 84: 6831-6839.

Smith, S.P. and J.H. Reynolds (1981) Excess ^{129}Xe in a terrestrial sample measured in a pristine system. Earth Planet. Sci. Lett. 54:236-238.

Srinivason, B., R.S. Lewis, and E. Anders (1978) Noble gases in the Allende and Abee meteorite and a gas-rich mineral fraction. Geochim. Cosmochim. Acta 42:183.

Staudacher, T., and C.J. Allegre (1981) ^{129}Xe excess in typical MORB from the Pacific Ocean. EOS 62:420.

Staudigel, H., S.R. Hart, A. Zindler, M. Lanphere, C.Y. Chen, and D. Clague (1981) Pb, Nd, and Sr Isotopes of Loihi Seamount. EOS 62:1087.

Stettler, A. and P. Bochsler (1979) He, Ne and Ar composition in a neutron activated sea-floor basalt glass. Geochim. Cosmochim. Acta 43:157-169.

Stevenson, D.J. and J.S. Turner (1979) Fluid models in mantle convection. In: The Earth: Its Origin, Structure and Evolution, M.W. McElhinny, ed., Academic Press, New York.

Suess, H. (1949) Die Haufigkeit der edelgase auf der Erde und im Kosmos. J. Geol. 57:699-707.

Sun, S. and G.N. Hanson (1975) Evolution of the mantle: geochemical evidence from alkali basalt. Geology 3:297-302.

Sun, S.S. and B.M. Jahn (1975) Lead and strontium isotopes in post glacial basalts from Iceland. Nature 255:527-530.

Sun, S.S., M. Tatsumoto, and J.G. Schilling (1975) Mantle plume mixing along the Reykjanes Ridge axis: lead isotopic evidence. Science 190:143-147.

Sun, S.S., R.W. Nesbitt, A. Ya Sharaskin (1979) Geochemical characteristics of mid-ocean ridge basalts. Earth Planet. Sci. Lett. 44:119-138.

Sun, S.S. (1980) Lead isotopic study of young volcanic rocks from mid-ocean ridges, ocean islands and island arcs. Phil. Trans. Royal Soc. London A297:409-445.

Swanson, D.A. (1972) Magma supply at Kilauea volcano 1952-1971. Science 175:169-170.

Takagi, J. (1969) Rare gas anomalies and intense muon fluxes in the past. Nature 227:362.

Takaoka, N. and M. Ozima (1978) Rare gas isotopic compositions in diamonds. Nature 271:45-46.

Tarling, D.H. (1980) Lithospheric evolution and changing tectonic regimes. J. Geol. Soc. London 137:459-467.

Tatsumoto, M. (1966) Genetic relations of oceanic basalts as indicated by the lead isotopes. Science 153:1330.

Tatsumoto, M. (1978) Isotopic composition of lead in oceanic basalt and its implication to mantle evolution. Earth Planet. Sci. Lett 38:63-87.

Taylor, S. R., and S. M. McLennon (1981) The composition and evolution of the continental crust: rare earth element evidence from sediment rocks. Phil. Trans. R. Soc. London A301: 381-3999.

Thompson, G., W.B. Bryan, and W.G. Melson (1980) Geological and geophysical investigation of the Mid-Cayman Rise spreading center: geochemical variation and petrogenesis of basalt glasses. J. Geol. 88:41-55.

Thomsen, L. (1980) ^{129}Xe on the outgassing of the atmosphere. J. Geophys. Res. 85:4374-4378.

Tilley, C.E. (1950) Some aspects of magmatic evolution. Proc. Geol. Soc. London 16:37-71.

Tolstikhin, I.N., B.A. Mamyrin, L.B. Khabarin, and E.N. Erlikh (1974) Isotope composition of helium in ultrabasic xenoliths from volcanic rocks of Kamchatka. Earth Planet. Sci. Lett. 22:75-84.

Tolstikhin, I.N. (1978) A review: some recent advances in isotope geochemistry of light rare gases. In: Terrestrial Rare Gases, E.C. Alexander and M. Ozima, eds., Japan Scientific Society Press, Tokyo.

Torgersen, T., J.E. Lupton, D.S. Sheppard, and W. Giggenbach (1982) Helium isotope variations in the thermal areas of New Zealand. J. Volc. Geotherm. Res. (in press).

Trimble, V. (1975) The origin and abundances of the chemical elements. Rev. Mod. Phys. 47:877.

Turcotte, D.L. and E.R. Oxburgh (1978) Intra plate volcanism. Phil. Trans. Royal Soc. London A288:561-579.

Turekian, K.K. (1959) The terrestrial economy of helium and argon. Geochim. Cosmochim. Acta 17:37-43.

Unni, C.K. and J. G. Schilling (1978) Cl and Br degassing by volcanism along the Reykjanes Ridge and Iceland. Nature 272:19-23.

Upton, B.G. and W.J. Wadsworth (1972) Aspects of magmatic evolution on Reunion Island. Phil. Trans. Royal Soc. London A271:105-130.

van Andel, T.H. and R. D. Ballard (1979) Galapagos rift at 86°W, 2, volcanism, structure and evolution of the Rift valley. J. Geophys. Res. 84:5390.

Vollmer, R. (1976) Rb-Sr and U-Th-Pb systematics of alkaline rocks: the alkaline rocks from Italy. Geochim. Cosmochim. Acta 40:283-295.

Voerwoerd, W.J. (1971) Geology of Marion and Prince Edward. In: Marion and Prince Edward Islands, E.M. Van Zinderen Bakker et al., eds., Balkema, Cape Town.

Wallington, M.J. (1971) The focal properties of electron bombardment ion sources. J. Phys. E.: Sci. Instru. 4:1-8.

Wancke, H. (1981) Constitution of terrestrial planets. Phil. Trans. R. Soc. London A303: 287-302.

Warasila, R.L. and O.A. Shaeffer (1974) $^{3}He/^{4}He$ ratios in the lower radiation belt as measured by trapped particles in a recovered satellite. Geophys. Res. Lett. 2:480-482.

Wasserburg, G.J. and D.J. DePaolo (1979) Models of earth structure inferred from neodymium and strontium isotopic abundances. Proc. Natl. Acad. Sci. 76:3594-3598.

Watts, A.B. and J.R. Cochran (1974) Gravity anomalies and flexure of the lithosphere along the Hawaiian-Emperor seamount chain. Geophys. J. Royal Ast. Soc. 38:119-141.

Watts, A.B. and S.F. Daly (1981) Long wavelength gravity and topography anomalies. Ann. Rev. Earth Planet. Sci. 9:415-448.

White, W. M., J. G. Schilling, and S. R. Hart (1976) Evidence for the Azores mantle plume from strontium isotope geochemistry of the Central North Atlantic. Nature 263:659-663.

White, W.M. (1977) Geochemistry of igneous rocks from the central North Atlantic. Ph.D. Thesis, U. Rhode Island.

White, W.M. and W.B. Bryan (1977) Sr-isotope, K, Rb, Cs, Sr, Ba, and rare-earth geochemistry of basalts from the FAMOUS area. GSA Bull. 88:51.

White, W.M. and J.B. Schilling (1978) The nature and origin of geochemical variations in Mid-Atlantic Ridge basalts from the Central North Atlantic. Geochim. Cosmochim. Acta 42:1501-1516.

Wilkinson, J.F.G. (1982) The genesis of mid-ocean ridge basalt. Earth Sci. Rev. 18:1-57.

Williams, D.L. and R.P. von Herzen (1974) Heat loss from the earth: new estimate. Geology 2:327-328.

Wilson, J.T. (1963) A possible origin of the Hawaiian Islands. Can. J. Phys. 41:863-870.

Windley, B.F. (1977) Timing of continental growth and emergence. Nature 270:426-428.

Windley, B.F. (1981) Precambrian rocks in the light of the plate tectonics concept. In: Precambrian Plate Tectonics, A. Kroner, ed., Elsevier.

Wood, D.A., J.L. Joron, M. Trevil, M. Norry, and J. Tarney (1979) Elemental and Sr isotope variations in basic lavas from Iceland and the surrounding ocean floor. Cont. Min. Petr. 70:319-339.

Wright, T.L. (1971) Chemistry of Kilauea and Mauna Loa lavas in space and time. U.S. Geol. Survey Prof. Paper 735.

Yoder, H.S. (1976) Generation of Basaltic Magma. National Academy of Sciences, Washington, D.C.

Zindler, A., S. Hart, F. Frey, and S. Jakobsson (1979) Nd and Sr isotope ratios and rare earth element abundances in Reykjanes Peninsula basalts: evidence for mantle heterogeneity beneath Iceland. Earth Planet. Sci. Lett. 45:249-262.

Zindler, A. (1981) Chapman Conference on the generation of oceanic crust. Airlie House, Virginia.

Zindler, A., E. Jagoutz, and S. Goldstein (1982) Nd, Sr, and PD isotopic systematics in a three component mantle: a new perspective. Submitted to Nature.